

Herbicide Safening in Maize (*Zea mays*)

Philip Alexander Watson

A thesis submitted for the degree of Doctor of Philosophy (PhD)



School of Natural and Environmental Sciences

Newcastle University

September 2019

Abstract:

Safeners are agrochemicals used in conjunction with herbicides to enhance selectivity in large grained cereals, by reducing crop damage. The safening effect is associated with an increase in herbicide detoxification, via increased expression of enzymes in the xenobiotic detoxification pathway, known as the xenome. In this biosystem, cytochrome P450 (CYP) enzymes catalyse oxidation/reduction reactions, and glutathione-S-transferase (GST) enzymes catalyse conjugation reactions, leading to reduced toxicity and vacuolar sequestration. Despite their extensive use, the basis of safener specificity is largely unknown. The objective of this research was to identify, characterise and understand the mechanism of safener selectivity, and to determine the effect on specific mechanisms of herbicide metabolism, focusing on maize (*Zea mays L.*). A hydroponic growth system was developed to allow rapid, controlled analyses to be performed, and to test its validity as a potential replacement of large scale metabolic studies.

Two safeners, metcamifen and benoxacor, are known to enhance the detoxification of triketone and chloroacetanilide classes of herbicides, respectively. The effects of these safeners on the metabolism of a triketone (mesotrione) and a chloroacetanilide (*S*-metolachlor) herbicide were investigated in maize to characterise their chemical specificity. The effects of the safeners on the metabolic rate and route of the radiolabelled herbicides were studied using thin layer chromatography. This study identified an enhanced rate of mesotrione metabolism by both safeners, with metcamifen causing significantly faster metabolism than benoxacor. The metabolism of *S*-metolachlor was unaffected by either safener. To identify if uptake rate was responsible for this selectivity, the translocation of the radiolabelled safeners was analysed through phosphorimaging. Benoxacor underwent more rapid uptake than metcamifen.

The GST superfamily was then analysed at the genome level through *in silico* phylogenetic analyses, to further understand their involvement in metabolism. 65 proteins from 56 genes were identified and characterised using a novel nomenclature system. Investigation of GST enzyme structures and catalytic sites, using sequence alignments, and homology modelling, provided an insight into their functional properties.

To determine if differential regulation of xenome enzymes was involved in safening, the expression of transcripts encoding GSTs and CYPs by the safeners was investigated by

quantitative real time polymerase chain reaction (qPCR). Safener-inducible candidate GSTs and CYPs genes were identified by next generation sequencing analysis. This study showed an early induction of these genes in maize stems with benoxacor, while metcamifen caused a later induction of these genes in the leaf, providing time and tissue specific effects that could explain the observed specificity. In addition, both Safeners caused greater induction of GSTs than CYPs. To investigate the effect of the safeners on the regulation of important GST enzymes, western blotting was performed using antibodies recognising *ZmGSTU1.2-1.2* and *ZmGSTF2.0-2.3*. Both safeners increased the levels of the proteins, with benoxacor showing the greatest effect, and the stem displaying larger increases than the leaf. *ZmGSTF2.0*, *ZmGSTF2.3* and *ZmGSTU1.2* enzymes were expressed in *E. coli*, allowing for verification and characterisation of conjugating activity. In order to understand the complex signalling pathways regulating GSTs, co-expression analyses were performed using a database of maize experiments, to determine the effect of abiotic stresses on their expression. This study identified similarities between the effects of a phytohormone (12-OPDA), submergence stress, and safener treatment, potentially indicating shared signalling systems. These analyses also investigated the tissue-specific and developmental profile of GST expression, generating a comprehensive understanding of how the GST superfamily is regulated.

Overall, this research has determined that the safeners, metcamifen and benoxacor, selectively enhance the metabolic rate of different herbicide classes through increased expression of specific GST and CYP enzymes involved in xenobiotic detoxification, at both the transcript and protein level. The safener-effect is both tissue and time specific, and occurs without long term alteration to the final metabolic profiles of the herbicides. The GST family has been extensively characterised, providing a better understanding of their safener selectivity. For regulation, new safeners may be subjected to such analyses, allowing for predictions of specificity and suitability, before expensive and time-consuming field trials are performed.

In dedication to David and Gillian Williams
For inspiring me to pursue a life of knowledge
I wouldn't be here without you

Acknowledgements

I would like to thank my supervisor Professor Robert Edwards, whose profound understanding of the field has guided me through many challenges. Rob, I have learned more in this four years than in a lifetime before, which I owe to you. Thank you for the opportunity to work in such an esteemed group.

To the other research associates, I owe enormous thanks. From helping me in the lab, to helping me to navigate complex analysis, and most importantly in making sure I didn't burn out; I would not have succeeded without you. To Melissa Brazier-Hicks, I owe all my knowledge of plant growth, laboratory experimentation, analysis and indeed my project. To Nawaporn Onkokesung I owe several hundred hours, for proof-reading every piece of nonsense I wrote. To Alina Goldberg-Cavalleri and Sara Franco-Ortega I owe my sanity, which would certainly have faltered without their support.

To BBRSC and Syngenta I am eternally grateful, for providing sponsorship which made this project possible. I offer all my gratitude to James Booth and Roobina Baloch for supervising me through my time at Jeallot's Hill. You housed me, fed me, and made me feel comfortable in a new place. James, I apologise for making you don a lab coat once again, and thank you for assisting me where I was struggling. Roobina, your encouragement to present my work has given me both confidence in speaking, and confidence in my abilities.

To my fellow colleagues, I must generously thank you all. Steven and George, in the trenches we have become brothers in arms, and your friendship and shared despair has kept me going. Misery loves company, and you were mine. Gabby and Stewart, may our mistakes pave the road to your success. Thank you both for shared yoga therapy.

Finally I would like to thank my friends and family for their constant support. For my grandparents inspiration to dedicate my life to science. For my parents emotional support. For my best friend's suggestion to get the title of Doctor for the sake of pop-culture jokes. And to all who listened to my complaints and boring presentations.

Declaration and copyright

I declare that this thesis is my own work and that I have correctly acknowledged the work of others. This submission is in accordance with University and School guidance on good academic conduct. I certify that no part of the material offered has been previously submitted by me for a degree or other qualification in this or any other University. Any reference to this work should be acknowledged and permission should be sought from the author prior to the publication of any quotation from this work. I confirm that the word length is within the prescribed range as advised by my school and faculty.

Word count

Total: 68621

Page count

Total: 249

Contents

Abstract:	i
Acknowledgements.....	iv
Declaration and copyright.....	v
Word count.....	v
Page count	v
List of figures	x
List of supplementary figures	xiii
List of tables.....	xv
List of supplementary tables	xvi
1 Chapter 1. Introduction: Herbicide action, selectivity and safening	1
1.1 Herbicides.....	1
1.2 Herbicide mode of action and chemistry.....	2
1.2.1 Disruption of the photosynthetic system	4
1.2.2 Disruption of cell metabolism	5
1.2.3 Disruption of cell division and plant growth	7
1.3 Herbicide selectivity.....	9
1.4 Herbicide history.....	9
1.5 Herbicides in maize	10
1.6 The xenome	11
1.6.1 Phase I	12
1.6.2 Phase II	13
1.6.3 Phase III	15
1.6.4 Phase IV.....	15
1.6.5 Xenobiotic metabolism vs secondary metabolism.....	16
1.7 Herbicide metabolism	17
1.8 Herbicide safeners	19
1.9 Safener history.....	20
1.10 Safener chemistry.....	22
1.11 Safener mode of action	29
1.11.1 Alteration of herbicide uptake and translocation	29
1.11.2 Competitive antagonism	29
1.11.3 Enhancement of herbicide detoxification.....	30
1.12 Agrochemical discovery	34
1.13 Regulation of agrochemicals.....	34

1.14	Aims and objectives	36
2	Chapter 2. Materials and methods	38
2.1	Materials	38
2.2	Instrumentation and software	38
2.3	Statistical analysis	40
2.4	Plant growth	40
2.5	Dosing maize plants	41
2.5.1	Dosing for gene induction studies	41
2.5.2	Dosing for translocation study	41
2.5.3	Dosing for metabolism study	42
2.5.4	Dosing for protein study	42
2.6	Gene study	42
2.6.1	Primer design.....	42
2.6.2	Standard curves	43
2.6.3	RNA extraction.....	43
2.6.4	Reverse transcription by polymerase chain reaction (PCR).....	43
2.6.5	Quantitative/real time polymerase chain reaction (qPCR)	43
2.6.6	Absolute quantification using gBlocks®	44
2.6.7	Separation of DNA molecules using agarose gel electrophoresis.....	44
2.6.8	Next generation sequencing	45
2.7	Protein studies.....	45
2.7.1	Protein extraction	45
2.7.2	Protein concentration determination	46
2.7.3	SDS polyacrylamide gel electrophoresis (SDS-PAGE)	46
2.7.4	Western blotting and immunodetection	47
2.7.5	Plasmid production.....	47
2.7.6	Sequencing of recombinant plasmid	48
2.7.7	Recombinant protein expression	48
2.7.8	Recombinant protein purification	49
2.7.9	Recombinant protein quantification	49
2.7.10	GST assay with CDNB	49
2.8	Bioinformatics	50
2.8.1	GST gene expression analysis.....	50
2.8.2	GST sequence searching	50
2.8.3	Alignment and phylogenetic tree synthesis.....	50
2.8.4	Domain and interface mapping.....	51

2.8.5	Chromosome mapping.....	51
2.8.6	Hydrogen bond interaction mapping	51
2.8.7	Homology modelling.....	51
2.8.8	Targeting sequence analysis.....	52
2.9	Radio-isotope metabolism studies	52
2.9.1	Stock quantification and purity	52
2.9.2	Metabolite extraction	52
2.9.3	Liquid scintillation counting (LSC).....	52
2.9.4	Thin layer chromatography (TLC)	53
2.10	Translocation study	53
2.10.1	Phosphorimaging of freeze-dried plants	53
3	Chapter 3. Comparative translocation of the safeners, benoxacor and metcamifen, and their effect on herbicide metabolism	55
3.1	Introduction.....	55
3.2	Results	57
3.2.1	Translocation of safeners.....	57
3.2.2	Effect of safeners on herbicide metabolism	65
3.3	Discussion	84
3.3.1	Safener effects on herbicides translocation	84
3.3.2	Safener translocation.....	84
3.3.3	Safener effects on herbicide metabolism	85
3.4	Appendix to Chapter 3	87
4	Chapter 4. <i>In silico</i> analysis of glutathione-S-transferases.....	101
4.1	Introduction.....	101
4.2	Results	103
4.2.1	Identification and classification of GSTs in maize	103
4.2.2	Functions of maize GSTs	109
4.2.3	Evolution of GSTs.....	112
4.2.4	Chromosome distribution of maize GSTs	113
4.2.5	Domain organisation and interface interactions of maize GST proteins.....	116
4.2.6	G-site of maize GSTs	120
4.2.7	H-site of maize GSTs	124
4.2.8	3D structure of maize GSTs	128
4.2.9	Targeting sequences of maize GSTs	132
4.2.10	GST expression throughout development and in different tissues of maize plants	137
4.3	Discussion	140

4.4	Conclusions.....	141
4.5	Appendix to Chapter 4	143
5	Chapter 5. The effect of safeners and stresses on xenome enzyme induction	148
5.1	Introduction.....	148
5.2	Results	149
5.2.1	Safener effects on GST transcript expression in maize cell culture	149
5.2.2	Safener effects on GST and CYP transcript expression in whole plants	155
5.2.3	Effect of safeners on the expression of GST proteins in maize plants	168
5.2.4	Effect of abiotic stress on maize GST transcripts	179
5.3	Discussion.....	181
5.3.1	Safener effects on GST and CYP transcript regulation	181
5.3.2	Effect of safeners on GST protein regulation.....	185
5.3.3	Effect of abiotic stresses on GST transcript induction.....	186
5.4	Conclusions.....	186
5.5	Appendix to Chapter 5	188
6	Chapter 6. Conclusions and future Work	195
6.1	Conclusions.....	195
6.2	Future work	207
7	Abbreviations.....	210
8	Bibliography.....	212

List of figures

Figure 1: Schematic of carotenoid biosynthesis from D-glyceraldehyde 3-phosphate to lutein and xanthophylls.	5
Figure 2: Graph displaying the discovery of different herbicidal modes of action (MoA).	10
Figure 3: Herbicides used in the cultivation of maize.	11
Figure 4: Diagram showing the xenome (the biosystem responsible for the detection, transport and detoxification of xenobiotics).	12
Figure 5: Graph showing the history of safener development from 1969 to 2009.	21
Figure 6: a; Maize growth schematic. b; Maize growth photograph.	40
Figure 7: Structures of radioactive Safeners used in this thesis. a; [aniline-U- ¹⁴ C]-metcamifen, b; [phenyl-U- ¹⁴ C]-benoxacor.	41
Figure 8: Structures of radioactive herbicides used in this study. a; [phenyl-U- ¹⁴ C]-metolachlor, b; [phenyl-U- ¹⁴ C]-mesotrione.	42
Figure 9: Anatomy of maize plant at 3 leaf stage (phenological developmental stage identifier; BBCH13).	59
Figure 10: Photograph of maize plants after freeze drying.	60
Figure 11: Phosphoimage of maize plants.	61
Figure 12: Graphs showing uptake of Safeners in maize plants determined by analysis of Figure 11.	62
Figure 13: Graphs showing the uptake of dose solution (μL) in maize plants over time (h)...	66
Figure 14: Graphs showing the uptake of radioactive herbicide (kBq μL ⁻¹) over time (h).	67
Figure 15: Bar chart showing the radioactive recovery of samples (%), over time (h).	69
Figure 16: Ultraviolet (UV) image of thin layer chromatograph (TLC) of mesotrione standards.	70
Figure 17: Phosphorimage of thin layer chromatograph (TLC) containing a [¹⁴ C]-sample and superimposed [¹² C]-mesotrione metabolite standards.	71
Figure 18: Phosphorimage of two dimensional thin layer chromatograph (TLC) test of [¹⁴ C]-S-metolachlor sample.	72
Figure 19: Ultraviolet (UV) image of thin layer chromatograph (TLC) of S-metolachlor non-radioactive standards.	73
Figure 20: Schematic describing oxidative metabolism of mesotrione in plants.	74

Figure 21: Graphs showing the effect of metcamifen and benoxacor safeners on the metabolism of mesotrione in different tissues, over time (h).	75
Figure 22: Schematic describing oxidative metabolism of S-metolachlor.....	79
Figure 23: Schematic showing glutathione-mediated metabolism of S-metolachlor.....	80
Figure 24: Graphs showing the effect of metcamifen and benoxacor safeners on the metabolism of S-metolachlor in different tissues, over time (h).	83
Figure 25: Circular tree of maize Glutathione-S-Transferases (GSTs) based on maximum likelihood phylogenetic analysis using an LG model.....	108
Figure 26: Schematic indicating proposed evolution of Glutathione-S-Transferases (GSTs) based on the literature and the information obtained in section 4.2.1.	113
Figure 27: Maize karyogram showing maize Glutathione-S-Transferase (GST) gene locations on chromosomes 1-10 and MT (mitochondrial chromosome) and Pltd (Chloroplast chromosome).....	115
Figure 28: <i>In-silico</i> domain and interface residue localisations of maize Glutathione-S-transferase (GST) proteins.	118
Figure 29: Pie charts describing percentage ratios of amino acid residues involved in dimer interface interactions of Glutathione-S-transferase (GST) classes.	119
Figure 30: a; Aligned maize Glutathione-S-Transferase (GST) sequences with identified Glutathione-binding (G-) sites displayed in red. b; Graph showing percent similarity of residues between positions 110-220 of the alignment, with important sites highlighted in red with data values.....	122
Figure 31: 2-Dimensional hydrogen-bond schematic of Glutathione-binding (G-) site interactions of resolved Glutathione-S-Transferase (GST) structures.	123
Figure 32: a; Aligned maize Glutathione-S-Transferase (GST) sequences with identified substrate binding (H-) sites displayed in red. b; Graph showing percent similarity of residues from alignment positions 250 to 290 and 380 to 550.....	126
Figure 33: Pie charts showing percentage ratio of amino acid residues involved in substrate binding.	127
Figure 34: Glutathione-S-Transferase (GST) homology structures, superimposed in ribbon format.....	131
Figure 35: Schematic of theta class Glutathione-S-Transferase (GST) fold.	132
Figure 36: Heat map showing expression of Glutathione-S-Transferases (GSTs) a; throughout development of maize plant and b; in different tissues.	139

Figure 37: Regression analysis showing the effect of safeners, metcamifen and benoxacor, on induction of Glutathione-S-Transferase (GST) classes.	152
Figure 38: Bar chart showing calculated molecular weights of reference gene replicated region of treated and untreated samples as defined by the legend (right).....	158
Figure 39: Bar chart showing percentage difference in molecular weight of calculated compared to expected product sizes of reference genes.	158
Figure 40: Quantification cycle (Cq) of reference gene primers with benoxacor treatment compared to control treatment.	159
Figure 41: <i>ZmGSTU1.2</i> gene sequence with primer positions.	161
Figure 42: Relative quantification of Glutathione-S-Transferase (GST) enzyme induction with safeners, metcamifen and benoxacor, showing N-fold induction against time (h).	162
Figure 43: Relative quantification of Cytochrome P450 (CYP) enzyme induction with safeners, metcamifen and benoxacor, showing N-fold induction against time (h).	163
Figure 44: gBlock® design for Glutathione-S-Transferase (GST) quantitative/real time polymerase chain reaction (qPCR) quantification.	164
Figure 45: gBlock® design for Cytochrome P450 (CYP) quantitative/real time polymerase chain reaction (qPCR) quantification.	165
Figure 46: gBlock® standard curves showing relationship between Log ₁₀ complementary DNA (cDNA) copy number per reaction and quantification cycle (Cq).	166
Figure 47: Absolute quantification of endogenous gene transcription showing complementary DNA (cDNA) copy numbers against time (h).....	167
Figure 48: <i>ZmGSTU1.2</i> protein sequence.....	169
Figure 49: <i>ZmGSTF2.0</i> protein sequence.	169
Figure 50: a; <i>ZmGSTF2.3</i> DNA insert sequence. b; <i>ZmGSTF2.3</i> protein sequence.....	169
Figure 51: a; Ultraviolet (UV) spectrum displaying purification of <i>ZmGSTU1.2</i> recombinant protein showing absorbance against volume eluted (mL). b; Concentration (mg mL ⁻¹) of <i>ZmGSTU1.2</i> recombinant protein in purified fractions.....	170
Figure 52: a; Ultraviolet (UV) spectrum displaying purification of <i>ZmGSTF2.0</i> recombinant protein showing absorbance against volume eluted (mL). b; Concentration (mg mL ⁻¹) of <i>ZmGSTF2.0</i> recombinant protein in purified fractions.	171

Figure 53: a; Ultraviolet (UV) spectrums displaying purification of <i>ZmGSTF2.3</i> recombinant protein showing absorbance against volume eluted (mL). b; Concentrations (mg mL ⁻¹) of <i>ZmGSTF2.3</i> recombinant protein in purified fractions.	171
Figure 54: Recombinant protein activity towards 1-chloro-2,4-dinitrobenzene (CDNB) (nkat mg ⁻¹).....	172
Figure 55: Western blot showing cross reactivity of <i>TaGSTU1-1</i> antibody with recombinant <i>ZmGSTU1.2</i> protein and crude protein from leaves of untreated maize plants (sample).	173
Figure 56: Western Blot showing cross reactivity of <i>ZmGSTF2.0-2.3</i> antibody with recombinant <i>ZmGSTF2.0</i> and <i>ZmGSTF2.3</i> proteins and crude protein from stems of metcamifen (25µM) treated maize plants (sample).....	174
Figure 57: a; Western blot of <i>TaGSTU1-1</i> antibody with 40 ng <i>ZmGSTU1.2</i> recombinant protein. Molecular weight ladder shows mass of markers (kDa). b; western blot of dilution curve of <i>TaGSTU1-1</i> antibody with <i>ZmGSTU1.2</i> recombinant protein. c; Graph of data in b, showing density of western blot bands against amount of recombinant proteins (ng).....	175
Figure 58: a; Western blot of <i>ZmGSTF2.0-2.3</i> antibody with 40 ng <i>ZmGSTF2.0</i> recombinant protein. Molecular weight ladder shows mass of markers (kDa). b; Western blot of dilution curve of <i>ZmGSTF2.0-2.3</i> antibody with <i>ZmGSTF2.0</i> recombinant protein. c; Graph of data in b, showing density of western blot bands against amount of recombinant proteins (ng).....	176
Figure 59: Expression of Glutathione-S-Transferase (GST) proteins in leaf and stem tissues, plotted as percentage of total protein (after normalisation to control) against time (h).	178
Figure 60: Study pipeline.....	196
Figure 61: Proposed system of safener selectivity.....	204

List of supplementary figures

Figure S 1: Phosphorimages of thin layer chromatographs (TLCs) with [¹⁴ C]-mesotrione-treated plant samples, for Figure 21.	89
Figure S 2: Phosphorimages of thin layer chromatographs (TLCs) with [¹⁴ C]-S-metolachlor-treated plant samples, for Figure 24.....	94

Figure S 3: Example data used to validate homology model quality. a; Ramachandran plot, b; global quality estimate,	144
Figure S 4: Alignment of Glutathione-S-Transferase (GST) class sequences based on homology models structure alignment.....	146
Figure S 5: Agarose gel electrophoresis of reference gene replicated region, for Figure 38 and Figure 39.	188
Figure S 6; Melting peaks for genes of interest (Table 24).	189
Figure S 7; Agarose gel electrophoresis of gene of interest primers (Table 24).	190
Figure S 8: Bar chart showing difference of in molecular weight of calculated compared to expected product sizes of genes of interest.	191
Figure S 9: pET-STRP3 expression vector sequence.	194

List of tables

Table 1: Herbicide classes organised by process and mode of action.	2
Table 2: The metabolic pathways of herbicide detoxification.	18
Table 3: Commercial products containing safeners.	22
Table 4: Safener classification.	24
Table 5: Known safener agonism of herbicides determined through survey of literature.	27
Table 6: The use of glutathione-S-transferase (GST) and cytochrome P450 (CYP) enzymes in safener-mediated detoxification of herbicide classes.	33
Table 7: Regulatory authorities for each country or region. Data extracted from ("ENV pesticide compliance," accessed 2020).	35
Table 8: Instrumentation used for experimental processes.	38
Table 9: Software and databases used for analysis.	39
Table 10: Conditions for maize growth.	41
Table 11: Quantitative/real time polymerase chain reaction (qPCR) conditions.	44
Table 12: Ratios of each active ingredient (in percentage of total active ingredients) in formulated products containing benoxacor.	56
Table 13: Physicochemical properties of metcamifen and benoxacor, and optimum properties for root translocation.	63
Table 14: Physicochemical properties of mesotrione and S-metolachlor and optimum properties for root translocation.	68
Table 15: List of Identified maize Glutathione-S-Transferase (GST) genes and proteins.	106
Table 16: Known maize Glutathione-S-Transferase (GST) activity against herbicide substrates.	111
Table 17: C- and N- terminal targeting sequences of Glutathione-S-Transferases (GSTs).	135
Table 18: Experimentally determined subcellular localisation of <i>Arabidopsis thaliana</i> GSTs, compiled from literature survey and using ProteomicsDB.	136
Table 19: Correlation and regression analysis of next generation sequencing data of Glutathione-S-Transferase (GST) classes (Figure 37).	153
Table 20: Perturbation of maize Glutathione-S-Transferase (GST) genes by safeners, metcamifen and benoxacor, determined through next generation sequencing. ...	154
Table 21; Reference gene primer sequences.	155

Table 22: Reference gene primer efficiency data.....	156
Table 23: Melting curves for reference gene primers.	157
Table 24: Gene of interest primer sequences.	160
Table 25: Properties of recombinant proteins.	172
Table 26: Perturbation of maize Glutathione-S-Transferase (GST) genes by abiotic stresses.	180
Table 27: Pearsons correlation of abiotic stress and safener perturbation.	181

List of supplementary tables

Table S 1: Uptake volume data (μL) for Figure 13.	87
Table S 2: Uptake volume statistics for Figure 13.	87
Table S 3: Radioactive herbicide uptake data ($\text{Bq } \mu\text{L}^{-1}$) for Figure 14.....	88
Table S 4: Radioactive uptake statistics for Figure 14.	88
Table S 5: Mesotrione metabolism data expressed in percent radioactivity (%), for Figure 21.	90
Table S 6: Mesotrione metabolism statistics for Figure 21.....	92
Table S 7: S-metolachlor metabolism data in percent radioactivity (%),for Figure 24.....	95
Table S 8: S-metolachlor metabolism statistics, for Figure 24.	96
Table S 9: Compounds used as identification standards for mesotrione metabolites.....	97
Table S 10: Compounds used as identification standards for S-metolachlor metabolites.....	98
Table S 11: Table describing details of Glutathione-S-Transferase (GST) models used in Figure 31.	143
Table S 12: Homology model characteristics, for Figure 34.	145
Table S 13: Statistical analysis of reference gene Cq values in stability test, for Figure 40. .	188
Table S 14; Primer efficiencies for genes of interest (Table 24).....	189
Table S 15: Obsolete gene of interest primers.	191
Table S 16: Heat map of quantitative/real time polymerase chain reaction (qPCR) data (Figure 42 and Figure 43).....	192
Table S 17: gBlock® absolute quantification summarised data (Figure 47).....	193

Chapter 1. Introduction: Herbicide action, selectivity and safening

1.1 Herbicides

It has been predicted that the world's population will exceed nine billion by 2050 (Fao, 2012). Therefore, food production needs to be increased significantly to prevent global shortages. The best strategy to cope with increasing demand is to maximise the efficiency of food production, which involves mitigating the heavy yield losses caused by pests, diseases and weed infestation. The effects of weeds can be reduced through a variety of techniques including mechanical methods, such as tillage and manual removal, cultural methods, such as crop rotation, and chemical methods, including the use of fertilisers and herbicides. The most effective means in protecting crops from weed infestation is the use of herbicides, which provide fast, effective protection against a range of species (Abrol et al., 2014).

Herbicides are chemical agents used for weed control, which mainly work through the inhibition of vital biological processes in the plant life cycle (Kraehmer et al., 2014). In agriculture, selective herbicides are used to control specific weeds while causing minimum damage to crop plants (Hatton et al., 1996). Exploiting biological differences between specific crops and competing weeds is an important factor in delivering herbicide selectivity. Modern agriculture's heavy reliance on herbicides has made it the largest chemical sector of the \$US 85 billion crop protection market, with herbicide sales reaching \$US 17 billion in 2014, exceeding the fungicide and insecticide markets, and continuing to grow in both developing and developed countries (Green, 2014)(Kraehmer, 2012). To this day herbicides remain the most effective, efficient and economical approach for weed control, and the economic costs of herbicides are fully compensated by the increase in crop production (Green, 2014; Scarponi et al., 2009b).

Herbicides are generally separated into three categories, which describe the time of their application. Pre-emergence herbicides are applied before the appearance of weeds, early in the growing season, and are designed to inhibit seed germination or establishment. They are usually separated into those targeting monocotyledonous (grassy) weeds or dicotyledonous (broad-leaf) weeds. Pre-plant incorporated (PPI) herbicides are mixed into the soil before any planting, and are often used to combat existing vegetation. Post-emergence herbicides are

used once plants have begun to grow and are categorised as selective or non-selective (Cobb et al., 2011).

1.2 Herbicide mode of action and chemistry

The diverse chemistries of herbicides cause toxicity to plants through a range of modes of action (MoA), which are described in Table 1. Herbicides are commonly classified based on their specific action in disrupting important biological processes, including the photosynthetic system, cell metabolism, and cell division. Herbicides will be discussed here with respect to their MoA.

		Reference codes					
Processes	Mode of action	HRAC	WSSA	Herbicide class			
Light processes	1. Inhibition of photosystem II	C1	5	Phenyl carbamates			
				Uracils			
				Pyridazinones			
				Triazinones			
				Triazolinone			
				Triazines			
		C2	7	Ureas			
				Amides			
		C3	5	Phenyl-pyridazines			
				Benzothiadiazinones			
			5/6	Nitriles			
	2. Inhibition of protoporphyrinogen oxidase	E	14	Diphenyl ethers			
				Thiadiazoles			
				Pyrimidinediones			
				Phenylpyrazoles			
				Oxadiazoles			
				Triazolinones			
				Oxazolidinedione			
				N-Phenylphthalimides			
				Other			
				3. PS-I-electron diversion	D	22	Bipyridyliums
				4. Inhibition of pigment Synthesis	PDS inhibitors	F1	12
	Pyridinecarboxamide						
	Other						
	4-HPPD inhibitors	F2	27		Isoxazole		
					Pyrazole		
					Triketone		
					Other		
	Unknown target	F3	1		Diphenylethers		
					Triazole		
					Urea		
	DXS inhibitors	F4	13		Isoxazolidinone		

Table 1: Herbicide classes organised by process and mode of action.

Data taken from the global classification lookup tool of HRAC (herbicide resistance action committee). N/A indicates no information given.

		Reference codes		
Processes	Mode of action	HRAC	WSSA	Herbicide class
Cell metabolism	5. Inhibition of ALS	B	2	Imidazolinones
				Sulfonylureas
				Sulfonylamino-carbonyl-triazolinones
				Pyrimidinyl (thio) benzoates
				Triazolopyrimidines
	6. Uncoupler (membrane disruption)	M	24	Dinitrophenols
	7. Inhibition of EPSP synthase	G	9	Glycines
	8. Glutamine synthetase inhibition	H	10	Phosphinic acids
	9. DHP-inhibition	I	18	Carbamates
	10. Lipid synthesis inhibition (ACCase)	A	1	Cyclohexanediones (DIMs)
				Aryloxyphenoxypropionates (FOPs)
				Phenylpyrazolines (DENs)
Growth/ cell division	11. Lipid synthesis inhibition (non-ACCase)	N	8	Phosphorodithioate
				Benzofuranes
				Thiocarbamates
			26	Chlorocarb. Acids
	12. Inhibition of microtubule assembly	K1	3	Benzoic acids
				Phosphoroamidates
				Dinitroanilines
				Pyridines
	13. Inhibition of microtubule organisation	K2	23	Carbamates
			N/A	Arylamino propionic acid
	14. Inhibition of cell division (inhibition of VLCFAs)	K3	15	Acetanilides
				Oxyacetamides
				Chloroacetanilides
				Tetrazolinones
				Other
	15. Inhibition of cellulose synthesis	L	N/A	Alkylazines
			20	Nitriles
			21	Benzamides
				Triazolocarboxamides
			26	Quinoline carboxylic acid
	16. Synthetic Auxins	O	4	Pyridine-carboxylic acids
				Quinolinecarboxylic acids
				Benzoic acids
				Phenoxy-carboxylic acids
				Arylpiccolinate
Unknown mode of action	17. Auxin transport inhibition	P	19	Semicarbazones
				Phthalamates
	18. Unknown mode of action	Z	17	Organoarsenical
			26	Pyrazolium

Table 1: (Continued).

1.2.1 *Disruption of the photosynthetic system*

Photosynthesis is the main source of energy for plants, the disruption of which reduces anabolism and invokes excessive photo-oxidation, which destroy the cells. Four classes of herbicide (Table 1. 1-4) cause toxicity through such disruption. Although the herbicides in these groups target different components in photosynthesis, leaf bleaching is the main phenotype caused, and hence they are also known as photobleaching herbicides. These can be classified based on MoA into four subgroups as defined in Table 1, namely; (1) the inhibition of photosystem II, (2) the inhibition of protoporphyrinogen IX oxidase (PPO), (3) photosystem I-electron diversion, and (4) the inhibition of carotenoid biosynthesis.

The photosystem II inhibitor herbicides (Table 1. 1), inhibit the electron transport chain in photosystem II, by binding to reaction centre protein D-1 located in the chloroplast thylakoid membranes, which then prevents the binding of plastoquinone to this protein (Devine et al., 1992). This competitive binding inhibits the redox system and causes an increase in reactive oxygen species, leading to oxidative stress and phytotoxicity (Devine et al., 1992; Santabarbara, 2006; Sherwani et al., 2015). This MoA is demonstrated by phenylureas (also known as arylureas), triazines, and uracils (Kraehmer et al., 2014).

The second MoA (Table 1. 2) is the inhibition of protoporphyrinogen IX oxidase (PPO), an enzyme important for the synthesis of chlorophyll. This inhibition results in a significant reduction of chlorophyll content and consequently leads to the reduction of photosynthesis. Furthermore, the disturbance to the synthesis of reactive porphyrins causes an associated accumulation of oxygen radicals, causing phototoxicity (Devine et al., 1992). This mode of action of herbicide is observed with diphenyl ethers, oxadiazoles and thiadiazoles (Kraehmer et al., 2014).

Photosystem I-diversion herbicides (Table 1. 3), such as diquat and paraquat, disturb the normal function of the photosystem I protein complex involved in photosynthesis. The herbicides are chemically reduced by photosystem I in place of endogenous cofactors, leading to a production of superoxide, causing oxidative damage (Devine et al., 1992). These herbicides are classified as the bipyridylium class (Kraehmer et al., 2014).

A number of herbicides inhibit the biosynthesis of carotenoids, important pigments that protect chlorophyll from excess light (Table 1. 4). Herbicides with this MoA cause photo-oxidation that leads to photobleaching. Herbicides target carotenoid synthesis by inhibiting

different biosynthetic enzymes, such as phytoene desaturase (PDS), 4-hydroxyphenyl pyruvate dioxygenase (HPPD) and 1-deoxy-D-xyulose 5-phosphate synthase (DXS) as shown in Figure 1 (Devine et al., 1992). The PDS enzyme catalyses an essential reaction in the synthesis of carotenes and the xanthophylls, zeaxanthin, antheraxanthin and violaxanthin (Kramer et al., 2007; Qin et al., 2007). HPPD is involved in the synthesis of plastoquinones, which act as vital electron acceptors in carotenoid synthesis, as a cofactor with PDS. The enzyme DXS is also involved in the early steps of the carotene and xanthophyll formation (Stange et al., 2008). The PDS inhibitor herbicides include the pyridazinones, while the HPPD inhibitors include the triketones, such as mesotrione (Kraehmer et al., 2014; O'sullivan et al., 2002).

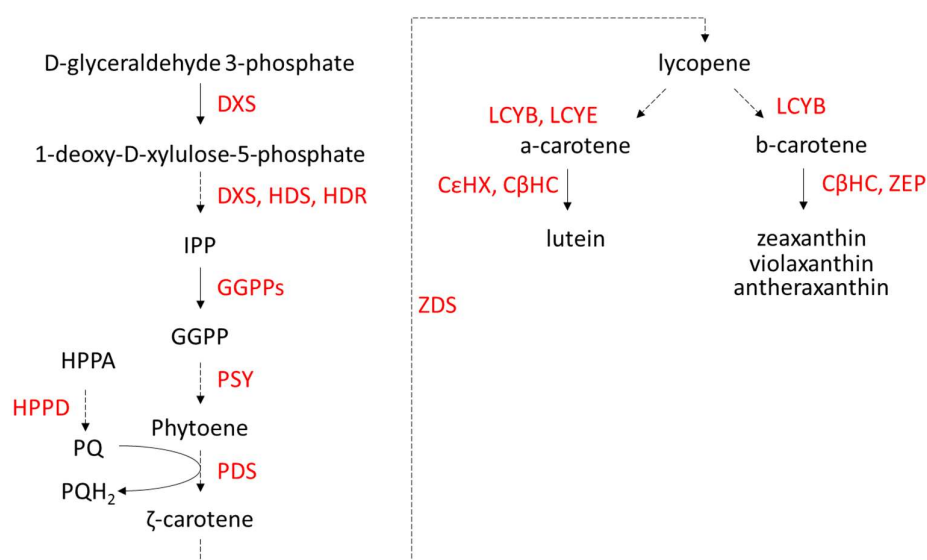


Figure 1: Schematic of carotenoid biosynthesis from D-glyceraldehyde 3-phosphate to lutein and xanthophylls.

IPP; isopentyl pyrophosphate, GGPP; geranyl geranyl pyrophosphate, DXS; 1-deoxy-D-xyulose 5-phosphate synthase, PDS; phytoene desaturase, HPPD; 4-hydroxyphenyl pyruvate dioxygenase, PQ/PQH₂; plastoquinone, HPPA; 4-hydroxyphenylpyruvate, PSY; phytoene synthase, ZDS; ζ-carotene desaturase, ZEP; zeaxanthin epoxidase, CεHX; ε-carotene hydroxylase, CβHX; β-carotene hydroxylase, LCYE; lycopene ε cyclase, LCYB lycopene β cyclase, HDS; HMBPP synthase, HDR; HMBPP reductase. Dotted lines indicate further steps may exist. (Stange et al., 2008; Xu et al., 2015).

1.2.2 Disruption of cell metabolism

A range of herbicides damage plants through the inhibition of primary biosynthetic pathways, including the synthesis of amino acids, fatty acids and micronutrients such as folic acid.

Acetolactate synthase (ALS) inhibitors (Table 1. 5), commonly known as amino acid synthase inhibitors, inhibit the ALS enzyme, responsible for the synthesis of branched chain amino acids in the plastids. This inhibition eventually causes plant wilting and death. The chemical class of

herbicides that work through this action include the sulfonylureas, imidazolinones, and pyrimidinylthiobenzoates (Devine et al., 1992; Kraehmer et al., 2014; Sherwani et al., 2015; Whitcomb, 2016).

The dinitrophenol herbicides, including dinitro-ortho-cresol, are oxidative phosphorylation uncouplers (Table 1. 6). This group of herbicides act as protonophores, causing a loss of proton gradient over mitochondrial membranes. This process inhibits ATP production by bypassing the ATP synthase enzyme, causing an energy deficit which leads to a compensating increase in metabolism and toxicity (Devine et al., 1992; Kraehmer et al., 2014; Moreland, 1993; Rensen et al., 1979).

5-enolpyruvylshikimate-3-phosphate (EPSP) is intermediate metabolite in shikimic acid biosynthetic pathway, responsible for production of aromatic amino acid precursors. The inhibition of the EPSP synthase enzyme, which produces EPSP, therefore results in the depletion of amino acids and secondary products, including lignins and flavonoids. These products are important in plant growth and development, and the inhibition of this pathway ultimately causes plant death. This mode of action (Table 1. 7) is used by herbicides such as the glycines, notably the well-known glyphosate. Due to the importance of the shikimate pathway, these herbicides non-specifically target all plants (Devine et al., 1992; Herrmann et al., 1999; Kraehmer et al., 2014; Sherwani et al., 2015).

Glutamine synthetase (GS) inhibitor herbicides (Table 1. 8), work by inhibiting the GS enzyme which catalyses the synthesis of the amino acid, glutamine. Under normal conditions, this reaction uses ammonia generated from respiration and deamination reactions, and herbicidal inhibition of GS thus leads to an accumulation of ammonia. This affects pH and ultimately disrupts various cell functions including the photosystems (Sherwani et al., 2015). Herbicides with this mode of action fall under the phosphinic acid class (Kraehmer et al., 2014; Obojska et al., 2004).

7, 8-dihydropteroate (DHP) synthase is an important enzyme involved in folic acid synthesis. Since folic acid is required for the synthesis of purines, pyrimidines and certain amino acids, such as glutamic acid, the inhibition of DHP synthase leads to reduced DNA and protein production, and ultimately causes cell death. Herbicides that target this enzyme are known as DHP inhibitors (Table 1. 9), the major chemical class of which is the carbamates, including

asulam. The DHP inhibitor herbicides are commonly used in the protection of sugarcane from johnsongrass (Ahrens, 1994; Devine et al., 1992; Pallett, 2003; Stryer, 1995).

Acetyl coenzyme A carboxylase (ACCase) is the primary enzyme involved in fatty acid biosynthesis, and herbicides that inhibit this enzyme are known as ACCase inhibitors (Table 1. 10) or lipid biosynthesis inhibitors. The inhibition of ACCase activity blocks the biosynthesis of phospholipids, and therefore prevents cell membrane production. Herbicide chemical classes in this category include the aryloxyphenoxypropionates (FOPs), cyclohexanediones (DIMs), and phenylpyrazolines (DENs). These classes of herbicide are typically used to control grass weeds during broadleaf crop cultivation (Delye et al., 2005; Konishi et al., 1994; Kraehmer et al., 2014; Sherwani et al., 2015).

Apart from the ACCase inhibitors, there is another MoA of lipid synthesis inhibition (Table 1. 11). The herbicides in this group inhibit the biosynthesis of lipids, fatty acids, flavonoids and gibberellins by targeting the lipid synthesis machinery in the cell membranes, possibly by conjugation of acetyl coenzyme A, which ultimately causes shoot growth inhibition (Fuerst, 1987). Herbicides in this class include the chlorocarbonic (chloroaliphatic) acids, phosphorodithioates and thiocarbamates (carbamothioates). These herbicides are used pre-emergence and are designed to control grass and broadleaf weeds (Colovic et al., 2013; Kraehmer et al., 2014; Sherwani et al., 2015).

1.2.3 *Disruption of cell division and plant growth*

Many herbicides function by inhibiting cell division, thus reducing plant growth. The reduction of weed growth rate may be enough for crop plants to outcompete weeds in the fields, and this growth inhibition effect may also prevent efficient photosynthesis of the weeds as a result of shading by crops.

Microtubule assembly inhibitor herbicides (Table 1. 12) inhibit the polymerisation of microtubules by binding to tubulin. This lack of microtubule function compromises formation of the cell wall and impedes correct mitosis, leading to prevention of replication and elongation, especially in the growing root tips. As a result of this physiological effect, these herbicides are also known as root growth inhibitors. This group of herbicides includes the dinitroaniline, benzamide, and pyridine chemical classes. Since root growth is a vital process in the early stages of plant development, these herbicides are normally applied pre-emergence (Kraehmer et al., 2014; Sherwani et al., 2015; Wloga et al., 2010).

Microtubule organisation inhibitor herbicides (Table 1. 13), such as carbamates and arylaminopropionic acids, disrupt mitosis through the disturbance of the spindle microtubule organising centres. The resulting improper localisation of the chromosomes, prevents correct cell division and thus inhibits plant growth. This mode of action is used in the pre-emergence control of monocot weeds (Kraehmer et al., 2014; Vaughn et al., 1991).

Very long-chain fatty acid (VLCFA) inhibitor herbicides (Table 1. 14) work by inhibiting acetyl coenzyme A, which is involved in the synthesis of VLCFAs in the cell membranes. Ultimately lipid synthesis inhibition prevents growth of the shoot, and hence this group of herbicides are often known as shoot-growth inhibitors. Besides growth inhibition, this group of herbicides also negatively affect leaf wax deposition. Herbicide classes with this mode of action include the chloroacetanilides (chloroacetamides), such as metolachlor, acetanilides, oxyacetamides, and tetrazolinones, and are typically used in pre-emergence control of grass and broadleaf weeds (Devine et al., 1992; Kraehmer et al., 2014; Sherwani et al., 2015; Trenkamp et al., 2004).

Cellulose synthesis inhibitor herbicides (Table 1. 15), inhibit the synthesis of the polysaccharide cellulose, the major component of cell walls. This inhibition prevents the efficient biosynthesis of cell walls and thus inhibits plant growth. Herbicides displaying this mode of action include nitriles, benzamides, alkylazines, and triazolocarbonylamides (Devine et al., 1992; Kraehmer et al., 2014).

Synthetic auxin herbicides (Table 1. 16) control weeds by mimicking the endogenous effect of indole acetic acid (IAA). The natural growth effect of auxins is agonistically hyper-stimulated by these herbicides, leading to increased protein biosynthesis in the cells, and uninhibited vascular growth. The organelles swell, generally the chloroplast first, followed by eventual bursting, cell rupture and plant death. Herbicides with this mode of action include the phenoxy-, pyridine-, and quinolone- carboxylic acids. These herbicides are used to control broadleaf weeds in cereal cultivation (Devine et al., 1992; Grossmann, 2010; Kraehmer et al., 2014; Sherwani et al., 2015).

Phthalamate and semicarbazone herbicides act as inhibitors of auxin transport, also known as phytotropins (Table 1. 17), and exert an opposite effect to the synthetic auxins. These herbicides inhibit auxin efflux from the cytoplasm to the periplasm, causing a lack of growth

signalling, leading to stunting. These herbicides are typically used for pre-emergence control of broadleaf weeds (Naylor, 2008).

1.3 Herbicide selectivity

For herbicides to be effective, they must be selective with respect to the target plants; i.e. toxic to the weed but not to the crop. This botanical selectivity takes advantage of the biochemical differences between tolerant crops and sensitive weeds (Kreuz et al., 1996). For example, herbicides which act as auxins (Table 1. 16) selectively target dicotyledonous (dicot) weeds in monocotyledonous (monocot) cereals crops (Grossmann, 2010; Kraehmer et al., 2014). This selective toxicity is believed to be due to differential metabolism of the herbicides and differential target-site or receptor sensitivity (Grossmann, 2010; Kraehmer et al., 2014). In contrast, the ACCase inhibitor (Table 1. 10) herbicide classes, aryloxyphenoxypropionates (FOPs) and cyclohexanediones (DIMs) selectively target grass (monocot) weeds in broadleaf (dicot) crop cultivation. This occurs due to the selectivity of the herbicides towards the homomeric, chloroplastic, ACCase enzyme exclusive to grasses (Delye et al., 2005; Kraehmer et al., 2014; Sherwani et al., 2015). Non-selective herbicides, such as the EPSP synthase inhibitor, glyphosate (Table 1. 7), and the photosystem I inhibitors (Table 1. 3), diquat and paraquat, target all plants, and selectivity must be provided by other means. Glyphosate is sometimes used with special genetically modified glyphosate-resistant crops which afford selectivity, while selectivity in the bipyridyliums, diquat and paraquat, is afforded by application prior to crop planting (Devine et al., 1992; Kraehmer et al., 2014; Sherwani et al., 2015; Springett, 1965). As mentioned, the primary system of selectivity between crop and weed plants is the ability of crops to detoxify the herbicide (Hatzios et al., 2004; Kraehmer et al., 2014). This has been confirmed in the sulfonylurea herbicides, and in many herbicide classes, such as the chloroacetanilides, ureas, and thiocarbamates in rice crops (*Oryza sativa*) (Brown, 1990; Usui, 2001).

1.4 Herbicide history

Figure 2 describes the year in which each herbicidal MoA was first used commercially. On average, between 1934 and 1984, one new MoA was discovered every three years, in a linear manner. It was thought that since then, no new herbicide MoA had been commercially adopted into agricultural practice (Kraehmer et al., 2014). However, the MoA for the unexploited molecule cinmethylin (Figure 2. x), commercialised in 1989, has recently been determined as novel (Campe et al., 2018). This herbicide inhibits fatty acid biosynthesis by

binding a novel target, acyl-ACP thioesterase, though HRAC has not assigned a MoA reference (Campe et al., 2018). The declining rate of discovery of new MoA is thought to be due to the cornering of the herbicide market by glyphosate and glyphosate-resistant crops, leading to a reduction in herbicide development. Also the cost of herbicide discovery and meeting regulatory requirements has increased drastically, with research and development costs increasing by 68% between 1995 and 2005 (Lamberth et al., 2013). As a result of this discovery plateau, a considerable degree of crop protection efficiency in weed control has been lost (Duke, 2012).

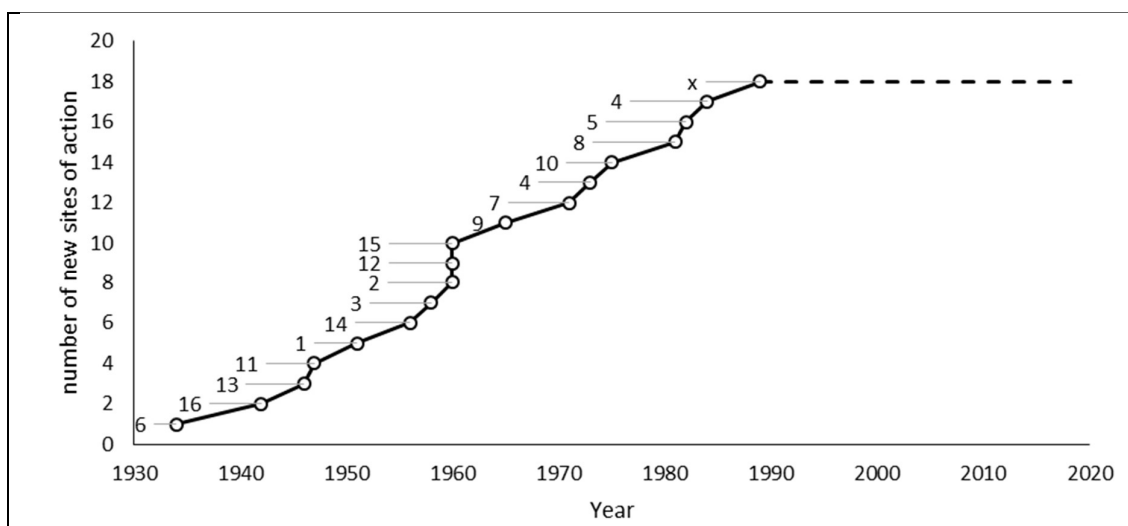


Figure 2: Graph displaying the discovery of different herbicidal modes of action (MoA).

Year of first commercial use is shown against number of MOA. Data labels indicate HRAC (herbicide resistance action committee) MOA reference number (Table 1). x indicates unassigned MOA for cinmethylin. Dashed line indicates no new discovery. Data taken from Campe et al. (2018); Kraehmer et al. (2014); Pallett (2003), and plotted using Excel.

1.5 Herbicides in maize

Maize represents one of the most important crops in the world, with 717 million metric tons grown globally per year (Ranum et al., 2014)(Rajcan et al., 2001; Tandzi et al., 2019). The gross production value of maize in 2016 was \$US 192 trillion (Faostat, Accessed 2020). It's uses include animal feed, food, seed, and ethanol production (Ranum et al., 2014). Considering the importance of maize, especially in North America, considerable research and development has focused on finding effective weed control for this crop (Rajcan et al., 2001). Over 30 herbicides, with 13 MoA have been developed, to control a huge range of weed species (Figure 3). Most of these herbicides are broad-spectrum, acting on both monocot and dicot weeds. Only a few of these herbicides are selective, with flumetsulam, bromoxynil, paraquat,

carfentrazone, flumiclorac, mesotrione, clopyralid and dicamba used for dicot weeds, and butylate and nicosulfuron for monocot weeds. Nine of the herbicides provide selectivity through pre-plant incorporation (see section 1.3), and the remainder are split between pre- and post- emergence application. It should be noted that many of these herbicides have been superseded by others, or removed from the market, with 17 herbicides currently approved for use in the European Union (EU).

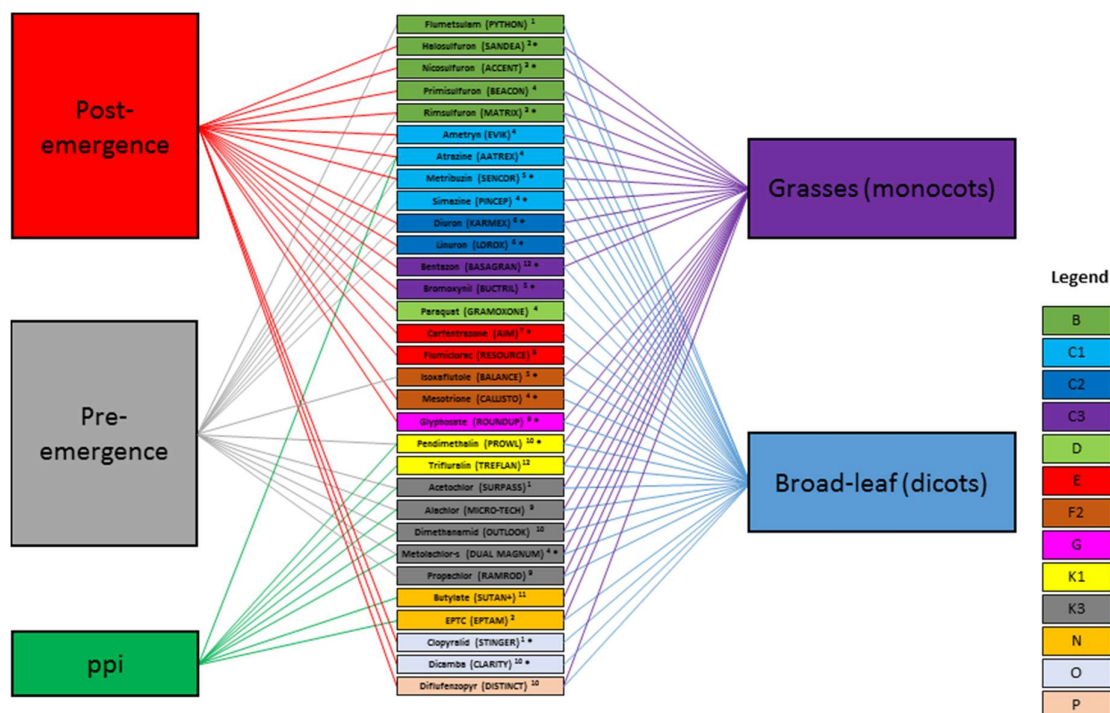


Figure 3: Herbicides used in the cultivation of maize.

Application (left), herbicide with trade names in brackets (middle) and target weeds (right) are shown. PPI; Pre-plant incorporated. Herbicide mode of action (MoA) is described by the HRAC (herbicide resistance action committee) letters in the legend (right). *; approved for use in the EU according to Lewis et al. (2016). Manufacturers represented by superscripts: 1; Dow AgroSciences, 2; Gowan, 3; DuPont, 4; Syngenta, 5; Bayer Crop Science, 6; Griffin, 7; FMC, 8; Valent, 9; Monsanto, 10; BASF, 11; Helm AgroScience, 12; several. Data was obtained from the University of Kentucky horticulture database (Section 2.2), and Lewis et al. (2016).

1.6 The xenome

As mentioned in section 1.3, the primary system of selectivity between crop and weed plants is the ability of crops to detoxify the herbicide. This occurs through the xenome, defined as ‘the biosystem responsible for the detection, transport and detoxification of xenobiotics’ (Edwards et al., 2011). Generally this follows a four-phase detoxification pathway involving the activation of the parent xenobiotic during phase I, the subsequent conjugation with endogenous substrates during phase II, and the sequestering or further processing of the

metabolites in the vacuole during phase III and IV respectively, as described in Figure 4 (Davies et al., 1999).

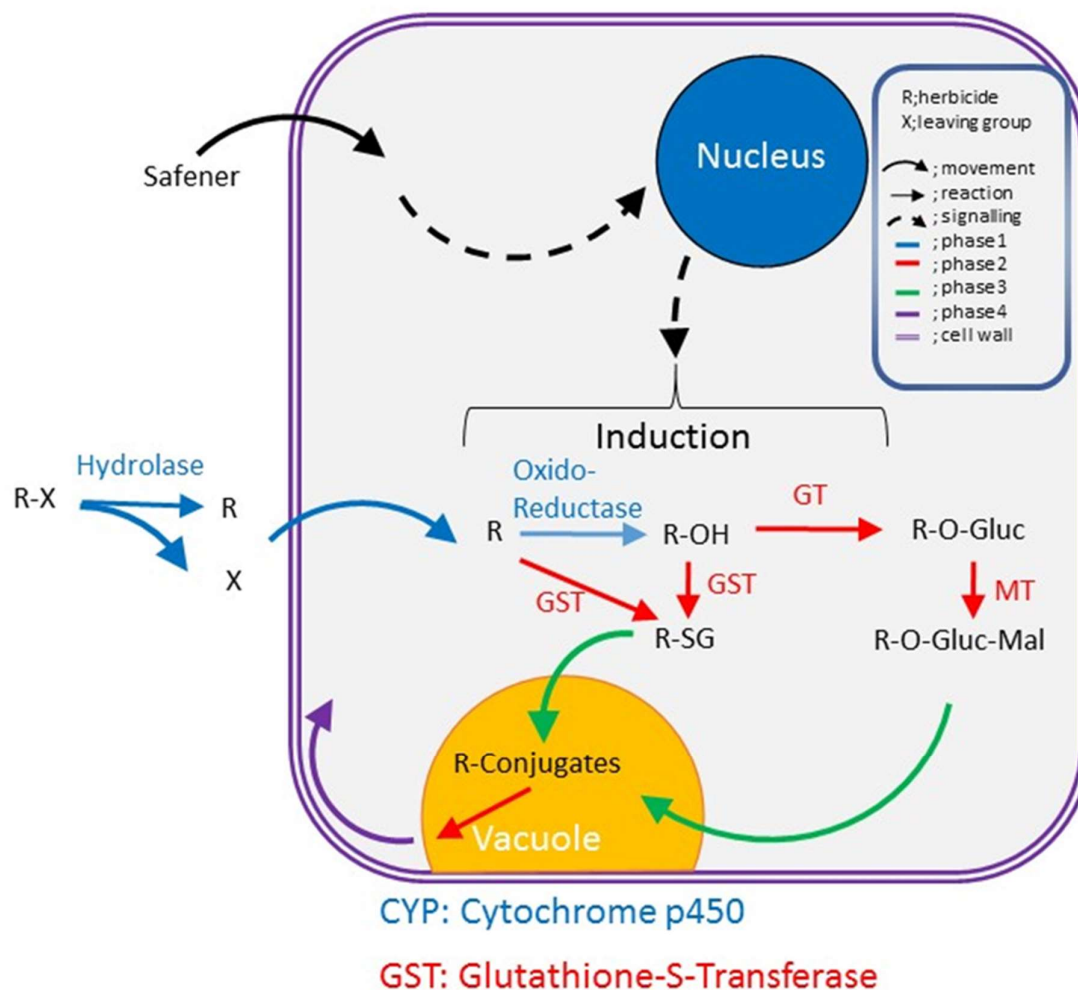


Figure 4: Diagram showing the xenome (the biosystem responsible for the detection, transport and detoxification of xenobiotics).

The route of a xenobiotic molecule through a typical plant cell is shown, along with the basic Safener signalling pathway. Legend (top right) explains reactions and structures. Figure is based on a figure from Edwards et al. (2011).

1.6.1 Phase I

1.6.1.1 Hydrolysis

In phase I metabolism, xenobiotics may undergo hydrolysis in the apoplast by hydrolase enzymes, which increase the bio-activity and/or mobility of the xenobiotics, allowing them to pass into the cell and exposing them to further processing. In the case of herbicides, this is often described as the activation of a 'pro-herbicide' into the 'active herbicide' (Edwards et al., 2011). These hydrolytic enzymes can be divided into two families, carboxylesterases and

amidases, with the former split further into subfamily I, II and III carboxylesterases (Cummins et al., 2001; Leah et al., 1994). Each hydrolase acts upon a specific chemical group, for instance, esterases act upon ester bonds, and amidases act upon amide bonds. The role of hydrolases in xenobiotic bio-activation have often been demonstrated *in planta*, and have been suggested as one mechanism determining herbicide selectivity (Edwards et al., 2011; Reinemer et al., 1996; Riechers et al., 2010).

1.6.1.2 *Oxidation/reduction*

Herbicides may also be exposed to oxido-reductase enzymes, which introduce reactive functional groups suitable for further metabolic phases. The majority of these reactions involve oxidation, dealkylation, hydroxylation, isomerisation, desaturation, demethylation, dehalogenation, epoxidation, or sulfoxidation, which are often catalysed by cytochrome P450-dependent mono-oxygenases (CYPs), membrane associated haemoproteins (Guengerich, 2001). CYPs are often considered the most important enzymes involved in this phase of xenobiotic detoxification, as these enzymes can metabolise diverse classes of herbicides. CYPs are also implicated as important factors in crop selectivity. Besides CYPs, peroxidases which catalyse oxidative reactions using hydrogen peroxide, are also implicated in phase I xenobiotic metabolism. Alternatively, the xenobiotic may be sufficiently reactive to directly undergo phase II metabolism (Davies et al., 1999; Edwards et al., 2011; Riechers et al., 2010).

1.6.2 *Phase II*

During phase II metabolism, phase I metabolites undergo conjugation reactions with endogenous substrates, such as glucose, amino acids or glutathione, through catalysis by a range of enzymes (Davies et al., 1999; Edwards et al., 2011). In general, metabolites of phase II conjugation have low or no herbicidal activity (Carvalho et al., 2009; Van Eerd et al., 2003).

1.6.2.1 *Glutathione conjugation*

Glutathione (GSH), the major cellular thiol, is a tripeptide of glutamic acid, cysteine and glycine, widely distributed in plant tissues, endogenously functioning in protecting cells from oxidative stress (Davies et al., 1999; Riechers et al., 2010). During xenobiotic metabolism, this tripeptide may be directly conjugated to a herbicide or to phase I generated metabolites, by glutathione-S-transferase (GST) enzymes (Davies et al., 1999). These enzymes have displayed diverse subcellular localisations, but are most commonly cytosolic (soluble) or microsomal proteins, though microsomal GSTs have not been implicated in xenobiotic detoxification (Davies et al., 1999; Edwards et al., 2011; Riechers et al., 2010). GSH is activated in the active site of GSTs to

form a highly nucleophilic thiolate anion, which is in turn conjugated to the electrophilic site of a lipophilic xenobiotic, through addition or substitution reactions (Edwards et al., 2011; Riechers et al., 2010). In some cases the substitution reactions can significantly reduce the toxicity and increase the polarity of xenobiotics, thus effectively detoxifying the xenobiotic before subsequent phases (Edwards et al., 2011). In many cases crop tolerance to some of the major herbicide classes, including chloroacetanilides, chlorotriazines, diphenylethers and aryloxyphenoxypropionates, may be due to rapid GST-mediated detoxification, implicating GST specificity as a mechanism for selectivity (Edwards et al., 2011). Quite understandably, the availability of GSH plays an important role in GST-mediated detoxification. A high level of GSH can increase enzymatic, and also spontaneous conjugation, while a low level of GSH can hinder metabolism, especially when the plant is exposed to large quantities of, or highly reactive, xenobiotics (Brazier-Hicks et al., 2008; Edwards et al., 2011).

1.6.2.2 *Glucose Conjugation*

Some herbicides or phase I metabolites are conjugated with glucose, a reaction catalysed by glucosyl/glycosyl transferases (GTs), producing the corresponding O- or N- glucosides or glucose esters (Davies et al., 1999; Edwards et al., 2011; Riechers et al., 2010). Herbicide substrates of GTs include phenylcarbamates, phenylureas, sulfonylureas and imidazolinones (Davies et al., 1999). The GTs can be categorised into different groups, based upon their function and glucose donors (Edwards et al., 2011). The GT group most commonly observed catalysing xenobiotic conjugation is the UDP-glucosyltransferase (UGT) class (Pflugmacher et al., 1998). These enzymes utilise uridine diphosphate glucose (UDPG) as the glucosyl donor (Davies et al., 1999; Edwards et al., 2011). This class comprises a large multigene family and has been reported to glycosylate xenobiotics throughout the plant kingdom (Edwards et al., 2011; Riechers et al., 2010).

1.6.2.3 *Malonic acid Conjugation*

Xenobiotics may also be conjugated to malonic acid through the catalytic action of specific malonyltransferases (MTs), using malonyl CoA as the donor species (Cole et al., 2000; Davies et al., 1999; Edwards et al., 2011). Target groups for malonylation include the amino groups of anilines, S-cysteinyllated conjugates, and the 6'-O position of glucose conjugates (Edwards et al., 2011).

1.6.3 *Phase III*

During phase III metabolism, phase II conjugates are specifically imported into the vacuole by ATP-dependent transport proteins (Edwards et al., 2011). The compartmentalisation of tagged xenobiotics within the vacuole may function to protect GSH-dependent enzymes from product inhibition, or to avoid reactivation of the metabolites by catabolism of phase II conjugates (Riechers et al., 2010). Glutathione and glucose tagged herbicides are recognised and transported into the vacuole by ATP-binding cassette (ABC) transporter proteins (Edwards et al., 2011; Riechers et al., 2010). These proteins use magnesium-adenosine-trisphosphate (MgATP) to actively drive transport (Edwards et al., 2011; Rea, 2007). The large ABC transporter family is arranged into 13 subfamilies based on size, orientation, structure and sequence. Many studies have reported that glutathionylated xenobiotics are transported into the vacuoles by the ABC subfamily C (Edwards et al., 2011; Klein et al., 2006; Leier I, 1994). As is common with xenobiotic detoxifying enzymes, the ABC proteins possess intrinsic roles in plant secondary metabolism, and have evolved additional functions in xenobiotic processing (Edwards et al., 2011). Glucose conjugates may also be sequestered in the vacuole by virtue of electrochemical potential gradients caused by vacuolar enzymes, H⁺-ATPase (V-ATPase) and H⁺-pyrophosphatase (Bartholomew et al., 2002; Riechers et al., 2010). Subsequent hydrolysis of the phase II tags, catalysed by specific enzymes within the vacuole, effectively recycles them for reuse (Edwards et al., 2011). Alternatively phase II metabolites may be further conjugated into insoluble residues, which are sequestered in the vacuole or bound in lignin polymers, thereby removing the xenobiotic from the cytosol (Davies et al., 1999).

1.6.4 *Phase IV*

Following vacuolar sequestration, the xenobiotics are either retained in the vacuole, where they may be further metabolised, or they are exported and incorporated into cell wall components or bound residues, rendering them insoluble and inactive (Edwards et al., 2011; Lamoureux, 1993). Glutathione conjugated xenobiotics are processed by vacuolar enzymes such as carboxypeptidases and γ -glutamyl transpeptidases, producing the equivalent cysteine conjugates (Riechers et al., 2010). These cysteine conjugates are further processed, either by conjugation to malonate, or by cysteine conjugate β -lyase and S-methyltransferase catalysis, producing S-methyl derivatives (Brazier-Hicks et al., 2008; Riechers et al., 2010). It has also been demonstrated that cysteine conjugates may be formed via a cytosolic processing pathway, by the enzyme phytochelatase, and some studies proposed that glutathione

conjugate degradation occurs in several compartments through several routes, using this enzyme (Blum et al., 2007; Brazier-Hicks et al., 2008)(Edwards et al., 2011; Riechers et al., 2010). The routes through which S-glutathionylated xenobiotics are further metabolised is thought to be dependent on cell type and relative conjugate availability (Edwards et al., 2011). Similarly, it has been demonstrated that the order of reactions in xenobiotic metabolism may be species or substrate specific (Edwards et al., 2011).

Since xenobiotics are rarely secreted or mineralised in plants, their fate is often long term storage in a form less toxic than the parent molecule (Edwards et al., 2011). This may be via vacuolar compartmentalisation of soluble polar residues as previously discussed; or alternatively during phase IV, intermediates of further processing may be incorporated into natural products such as cell wall-bound polysaccharides or polyphenolics, lignin, lipids, or proteins, thereby rendering them inactive (Edwards et al., 2011).

1.6.5 *Xenobiotic metabolism vs secondary metabolism*

Each of the enzymes discussed, also serve functions in the regulation of plant secondary metabolites, plant synthesised compounds not involved in growth, development or reproduction. Hydrolases are involved in the hydrolysis of a wide range of secondary metabolites, including glucosynolate precursors (Minic, 2008). CYPs are involved in biosynthesis of a range of secondary metabolites, including isoflavanoids, and alkaloids (Mizutani et al., 2011). Similarly, peroxidases have been implicated in the biosynthesis of alkaloids (Sottomayor et al., 2008). GSTs have been shown to be involved in the synthesis of volatiles and glucosinolates, as well as the conjugation of oxylipids, phenolics and flavonoids (Dixon et al., 2010b). Glycosylation by glycosyltransferases, is important for the synthesis and regulation of many secondary metabolites, including flavonoids and glucosinolates (Gachon et al., 2005). ABC transporters have been shown to be involved in the vacuolar uptake of secondary metabolites including flavone glucuronides (Klein et al., 2000). Considering these enzymes are not exclusively involved in foreign compound metabolism, it is possible that their role in xenobiotic metabolism may be an evolution of their own secondary metabolism system. This is supported by the large size of plant xenomes, when compared to animals, and the electrophilicity of most xenobiotics and secondary metabolites (Coleman et al., 1997; Edwards et al., 2011).

In summary, the xenome describes the major pathways for xenobiotic metabolism in plants, and has demonstrated a role in determining herbicide selectivity through the use of large, diverse gene families and similarly diverse pathways.

1.7 Herbicide metabolism

Each herbicide class is metabolised in plants through different pathways of the xenome. As such the pathways involved in detoxifying the major classes of herbicide will be discussed here. Table 2 describes the known metabolic systems of specific herbicides with respect to oxidative or glutathione conjugation-based detoxification.

The chloroacetanilide herbicides are detoxified in crops by conjugation with glutathione, resulting in non-phytotoxic conjugates (Fuerst, 1987; Riechers et al., 2010). This occurs non-enzymatically as well as via catalysis with GSTs (Fuerst, 1987). Some oxidation-based metabolism has also been shown. For example, *S*-metolachlor has two pathways of metabolism in maize, through the action of GSTs or CYPs (Ohkawa et al., 1999 ; Syngenta personal comm). Thiocarbamates, such as *S*-ethyl dipropylcarbamothioate (EPTC), are also detoxified by conjugation with glutathione (Fuerst, 1987; Riechers et al., 2010), after oxidation to the respective sulfoxide, via catalysis by peroxidases or oxidases, in maize (Carringer et al., 1978; Fuerst, 1987). Further metabolism leads to malonylcysteine conjugates or malonyl-3-thiolactic acid conjugates in the case of thiocarbamates (Fuerst, 1987). Thiocarbamates may also be hydrolysed completely to their respective elements (Hatzios et al., 1982). Many of the sulfonylurea herbicides are detoxified by hydrolytic reactions of phase I, while some are subject to glutathione-mediated detoxification (Hatzios et al., 2004). In fact, chlorimuron-ethyl is metabolised by both aryl-hydroxylation and glutathionylation in maize (Hatzios et al., 2004; Lamoureux et al., 1991; Siminszky, 2006). Chloro-*S*-triazines, such as atrazine, have been metabolised by glutathione-dependent detoxification (Hatzios et al., 2004; Hatzios et al., 1982), but have also been metabolised by *N*-dealkylation, in maize (Hatzios et al., 1982; Ohkawa et al., 1999). Aryloxyphenoxypropionate herbicides such as fenoxaprop-ethyl, diphenylethers such as flurodifen, and sulphonamides, such as cloransulam-methyl have been metabolised by glutathione-dependent detoxification in crops including maize (Hatzios et al., 2004; Romano et al., 1993). Triketones, are detoxified by oxidation only, including mesotrione in maize (Alferness et al., 2002 ; Syngenta personal comm).

Herbicide (type)	Herbicide	Oxidative	Glutathione conjugated
Chloroacetanilide	Alachlor	<i>Vr</i> ^a	
	Acetachlor	<i>Sb, Zm</i> ^a	
	Metolachlor	<i>Vr</i> ^a <i>Unk</i> ^b <i>Zm</i> ^[pc]	<i>Zm</i> ^{c[pc]}
	Dimethenamid		<i>Ta</i> ^e
	Metazachlor		
Aryloxyphenoxypropanoate	Diclofop	<i>Ta</i> ^a <i>Unk</i> ^b	<i>Unk</i> ^b
	Fenoxaprop-ethyl		<i>Unk</i> ^b <i>Ta, Hv</i> ^l
Imidazolinone	Imazapic	<i>Zm</i> ^a	
	Imazethapyr	<i>Zm</i> ^a	
Phenoxyalkanoic acid	2-4D	<i>Tsp.</i> ^a <i>Unk</i> ^b	
Phenylurea		<i>Ht, Gm, Nsp., Ta, Zm</i> ^a	
	Chlortoluron	<i>Unk</i> ^b <i>Ta</i> ^c	
	Diuron	<i>Gm</i> ^a	
	Fluometuron	<i>Gsp., Gm</i> ^a	
	Isoproturon	<i>Gsp., Ta</i> ^a	
	Linuron	<i>Ta, Gm, Ht</i> ^a	
Sulfonamide	Flumetsulam	<i>Zm</i> ^a <i>Unk</i> ^b	
	Cloransulam-methyl		<i>Unk</i> ^b
Sulfonylurea	Bensulfuronmethyl	<i>Ta</i> ^a	
	Chlorimuron-ethyl	<i>Zm</i> ^a	<i>Zm</i> ^h
	Chlorsulfuron	<i>Ta</i> ^a	
	Metsulfuronmethyl	<i>Ta</i> ^a	
	Nicosulfuron	<i>Zm</i> ^a	
	Primisulfuron	<i>Ev, Zm</i> ^a	
	Prosulfuron	<i>Zm, Sb, Ta</i> ^a	
	Rimsulfuron	<i>Zm</i> ^a	
	Triasulfuron	<i>Zm, Ta</i> ^a	
	Tribenuronmethyl	<i>Ta</i> ^a	
	Triflurosulfuron-methyl		<i>Bv</i> ⁱ
	Thifensulfuron-methyl		<i>Unk</i> ^b
Chloro-S-triazines	Atrazine	<i>Zm</i> ^c	<i>Unk</i> ^{bf} <i>Zm</i> ^c
Triazinone sulfoxides			<i>Unk</i> ^b
Diphenylethers	Fluorodifen		<i>Unk</i> ^b <i>Zm</i> ^k
Thiocarbamates/thiolcarbamates	EPTC	<i>Zm</i> ^g	<i>Zm</i> ^g
Triketone	Mesotrione	<i>At</i> ^d <i>Zm</i> ^[pc]	
	Tembotrione	<i>At</i> ^d	
Pyrazolone	Topramezone	<i>At</i> ^d	
Unclassified	Bentazon	<i>Zm, Ev, Sb, Vr, Ta</i> ^a <i>Unk</i> ^b	
	Clomazone	<i>Zm</i> ^a	

Table 2: The metabolic pathways of herbicide detoxification.

Superscripts denote sources: *a*; Siminszky, 2006 , *b*; Hatzios et al., 2004 , *c*; Ohkawa et al., 1999 , *d*; Oliveira et al., 2018 , *e*; Dixon et al., 1998b , *f*; Hatzios et al., 1982 , *g*; Carringer et al., 1978 , *h*; Lamoureux et al., 1991 , *i*; Wittenbach et al., 1994 , *j*; Romano et al., 1993 , *k*; Dixon et al., 1997 , *l*; Alferness et al., 2002 , *[pc]* personal communication. *Unk*; unknown crop, *Vr*; *Vigna radiate* (mung bean), *Zm*; *Zea mays* (maize), *Tsp.*; *Tulipa sp.* (tulip), *Ht*; *Helianthus tuberosus* (jerusalem artichoke), *Gsp.*; *Gossypium sp.* (cotton), *Ta*; *Triticum aestivum* (wheat), *Nsp.*; *Nicotinia sp.* (tobacco), *Gm*; *Glycine max* (soybean), *Sb*; *Sorghum bicolor* (sorghum), *Ev*; *Eriochloa villosa* (woolly cupgrass), *At*; *Amaranthus tuberculatus* (waterhemp), *Bv*; *Beta vulgaris* (sugar beet), *Hv*; *Hordeum vulgare* (barley).

1.8 Herbicide safeners

Even though various herbicidal MoA are used in rotation to control grass weeds, herbicide efficacy has been significantly declining for decades due to the development of herbicide resistant weeds. In the United States, correctly applied herbicides still leave 12% losses of potential crop yield due to weeds (Pimentel, 1997). In addition, herbicides may reduce crop yields themselves by inhibiting crop growth through a lack of selectivity, as mentioned in section 1.3 (Abrol et al., 2014). In this case, selectivity must be artificially augmented, the most effective method being the use of herbicide safeners.

Herbicide safeners are a group of agrochemicals that protect monocotyledonous crops against injury from herbicides without reducing chemical control in target weed species, thus improving selectivity (Cataneo et al., 2013; Matola et al., 2007; Scarponi et al., 2009a; Scarponi et al., 2009b; Scarponi et al., 2006). It has been widely acknowledged that the reduction of herbicide injury in crop plants by safeners is caused by an enhancement in herbicide metabolism/detoxification, as discussed in section 1.11 (Cataneo et al., 2013). Safeners upregulate components of the xenome, including CYPs, GTs, and GSTs (Del Buono et al., 2007; Edwards et al., 2011; Scarponi et al., 2009a; Scarponi et al., 2009b; Scarponi et al., 2006). The majority of herbicide safeners are active in cereal crops, such as maize, wheat, rice and sorghum, however a few studies indicate that some non-crop species may also be responsive to safeners (Scarponi et al., 2009a; Scarponi et al., 2009b; Scarponi et al., 2006). Herbicide safeners are normally applied either through seed treatment, or addition to sprayed tank mixes, formulated with herbicides (Cataneo et al., 2013; Scarponi et al., 2009b).

The ability of safeners to protect crops from herbicides, thereby enhancing selectivity between crop and weed, affords them many potential applications. These applications include; 1. The use of higher herbicide doses to achieve more effective weed control, 2. Providing greater flexibility in crop choice in crop rotation systems, and to address the problem of 'volunteer' crops from previous rotations, 3. Affording the possibility of providing weed control options for minor crops, which are not generally targeted for development of new herbicide compounds because of their small market value, 4. Using herbicides under environmental conditions likely to cause some crop damage, 5. Extending the usage patterns of commercial herbicides, and 6. Developing molecules with desirable toxicological profiles, despite showing poor selectivity (Davies et al., 1999). Many herbicide safeners are now

commercially available, with 30% of all herbicide sales in 2011 associated with products containing a safener (Scarponi et al., 2006; Sivey et al., 2015).

1.9 Safener history

Safeners were conceptually discovered in 1947, and since then over twenty safeners have been developed and commercialised. The timeline of safener development and commercialisation, from discovery to the early 21st century, is shown in Figure 5.

The first example of the safening effect was discovered accidentally by Otto Hoffmann, finding that the chemical 2,4,6-trichlorophenoxyacetic acid protected tomato (*Solanum lycopersicum*) plants from 2,4-dichlorophenoxyacetic acid (2,4-D) injury (Davies et al., 1999; Hoffmann, 1953, 1977; Kraehmer et al., 2014). While this compound proved too ineffective for commercialisation, it prompted a search for other chemicals displaying this phenomenon, and in 1971 the Gulf Oil company patented 1,8-Naphthalic anhydride (1,8-NA), a safener developed as a seed treatment for the protection of maize from thiocarbamate herbicide injury (Davies et al., 1999; Hoffman, 1969; Kraehmer et al., 2014; Stephenson et al., 1991). A competitor company, Stauffer Chemicals, quickly developed their own safener, dichlormid, affording similar protection, which by virtue of its greater selectivity and direct application with the herbicides instead of seed treatment, outcompeted 1,8-NA (Pallos et al., 1972)(Davies et al., 1999; Stephenson et al., 1991). While seed treatments have the benefit of affording a spatial selectivity, providing no protection to the weeds, pre-emergence sprayed safeners have the benefit of simplified agricultural practice, and control over the products used (Jablonkai, 2013; Kraehmer et al., 2014). However, due to the need for greater selectivity with pre-emergence sprayed safeners, seed treatments are sometimes necessary, especially when the weed is related to the crop, such is the case with rice (*Oryza sativa*) and competing wild rice weeds (*Oryza sp.*) (Kraehmer et al., 2014). Research into finding new safeners proceeded intensively during the 1970's, focusing mainly on seed treatment and other sprayed pre-emergence safeners (Jablonkai, 2013; Kraehmer et al., 2014). Notably, these safeners were targeted towards cereals and herbicides of the chloroacetanilide and thiocarbamate class (Davies et al., 1999). The oxime-ether safeners, cyometrinil, oxabetrinil and fluxofenim, were developed by Ciba-Geigy (now Syngenta) as seed treatments for chloroacetanilide and thiocarbamate herbicides in sorghum (*Sorghum bicolor*) (Davies et al., 1999; Kramer et al., 2007). The pre-emergence safener, benoxacor was developed by Ciba-Geigy (now Syngenta) for maize protection from chloroacetanilide herbicides (Kramer et al., 2007). Fenclorim and flurazole

were developed as seed treatments for rice and sorghum, respectively, for protection from chloroacetanilides (Jablonkai, 2013; Kramer et al., 2007; Stephenson et al., 1991).

In the late 1980's, leaf active safeners were discovered, allowing for protection of post-emergence herbicides. These included fenchlorazole-ethyl, and cloquintocet-mexyl, developed for protection of cereals from arloxyphenoxypropionate herbicides (Kraehmer et al., 2014; Kramer et al., 2007). Post-emergence safeners, including mefenpyr-diethyl and isoxadifen-ethyl, were also developed to protect cereals from ACCase inhibitor and sulfonylurea herbicide classes (Kramer et al., 2007).

The rate of safener development peaked in the late 1980's and has since decreased, such that, until the recent development of metcamifen, no new safener had been commercialised for approximately a decade (Figure 5). This is, in part, because the molecular mechanisms of safeners are so poorly understood. Furthermore, the discovery of new chemistries is largely based on trial and error, using old chemistries as the basis for derivatisation. The high costs and time associated with satisfying the ever increasing demands of regulatory authorities, as discussed in section 1.13, also contributes to the reduced rate of development. Of the wide range of safeners developed, only seven are currently used in agricultural practice, as many chemistries have been removed or superseded. Table 3 lists the herbicide products containing safeners, currently commercialised by major agricultural companies, as of 2018.

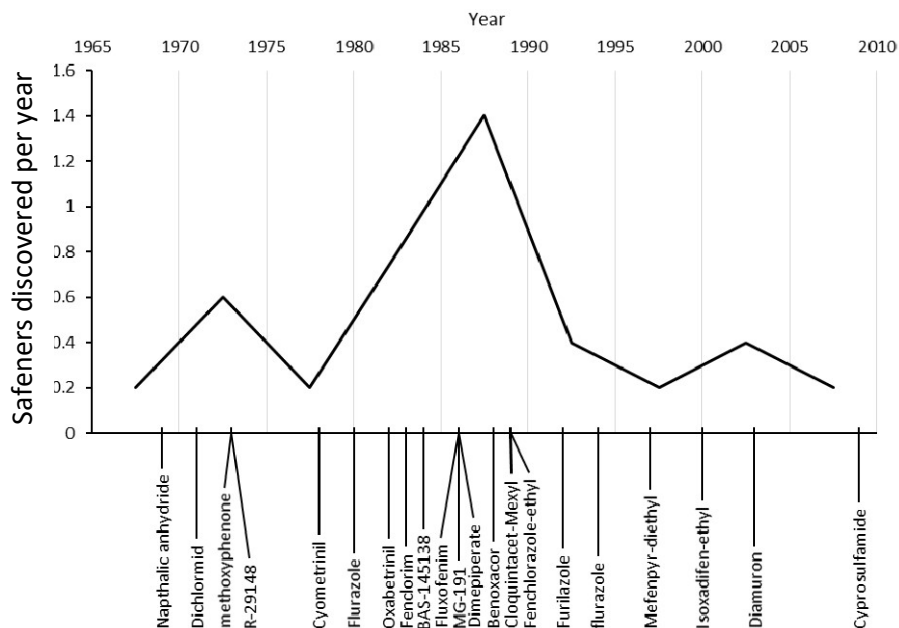


Figure 5: Graph showing the history of safener development from 1969 to 2009.

A timeline of safener year of development is shown with the average rate of safener development per year (in 5 year intervals) displayed in a connected scatter graph. Data extracted from Jugulam (2017); Lewis et al. (2016); Ota (2013), and plotted using Excel.

Company	Safener	Product	Herbicide
Syngenta	Benoxacor	Acuron	Atrazine
			S-Metolachlor
			Mesotrione
			Bicyclopyrone
		Dual	S-Metolachlor
		Bicep	Atrazine
			S-Metolachlor
		Lumax	Atrazine
			S-Metolachlor
			Mesotrione
		Lexar ex	Atrazine
			S-Metolachlor
			Mesotrione
Bayer	Isoxadifen-ethyl	Capreno	Thiencarbazone-methyl
			Tembotrione
		Laudis	Tembotrione
		Ricestar	Fenoxaprop-P-ethyl
	Cyprosulfamide	Corvus	Thiencarbazone-methyl
			Isoxaflutole
		Diflexx	Dicamba
		Balance	Isoxaflutole
	Mefenpyr-diethyl	Huskie	Pyrasulfotole
			Bromoxynil Octanoate
			Bromoxynil Heptanoate
		Osprey	Mesosulfuron-Methyl
		Rimfire	Propoxycarbazone-sodium
		Varro	Thiencarbazone-methyl
		Atlantis	Iodosulfuron-methyl-sodium
			Mesosulfuron-methyl
Monsanto	Furilazole	Harness	Acetochlor
Dupont	Isoxadifen-ethyl	Realm	Rimsulfuron
			Mesotrione
		Resolve	Rimsulfuron
			Thifensulfuron-methyl
Dow Agrosiences	Furilazole	Surpass	Acetochlor
	Dichlormid	Topnotch	Acetochlor

Table 3: Commercial products containing safeners.

Data taken from websites of the relevant company as of 2018. Products are registered trademarks and simplified names are given.

1.10 Safener chemistry

The safeners, summarised in Table 4, comprise diverse chemical classes and have various applications, protecting different crops from specific herbicides at certain times. Here the commercially verified herbicide and crop targets will be discussed, along with their applications.

As mentioned, a large number of safeners have been developed to protect maize from a variety of herbicide classes. 1,8-naphthalic anhydride (1,8-NA), is the only member of the anhydride safener class, and is used in seed treatment to protect maize from thiocarbamate herbicides (Kramer et al., 2007). The dichloroacetanilide safeners, including dichlormid, furilazole and AD-67, are generally used pre-emergence in maize against chloroacetanilide herbicides. The arylsulfonyl–benzamide, cyprosulfamide, is used post-emergence to protect maize from HPPD inhibitor and ALS inhibitor herbicides (Kramer et al., 2007). MG-191, the only member of the dichloromethyl-ketal class of safeners, was developed to protect maize from thiocarbamate and chloroacetanilide herbicides (Jablonkai et al., 1995). Dicyclonon is an obsolete safener used to protect maize from a variety of herbicides (Lewis et al., 2016). Benoxacor (4-(dichloroacetyl)-3,4-dihydro-3-methyl-2H-1,4-benzoxazine) is a dichloroacetamide safener, developed by Ciba-Geigy (now Syngenta) to be used in conjunction with the herbicide metolachlor, in pre-emergence or pre-plant products for use in maize (Cottingham et al., 1991; Kramer et al., 2007). Metcamifen (2-methoxy-N-[[4-[[[(methylamino)carbonyl]amino]phenyl]sulfonyl] benzamide) is a new safener, of the aronyl-sulfonamide class, developed by Syngenta. It was released in 2016 under the name Epivio™ C as a seed treatment, and has displayed protection of maize from mesotrione and other HPPD inhibitors (Syngenta personal comm). It has also shown effective safening against ACCase inhibitors, VLCFA synthesis inhibitors, auxins and ALS inhibitors (Syngenta personal comm.).

In addition to these, a number of safeners have been developed for other cereal crops, which will be briefly discussed. Mefenpyr-diethyl was used in the post-emergence protection of cereals from ACCase inhibitors and sulfonylurea herbicides (Kramer et al., 2007). The 8–Quinolinoxy–carboxylic ester, cloquintocet-mexyl, and the 1,2,4–Triazole–carboxylate, fenclorazole-ethyl, are both used for post-emergence protection of cereals from clodinafop-propargyl and fenoxaprop-ethyl, respectively (Kramer et al., 2007). The oxime-ether safeners, cyometrinil, fluxofenim and oxabetrinil, are used as seed treatment to protect sorghum from thiocarbamate or chloroacetanilide herbicides (Kramer et al., 2007). Flurazole is a thiazole carboxylic acid used in a similar manner (Kramer et al., 2007). The rice safeners contain the phenyl–pyrimidine, fenclorim, the urea, diamuron, the alkylbenzene, cumyluron, and the piperidine–1–carbothioate, dimepiperate. Apart from fenclorim, safeners in this group are used post-emergence to protect against sulfonylureas. In contrast, fenclorim is used pre-emergence to protect rice against the chloroacetanilide, pretilachlor (Kramer et al., 2007). The

dihydroisoxazole–carboxylate, isoxadifen ethyl, is used post-emergence to protect rice and maize against ACCase inhibitors and sulfonylureas (Kramer et al., 2007). A number of unclassified safeners are shown in Table 4, with little information on their herbicide partners.

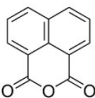
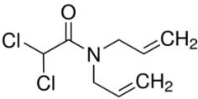
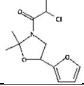
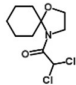
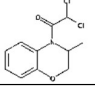
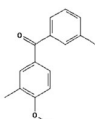
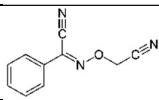
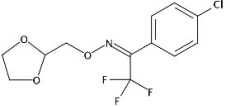
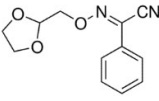
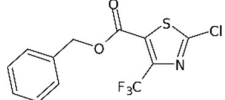
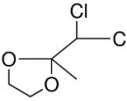
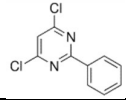
Chemical class	Safener	Pubchem reference	Structure
Anhydride	1-8 naphthalic anhydride	6693	
	Dichlormid	37829	
	Furilazole	86187	
Dichloroacetamide/ Dichloroacetanilide	AD-67	3482402	
	Benoxacor	62306	
	Dicyclonon	115203	
Oxime ether	Cyometrinil	9576090	
	Fluxofenim	91747	
	Oxabetrinil	5484132	
Thiazole carboxylic acid	Flurazole	91715	
Dichloromethyl-ketal	MG-191	115289	
Phenyl–pyrimidine	Fencloirim	77338	

Table 4: Safener classification.

Safener chemical class, pubchem reference ID, and structure are shown. Classification from Jablonkai (2013), Hatzios et al. (2004), Kramer et al. (2007), or pubchem database.

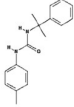
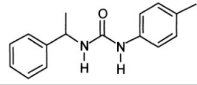

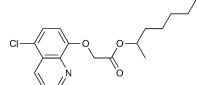
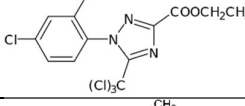
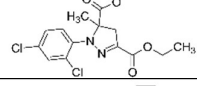
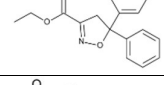
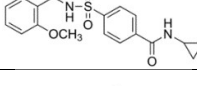
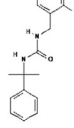
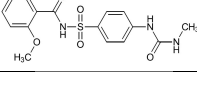
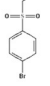
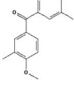
Chemical class	Safener	Pubchem reference	Structure
Urea	Dymron/ Diamuron	39238	
	S-PEU	19165564	
Piperidine-1-carbothioate	Dimepiperate	91679	
8-Quinolinoxy-carboxylic esters	Cloquintocet-mexyl	93528	
1,2,4-Triazole-carboxylate	Fenchlorazole-ethyl	3033865	
Dihydropyrazole-dicarboxylate	Mefenpyr-diethyl	10937610	
Dihydroisoxazole-carboxylate	Isoxadifen ethyl	6451155	
Arylsulfonyl-benzamide	Cyprosulfamide	11707647	
Alkylbenzene	Cumyluron	11709249	
Aronyl-sulfonamide	Metcamifen	11559601	
Unclassified	BCS	40989	
	Methoxyphenone	38839	

Table 4: (Continued).

While these safeners have been used in agricultural practice with specific crop and herbicide partners, many studies have indicated they may have more targets. Based on available information, safeners likely work on a diverse range of herbicide chemistries, in a variety of crops, as described in Table 5. Few trends can be seen between safener and herbicide classes, with respect to agonistic effects, though the research is far from comprehensive. Further research is certainly needed to identify the exact safener-herbicide-crop combinations that result in protection. This table was compiled to highlight the lack of understanding present in this system, and to encourage a process of comprehensive safener-target review. It also aims to be a guide for safener research, with respect to specific studies.

Herbicide (type)	Herbicide	1-8 naphthalic anhydride	Dichlormid	Furilazole	AD-67	Benoxacor	Dicyclonon	Cyometrinil	Fluxofenim	Oxabtrinil	Flurazole	MG-191	Fencloirim	Fymron/ diamuron	S-PEU	Dimepiperate	Cloquintocet- mexyl	Fenclorazole -ethyl	Mefenpyr- diethyl	Isoxadifen ethyl	Cypro- sulfamide	Cumyluron	BCS	Metamifen
Chloroacetanilide	General*	Zm ^a	Zm ^{abcd}			Zm ^d	Zm ^a	N/A ^c , Sb ^d O ^s	Sb ^d O ^s	Sb ^d O ^s	Sb ^{ad} O ^s	Zm ^b	O ^s Sb ^f	Sb ^f	Sb ^f	Sb ^f								Sb ^f
	alachlor										Sb ^{be} N/A ^c													
	acetachlor			Zm ^{bd}	Zm ^{bd}																			Zm, O ^s [pc]
	butachlor																							Zm, O ^s [pc]
	metolachlor					Zm ^{bce}		Sb ^{be}	Sb ^{bce}	Sb ^{bce}	N/A ^c													
	pretilachlor												O ^s bde, N/A ^c	O ^s b										
Aryloxyphenoxy- propanoate	General*	Hv ^a															Ta ^f Hv ^a	Ta ^{af} ,As ^a	Ta ^f					
	Fenoxaprop- ethyl/fenoxaprop- p-ethyl																	Ta ^{ae} C ^b dg	Ta,Sc,x T,Hv ^e C ^c _g					Zm,C,O s,So[pc]
	Clodinafop propargyl																	Ta ^e C ^b gd			Zm ^h			Zm[pc] ^h , C,O ^s ,So [pc]O ^s ^h
Imidazolinone	General*	Zm ^a																						
	Imazethapyr																							Zm,C,O s,So[pc]
Sulfonylurea	General*	Zm,Sb ^a	Zm,Sb ^a					O ^s	O ^s	O ^s	O ^s			O ^s		O ^s ^{abd}	Ta ^f	Ta ^f	Ta ^{af} ,Sc, xT, Hv ^b ,C ^d	Zm,O ^s _d			O ^s	
	Nicosulfuron																							Zm,C,O s,So[pc]
	Pyrazosulfuron- ethyl													O ^s _b										
	halosulfuron- methyl			C ^c ,Zm ^b																				

Table 5: Known safener agonism of herbicides determined through survey of literature.

Superscripts denote sources: *a*; Hatzios, 1991 , *b*; Jablonkai, 2013 , *c*; Lewis et al., 2016 , *d*; Kramer et al., 2007 , *e*; Davies et al., 1999 , *f*; Hatzios et al., 2004 , *g*; Kraehmer et al., 2014 , *h*; Brazier-Hicks et al. , *i*; Dutka et al., 1987 , [*pc*]; personal communication. * denotes cases where only the herbicide class was mentioned. Zm; *Zea mays* (maize), Sb; *Sorghum bicolor* (sorghum), Sc; *Secale cereale* (rye), Ta; *Triticum aestivum* (wheat), Os; *Oryza sativa* (rice), C; Cereals, Hv; *Hordeum vulgare* (barley), xT; x-*Triticosecale* (triticale), So; *Saccharum officinarum* (sugarcane), As; *Avena sativa* (oat), N/A; no crop mentioned. Chemistries with no agonistic effects were excluded from the table.

Herbicide (type)	Herbicide	1-8 naphthalic anhydride	Dichlorimid	Furilazole	AD-67	Benoxacor	Dicyclonon	Cyometrinil	Fluxofenim	Oxabetrinil	Flurazole	MG-191	Fencloirim	Dymron/ diamuron	S-PEU	Dimepiperate	Cloquintocet- mexyl	Fenchlorazole -ethyl	Mefenpyr- diethyl	Isoxadifen ethyl	Cypro- sulfamide	Cumyluron	BCS	Metcamifen
Sulfonylurea	iodosulfuron																		C ^c					
	foramsulfuron																			N/A ^c				
Diphenylethers	fomesafen																							Zm, Os, So ^[pc]
Thiocarbamates/ thiolcarbamates/ (sulfoxided)	General*	Ta, Os ^a , Zm ^{abd}	Ta, Os ^a , Zm ^{abcd}					Sb ^d	Sb ^d	Sb ^d		Zm ^{ebi}												Zm, Ta, Os ^a
	EPTC	Zm ^e	Zm ^e																					
	butylate	Zm ^e	Zm ^e																					
	vernolate	Zm ^e	Zm ^e																					
HPPDinhibitors	General*																				Zm ^{dg}			
	mesotrione																							Zm, C, O s, So ^[pc]
	Tembotrione																			N/A ^c				
	topramezone																							Zm, C, O s, So ^[pc]
	isoxaflutole																				Zm ^b			
Isoxazolidinones	General*	Zm, Ta ^a	Zm, Ta ^a																					
Cyclohexanediones	General*	Zm, Sb ^a	Zm, Sb ^a																					
Accase inhibitors	General*																		Ta, Sc, xT, Hv ^b , C ^d	Zm, Os ^{bdg}				
phenoxy-carboxylicacids	2,4-D																							Zm, Os ^[pc]
quinolinecarboxylic acids	quinclorac																							Zm, Os ^[pc]
Pyrimidinyl (thio) benzoates	bispyribac-sodium																							Zm, C, Os, So ^[pc]
	pyribenzoxim																							Zm, C, O s, So ^[pc]
Dichloroacetamides	General*				N/A ^c																			
ALS inhibitors	General*																			Zm, Os ^a	Zm ^{dg}			
unclassified	Pyributicarb													Os ^b										
	florpyrauxifen- benzyl																							Zm, Os ^[pc]

Table 5: (Continued).

1.11 Safener mode of action

Safeners are known to inhibit the phytotoxicity of partner herbicides, but this may be mediated by a variety of effects. It has been proposed that safeners prevent herbicides from reaching their target sites by biochemical antagonism, or by interactions between herbicides and safeners through competitive or physiological antagonism (Komives, 1992). The current understanding of safener mode of action from the literature will be reviewed.

1.11.1 *Alteration of herbicide uptake and translocation*

One explanation for safener MoA, is that safeners inhibit the uptake or translocation of herbicides, such that they cannot reach the site of action (Davies et al., 1999; Hatzios, 1991; Komives, 1992). This could occur through competition for the uptake active site, or through effects on membrane permeability (Hatzios, 1991). Alternatively, safeners may act indirectly on herbicide transport via effects on cuticular integrity (Hatzios, 1991). Although comprehensive studies have been designed to test this hypothesis, there have been no conclusive results. In fact, it was found that in most cases safeners had no effect on herbicide uptake, and in some cases even enhanced absorption (Davies et al., 1999; Kraehmer et al., 2014). Any changes were subsequently considered to be side effects from safener interactions on other processes (Davies et al., 1999). Additionally, it has been demonstrated that safeners may protect plants even after herbicide application, at a time where the potential for inhibition of herbicide uptake and translocation would be limited (Davies et al., 1999). According to available information, it is considered that any changes in herbicide uptake or translocation do not account for the safening effect (Hatzios, 1991).

1.11.2 *Competitive antagonism*

Another hypothesis proposed that safeners may antagonise herbicides by acting as competitive inhibitors at the site of action. It is interesting that safeners and their herbicide partners have, in many cases, shown a high similarity in structure and even bonding properties. Examples of this include the safener-herbicide partners; dichlormid-EPTC, flurazole-alachlor, fluxofenim-metolachlor, fenclorim-pretilachlor and benoxacor-metolachlor (Hatzios, 1991). Some studies have provided evidence to support this theory, such as that of the safener R-29148, competing with herbicides EPTC and alachlor for binding in maize (Kraehmer et al., 2014). In addition, the safening activity of dichloroacetanilide compounds has been correlated with competitive binding (Kraehmer et al., 2014). One comparative study provided support for this competitive antagonist theory, with some

safener-herbicide partners, though many studies have found no safener-herbicide interactions at target sites (Kraehmer et al., 2014). Based on the discrepancy among various studies, it has been proposed that while the structural similarity between herbicides and their partner safeners is advantageous, this property is not necessary for the safening effect (Komives et al., 1991). To date, it is still unclear whether the competitive antagonism plays any part in the safener MoA.

1.11.3 *Enhancement of herbicide detoxification*

The safener MoA theory with the most support is that safeners enhance the metabolism of herbicides to less active metabolites, thereby reducing the concentration of herbicide at its site of action (Davies et al., 1999; Kraehmer et al., 2014). This theory, proposed in the 1970's, is supported by considerable evidence (Kraehmer et al., 2014). Seed treatment and pre-emergence safeners have been shown to enhance the metabolism of target herbicides (Kraehmer et al., 2014). This could occur through an increased expression of xenome enzymes, or through increased production of vital xenome cofactors, such as the tripeptide glutathione (GSH) required for glutathione conjugation.

1.11.3.1 *GSH regulation*

An increase in GSH content by safeners has been considered in many studies to be involved in the safening effect, with many safeners causing an elevation in GSH in maize, sorghum, tobacco (*Nicotiana sp.*) and rice (Davies et al., 1999; Hatzios, 1991; Komives, 1992). In many cases this has been attributed to enhanced expression of enzymes involved in glutathione biosynthesis (Davies et al., 1999; Hatzios, 1991). However, the involvement of this effect in safener protection is considered unlikely, as many studies suggest that the increase in GSH content does not correlate with increases in herbicide conjugation or safener efficacy (Davies et al., 1999).

1.11.3.2 *Enzyme regulation*

The hypothesis that safening occurs through enhanced expression of xenome enzymes involved in herbicide detoxification, has gained considerable support. Xenome enzymes have been shown to be induced by safeners within a few hours of safener application as highlighted in Table 6 (Kraehmer et al., 2014). Considering the role of GSTs in glutathionylation-based herbicide metabolism, the increased expression of these enzymes has been considered as a plausible method for safener action (Hatzios et al., 2004). Indeed, it was found in many studies that safeners, including flurazole, oxabetrinil, 1,8-NA, dichlormid and benzenesulfonamide

safeners, induced the expression of GST enzymes (Hatzios et al., 2004; Komives, 1992). Furthermore, this enhancement of GST level is strongly correlated with the protective effects of safeners such as dichlormid, benoxacor, fencloirim and flurazole against chloroacetanilide and thiocarbamate herbicides in maize, sorghum, rice and wheat (*triticum aestivum*) (Hatzios et al., 2004; Riechers et al., 2010). Specifically, an increased GST-mediated metabolism of the chloroacetanilides, metolachlor and metazachlor, and the thiocarbamate, EPTC-sulfoxide, has been demonstrated in maize upon safener application (Riechers et al., 2010). It is believed that an increased accumulation of the enzymes is mediated by transcriptional activation, as has been demonstrated in maize and arabidopsis (*Arabidopsis thaliana*) (Hatzios et al., 2004).

Besides GSTs, safeners have also been shown to protect crops from herbicides by enhanced phase I herbicide metabolism. The widespread involvement of CYP enzymes in phase I herbicide metabolism identified these enzymes as potential mediators of safener MoA (Davies et al., 1999). Studies indicated the safeners 1,8-NA and dichlormid were able to enhance the oxidative metabolism of herbicides chlorsulfuron, metsulfuron-methyl and sulfometuron-methyl in maize and wheat plants, with enhancement of CYPs implicated in this effect (Davies et al., 1999). Benoxacor and cloquintocet-mexyl have also been shown to enhance CYP levels (Davies et al., 1999).

In addition, GTs, also involved in phase II metabolism, have been shown to be involved in the safener effect. Cloquintocet-mexyl and BAS-145138 safeners enhance the glucosylation of herbicides, with cloquintocet-mexyl and dichlormid enhancing GT levels (Davies et al., 1999; Hatzios et al., 2004).

Similarly, the expression of an ABC transporter, *ZmMRP1*, was induced by the Safener dichlormid in maize (Pang et al., 2012), and a multidrug resistant protein (MRP), potentially involved in the removal of glucosylated herbicide metabolites, was induced by cloquintocet mexyl in wheat (Theodoulou et al., 2003). This indicates that enzymes involved in vacuolar transport of herbicide metabolites are upregulated by Safeners. In support of this, cloquintocet mexyl has been shown to induce MRP-mediated transport of glutathione and glucose conjugates of herbicides into vacuoles in barley (Gaillard et al., 1994).

A number of transcriptomic studies have identified common enzymes induced by Safeners, supporting their involvement in the safening effect. Behringer et al. (2011) identified a large range of Safener-induced detoxification genes through transcriptomic analyses in arabidopsis.

These enzymes included CYPs, oxygenases, oxidases peroxidases, glycosyl hydrolases, esterases, GSTs, GTs, ABC transporters and glutathione-conjugate degradation enzymes. The expression of these genes were induced at least 2-fold in response to treatment with the Safeners isoxadifen-ethyl and mefenpyr-diethyl. Skipsey et al. (2011) also demonstrated an induction of xenobiotic detoxification gene transcripts in arabidopsis, by treatment with derivatives of the safener fenclorim, including GSTs, GTs, CYPs and ABC transporters. GSTs, UGTs and CYPs transcripts were induced by metcamifen in rice and by fenclorim in arabidopsis and rice (Brazier-Hicks et al., 2017; Brazier-Hicks et al., 2020).

		Enzyme-mediated metabolism	
Herbicide (type)	Herbicide	CYP	GST
Chloroacetanilide	General*	Grass crops ^a	Zm, Sb, Os, Ta ^a Unk ^{a,b,d}
	alachlor		
	acetachlor		
	metolachlor		Zm ^e
	dimethenamid		
	metazachlor		Zm, Ta, ^e
Aryloxyphenoxypropanoate	General*	Grass crops ^a Unk ^{a,b}	
	Diclofop		
	Fenoxaprop-ethyl	Hv, Ta ^c	
Imidazolinone	general	Grass crops ^a Unk ^{a,b}	
	Imazapic		
	Imazethapyr	Zm ^c	
Phenoxyalkanoic acid	general		
	2-4D		
Phenylurea	General*		
	Chlortoluron	Zm ^d	
	Diuron		
	Fluometuron		
	Isoproturon		
	Linuron		
Sulfonamide	General*	Grass crop ^a	
	Flumetsulam	Zm ^c	
Sulfonylurea	General*	Grass crops ^a Unk ^{a,b}	
	Bensulfuronmethyl	Os ^c	
	Chlorimuron-ethyl	Zm ^c	
	Chlorsulfuron	Zm ^c	
	Metsulfuronmethyl	Ta, Zm ^c	
	Nicosulfuron	Zm ^c	
	Primisulfuron	Sb, Zm ^c Zm ^d	
	Prosulfuron		
	Rimsulfuron		
	Triasulfuron		
	Tribenuronmethyl		
	Sulfometuron-methyl	Ta ^c	
Unclassified	Bentazon	Zm, Sb ^c	
	Clomazone		
Phenoxyalkanoates			
chloro-S-triazines			Unk ^d
triazinone sulfoxides			
diphenylethers			
thiodiazolidines			
Thiocarbamates/thiolcarbamates/(sulfoxided)	General*		Unk ^{bd} Grass crops ^a
	EPTC-sulfoxide		Zm ^e
HPPD inhibitors	mesotrione		
	Tembotrione		
	toprmezone		

Table 6: The use of glutathione-S-transferase (GST) and cytochrome P450 (CYP) enzymes in safener-mediated detoxification of herbicide classes.

Superscripts denote sources: a; Hatzios et al., 2004 , b; Hatzios, 1991 , c; Davies et al., 1999 , d; Komives, 1992 , e; Riechers et al., 2010 . Empty boxes indicate no available data. General*; data refers to whole class, Unk; unknown crop, Zm; *Zea mays* (maize), Sb; *Sorghum bicolor* (sorghum), Ta; *Triticum aestivum* (wheat), Hv; *Hordeum vulgare* (barley), Os; *Oryza sativa* (rice).

1.12 Agrochemical discovery

New agrochemicals are mainly discovered through a combination of scientific knowledge and trial and error. New chemical leads are based on natural products or chemistries used for a similar purpose (Loiseleur, 2017). These are screened for desired agrochemical characteristics and optimised through cycles of 'design-synthesis-test-analysis'. In each cycle, effective chemistries are identified and chemical analogies with similar structures are added. Chemistries are screened for activity against the target organism, favourable kinetic and chemical properties, low toxicity, and environmental fate, through whole organism testing or *in vitro* assays. Structure-based design, a tool adopted from the pharmaceutical industry, offers an additional method for finding chemical leads. Advances in gene sequencing, protein crystallography and modelling have allowed predictions of agrochemically effective chemistries to be made. In addition, virtual screening offers a method of aiding agrochemical discovery by computer-based modelling of binding efficacy (Lamberth et al., 2013).

As mentioned, natural products are often used as chemical leads. As a result of evolution, these compounds typically possess high biological activity. They also often display low environmental persistence, and have high target specificity, ideal for new agrochemicals. Candidate chemistries may be sufficient to use directly, or may require synthetic modification. Alternatively, they may inspire synthetic mimics or highlight target sites of action (Loiseleur, 2017).

1.13 Regulation of agrochemicals

The development and marketing of new agrochemicals, including Safeners and herbicides, is strongly regulated by the relevant governing authorities, which must approve each chemical (Bijman et al., 2002). This system is put in place to ensure the safety of plant protection products to organisms and the environment. For a company to market a new compound, they must apply for regulatory approval, supplying data on many aspects of the chemical. It is important to note that individual combinations of plant protection products require individual regulatory approval. The regulatory authorities for each country or region are shown in Table 7.

Country/Region	Regulatory authority
Australia	Australian Pesticides and Veterinary Medicines Authority
Austria	Austrian Agency for Health and Food Safety
Brazil	Ministry of Agriculture, Livestock and Food Supply
Canada	Pest Management Regulatory Agency, Health Canada
Czech Republic	State Phytosanitary Administration
Germany	Federal Office of Consumer Protection and Food Safety, State Ministry of Economy/Transport/Innovation
Ireland	Department of Agriculture, Food and the Marine
Korea	National Academy of Agriculture Science
The Netherlands	Netherlands Food and Consumer Product Safety Authority
New Zealand	Ministry for Primary Industries
United Kingdom	Compliance Team Chemicals Regulation Directorate Health and Safety Executive
United States	Environmental Protection Agency
European Commission	Director General Health and Consumers Sector F.4.2 Pesticides and Import Controls

Table 7: Regulatory authorities for each country or region. Data extracted from "ENV pesticide compliance," accessed 2020 .

A variety of factors are considered in deciding the regulatory status of new agrochemicals, depending on the governing body. These criteria will be discussed here, focusing on herbicide products, based on the European Union (EU) regulatory approval process (Parliament, 2011).

The efficacy of the agrochemical is considered, taking into account the necessity of agrochemical control and the effectiveness of control afforded by the agrochemical. The performance is validated by testing the product in a range of conditions likely to be encountered in product use.

The agrochemical must display an absence of unacceptable effects on plants or plant products. Phytotoxicity studies are required to identify adverse effects and determine their degree, localisation, and effects, including those on neighbouring plants.

The impact of the agrochemical on human or animal health is reviewed. This includes effects arising from the product and its residues. The likelihood and risk of exposure of operators or bystanders to the active ingredients or toxic compounds is evaluated. This is determined through toxicological and metabolic studies, and analysis of application procedures. The metabolic pathways of the plant product, and the behaviour of the active substance and its metabolites in treated plants is also considered, which is determined through metabolic studies and toxicological analyses. In addition, consumer and animal exposure to residues is estimated.

The authorities also investigate the potential influence of the agrochemical on the environment, including the environmental fate and distribution, and also the impact on non-target species. The possibility of the product reaching the soil, groundwater, surface water and air is evaluated, with consideration of the chemical degradation pathways. Physicochemical properties are determined experimentally, and calculation models are used to predict the likelihood of this occurrence. The possible exposure of non-target organisms, including aquatic organisms, honeybees, beneficial arthropods, soil macro-organisms, birds, mammals and other terrestrial vertebrates, to the plant product is evaluated. Toxicological studies are carried out to determine the effects of exposure on health and reproduction of non-target organisms and the likelihood of exposure is estimated.

1.14 Aims and objectives

Despite their extensive use and importance in agriculture, the precise effects of herbicide safeners on crops are still uncertain. To ensure consumer safety, and to address questions raised by regulatory authorities, these effects were investigated. The question of whether safeners cause the production of aberrant metabolites, modified levels of conventional metabolites, and alterations in final residue composition, was considered. This work forms part of a longer term priority to develop a framework to address questions raised by regulatory authorities regarding long term safener effects on crops. In addition, a comprehensive understanding of safener effects, and the method of chemical selectivity, would allow predictions of effective safener-herbicide combinations, and may assist the development of novel safener technologies.

The main objective of this project was to obtain in-depth understanding of the generic impact of safeners on the metabolism and residue profile of agriculturally important herbicides in maize. This was to be performed using a combination of *in silico*, *in vitro* and *in vivo* experimentation. The underlying mechanism of the safening effect was to be investigated at the genome and transcriptome level. To ensure the greatest impact on the agriculture sector, the focus of this study was placed on agriculturally important crops, herbicides, and safeners. Maize was chosen as the study model, due to the widespread application of safeners in this crop plant. Herbicide-safener combinations were chosen such that a range of agriculturally important chemistries would be tested. Also, a hydroponic system was used in order to achieve rapid, accurate results, and to test whether such small-scale studies could be used to

predict the results of large-scale field trials. The research and thesis was split into three key projects.

The first study was designed to address three specific questions: does the presence of a safener lead to a significant and long term change in metabolic/profile residue by;

1. Leading to analytically quantifiable changes in the metabolic profile of the herbicide?
2. Generation of different metabolite(s) due to a change in the route of metabolism and/or;
3. Increased levels of known metabolite(s) due to enhanced rate of metabolism?

To address these key questions, the metabolic effects of the safeners on herbicide metabolism *in vivo* were investigated with the use of radiolabelled herbicides. The uptake and systemic mobility of the safener compounds were also tested *in vivo*, using radiolabelled safeners, and the uptake rates explored with respect to physicochemistry. The results from these studies will provide evidence to help explain the effect of safeners on the herbicide metabolic pathways, rates of detoxification and longevity of safening effect.

The second study aimed to investigate whether *in silico* analyses could be used to understand how herbicide selectivity is mediated by xenome enzymes involved in herbicide metabolism. A family of xenome enzymes known to be involved in safening were investigated *in silico*, at the genome, transcriptome and proteome levels. The GST superfamily was analysed in detail, with respect to general function and properties important for herbicide detoxification.

The third objective was to determine if safener effects on herbicide metabolism could be understood and predicted by *in vivo* studies of gene and protein expression. As such, the regulatory effects of safeners on key xenome enzymes were explored, at the transcript and protein level, using polymerase chain reaction (PCR) and western blotting, respectively. The time-dependency, magnitude, tissue specificity, and selectivity of the effects were investigated by use of time course studies.

Chapter 2. Materials and methods

2.1 Materials

Unless stated otherwise, all chemicals were of analytical grade and purchased from Sigma-Aldrich (now Merck). Herbicides and safeners (including radioactive isotopes) were provided by Syngenta (Jealott's Hill, UK). Oligonucleotide primers were synthesized and purchased from Integrated DNA Technologies. All molecular biology reagents and enzymes were purchased from Biotin. DNA extraction kits were purchased from Qiagen, protein gels from Bio-Rad and qPCR plates from Roche diagnostics. All buffers were formulated in ultrapure water ($18.2 \text{ M}\Omega \text{ cm}^{-1}$) and growth media autoclaved prior to use. Plant material (*Zea mays* cv. *Coxximo*) was provided by Syngenta.

2.2 Instrumentation and software

The instrumentation used for each experimental process, and software used for analyses, are listed in Table 8 and 9, respectively.

Process	Instrument	Company
Polymerase chain reaction	Mastercycler® gradient thermal cycler	Eppendorf
qPCR	LightCycler® 96 Real-Time PCR System	Roche Diagnostics Ltd
Agarose-Nitrocellulose transfer	IBlot(2) Dry Blotting System	ThermoFisher scientific
Protein purification	AKTA-purifier FPLC system with Frac-950 fractionator	GE Healthcare
Spectrophotometry	Shimadzu UV-1800 UV spectrophotometer	Shimadzu Corporation
Radioactive tissue maceration	FastPrep®-24 instrument	MPBio
Phosphorimaging	Typhoon FLA 9500 phosphorimager	GE Healthcare
Plant material growth	MLR-352 series growth cabinets	Panasonic Biomedical
HPLC	1220 Infinity Series LC	Agilent
Radio-HPLC	1200/1290 Infinity Series LC, Beta-RAM 5B Radio Flow Detector	Agilent
qDA	Acquity UPLC® class I	Waters
pH measurement	edge ^{pH}	HANNA
H ₂ O bath Sonication	Clifton SW3H	WolfLabs
Probe Sonication	Q55	Q Sonica
DNA gel analysis	Genoview UV light plate	VWR
DNA quantification	Nanodrop lite spectrophotometer	Thermo Scientific
H ₂ O bath	SUB Aqua Pro	Grant
Mass measurement	BP211D balance	Sartorius
Gel Imaging	ChemiDoc™ XRS + Imager	Bio-Rad
Mass spectrometer	XEVO G2-XS QTOF	Waters
TLC applicator	Automatic TLC Sampler (ATS) 4	Camag
TLC imager	Reprostar 3	Camag
Centrifuges	Megafuge 16R & Sorvall LYNX 4000	ThermoScientific

Table 8: Instrumentation used for experimental processes.

Process	Software or database	Version	Company or institute	Available from:	References
Statistical analyses	Graphpad	8	Prism	graphpad.com	-
In silico analyses	NCBI	-	United States National Library of Medicine	ncbi.nlm.nih.gov	(Johnson et al., 2008)[BLAST] (Ncbi-Resource- Coordinators, 2016)
Sequence alignment	Seaview	4.7	PRABI	doua.prabi.fr	(Gouy et al., 2010)
	Clustal X software	2	UCD	clustal.org	(Larkin et al., 2007)
X-ray/NMR structure organisation	Jalview	2.11.0	-	jalview.org	(Waterhouse et al., 2009)
Chemical Drawing	Biovia Draw	2017 R2	Dessault systemes	3dsbiovia.com	-
Primer design	Primer3	4.1.0	Whitehead Institute for Biomedical Research	primer3.ut.ee	(Untergasser et al., 2012)
Gel analysis	Gelanalyzer software	2010	-	gelanalyzer.com	-
Gene expression database	Genevestigator	7.3.1	Nebion	genevestigator.com	(Hruz et al., 2008)
Protein modelling	Chimera	1.13.1	UCSF	cgl.ucsf.edu/chimera	(Pettersen et al., 2004)
Homology modelling	Swiss-Model	-	Swiss Institute of Bioinformatics	swissmodel.expasy.org	(Waterhouse et al., 2018)
	Procheck	3.5	UCLA Molecular Biology Institute	servicesn.mbi.ucla.edu/PROCHECK	(Laskowski et al., 1993)
Targeting sequence analysis	Wolf psort	-	-	wolfpsort.hgc.jp	(Horton et al., 2007)
	Cello	2.5	National Chiao Tung University	cello.life.nctu.edu.tw	(Yu et al., 2006)
	LocSigDB	-	Guda Lab	genome.unmc.edu/LocSigDB	(Negi et al., 2015)
	TargetP	1.1	DTU Bioinformatics	cbs.dtu.dk/services/TargetP	(Emanuelsson et al., 2000)
Proteomics	ProteomicsDB	-	Technische Universität München (TUM) and Cellzome GmbH, a GSK company	www.proteomicsdb.org	(Samaras et al., 2020)
Protein property prediction	ExPASy software	-	Swiss Institute of Bioinformatics	expasy.org	(Gasteiger et al., 2003)
qPCR analysis	Lightcycler96	1.1	Roche Life Science	lifescience.roche.com	-
Data and word processing	Micorosoft Office	2013	Micorosoft	products.office.com	-
Phosphorimage analysis	ImageJ	1.8.0	National Institutes of Health and the Laboratory for Optical and Computational Instrumentation	imagej.nih.gov/ij	-
	Multiguage (TLC)	2.2	Fujifilm	-	-
Phylogenetic tree processing	Figtree	1.4.4	-	tree.bio.ed.ac.uk	-
	ITOL	3	-	itol.embl.de	(Letunic et al., 2016)
Herbicide usage data	Horticulture	-	University of Kentuky	uky.edu/Ag/Horticulture/masabni/index.htm	-

Table 9: Software and databases used for analysis.

URL prefixes for websites are excluded. Dashes indicate no information available.

2.3 Statistical analysis

To determine statistical significance for all comparisons, multiple T-test or two-way anova analyses were performed as appropriate. Statistical significance was determined for multiple T-tests using the Holm-Sidak method, with $\alpha = 0.05$. Individual parameters were analysed individually, without assuming a consistent standard deviation. Statistical significance was determined for two-way anova using the Tukey method, with $\alpha = 0.05$. All analyses were completed using graphpad software (Table 9).

2.4 Plant growth

Zea mays cv. *Coxximo* seeds were germinated for 3 d on wet paper towels. Seedlings were then placed in nutrient solution (0.8 mg mL^{-1} (50%) Hoaglands solution (Sigma-Aldrich, Cat/Id: H2395), pH 5.0) in appropriate size tubes, and allowed to grow for 7 d to two leaf stage (Figure 6) under the light conditions detailed in Table 10.

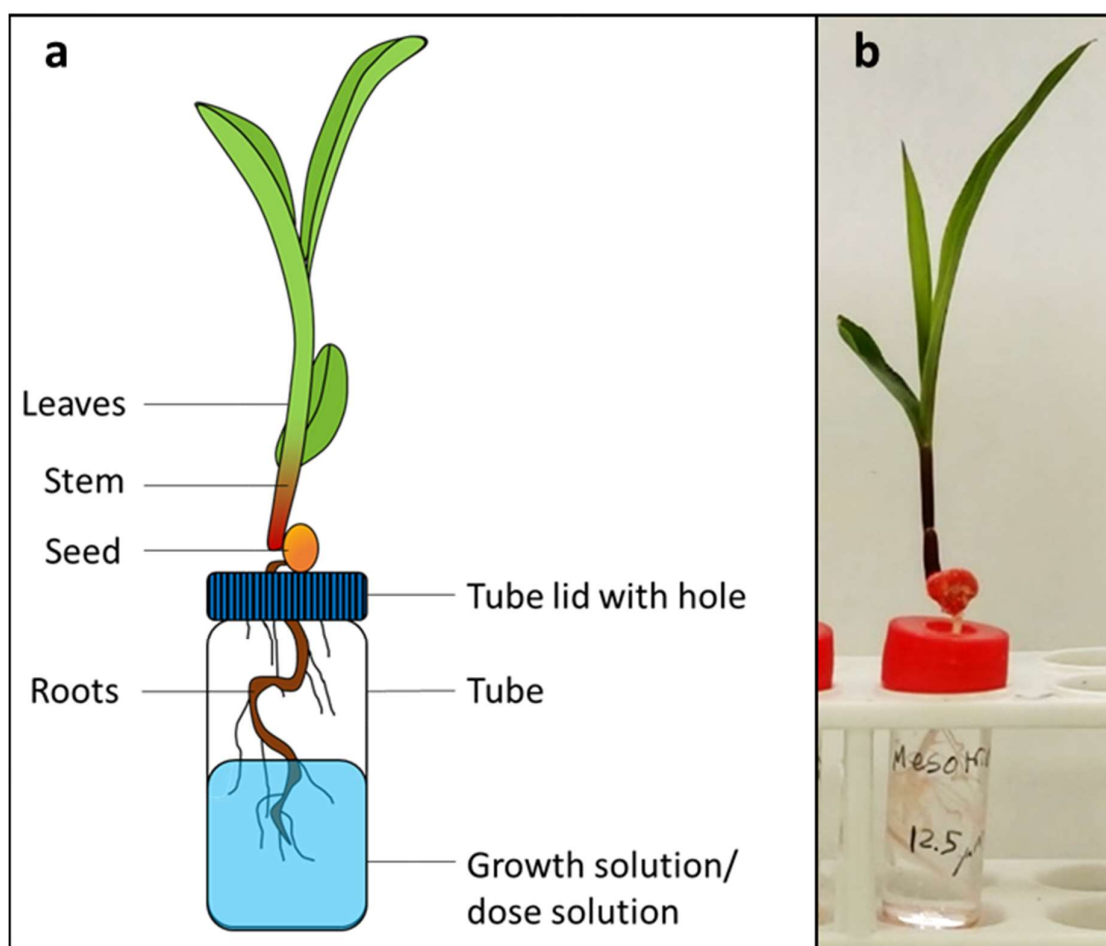


Figure 6: a; Maize growth schematic. b; Maize growth photograph.
Important descriptions are annotated in a.

Time	Temperature (°C)	Humidity (%)	Light ($\mu\text{mol m}^{-2} \text{s}^{-1}$)
06:00	24	70	600
21:00	18	70	0

Table 10: Conditions for maize growth.

Start time of condition given. Temperature (°C), Humidity (%) and Light levels ($\mu\text{mol m}^{-2} \text{s}^{-1}$) are given.

2.5 Dosing maize plants

2.5.1 Dosing for gene induction studies

Plants grown as described in section 2.4, were dosed after 7 d by transfer to 0.1% (v/v) DMSO (dimethyl sulfoxide), nutrient solution containing 25 μM metcamifen or benoxacor or no safener for 1 h, then returned to nutrient solution. Plants were harvested 3 h, 24 h, 48 h and 72 h later and frozen in liquid nitrogen before storage at -80 °C. Each application was performed in triplicate. Plants were separated into root, stem and leaf as defined in Figure 6. a.

2.5.2 Dosing for translocation study

Plants grown as described in section 2.4, were dosed after 7 d by transfer to 6.5 mL 0.1% (v/v) DMSO, nutrient solution containing 25 μM [aniline- $\text{U-}^{14}\text{C}$]-metcamifen (5.03 MBq mg^{-1}) or with 25 μM [phenyl- $\text{U-}^{14}\text{C}$]-benoxacor (1.80 MBq mg^{-1}), for 4.5 h, 24 h, 48 h and 72 h. Structures are shown in Figure 7. This was equivalent to 45.875 Bq μL^{-1} and 11.75 Bq μL^{-1} of dosed radioactivity respectively. Plants were then harvested, the seed removed, and the roots washed with 100% acetonitrile. The plants were then frozen between blotting paper at -20 °C, mounted to cardboard and freeze dried for 4 h.

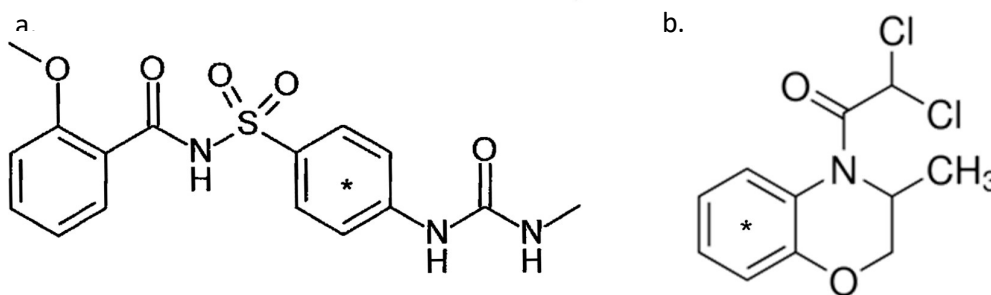


Figure 7: Structures of radioactive Safeners used in this thesis. a; [aniline- $\text{U-}^{14}\text{C}$]-metcamifen, b; [phenyl- $\text{U-}^{14}\text{C}$]-benoxacor.

* denotes ^{14}C ring labelled material.

2.5.3 Dosing for metabolism study

Plants grown as described in section 2.4 were dosed after 7 d by transfer to 0.1% (v/v) DMSO nutrient solution containing 25 μM metcamifen, benoxacor or no safener, with combinations of 25 μM [phenyl- $\text{U-}^{14}\text{C}$]-S-metolachlor (1.94 MBq mg^{-1}) or [phenyl- $\text{U-}^{14}\text{C}$]-mesotrione (4.07 MBq mg^{-1}). Structures are shown in Figure 8. At 4.5 h, 24 h, 48 h and 72 h, plants were harvested and separated into root, seed, stem and leaf tissues, as defined in Figure 6 a. The roots were washed with 100% acetonitrile, which was retained for analysis, as was the remaining dose solution. Samples were frozen at $-20\text{ }^{\circ}\text{C}$ until analysed.

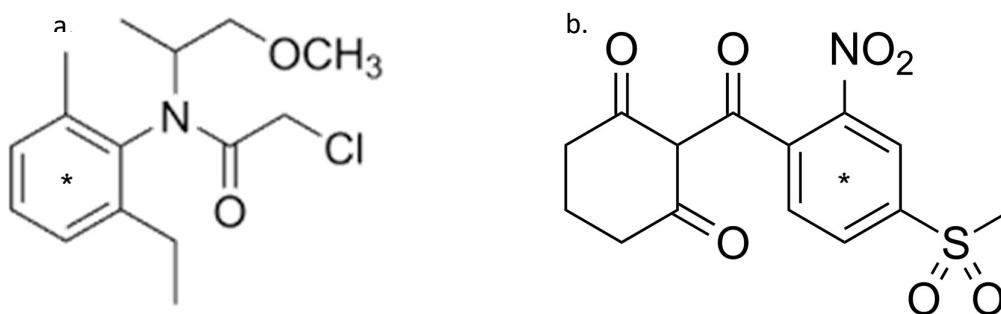


Figure 8: Structures of radioactive herbicides used in this study. a; [phenyl- $\text{U-}^{14}\text{C}$]-metolachlor, b; [phenyl- $\text{U-}^{14}\text{C}$]-mesotrione.

* denotes ^{14}C ring labelled material.

2.5.4 Dosing for protein study

Plants grown as described in section 2.4, were dosed after 7 d by transfer to 0.1% (v/v) DMSO, nutrient solution containing 25 μM metcamifen or benoxacor or no safener for 1 h, then returned to nutrient solution. Plants were harvested 0 h, 1 d, 3 d, 5 d and 7 d later and frozen in liquid nitrogen before storage at $-80\text{ }^{\circ}\text{C}$. Plants were separated into stem and leaf as defined in Figure 6 a.

2.6 Gene study

2.6.1 Primer design

All primers were designed using primer3 software (Table 9). The required parameters were a product size of 80-160 base pairs (bp), a primer melting temperature (T_m) of $57\text{--}62\text{ }^{\circ}\text{C}$ with an optimum of $60\text{ }^{\circ}\text{C}$, and a guanine/cytosine content (GC%) of $45\text{--}60\%$ with an optimum of 50% . The resulting primers were then verified using the primer blast function of NCBI (Table 9).

2.6.2 *Standard curves*

Mixtures of complementary DNA (cDNA) from different treatments (section 2.6.4) at final concentrations of 5, 1.67, 0.56 and 0.19 ng μL^{-1} were analysed with each primer to obtain standard curves. These were then analysed for primer efficiency, gradient uniformity (R^2), and quality of melting curves using lightcycler96 software (Table 9).

2.6.3 *RNA extraction*

Plant material grown as per section 2.4 and dosed as per section 2.5.1 was homogenised with a pestle and mortar while cooling with liquid nitrogen. RNA was extracted from homogenised plant material using the Qiagen RNeasy® mini kit (Cat No./ID: 74104), following the *RNeasy Mini Protocol for Isolation of Total RNA from Plant Cells and Tissues and Filamentous Fungi* protocol, including the optional DNase digestion step (appendix D). 100 mg of plant tissue was used for each sample.

2.6.4 *Reverse transcription by polymerase chain reaction (PCR)*

Reverse transcription of RNA from section 2.6.3, for cDNA synthesis, was performed using the Bioline Tetro cDNA Synthesis Kit (Cat No./ID: 65043). 0.5 μM Oligo (dT)₁₈, 50 ng μL^{-1} RNA, 0.5 mM dNTP mix, 1*RT Buffer, 1 μL Ribosafe RNase inhibitor, and 10 u μL^{-1} Tetro Reverse Transcriptase, were combined in 20 μL DEPC-treated Water. Samples were incubated using a Mastercycler gradient thermal cycler (Table 8), at 45 °C for 30 min and the reaction terminated by incubation at 85 °C for 5 min, followed by chilling on ice. cDNA was stored at -20 °C for long term storage, or amplified immediately by qPCR.

2.6.5 *Quantitative/real time polymerase chain reaction (qPCR)*

qPCR was performed using a lightcycler96 (Table 8) with conditions summarised in Table 11. 0.4 μM Forward and Reverse Primers, 18.75 ng cDNA and 7.5 μL Fast SYBR® Green Master Mix (Thermofisher Scientific), were combined in 15ul RNase free water per reaction. Before running, the plate was covered in a plastic film and centrifuged for 1 min at 1500 RCF. Relative expression levels (n-fold induction) were calculated using the comparative Ct method ($\Delta\Delta\text{CT}$), as per Equation 1, for each analysis. Three biological replicates were analysed, each with three technical replicates. Standard deviations were generated at the technical replicate level, and propagated throughout the analysis.

Phase	Cycles	Temperature (°C)	Duration (s)
Pre-incubation	1	95	600
3 step amplification	45	95	10
		60	10
		72	20
		95	10
Melting	1	65	60
		97	1

Table 11: Quantitative/real time polymerase chain reaction (qPCR) conditions.

The number of cycles for each phase is given. Temperature (°C) and duration of each cycle (s) are shown.

- $\Delta CT = Cq \text{ GOI} - Cq \text{ ref}$
- $\Delta\Delta CT = \Delta CT \text{ treatment} - \Delta CT \text{ control}$
- $n - \text{fold induction} = 2^{-\Delta\Delta CT}$

Equation 1: Quantitative/real time polymerase chain reaction (qPCR) analysis equation. a. ΔCT , b. $\Delta\Delta CT$, c. n-fold induction.

ΔCT ; change in cycle threshold difference when normalising to reference gene. Cq ; quantitation cycle for GIO (gene of interest) or ref (reference gene). $\Delta\Delta CT$; change in ΔCT when normalising treatment to control samples.

2.6.6 Absolute quantification using gBlocks®

gBlock® standard curves were designed to cover the expected range of Cq values seen in the relatively quantified data. gBlocks® were applied in 10* serial dilutions from 10^8 copies μL^{-1} to 10 copies μL^{-1} and were run in triplicate, as described in section 2.6.5. The standard curve equations were used to convert the Cqs of relatively quantified control data into DNA copy number.

2.6.7 Separation of DNA molecules using agarose gel electrophoresis

Agarose solution comprised of 1.2% Agarose, and 1*TAE buffer (0.484% tris-[hydroxymethyl]-aminomethane, 1.142% acetic acid and 1 mM Ethylenediaminetetraacetic acid) was microwaved at max power for 2 min. After cooling to approximately 50 °C, 1 μL ethidium bromide, or 1* gel red™ (Cambridge Biosciences) was added. 60 mL of the solution was then poured into gel casting apparatus (Bio-Rad) and left to set for a minimum of 15 min. The gel was covered with 1*TAE buffer and 5 μL samples of qPCR product (section 2.6.5) in 1*DNA loading buffer, consisting of 2.5% Ficoll 400, 0.04167% bromophenol blue dye, 0.04167% and Xylenecyanol FF dye, were added to the wells of the gel along with DNA ladder (1*DNA loading buffer, 0.1 $\mu\text{g} \mu\text{L}^{-1}$ 1Kb plus DNA Ladder (Invitrogen). A maximum of 125 V was applied to the gel for approximately 30 min. The gel was then imaged using a ChemiDoc™ XRS + Imager (Table 8). Molecular weights of samples were determined by reference to the standard curve generated by the DNA ladder. The \log_{10} of the ladder marker weights were plotted against the

retention factor (Rf) values producing a linear trendline. The equation for this trendline was used to convert sample Rf values into molecular weights. Rf values were determined using Gelanalyzer software (Table 9).

2.6.8 *Next generation sequencing*

Next generation sequencing experiments were performed by Melissa Brazier-Hicks (Syngenta, UK) and the bioinformatics analysis performed by Johnathan Cohn (Syngenta, USA). Black Mexican sweetcorn (BMS) cell suspension cultures were dosed with 5 μ M metcamifen or benoxacor or no safener control in triplicate. Cultures were sampled at 30, 90, and 240 min after treatment. Total RNA samples were prepared at the University of York. Total RNA was extracted using TRI-reagent (Sigma) and then cleaned up using RNeasy plant mini kit (Qiagen) and then shipped to Syngenta. Samples were processed and libraries for sequencing were sent to collaborators at the National Center for Genome Resources (NCGR) in Santa Fe, New Mexico for sequencing on the HiSeq. Sequences generated were aligned to the most recent available nuclear genome reference with reliable gene models as well as organellar genomes. Sequence alignment files in the .bam format were deposited in the NGS repository in the Syngenta data center in Alpharetta, GA. Count data were generated from BAM files using gene feature format (GFF3) files indicating location of genes on the maize reference genomes. All reads were counted at the gene level to avoid potential data loss associated with using only uniquely aligning reads. Gene regions for maize were identified as reads aligning to the genome in the same physical location as predicted gene models. For these studies, the nuclear, chloroplast, and mitochondrial genomes were concatenated. Log₂ fold change values with each safener treatment compared to a control were annotated with transcript sequences, identified by GRMZM codes, and an associated P-value indicating significance. Correlation statistics were performed using the correlation matrix tool of graphpad software (Table 9). Data alignment and conditional formatting was performed using Microsoft Excel software (Table 9).

2.7 Protein studies

2.7.1 *Protein extraction*

Tissue grown as per section 2.4 and dosed as per section 2.5.4 was homogenised using a pestle and mortar, cooled with liquid nitrogen. All further steps were carried out on ice. Protein was extracted with 3* (w/v) buffer (50 mM Tris-HCl, 2 mM EDTA [ethylenediaminetetraacetic acid], 1 mM DTT [dithiothreitol] pH 7.5) and 50 g L⁻¹ polyvinylpolypyrrolidone (PVPP). The resulting extract was filtered through a double layer of Miracloth (22-25 μ m pore size) (Merk Millipore).

The filtrate was transferred to Oakridge centrifuge tubes and centrifuged at 10,000*g for 15 min at 4 °C. The protein in the supernatant was precipitated through the addition of ammonium sulphate to 80% saturation and recovered following further centrifugation at 4000*g for 20 min at 4 °C. Pellets were then stored at -20 °C and desalted prior to use on a Sephadex G-25 column (Sigma-Aldrich).

2.7.2 *Protein concentration determination*

Protein concentration was determined using the Thermo Scientific™ Pierce™ BCA Protein Assay Kit with minor modifications from the test-tube procedure. The working reagent (WR) was prepared by mixing 50 parts of BCA Reagent A (500 mL solution containing: sodium carbonate, sodium bicarbonate, bicinchoninic acid and sodium tartrate in 0.1M sodium hydroxide), with 1 part of BCA Reagent B (25 solution containing 4% cupric sulfate). Each standard contained a total WR volume of 1 mL (50:1, Reagent A:B) and 50 µL of the protein bovine serum albumin (BSA) and were used to generate a standard curve ranging from 2,000 to 0 µg mL⁻¹. The unknown(s) were assayed alongside, in order to determine their concentration. The samples were measured at 562 nm with a UV-1800 spectrophotometer (Table 8) following an incubation period of 30 min at 37 °C. The generated standard curve was plotted once the blank (background interference) value was removed, to establish the amount of protein in the samples in µg mL⁻¹.

2.7.3 *SDS polyacrylamide gel electrophoresis (SDS-PAGE)*

4-20% SDS-PAGE gradient gels (Mini-PROTEAN TGX Gels, 4-20%, 15-well, 15 µL, BioRad) were purchased, and 12% SDS-PAGE gels were prepared as follows. The resolving gel solution was composed of 12.8% acrylamide/bis acrylamide, 1*resolving buffer (0.375 M Tris-HCL, pH9.0, 0.1% TEMED [tetramethylethylenediamine], 0.1% SDS [sodium dodecyl sulphate]), and 0.1% ammonium persulfate (APS). The stacking gel solution was composed of 4% acrylamide/bis acrylamide, 1*stacking buffer (0.13M Tris-HCl, pH 6.8, 0.1% TEMED and 0.1% SDS) and 1% APS. Each gel solution was degassed prior to APS addition, followed by transfer to pre-assembled gel-apparatus for polymerisation, with the resolving gel solution poured before the stacking gel solution. Water-saturated butan-1-ol was applied to ensure an even gel meniscus. A ten or fifteen well comb was added to the stacking gel solution before polymerisation. Gels were stored at 4 °C, wrapped in water-saturated paper towels, or used directly. The tank apparatus was assembled with one or two gels, using a buffer dam as required, and filled with running buffer (25 mM Tris, 192 mM glycine, 0.1% (w/v) SDS, pH 8.3). Polypeptide samples were

prepared in 1*SDS loading buffer (50 mM Tris-HCl, 10% (v/v) glycerol, 2% (w/v) SDS, 0.1 M DTT [dithiothreitol], 0.1% (w/v) Bromophenol Blue) prior to heating at 95 °C for 5 min, and stored at -20 °C or used directly. 5-10 µL protein sample was added to the gel wells after the comb was removed, alongside 5-10 µL protein ladder (PageRuler Prest) for molecular weight determination of samples. Gels were run at 60 mA, 200 V for 50 min or until the dye front eluted from the gel base. For total protein visualisation, gels were washed twice with water for 10 min, and stained by exposure to InstantBlue dye reagent (Expedeon Inc), for 16-18 h.

2.7.4 *Western blotting and immunodetection*

SDS page gels (section 2.7.3) were washed twice with water for 10 min, and polypeptides transferred to an iBlot® transfer stack polyvinylidene difluoride (PVDF) membrane (0.2 µm pore size, low fluorescence and protein binding capacity of 240 µg cm⁻²) (Thermo Fisher Scientific) using an iBlot(2)® Semi-dry blotting system (Table 8) according to the manufacturer's instructions. Membranes were then washed with 25 mL buffer A (5% milk in 1*TBS [tris buffered saline] + 0.05% tween 20) for 1 h, prior to incubation in 0.2% (v/v) dilution of primary antibody in buffer B (1% milk in 1XTBS + 0.05% tween 20) for 1 h at room temperature, or overnight at 4 °C. Membranes were washed thrice with 20 mL buffer B for 10 min, and exposed to 0.0067% secondary antibody (anti-rabbit IgG (whole molecule)-alkaline phosphatase antibody (Sigma-Aldrich)) in buffer B for 1 h. Membranes were then washed twice with 20 mL buffer B for 10 min, and once with 20 mL 1*TBS for 10 min. For chemical visualisation, membranes were washed with 20 mL developing buffer (100 mM Tris-HCl, pH 9.5) for 2 min and developed in 10 mL developing buffer containing 0.33% (v/v) nitro blue tetrazolium (NBT) and 0.33% (v/v) 5-bromo-4-chloro-3-indoyl phosphate (BCIP), for 15 min in the dark. For chemiluminescent visualisation, membranes were stored in 1*TBS at 4 °C until analysis and then developed using a Clarity western ECL substrate, 200 mL, kit (Cat./ID:170-5060), visualised using a ChemiDoc imager (Table 8). The data was first quantified into protein concentration (ng µL⁻¹), then converted into percentage of total protein concentration (%), followed by a subtraction of the non-treated control samples.

2.7.5 *Plasmid production*

14.22 ng µL⁻¹ pET-Strp3 plasmid vector (Figure S 9) was mixed with 1*NE4 and 1*BSA, 5% NDE1 and 5% Sal1, in a 40 µL reaction, and incubated overnight at 37 °C for restriction. The reaction mixture was then run on a 0.8% agarose gel, as described in 2.6.7. The restricted plasmid was isolated from the gel using Prep-A-Gene® DNA Purification System (BioRad). 5 ng µL⁻¹ of the

pET-Strp3 plasmid vector and 5 ng μL^{-1} DNA insert (Figure 50), restricted with Nde1 and Sal1 were mixed in 10 μL water and added to 140 μL XL-10 Gold cells, ice shocked for 20 min, heat shocked for 40 s at 42 °C, and ice shocked again for 2 min. 500 μL S.O.C. (2% Tryptone, 0.5% Yeast Extract, 40 mM MgSO_4 , 20 mM dextrose, 8.6 mM NaCl, 2.5 mM KCl, autoclaved) was added, followed by incubation at 37 °C, 200 RPM for 1 h. 100 μL of the solution was added to Agar plates with 100 $\mu\text{g mL}^{-1}$ Kanamycin, for incubation at 37 °C overnight. Individual colonies were then added to 24 mL of a solution of lysogeny broth (LB) media (2.5% LB, autoclaved) with 100 $\mu\text{g mL}^{-1}$ Kanamycin, and incubated overnight at 37 °C, 200 RPM. The recombinant plasmid was then isolated using the Wizard® plus SV miniprep DNA purification system (Promega).

2.7.6 *Sequencing of recombinant plasmid*

The isolated recombinant plasmid (section 2.7.5) was sequenced using the Sanger sequencing service from GATC (Eurofins) and determined to contain the correct sequence for recombinant protein expression.

2.7.7 *Recombinant protein expression*

LB Agar (1.5% Agar, 2.5% LB, autoclaved) was melted in boiling H_2O , cooled to 55 °C, and dosed with 34 $\mu\text{g mL}^{-1}$ chloramphenicol and 100 $\mu\text{g mL}^{-1}$ kanamycin. The solution was then mixed and poured into petri-dishes to set. 1 μL of pET-Strp3 plasmid vector (Figure S 9), containing the gene of interest, was combined with 50 μL Tunetta cells. The mixture was ice shocked for 2 min, heat shocked at 42.5 °C for 30 s, and ice shocked again for 2 min. 250 μL of S.O.C (see section 2.7.5) was then added, followed by mechanical shaking at 37 °C, 200 RPM for 1 h. 100 μL of the mixture was then spread onto each plate and incubated overnight at 37 °C, and then placed in a 4 °C room until needed. 34 $\mu\text{g mL}^{-1}$ chloramphenicol and 100 $\mu\text{g mL}^{-1}$ kanamycin were added to 10 mL LB Medium, and inoculated with colonies from plates. The culture was incubated overnight at 37 °C, shaking at 200 RPM. 34 $\mu\text{g mL}^{-1}$ chloramphenicol and 100 $\mu\text{g mL}^{-1}$ kanamycin were added to 250 mL LB. 5 mL of overnight culture was added and shaken at 37 °C, 200 RPM until an OD600 nm of approximately 0.6 was reached. 1 mM Isopropyl β -D-1-thiogalactopyranoside (IPTG) was then added, followed by incubation for 3 h at 37 °C, 200 RPM. Alternatively 0.1 mM IPTG was then added, followed by incubation overnight at 20 °C, 200 RPM. 1 mL was then aliquoted, centrifuged for 2 min, 10,000 RPM, and the pellet stored at -20 °C for non-purified protein analysis. The main culture was centrifuged at 8000*g for 10

min at 4 °C. The pellet was resuspended in 100 mL H₂O, separated into 20 mL fractions, and centrifuged at 4696*g for 10 min at 4 °C. The pellets were stored -20 °C prior to purification.

2.7.8 *Recombinant protein purification*

Pellets from section 2.7.7 were resuspended in an appropriate amount of degassed buffer W (20 mM HEPES-OH, 150 mM NaCl, 1 mM EDTA, pH 7.6). 0.1 µg mL⁻¹ culture avidin and 2 mM DTT were added to the solution along with a small amount of DNase I and RNase powder. The solution was sonicated at 50 mA for 2*15 s cycles in 1 mL fractions. Cell material was removed by centrifugation at 10,000*g for 10 min at 4 °C, and retained as the insoluble fraction, while the supernatant was pooled for injection onto the AKTA purifier (Table 8). Purification using the AKTA purifier was performed according the manufacturers guidelines, using a Strep-Tactin(R) Superflow(R) high capacity cartridge H-PR (Fisher Scientific). Protein was loaded using Buffer W, and eluted using Buffer E (2.5 mM Desthiobiotin in buffer W). Buffer W was used to wash the column before elution, which was retained as flowthrough. Purified recombinant protein was stored in 33% glycerol at -80 °C.

2.7.9 *Recombinant protein quantification*

Purified protein samples, flowthrough, and insoluble fraction, resuspended in appropriate volume buffer W (section 2.7.8), were analysed using a UV-1800 spectrophotometer (Table 8) at 280 nm. Buffer W was used to autozero the machine. The protein concentration was determined using Equation 2. Molecular mass and extinction coefficient predictions were generated by ExPASy software (Table 9).

$$A = \epsilon * b * c$$

Equation 2: Beer lambert law.

A; Absorbance at 280 nm, ϵ ; Extinction coefficient of the protein (M⁻¹ cm⁻¹), b; Pathlength (cm), c; Concentration (M).

2.7.10 *GST assay with CDNB*

1 mM 1-Chloro-2,4-dinitrobenzene (CDNB) in 0.1 M Potassium phosphate buffer pH 6.5 was incubated at 30 °C for >5 min. 25 µL purified protein (section 2.7.8), diluted in 0.1 M Potassium phosphate buffer pH 6.5 if necessary, was added to the reaction, followed by 10 mM glutathione (GSH). The reaction was immediately placed in a UV-1800 spectrophotometer (Table 8) and measured at 340 nm for 1 min. Each assay was run in triplicate reactions and a non-enzyme control reaction was performed by replacing the 25 µL enzyme with 0.1 M

Potassium phosphate buffer pH 6.5. The increase in absorbance at 340 nm, within a linear range, was used to calculate the rate of CDNB metabolism, using Equation 3, assuming an extinction coefficient of 9.6 mM⁻¹ cm⁻¹.

$$Activity = \left(\frac{(\Delta A_{enzyme} - \Delta A_{control})}{\epsilon} \right) / (c * v)$$

Equation 3: Determination of protein activity.

ΔA_{enzyme} or $\Delta A_{control}$; Change in absorbance at 340 nm per minute of enzyme or control sample respectively. ϵ ; Extinction coefficient (nM⁻¹ cm⁻¹), c ; Concentration of protein (mg mL⁻¹), v ; Volume of protein (mL). Activity is expressed in nkats mg⁻¹.

2.8 Bioinformatics

2.8.1 *GST gene expression analysis*

GST Gene IDs were inputted into Genevestigator software (Table 9) within platform ‘mRNA-Seq Gene Level Zea Mays (ref: AGPv4) (Default)’. Anatomy, development and perturbation tools within ‘Compendium-wide analysis’ condition search were used to generate log₂ values of gene expression changes, which were converted into heatmaps using Microsoft Excel and Graphpad software (Table 9) (Stelpflug et al., 2016).

2.8.2 *GST sequence searching*

Identification of maize GSTs was performed using the B73 RefGen_v4 maize genome, sequenced by BAC-by-BAC approach (Jiao et al., 2017; Schnable et al., 2009). A database of GSTs from Mcgonigle et al. (2000) was subjected to a Position-Specific Iterated (PSI) BLAST of non-redundant protein sequences in the *Zea mays* taxid 4577, using NCBI (Table 9). The sequences for each BLAST search, producing significant alignments with Expect-value lower than 10, were downloaded, and duplicate sequences were deleted. The remaining sequences were then restricted based on the given protein names. Those labelled as non-GST proteins were removed along with hypothetical, predicted, partial, and low quality, sequences.

2.8.3 *Alignment and phylogenetic tree synthesis*

Phylogenetic tree generation and sequence organisation both utilised Seaview software (Table 9). Sequences were aligned using the Clustal Omega drive and trees were produced using the maximum likelihood driving program PhyML 3.1. Invariable sites (P-inv) and across site rate variation (α) values were first determined with optimised parameters, which were used as values for fixed runs. Fixed run parameters include LG model, Bootstrap with 100 replicates branch support, model-given amino acid equilibrium frequencies, best of NNI & SPR

tree searching operations, optimised tree topology, and BioNJ starting tree with 5 random starts. Produced trees were analysed and sequences showing considerable similarity, as determined by low branch lengths and alignment similarity, were restricted to a single sequence. NCBI (Table 9) was used to aid this process by comparing other factors such as gene loci, naming, and source. Trees were annotated and edited using ITOL and Figtree software (Table 9). Alignment for G- and H- sites was achieved using Clustal X software (Table 9).

2.8.4 *Domain and interface mapping*

Protein sequence identifiers were used to identify protein domains and dimer interface regions, using the Batch Web CD-Search Tool of NCBI with default settings (Table 9). Data was downloaded into Microsoft Excel (Table 9). Domain data was given as residue length and position, while dimer interface region was given as residue positions, which were mapped as horizontal bar charts. Multiple domain suggestions were restricted to specific or superfamily hit types, with the lowest Expect (E)-Value.

2.8.5 *Chromosome mapping*

Gene sequence identifiers were used to identify chromosome number and position, using the Batch Entrez Tool of NCBI (Table 9). Data (gene chromosome number and position) were downloaded into Microsoft Excel (Table 9). Chromosome sizes were also identified using NCBI. The data were compiled into vertical bar charts.

2.8.6 *Hydrogen bond interaction mapping*

X-ray crystal and nuclear magnetic resonance (NMR) structures of plant GSTs were obtained through NCBI (Table 9). The sequences were restricted to those containing GSH as ligand using Jalview (Table 9). 2D interpretation was generated using Biovia Draw (Table 9).

2.8.7 *Homology modelling*

Individual sequences were inputted into Swiss-Model software (Table 9), and templates chosen based on oligomeric-state, GSH ligand, and sequence similarity. Models were built based on the target-template alignment using ProMod3. Coordinates which were conserved between the target and template were copied from the template to the model. Insertions and deletions were remodelled using a fragment library. Side chains were then rebuilt. The geometry of the resulting model was regularised using a force field. Global and per-residue model quality was assessed using the QMEAN scoring function, and Ramachandran plots (Benkert et al., 2011; Laskowski, 2006). Models were edited and superimposed using

matchmaker tool in Chimera Software (Table 9). Structure based alignment was performed using the *match -> align* tool in Chimera Software.

2.8.8 *Targeting sequence analysis*

Protein sequences were analysed for subcellular targeting sequences using four software programs: Wolf psort, Cello, LocSigDB and TargetP (Table 9). The most likely predictions from each program were collated.

2.9 Radio-isotope metabolism studies

2.9.1 *Stock quantification and purity*

Radioactivity of [^{14}C]-mesotrione, [^{14}C]-S-metolachlor, [^{14}C]-metcamifen and [^{14}C]-benoxacor were analysed by liquid scintillation counting (LSC) (Table 8) upon receipt. This was compared with expected radioactivity to determine accuracy, which met the 5% variability limit. This was repeated for plant dose solutions to determine their accuracy of preparation, and adjusted as necessary. The average measured radioactivity for each compound was within 10% of the expected value. To determine purity, [^{14}C]-mesotrione and [^{14}C]-S-Metolachlor were analysed by radio-HPLC (high performance liquid chromatography) (Table 8) alongside their respective standard [^{12}C]-counterparts by UV-HPLC (Table 8) at 254 nm. The Integrated peak density of the chromatogram was used to determine the degree of radiolysis. All dosed parent compounds exceeded 90% purity.

2.9.2 *Metabolite extraction*

Radioactive metabolites were extracted from tissue samples (section 2.5.3) by sequential maceration in various solvent mixtures. Maceration was performed using a fast prep macerator (Table 8) at 4.0 m s^{-1} for 60 second intervals, in 2 mL extraction tubes. The tissue was first macerated without solvent, after cooling with dry ice, followed by maceration with 2*(v/w) 80% acetonitrile. After centrifugation at 13000 RPM for 10 min, the supernatant was decanted and retained for analysis as the primary extraction. A second maceration of the tissue with 2*(v/w) 50% acetonitrile, followed by centrifugation and decanting, generated the secondary extraction. Plant tissue and extraction solutions were kept on ice and stored at $-20\text{ }^{\circ}\text{C}$.

2.9.3 *Liquid scintillation counting (LSC)*

50ul standards or samples (section 2.9.2) were diluted in 5 mL prosafe⁺ scintillation fluid and measured by liquid scintillation counting (Table 8). Machine conditions were set to single DPM

assay, tSIE/AEC quench indicator, 3 min count time, with a 10 min background subtract of prosafe⁺ scintillation fluid only.

2.9.4 *Thin layer chromatography (TLC)*

Metabolite extracts (section 2.9.2) were applied onto *TLC silica gel 60 F254* plates using an automatic TLC applicator (Table 8), along with non-radioactive metabolite standards. The volume of sample applied was varied based upon LSC count data (section 2.9.3) to ensure equal levels of radioactivity were applied to the same plate for comparison. Samples were applied 20 mm from the bottom of the plate, in 8 mm bands with 15 mm spaces between bands. The 20 mm application line was marked with pencil. After drying, TLC plates were lowered into TLC tanks equilibrated with 100 mL mobile phase solvent, and lined with saturation pads. When the solvent front was approximately 40 mm from the top of the plate, the plate was removed from the tank and the solvent front marked with pencil. TLC plates were visualised and photographed under white light and UV light (254 nm), using a Canon camera mounted to a light box (Table 8). TLC plates were exposed to radiofilm (Fujifilm) in lead cassettes for variable time, depending on level of radioactivity applied. The films were then scanned using a phosphorimager (Table 8). Calibration and superimposition of UV images and phosphorimages was achieved by applying 4 dots of radioactive ink to the TLC plates, 2 on the origin line and 2 on the solvent front line. Multiguage software (Table 9) was used to analyse the phosphorimage data. Regions of interest (ROI) were identified in each TLC band, along with intermediate regions and background. %ROI values were used for further data manipulation. Peak identification for the mesotrione study was achieved by co-chromatography with [¹²C]-standards at 254 nm. Since the [¹²C]-standards for the S-metolachlor study were of low visibility, R_f values from the preliminary test were used to identify peaks.

2.10 Translocation study

2.10.1 *Phosphorimaging of freeze-dried plants*

Freeze dried plants (section 2.5.2) were pressed against radiofilm (Fujifilm) in a cassette and left for 2 d. The exposed film was then imaged using a phosphorimager (Table 8) set to a pixel size of 100 µm, at a wavelength of 635 nm. The phosphorimager converted absorbed counts per second into a density map which was used to relatively quantify radioactivity. The density map was converted into a colour map by processing of the phosphorimage data using imageJ and plugin phosphoimageJ (Table 9). The linear range of radioactivity was defined by the

phosphoimager and radiation exceeding the linear range were highlighted as oversaturated density.

Chapter 3. Comparative translocation of the safeners, benoxacor and metcamifen, and their effect on herbicide metabolism

3.1 Introduction

It is well documented that herbicide safeners enhance the metabolism of certain herbicides, thereby reducing herbicide damage on monocotyledonous cereal crops (Davies et al., 1999; Jablonkai, 2013). In contrast, safeners do not protect the weed species being targeted, and also may protect only certain crops. This selective protection of plant types is known as botanical selectivity. In addition to this, certain safeners are more effective at increasing the metabolism of specific herbicides, a phenomenon known as chemical selectivity (Hatzios, 1991; Jablonkai, 2013). For this reason, safeners are partnered with specific herbicides in commercial products used for cereal crops (Edwards et al., 2011). While it is known that safeners increase the metabolism of herbicides through upregulation of xenobiotic detoxifying enzymes, such as glutathione-S-transferases (GSTs) and cytochrome P450s (CYPs), it is not fully understood how this chemical selectivity is achieved (Komives, 1992). This chapter aims to understand how safeners are distributed through the plant when applied hydroponically, and how different safeners affect the metabolism of different herbicides. Whether safener-mediated enhancement of metabolism is caused by changes in rate or route of metabolism will also be investigated, and the longevity of effect will be elucidated. The results also give a broader understanding of where safening occurs.

To understand the basis of chemical selectivity, a system was designed to compare the effects of safeners on the metabolism of different herbicides. Chemical partners known to be effective were cross-compared with novel combinations. Benoxacor (4-(dichloroacetyl)-3,4-dihydro-3-methyl-2H-1,4-benzoxazine) is a dichloroacetamide safener developed by Ciba-Geigy (now Syngenta) to be used in conjunction with the herbicide *S*-metolachlor (*S*-moc), also developed by Ciba Geigy, in pre-emergence products for use in maize (Cottingham et al., 1991). A comprehensive list of commercial products containing these two chemicals is shown in Table 12. It has previously been shown that benoxacor is able to increase the metabolism of metolachlor to its glutathione conjugate in maize by stimulating GST activity (Cottingham et al., 1991; Jablonkai, 2013). However the metabolic effect of benoxacor on mesotrione has not previously been reported. Metcamifen, 2-methoxy-N-[[4-[[[(methylamino)carbonyl]amino]phenyl]sulfonyl] benzamide, is a new safener, developed by

Syngenta, for use in maize. Metcamifen has displayed protection against HPPD inhibitors including mesotrione, a herbicide developed by Zeneca (Syngenta personal comm.). Due to its recent commercialisation, no data is available for products containing metcamifen. The metabolic effect of metcamifen on *S-moc*, has not previously been reported. The cross comparison of these safeners and herbicides should therefore provide insight into the phenomenon of chemical specificity.

Company	Product	Benoxacor (%)	S-metolachlor (%)	Atrazine (%)	Mesotrione (%)	Bicyclopyrone (%)
Syngenta	Acuron®	<5	23.40	10.93	2.60	0.65%
	BICEP II Magnum®	<5	26.10	33	-	-
	DUAL II Magnum®	<5	71%	-	-	-
	BICEP LITE II Magnum®	<5	35.80	28.10	-	-
	Lumax®	<5	29.40	11	2.94	-
	Lexar ex®	<5	19.00	19	2.44	-
	Camix®	1.80	36.80	-	3.68	-

Table 12: Ratios of each active ingredient (in percentage of total active ingredients) in formulated products containing benoxacor.

Data obtained from product labels from Syngenta webpages.

To better understand the chemicals being investigated, a summary of the Safeners and herbicides is presented here. Since Metcamifen is a relatively new compound, little published research is available. The protection of rice from the herbicide clodinafop-propargyl by metcamifen has been demonstrated, and the transcriptomic effects reported (Brazier-Hicks et al., 2020). In contrast, the wide use of benoxacor has resulted in more extensive characterisation of the Safener. Benoxacor has been shown to protect maize from the herbicide metolachlor through increased GST activity and thus herbicide metabolism (Cottingham et al., 1991; Del Buono et al., 2006; Fuerst et al., 1993; Irzyk et al., 1993; Miller et al., 1994). It has also been shown to enhance detoxification of the herbicide, terbuthylazine, in maize and the grass, *festuca arundinacea*, through increased GST activity (Del Buono et al., 2007; Scarponi et al., 2005). Mesotrione is a member of the triketone herbicides, which cause toxicity through HPPD inhibition (O'sullivan et al., 2002). It was developed for the selective

control of dicotyledonous weeds, including jimsonweed (*Xanthium strumarium*), and some monocotyledonous weeds, including *Digitaria* species in maize crops, and may be used pre- or post- emergence. Foliar uptake in maize occurs rapidly and results in both acropetal and basipetal translocation. The selectivity of mesotrione to maize is caused by rapid metabolism (Mitchell et al., 2001). However, while maize is tolerant to mesotrione applied pre-emergence, some cultivars show toxicity when applied post-emergence (O'sullivan et al., 2002). Metolachlor is a pre-emergence chloroacetanilide herbicide, which acts through the inhibition of elongases and gibberellic acid biosynthesis (Munoz et al., 2011). The molecule is chiral, and the (*S*)-enantiomer is used since this shows higher toxicity than the (*R*)-enantiomer (Xie et al., 2010). It is used in the control of annual monocot and dicot weeds, in maize and soybean. Seed applied metolachlor is taken up rapidly in both species, and is acropetally translocated (Scarponi et al., 1992). Its selectivity is afforded by high metabolism in the crops (Scarponi et al., 1992). However, crop damage can occur at certain application rates, and in certain maize cultivars (Li et al., 2017).

A range of studies have focused on understanding the uptake and translocation of agrochemicals, which will be summarised here. For root applied agrochemicals, the uptake generally follows a hyperbolic trend, with an initially high rate tending to a steady state. This is the case for the Safener MG-191 (Jablonkai et al., 1995), and the herbicides, atrazine, atratone, simazine, diuron, 2,4-D (Shone et al., 1974) and cinmethylin (Hsu et al., 1990). While the differences in experimental protocols make it hard to compare the uptake rates of different agrochemicals, there is evidence that uptake is related to physicochemical properties, with more lipophilic chemicals showing greater rates of uptake (Hsu et al., 1990; Shone et al., 1974). Xylem loading and translocation into the aerial tissues, known as acropetal movement, has been demonstrated (Hsu et al., 1990; Jablonkai et al., 1995; Shone et al., 1974; Yenne et al., 1990). For seed applied compounds, basipetal movement via phloem to the roots occurred less than acropetal movement (Yenne et al., 1990). For the Safener MG-191, acropetal movement resulted in compound concentration in the mesocotyl, coleoptile and second leaf (Jablonkai et al., 1995).

3.2 Results

3.2.1 Translocation of safeners

One hypothesis explaining the observed chemical selectivity of safeners, defined by differential metabolic effects with partnered herbicides, was that safeners undergo

differential translocation. It is likely that tissue localisation is an important determinant of efficacy on target herbicides, and safeners have been shown to work in specific tissues, often inducing enzymes differentially in the leaf and stem (Riechers et al., 2003). To test this hypothesis, [^{14}C] -tagged safeners, metcamifen and benoxacor, were applied to maize plants via hydroponic solution at 25 μM , similar to the concentration used in (Brazier-Hicks et al., 2020), for 4.5, 24, 48 and 72 hours before analysing the translocation via phosphorimaging. Dosing through the roots was used to simulate the uptake of pre-emergence herbicides. When harvested, the plants were at the 3 leaf stage (phenological developmental stage identifier BBCH13 (Zadoks et al., 1974)), as shown in Figure 9. Figure 10 shows the position of the harvested plants, and Figure 11 details the radioactivity observed within the plants, associated with the safeners. Together they describe the rate and tissue specificity of the safener translocation. The roots showed high levels of radioactivity, which increased with time until exposure saturation at 48 h. This saturation occurred due to the radiation exposure exceeding the saturation limit of the phosphorimager. This early display of high radioactivity indicated a rapid root uptake of both safeners. It is important to note that while the roots were washed with acetonitrile after removal from the dose solutions, some radioactivity may have remained on the surface resulting in an overestimation of the observed effect. Translocation of both compounds into the aerial tissues occurred as early as 4.5 h, and increased steadily with time. The direction of movement was initially through the stem and the tertiary leaf followed by the secondary leaf and finally the primary leaf. The most concentrated regions at the latest time points are the leaf tips, indicating a consistent movement to the upper tissues. It should be noted that different levels of radioactivity were applied for each of the safeners. This was done to keep equivalent molar concentrations for all treatments to ensure concentration effects on translocation would be eliminated. Since the specific radioactivity (Bq mol^{-1}) varied between the safeners, this resulted in a difference in applied radioactivity. Metcamifen and benoxacor were applied at 45.875 $\text{Bq } \mu\text{L}^{-1}$ and 11.75 $\text{Bq } \mu\text{L}^{-1}$ respectively, representing a total dose of 25 μM safener. Digital measurement of the radiation intensity was performed to correct for the different radioactive doses and allow comparison between safeners. It also allowed for more accurate assessment of the translocation. A plot of the measured radioactive intensity of the aerial tissues, leaves and stem, adjusted for specific activity, plotted against harvest time, is shown in Figure 12. In the aerial tissue (Figure 12.a) the data showed that benoxacor content was greater than that of metcamifen in the aerial tissues at all harvest times. This indicated that benoxacor was more readily translocated

through the plant. The data also indicated that the two safeners did not reach the same concentration in the plant tissues over the tested time frame. Metcamifen reached a maximum uptake at 48 hours, followed by a slight decrease to 72 hours, while benoxacor showed no such plateau. The plots of individual tissues (Figure 12. b and c) indicated benoxacor was present at a higher concentration than metcamifen in both tissues and all time points. In addition the leaf tissues contained more radioactivity than the stem for both safeners. This effect progressed with time, supporting the conclusion of leaf accumulation.

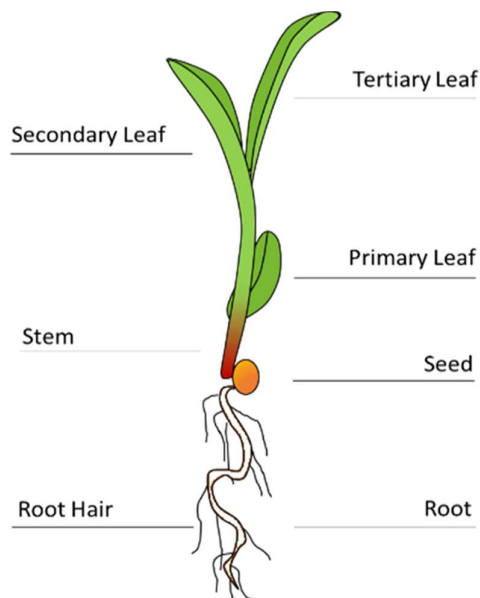


Figure 9: Anatomy of maize plant at 3 leaf stage (phenological developmental stage identifier; BBCH13).

Important descriptions are annotated.

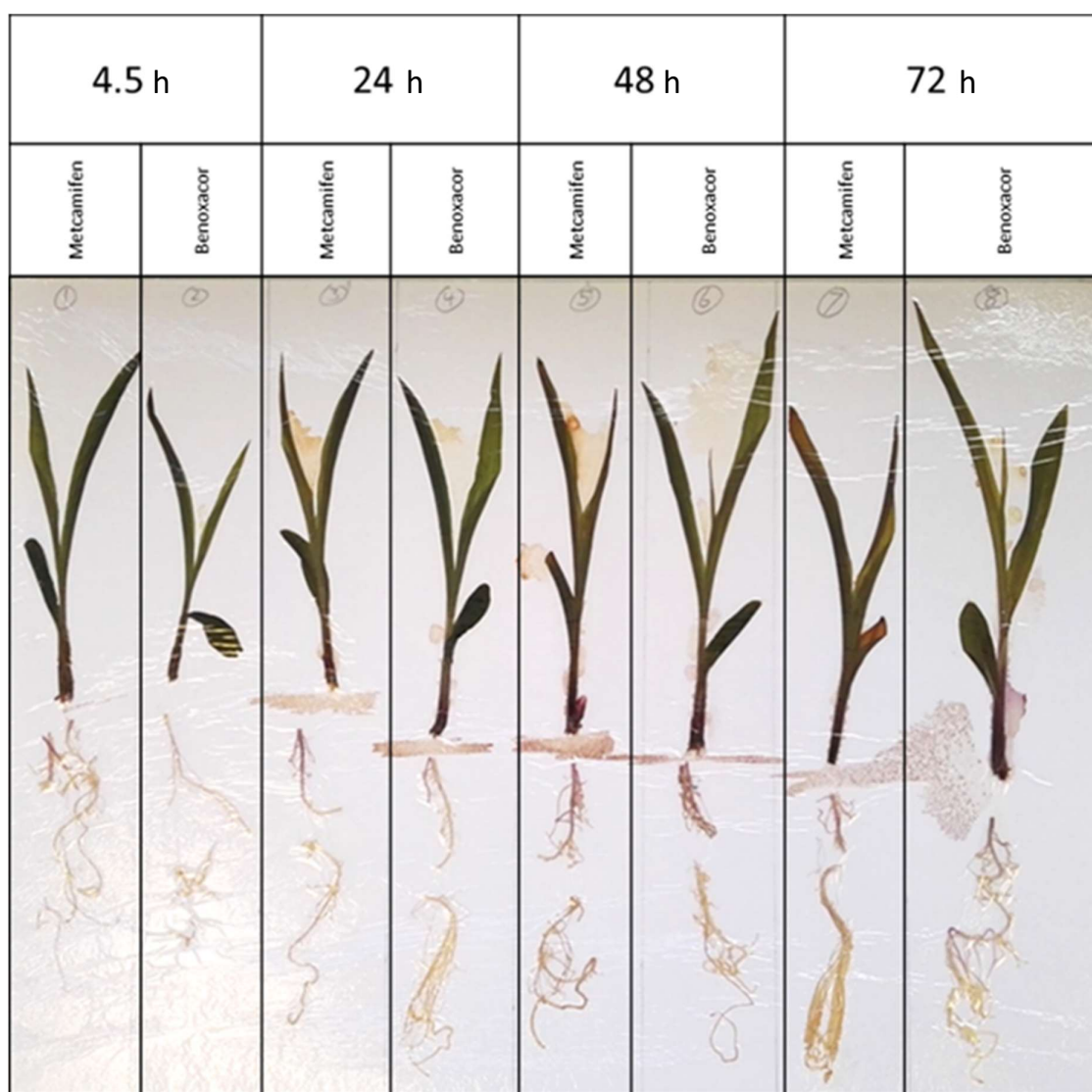


Figure 10: Photograph of maize plants after freeze drying.

Plants grown for 7 days hydroponically were treated with 0.1% (v/v) DMSO containing 25 μ M [14 C]-safener. Plants were harvested at 4.5, 24, 48 and 72 h and freeze dried. Plants are separated at the stem-root interface with the seed removed. Harvest time (h), and safener applied are shown (top).

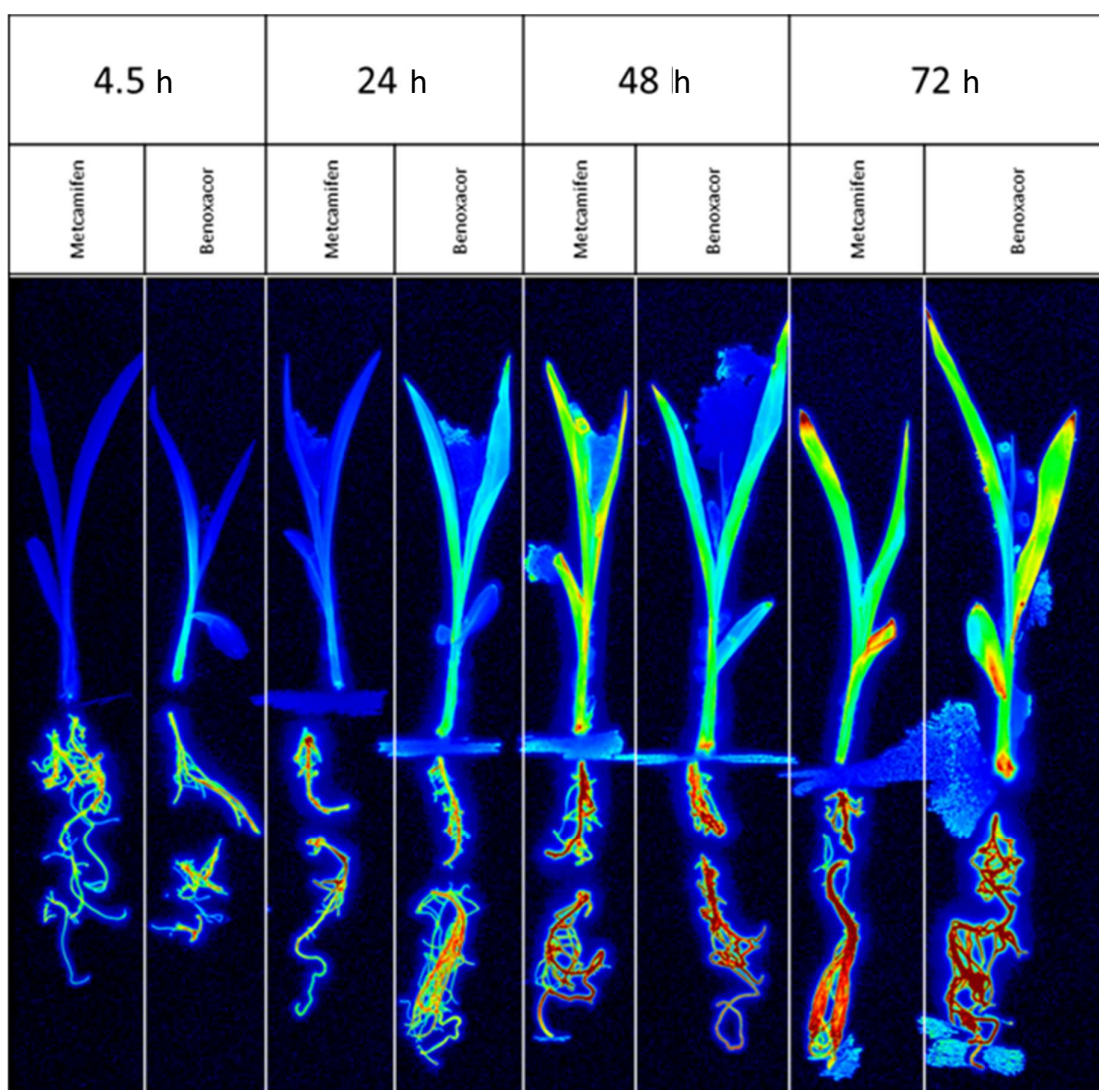
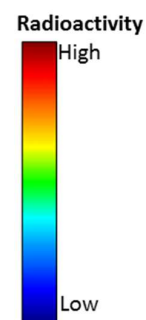


Figure 11: Phosphoimage of maize plants.

Plants grown for 7 days hydroponically were treated with 0.1% (v/v) DMSO containing 25 μ M [14 C]-safener. Plants were harvested at 4.5, 24, 48 and 72 h and freeze dried. Radioactivity was measured by phosphorimaging (film exposure time; 2 d, pixel size; 100 μ m, wavelength 635 nm). Plants are separated at the stem-root interface with the seed removed. Colour chart (bottom right) shows relative degree of radioactivity. Harvest time (h), and safener applied are shown (top).



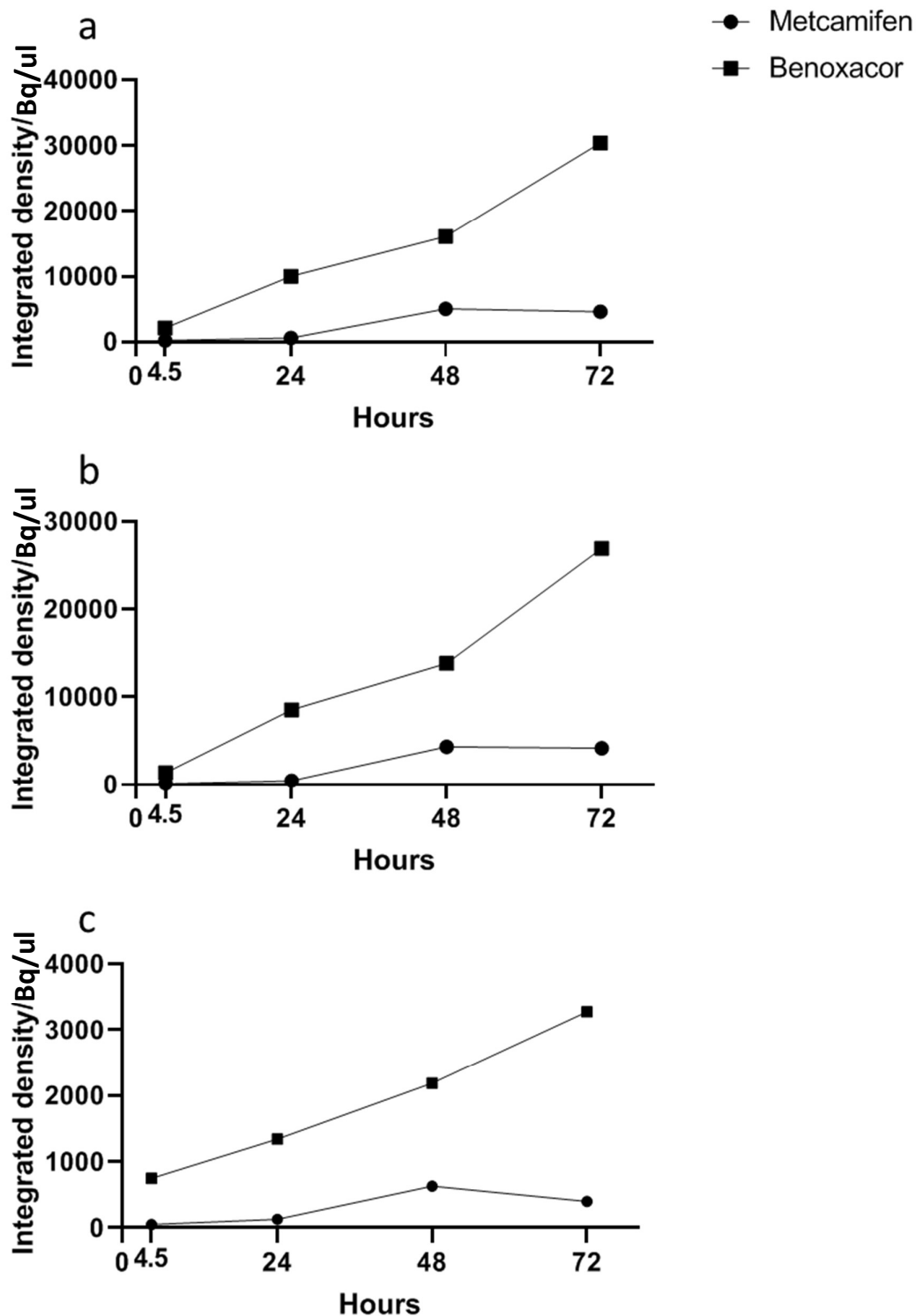


Figure 12: Graphs showing uptake of Safeners in maize plants determined by analysis of Figure 11.

Radiation measured by integrated density of digital image adjusted to specific radioactivity (Bq/ul) is plotted against time of harvest (h). a; Aerial tissues, b; Leaf, c; Stem. Legend shown (top right). Sample number (n) = 1.

The results showed rapid and even translocation of both safeners. This was expected, as it is known that systemically mobile pesticides enter the xylem and distribute uniformly into plant tissues (Deboer et al., 2014). The observed safener aggregation in the leaf margin is also well documented (Deboer et al., 2014). The results clearly indicated different rates of translocation of the two safeners throughout the plants; benoxacor translocated more rapidly than metcamifen in all tissues when applied at the same concentration. This differential uptake and translocation can be understood by investigating their physicochemical properties.

Since this experiment was conducted using hydroponically grown plants with solution-applied safener, root uptake was first investigated. Crossing the root barrier is often considered the limiting step in compound uptake from soil, as the xylem indiscriminately moves compounds to the aerial tissues (Limmer et al., 2014). Molecules may enter the root xylem apoplastically, through cell wall spaces, or symplastically, across cell membranes, but both pathways require passage through cell walls of the Casparian strip, which most severely limits root uptake (Hsu et al., 1990). Limmer et al. (2014) describes the optimum properties for chemical transport across the root barrier, which are summarised in Table 13 along with the chemical properties of metcamifen and benoxacor. The transpiration stream concentration factor (TSCF) is used as a measure of translocatability across the root barrier and is used here to describe root uptake. Values with higher TSCF will be more likely to be taken up through the root.

	LogKow/ LogP	Molecular Mass (Da)	Hydrogen Bond Donors	Hydrogen Bond Acceptors	Polar Surface Area (Å ²)	Rotable bonds
Optimum	1-4	<350	<4	<7	<90	<7
metcamifen	1.49 ^a	363.388 ^b	3 ^a	8 ^b	122 ^b	5 ^a
benoxacor	3.19 ^a	260.116 ^a	0 ^a	3 ^a	30 ^a	1 ^a

Table 13: Physicochemical properties of metcamifen and benoxacor, and optimum properties for root translocation.

Superscripts describe values: a; within optimum range, b; without optimum range. Physicochemical property data for metcamifen and benoxacor was taken from Chempider, predicted ACD/Labs. Molecular mass (Da) and polar surface area (Å²) are shown.

The octanol-water partition coefficients (logKow/LogP) of both safeners fall within the optimum range for translocation and Limmer et al. (2014) suggested there is little difference between logKow of 1-2 or 3-4. This indicates that the octanol-water partition coefficient of the safeners would not significantly contribute to their observed differences in translocation. Hsu et al. (1990) however, suggested that in hydroponic experiments, a logKow of 3-4 is significantly more effective at root to shoot translocation than a logKow of 1-2, which would

help to explain the increased uptake of benoxacor. In addition, logKow is used for un-ionized solutes, and when taking the pH of solutions into account, distribution coefficient (logD) is typically used (Manners et al., 1988). Taking into account the pH of the hydroponic solution (~5), the logD values for metcamifen and benoxacor are 0.28 and 2.8, respectively, at pH 5.5. This indicates a lower lipophilicity of metcamifen than benoxacor at the pH used, which may reduce its translocatability. Therefore, the distribution coefficients may, in part, explain the differences in observed safener uptake. The molecular mass of benoxacor, unlike that of metcamifen, is within the optimal range for root translocation. While metcamifen is close to the 350 Da limit, Limmer et al. (2014) described values of 250-300 Da as more suitable for system mobility than 350-400 Da showing a 29 times higher average TSCF. This value would predict that benoxacor was the more translocatable chemical. Both metcamifen and benoxacor have hydrogen bond donors within the optimal range of 0-4. However, Limmer et al. (2014) described the optimal value as 0, showing 4.3 times higher TSCF than 3. In addition benoxacor, unlike metcamifen, has a number of hydrogen bond acceptors that falls within the optimum range of 0-7, with values for benoxacor displaying a TSCF value 180 times higher than metcamifen. As such benoxacor has a hydrogen bond acceptor and donor number more suitable for translocation, than metcamifen. The polar surface area of benoxacor (25-50 Å²) falls within the ideal range of 0-90 Å² and predicting a TSCF value at least 6.6 times higher than that of metcamifen (100-125 Å²) (Limmer et al., 2014). Therefore the polar surface area of benoxacor is more suitable for translocation than metcamifen. Both metcamifen and benoxacor have rotatable bond numbers within the optimal range of 0-7. However, the value displayed by benoxacor has a TSCF value 1.7 times higher than that of metcamifen which is slightly more suitable for translocation (Limmer et al., 2014). Taken together all of these data suggest benoxacor as more translocatable through the root barrier than metcamifen. This provides support for the hypothesis that the physicochemical properties of the safeners are contributing to the differences in translocation observed, through differential loading of the root tissue during primary uptake.

While this study was performed hydroponically, and may not accurately replicate the effects in the field, benoxacor is generally used in pre-emergence products, and metcamifen is used in seed treatments (Su et al., 2019 ; Syngenta personal comm.). Therefore the roots would be the primary uptake route of both safeners. Since the safeners were applied via the roots, phloem transport ability was unlikely to affect translocation, since the phloem directs

compounds mostly basipetally (Deboer et al., 2014). Xylem transport could play a further role in differential translocation from the roots to the aerial tissue, though benoxacor and metcamifen are predicted to be equally xylem mobile, as their logKow values fall within the optimal range of 1 to 4 (Deboer et al., 2014).

In conclusion, differences in translocation were observed with the two safeners, providing a potential basis for differential safening with different herbicide partners.

3.2.2 Effect of safeners on herbicide metabolism

It is important to know whether safeners cause an enhancement of metabolism through increased flux of existing pathways, or through activation of differential metabolic routes, especially when considering their registration. In order to investigate this relationship, the effect of two safeners, benoxacor and metcamifen, on the metabolism of two herbicides, mesotrione and S-metolachlor, were tested in hydroponically grown maize plants. This was performed over 72 hours, with metabolism monitored in separate plant tissues. The hypothesis being tested was that certain safener-herbicide combinations would be more effective than others. This would give an insight into the mechanisms of chemical specificity of safeners. In addition, the longevity of the safening effect and route of metabolism could be determined, along with whether tissue specificity could explain chemical specificity.

The metabolism of S-moc and mesotrione was investigated in hydroponically grown maize, treated with either metcamifen or benoxacor. Root, stem and leaf tissues were harvested after 4.5, 24, 48 and 72 hours of treatment. Samples were extracted and analysed for radioactive content by liquid scintillation counting (LSC), and for metabolic profile by radio-thin layer chromatography (TLC).

3.2.2.1 Uptake of dose solution and herbicide

To determine dose solution uptake, the volume remaining after harvest was determined by weighing, and subtracted from the applied volume. As shown in Figure 13, the uptake was consistent for all safener and herbicide treatments, at around 2 mL per day. There was no statistical difference in uptake volume between safener treatments. The numerical data and supporting statistics are shown in Table S 1 and Table S 2, respectively.

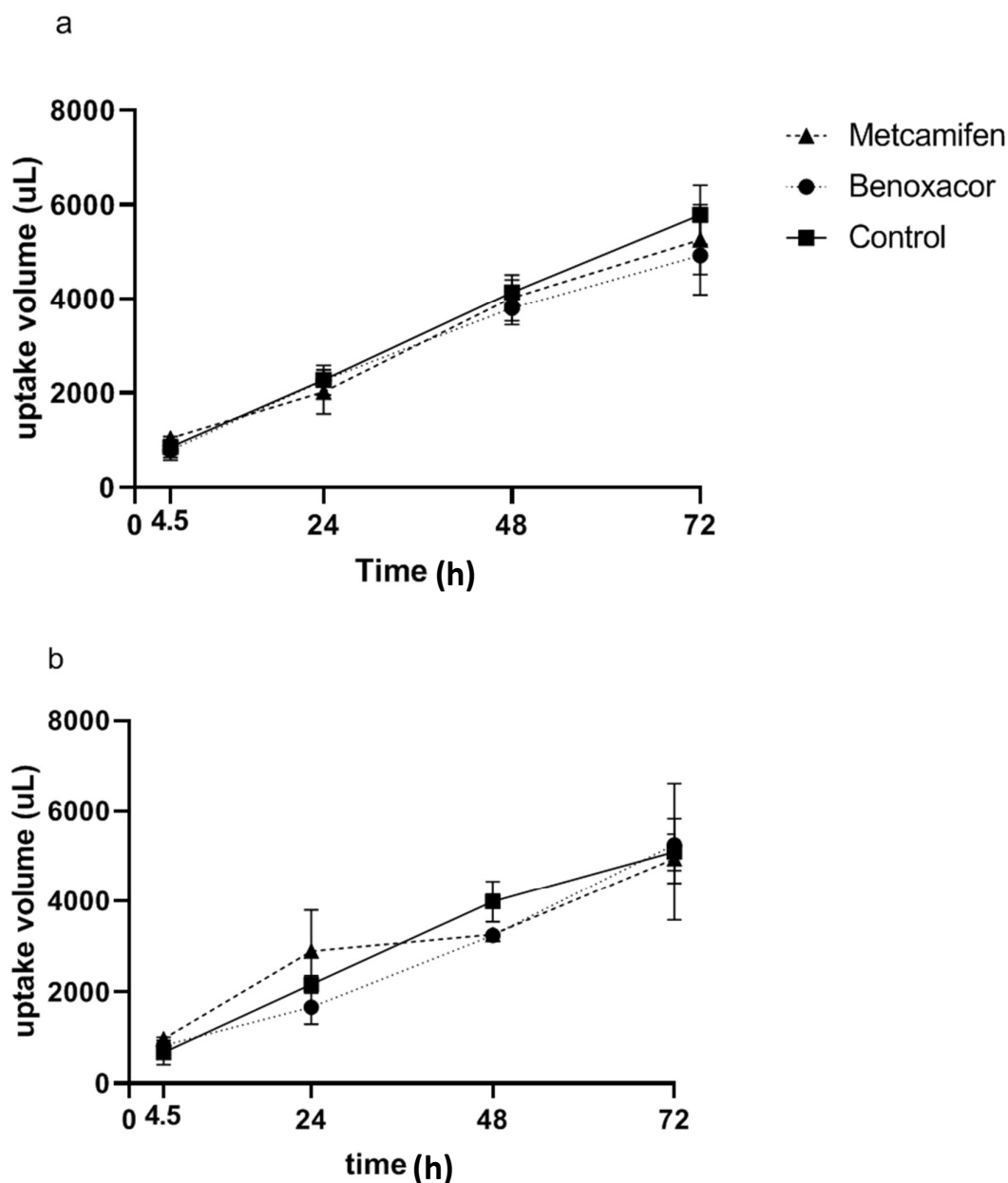


Figure 13: Graphs showing the uptake of dose solution (μL) in maize plants over time (h). 7 day old maize plants were treated with 0.1% (v/v) DMSO containing 25 μM a; [^{14}C]-Mesotrione or b; [^{14}C]-S-metolachlor and 25 μM Safener or no safener control as described in the legend (top right). Plants were harvested at 4.5, 24, 48 and 72 h. Remaining dose solution was measured by weighing. Results represent mean values and standard deviation ($n = 3$).

To determine consistency of radioactive herbicide uptake, the ratio of compound to volume taken up ($\text{kBq } \mu\text{L}^{-1}$) was calculated (Figure 14). The radiation uptake was calculated by subtraction of the acetonitrile wash and remaining dose solution counts from the applied radioactivity. This value was divided by the volume taken up. There was no statistical difference in uptake ratio between safener treatments. The numerical data and the supporting statistics are shown in Table S 3 and Table S 4, respectively. It has previously been shown that

certain safeners affect herbicide uptake whilst others have no effect, though any differences are unlikely to be responsible for safener protection (Jablonkai, 2013). Interestingly, while mesotrione is taken up in a consistent ratio, the uptake ratio of *S*-moc decreased over time, suggestive of associated plant damage. When the uptake ratio was taken as a percentage of applied concentration, mesotrione was taken up below 100%, indicating solution is taken up more readily than compound. *S*-moc however showed an uptake concentration of 283-431% at 4.5 h, decreasing to 71-85% at 72 h, indicating an initial preferential uptake of compound, switching to a preference for solution over time.

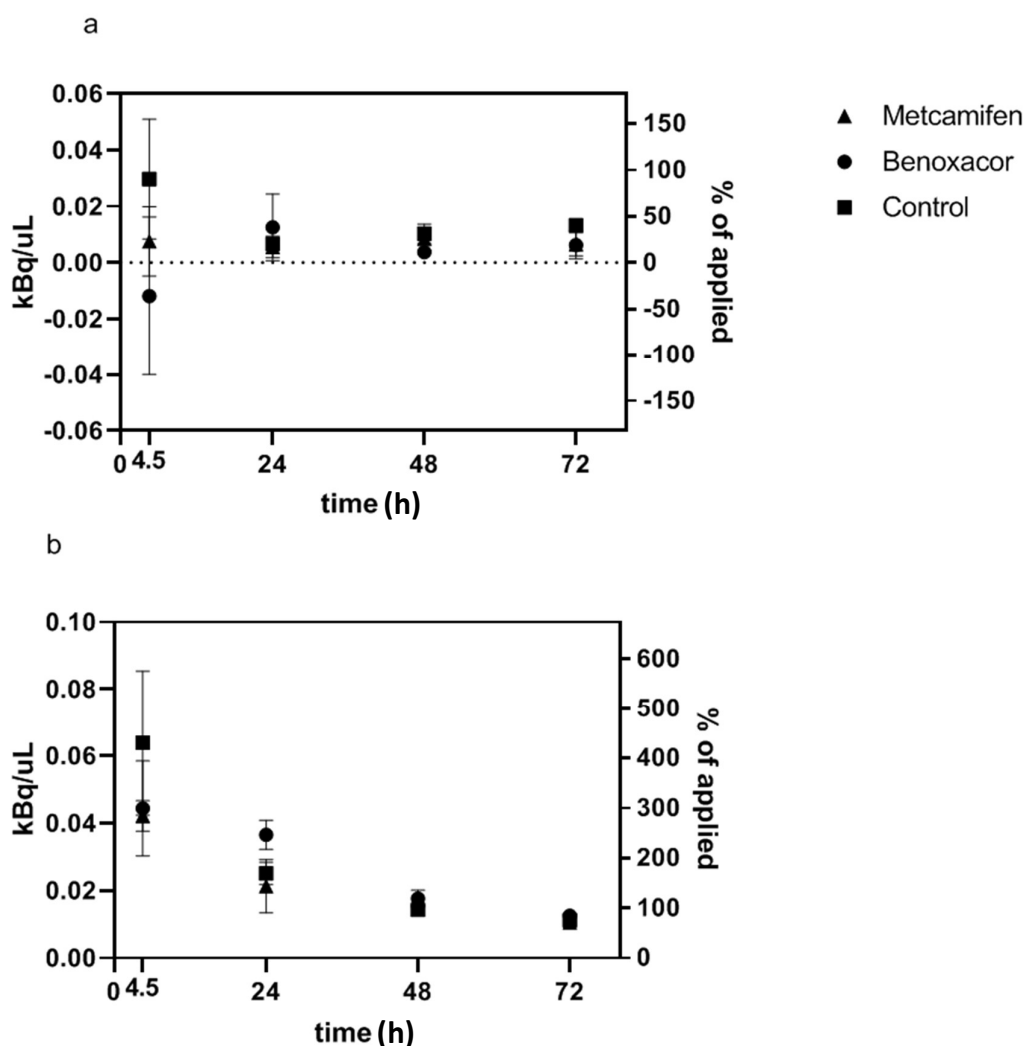


Figure 14: Graphs showing the uptake of radioactive herbicide (kBq μL^{-1}) over time (h).

Uptake also shown as percentage of applied concentration (secondary Y-axis). 7 day old maize plants were treated with 0.1% (v/v) DMSO containing 25 μM a; [^{14}C]-Mesotrione or b; [^{14}C]-*S*-metolachlor and 25 μM Safener or no safener control as described in the legend (top right). Plants were harvested at 4.5, 24, 48 and 72 h. Radioactive uptake determined by liquid scintillation counting of remaining dose solution and acetonitrile wash. Results represent mean values and standard deviation ($n = 3$).

As with the safener translocation, the physicochemical properties of the herbicides may explain their differential uptake rates (Table 14). Since *S*-moc was taken up into the plants at a higher rate than mesotrione, it would be expected that *S*-moc would possess more optimal physicochemical properties for uptake as described by Limmer et al. (2014).

As expected, the octanol-water partition coefficient (logKow/LogP) of *S*-moc falls within the optimal range, while mesotrione does not. Taking into account the pH of the hydroponic solution (~5), the logD values of *S*-moc and mesotrione are 3.21 and -1.27, respectively. The negative value of mesotrione indicates poor membrane permeability as compared to *S*-moc. Both herbicides fall within the optimum molecular mass range, though the mass of *S*-moc (284 Da) is considered more effective for system mobility than that of mesotrione (339 Da), with a TSCF approximately 2 times greater (Limmer et al., 2014). Both herbicides possess the same number of hydrogen bond donors, considered optimal for root uptake, though only *S*-moc has a number of hydrogen bond acceptors within the optimal range for membrane permeation (Limmer et al., 2014). The polar surface area of *S*-moc also falls within the optimal range, whereas mesotrione does not (Limmer et al., 2014). In contrast while both herbicides possess rotatable bond numbers within the optimal range, the value of mesotrione (4) indicates better translocatability than that of *S*-moc (6), with a TSCF 4 times higher (Limmer et al., 2014). Thus most of the physicochemical properties suggest *S*-moc would have improved root uptake as compared to mesotrione, consistent with the observed uptake rate.

	LogKow/ LogP	Molecular Mass (Da)	Hydrogen Bond Donors	Hydrogen Bond Acceptors	Polar Surface Area (Å ²)	Rotatable bonds
Optimum	1-4	<350	<4	<7	<90	<7
Mesotrione	-0.70 ^b	339.320 ^a	0 ^a	8 ^b	140 ^b	4 ^a
<i>S</i>-metolachlor	3.00 ^a	283.794 ^a	0 ^a	3 ^a	30 ^a	6 ^a

Table 14: Physicochemical properties of mesotrione and *S*-metolachlor and optimum properties for root translocation.

Superscripts define values: a; within optimum range, b; without optimum range. Physicochemical property data for metcamifen and benoxacor was taken from Chemspider, predicted ACD/Labs. Molecular mass (Da) and polar surface area (Å²) are shown.

3.2.2.2 Radioactive recovery

The recovery of radioactivity was determined through LSC analysis of individual or combined extractions, remaining dose solution and wash samples, followed by comparison with the applied radioactivity. The overall and specific recovery rates are shown in Figure 15. The optimal recovery was considered 100% ± 30%, which was met by 22 of 24 samples. The

recovery in the remaining dose solution was generally highest in the earlier samples, due to low uptake of solution. The wash solution contained a significant proportion of the recovered radioactivity at $15.4 \pm 9.5\%$ (mean \pm standard deviation). In all cases the root showed the highest proportion of recovered radioactivity among the tissues. This is not unexpected, since the roots were in constant contact with the dose solution and would likely be the limiting step for uptake. In addition root washing may not have been completely effective in removing all root-bound compound. In all but two cases, leaf extracts contained more radioactivity than stem extracts. This may be a function of tissue mass, or may represent the accumulation of compound in the most aerial regions of the plant as a result of constant xylem transport.

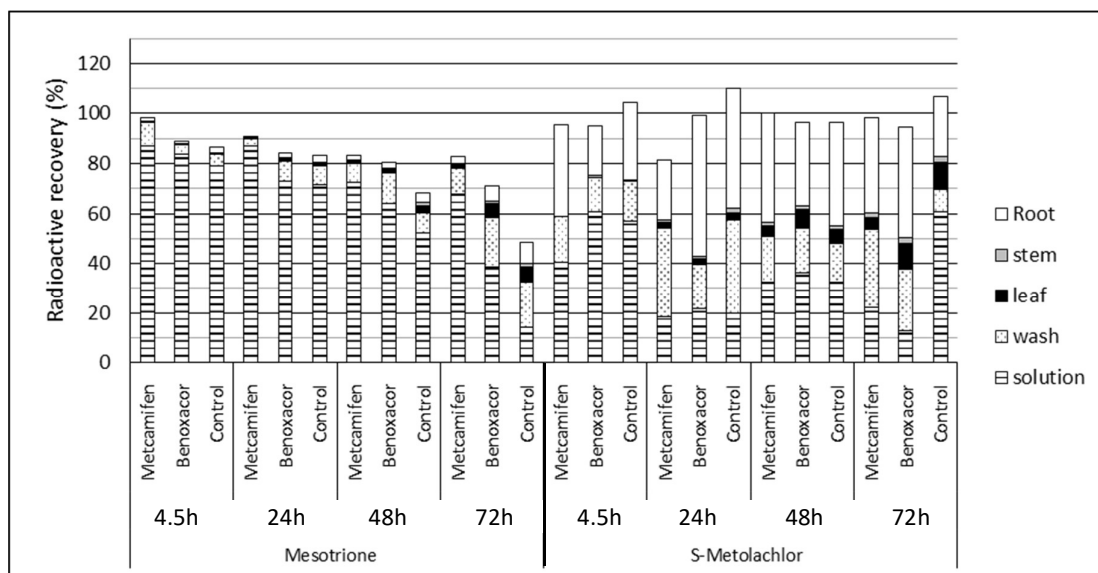


Figure 15: Bar chart showing the radioactive recovery of samples (%), over time (h).

7 day old maize plants were treated with 0.1% (v/v) DMSO containing 25 μM a; [^{14}C]-Mesotrione or b; [^{14}C]-S-metolachlor and 25 μM Safener or no safener control. Plants were harvested at 4.5, 24, 48 and 72 h. Recovery of radioactivity was determined through liquid scintillation counting of extractions, acetonitrile washes and remaining dose solutions. Y-axis describes extractable radiation as a percentage of applied radiation. X-axis describes time of harvest (h) and treatment. Legend (right) describes subsamples. Data represents means ($n = 3$).

3.2.2.3 Mesotrione TLC method development

The [^{14}C]-mesotrione-treated plant extracts were chromatographed by TLC using a mobile phase consisting of chloroform:ethyl acetate:methanol:formic acid (30:20:20:2 (v/v)). In order to validate this TLC system, and ensure metabolite separation, non-radioactive mesotrione and reference metabolites were analysed. Figure 16 shows the relative position of metabolite standards using the TLC system. Figure 17 shows a representative TLC phosphorimage of radioactive samples co-chromatographed with a non-radioactive standard mixture, visualised

under UV light (254 nm). Standard spot separation was found to be satisfactory, and alignment with radioactive bands clear and defined.

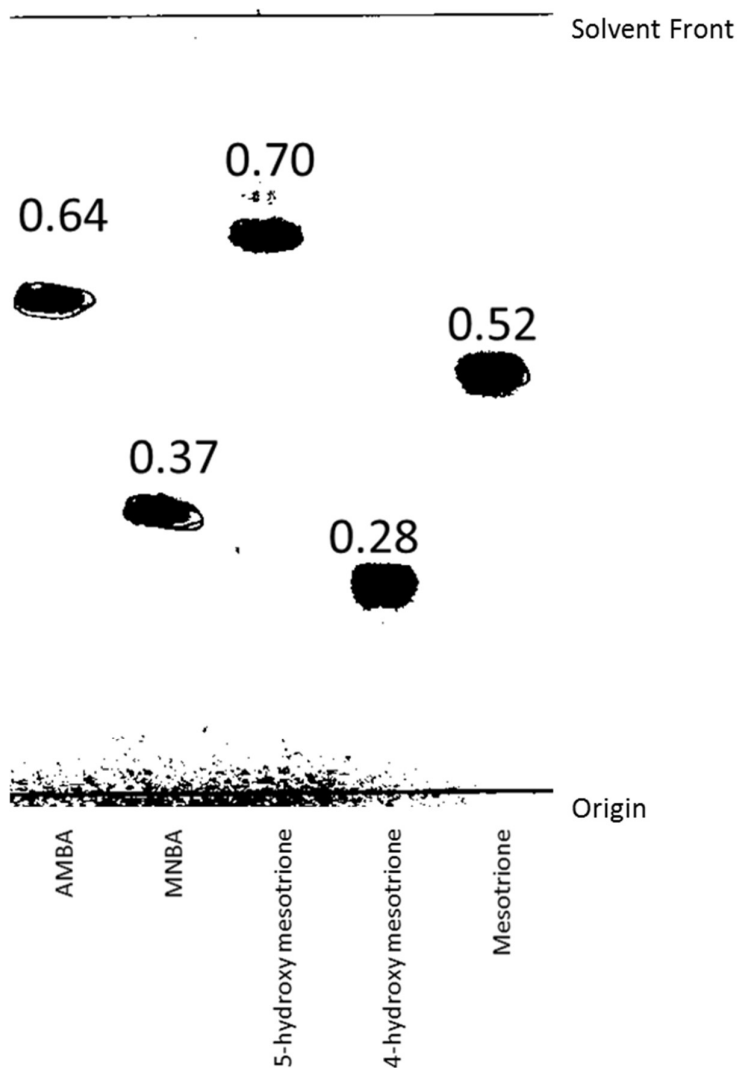


Figure 16: Ultraviolet (UV) image of thin layer chromatograph (TLC) of mesotrione standards.

Mesotrione standards applied to TLC plate at 5 μ l. Mobile phase; Chloroform:ethyl acetate:methanol:formic acid (30:20:20:2 (v/v)). X-axis describes mesotrione metabolite standards. Values represent retention factor (R_f) values. Origin and solvent front lines are shown.

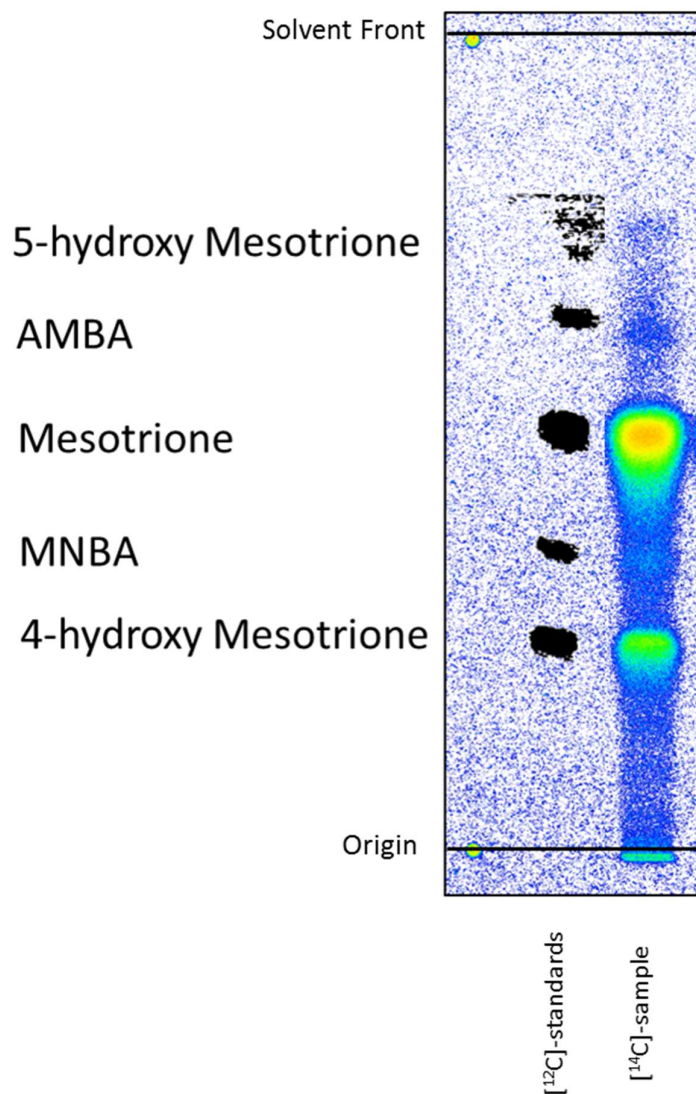


Figure 17: Phosphorimage of thin layer chromatograph (TLC) containing a [^{14}C]-sample and superimposed [^{12}C]-mesotrione metabolite standards.

Standard applied at 5 μl . Sample (Mesotrione and benoxacor treatment, 24 h harvest, root tissue) applied at 50 Bq. Y-axis describes mesotrione metabolites. X-axis describes sample/standard. Origin and solvent front lines are shown. Mobile phase; Chloroform: ethyl acetate: methanol: formic acid (30: 20: 20: 2 (v/v)).

3.2.2.4 *S-metolachlor* TLC method development

In order to determine the best TLC system, non-radioactive *S*-moc and reference metabolites were analysed via two-dimensional TLC, utilising two mobile phases, to find conditions optimal for spot separation of sample metabolites. Figure 18 shows the separation of *S*-moc and metabolites using the 2D-TLC system. The system was first run using chloroform:methanol:water:formic acid (75:25:4:2 (v/v)), then using ethyl acetate:n-

propanol:water (64:24:12 (v/v)). Due to the higher degree of spot separation using the first mobile phase, compared to the second, this was chosen for subsequent analyses. In order to validate this TLC system and assign R_f values for regions of interest (ROI), non-radioactive *S*-moc and respective metabolites were analysed (Figure 19). Resolution of the spots was found to be difficult due to the high number of metabolites present.

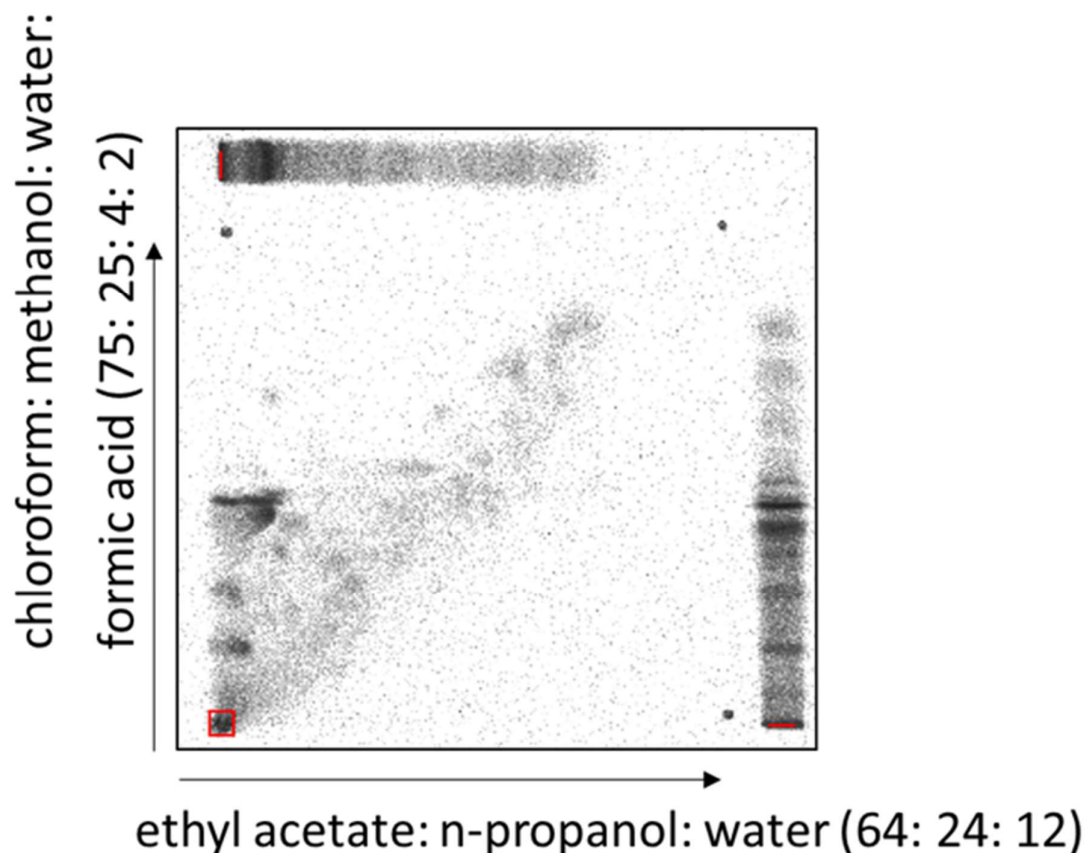


Figure 18: Phosphorimage of two dimensional thin layer chromatograph (TLC) test of [¹⁴C]-*S*-metolachlor sample.

Axes indicate mobile phase (v/v). Mobile phase direction and length are shown with arrows. 100 Bq sample (*S*-Metolachlor and no safener control treatment, 72 h harvest, Leaf tissue) applied, as indicated by the red lines/square (area to scale). The system was first run using chloroform:methanol:water:formic acid (75:25:4:2 (v/v)), then using ethyl acetate:n-propanol:water (64:24:12 (v/v)).

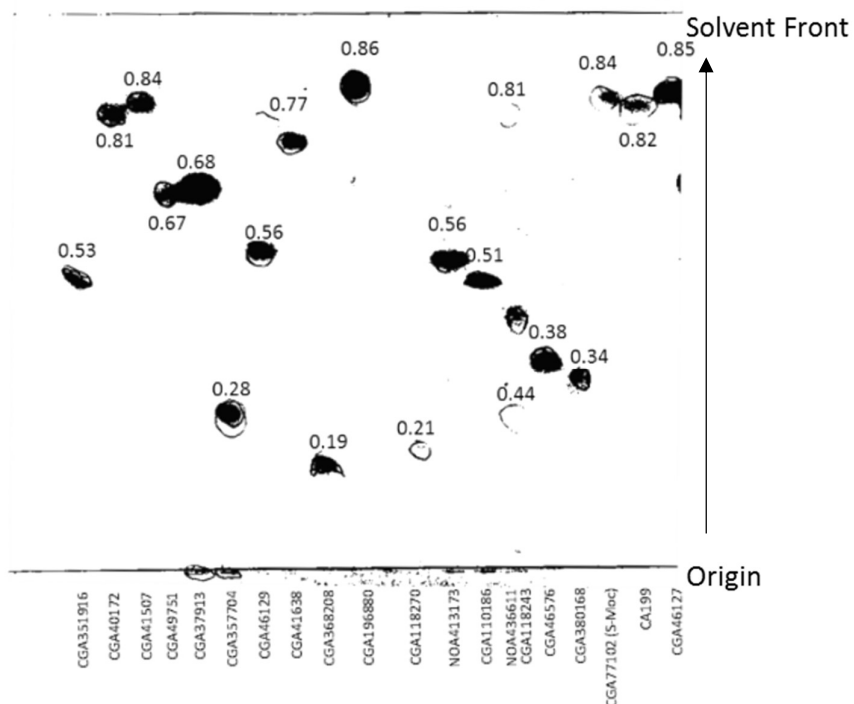


Figure 19: Ultraviolet (UV) image of thin layer chromatograph (TLC) of *S*-metolachlor non-radioactive standards.

Values represent retention factor (*R_f*) values. Origin and solvent front lines are shown. Arrow describes solvent direction. X-axis describes *S*-metolachlor degradation products shown in Table S 10. Mobile phase; Chloroform: methanol: water: formic acid (75: 25: 4: 2 (v/v)).

3.2.2.5 Effect of safeners on mesotrione metabolism

The metabolism of mesotrione in maize is shown in

Figure 20, based on metabolic studies carried out by Syngenta (personal comm.) and as reported in limited studies (Joy et al., 2009; Low et al., 2014). A comprehensive list of possible metabolites (Table S 9), was used to identify the metabolites in the plant extracts. Only oxidative metabolism is known, the primary reaction being hydroxylation of mesotrione (ZA1296) to 4-hydroxy-mesotrione (R282813) which results from cytochrome P450-catalysed aromatic hydroxylation of ring 2 C3. Mesotrione, or 4-hydroxy-mesotrione, is then oxidised to MNBA (4-methylsulfonyl-2- nitrobenzoic acid/NOA437130) formed via oxidative cleavage between the two rings, thereby removing the 1,3-Cyclohexanedione moiety. Finally, the nitro group of MNBA is reduced to the amide, producing AMBA (2-amino-4-methyl sulfonyl benzoic acid/R044276). AMBA may then be further conjugated. A 5-hydroxy metabolite of mesotrione has also been identified in mouse and rat, and was therefore included (Low et al., 2014).

Though its placement in the pathway is not confirmed, it can be assumed to be caused by direct hydroxylation of mesotrione (Alferness et al., 2002; Low et al., 2014).

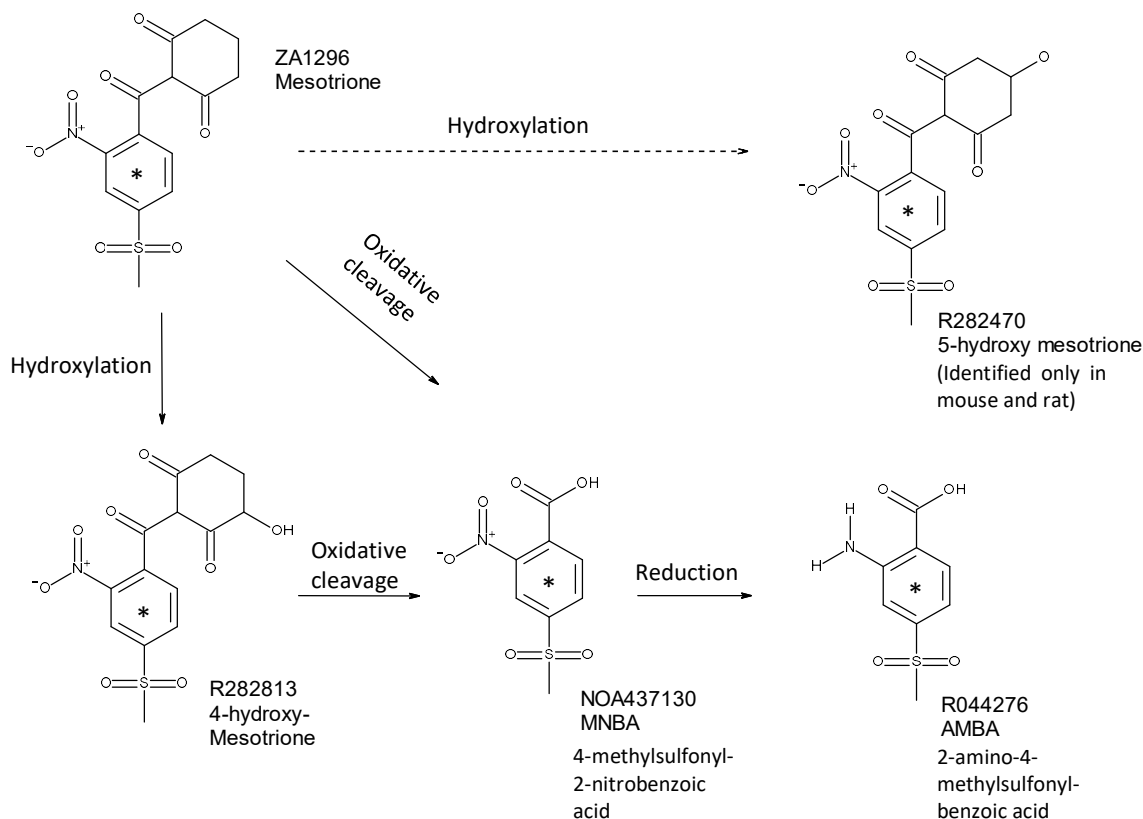


Figure 20: Schematic describing oxidative metabolism of mesotrione in plants.

* denotes position of ^{14}C . Dashed arrows indicate pathways with possible intermediates. Figure 21 shows the mesotrione parent and metabolite quantification in the current maize study. The numerical data and statistics are described in Table S 5 and Table S 6, respectively. Figure S 1 shows the TLC phosphorimages from which the data was extracted.

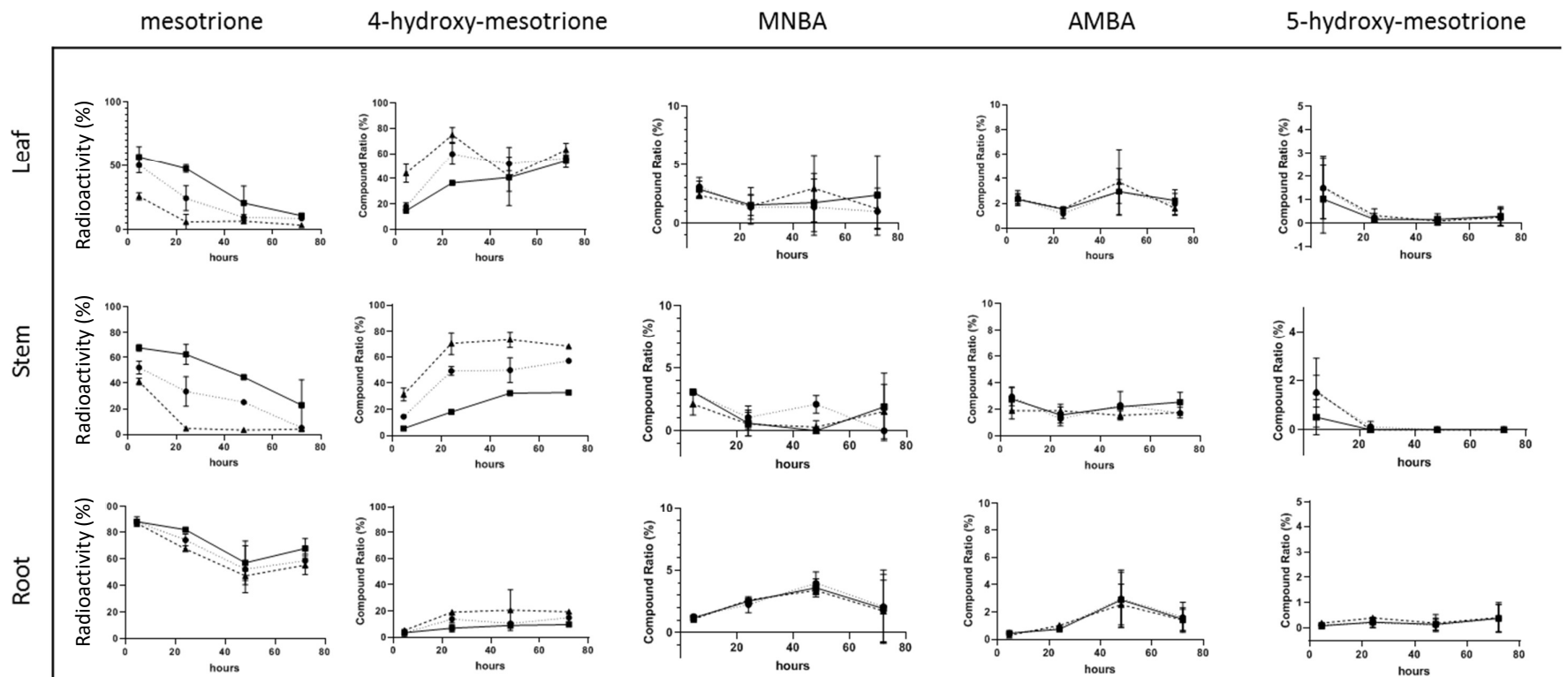


Figure 21: Graphs showing the effect of metcamifen and benoxacor safeners on the metabolism of mesotrione in different tissues, over time (h).

- 1 7 day old maize plants were treated continuously via roots with 0.1% DMSO (v/v) containing 25 μ M [14 C]-mesotrione and 25 μ M
- 2 Safener or no safener control as described by the legend (bottom right). Plants were harvested 4.5, 24, 48 and 72 h after
- 3 application. Each metabolite is shown as a percent of total radioactivity. Results represent means with standard deviations (n =
- 4 3).

--▲-- Metcamifen
●..... Benoxacor
 —■— Control

The results indicate that mesotrione was metabolised in the stem and leaf moderately quickly, showing approximately 50% detoxification between 4.5 and 72 hours, with a slightly faster rate observed in the leaf tissue. The trend suggests the metabolism would be complete at 90-100 hours. Less metabolism was observed in the root tissues, ranging from 10% to 40% metabolism between 4.5 and 48 hours. Interestingly, the levels of parent mesotrione increased by 10% of the dose between 48 and 72 hours in the root, reflecting continuous uptake of herbicide from the application solution, combined with a reduction in root metabolism. In all tissues, the appearance of the primary metabolite, 4-hydroxy-mesotrione, mirrored the decrease in parent mesotrione, increasing in content by 40% in the leaf and 30% in the stem, between 4.5 and 72 hours. However, the trend did not account for all of the metabolism of the parent. The root showed a 5% content increase in 4-hydroxy-mesotrione between 4.5 and 72 hours, which does not mirror the loss of parent, supporting the hypothesis of continuous herbicide uptake in the roots. The downstream metabolites, MNBA, AMBA and 5-hydroxy-mesotrione, accounted for only a small percentage of the overall metabolite profile. The secondary metabolite, MNBA, showed little change in the leaf over time, but displayed a minor biphasic trend in the stem. MNBA generation in the root displayed a parabolic trend, which accounts, in part, for the decrease in mesotrione parent. Similarly, the downstream metabolite, AMBA, contributes little to the metabolite profile. Little change in AMBA content is observed in the leaf over time, though does produce a biphasic trend in the stem. In the root, AMBA displays a parabolic trend, again accounting for some of the mesotrione parent metabolism. 5-hydroxy-mesotrione made almost no contribution to the metabolite profile, and may be considered a trace component. No differences in content can be observed over the time course.

The results indicate that metcamifen increased the metabolism of mesotrione in the leaf and stem tissues, as seen in previous studies (Syngenta personal comm.). The detoxification of mesotrione parent was significantly improved with metcamifen application at all time points in the aerial tissues. The lack of statistical significance in the leaf 48 hour samples and stem 72 hour samples was likely due to a high variation in the control samples, as metcamifen still caused a 14% and 18% increase in mesotrione detoxification, respectively. At all time points, metcamifen caused a decrease in mesotrione parent in the root tissue, though this effect was small and rarely significant. Only the 24 hour harvest time displayed a significant effect, with a 15% decrease (adjusted $p = 0.00$) in parent observed. It can therefore be gathered that

metcamifen detoxified mesotrione mainly in the aerial tissues. The increased metabolism of mesotrione in these tissues began as early as 4.5 hours and persisted to 72 hours. If the trends between 48 and 72 hours continued, the effect of metcamifen would be predicted to terminate at 99 hours at 0% parent in the leaf, and at 92 hours at 5% parent in the stem. Therefore, it is unlikely that metcamifen would cause any differences in parent mesotrione content at the time of crop harvest. Metcamifen caused an increase in 4-hydroxy-mesotrione levels, closely mirroring the detoxification of parent mesotrione. In the leaf, the appearance of 4-hydroxy-mesotrione was increased significantly at 4.5 and 24 hours, indicating that the effect was most prominent during the first two days of treatment. There was no significant effect of metcamifen in the leaf after 48 or 72 hours of treatment. In the stem, metcamifen caused a significant increase in 4-hydroxy-mesotrione at all time points, which closely mirrored the disappearance of parent mesotrione. This indicates that the effect of metcamifen began as early as 4.5 hours and may have lasted beyond three days. In the root, the levels of 4-hydroxy-mesotrione were increased all time points, though as with the parent, showed a lack of significance at many times. However, significant increases in 4-hydroxy-mesotrione of 12% (adjusted $p = 0.04$) and 10% (adjusted $p = 0.01$) were observed at 24 and 72 hours, respectively. This suggested some enhanced metabolism of mesotrione with metcamifen treatment in the root, though confirmation would require further study. Metcamifen caused no significant effect on the formation of the remaining metabolites, MNBA, AMBA or 5-hydroxy mesotrione, which existed in very low abundance in all tissues, irrespective of safener treatment.

The effect of benoxacor on mesotrione has not previously been reported, or compared with that of metcamifen. The results presented here indicate that benoxacor increased the metabolism of mesotrione. In the leaf, the detoxification of parent mesotrione was considerable, though not statistically significant at any reported harvest times. This lack of significance is likely due to the high degree of variation between biological samples. The largest effect on mesotrione metabolism occurred at 24 and 48 hours, suggesting a very transient effect. By extending the trend of 48 and 72 hours, the predicted termination of the benoxacor effect would be 77 hours, with 8% parent. In the stem, benoxacor caused an increase in mesotrione metabolism at all times, though not statistically significant at 72 hours. The complete metabolism of the parent was predicted to occur shortly after 72 hours, even without benoxacor. In the root tissue, benoxacor caused no statistically significant changes to

the metabolism of mesotrione. Small increases in 4-hydroxy mesotrione were observed with benoxacor treatment, mirroring the disappearance of parent mesotrione. In the leaf, benoxacor treatment resulted in increased 4-hydroxy mesotrione at all time points, though these were only statistically significant at 24 hours. Benoxacor produced a larger effect in the stem, causing a significant increase in 4-hydroxy mesotrione levels at 4.5 and 24 hours. As with the parent mesotrione, 4-hydroxy mesotrione levels were unaffected by benoxacor in the root tissue. The remaining metabolites, MNBA, AMBA and 5-hydroxy mesotrione, were unaffected by benoxacor at all times in all tissues, indicating the safener worked mainly by enhancing the first metabolic step.

Metcamifen caused a greater detoxification of mesotrione than benoxacor at all times, statistically significant at 4.5 hours in the leaves, and 4.5, 24 and 48 hours in the stem. This difference in tissue response may be explained by a lower abundance of safener in the leaves due to incomplete translocation. There was no difference between individual safener effects in the root, since no enhanced metabolism occurred with either safener. Similarly, metcamifen caused a greater generation of 4-hydroxy-mesotrione than benoxacor, statistically significant at the same time points. There was no difference between safener effects on 4-hydroxy-mesotrione levels observed in the root. There was no observed effect between the two safeners with respect to the generation of metabolites, MNBA, AMBA or 5-hydroxy-mesotrione, since neither safener had any effect compared to the control.

3.1.1.1 *Effect of safeners on S-metolachlor metabolism*

The metabolism of *S*-moc has previously been studied (Syngenta personal comm.) and the pathways in maize are shown in Figure 22 and Figure 23. A comprehensive list of possible metabolites, shown in Table S 10, was used to identify the metabolites in the plant extracts. *S*-moc is able to undergo oxidative or glutathione-mediated metabolism. The oxidative metabolism pathway (Figure 22) begins with a nucleophilic substitution of the chlorine of *S*-moc (CGA77102) to a hydroxyl group, producing CGA40172. Alternatively, the chlorine group is removed by dehalogenation, producing CGA41507. In a third reaction, the ether group is converted into a hydroxyl group forming CGA41638. Further downstream metabolism exists but will not be discussed in detail. The glutathionylation-mediated metabolism of *S*-moc (Figure 23) occurs by two main paths. In one pathway, a series of reactions causes cleavage of two nitrogen-bound groups, producing CGA212245. In the main pathway, *S*-moc is converted into its glutathione conjugate (CGA119393) by nucleophilic substitution of the chlorine atom

of S-moc by the sulphur atom of the glutathione molecule. Further metabolism of this conjugate occurs, but will not be discussed.

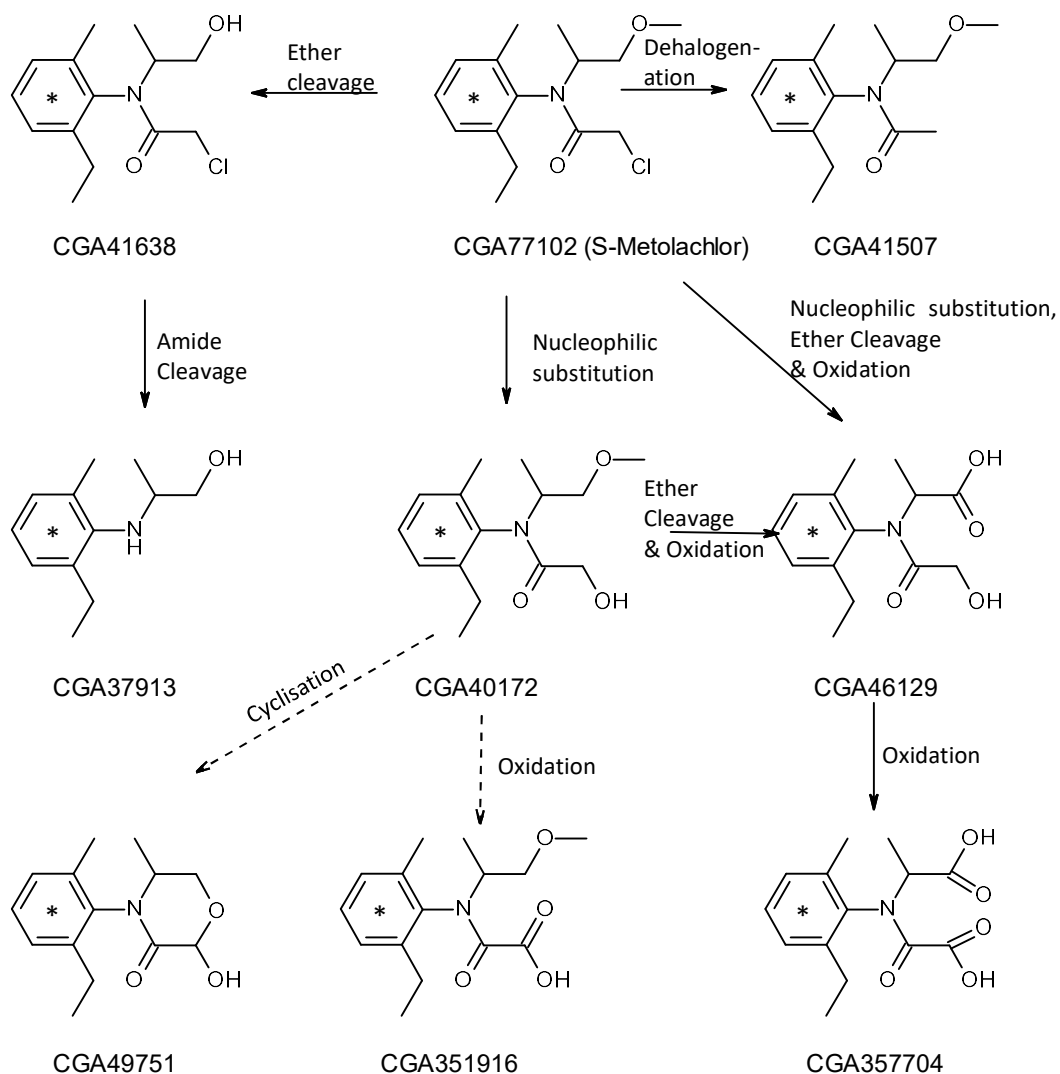


Figure 22: Schematic describing oxidative metabolism of S-metolachlor.

* denotes the position of ^{14}C . Dashed arrows indicate pathways with possible intermediates. Pathway provided by Syngenta.

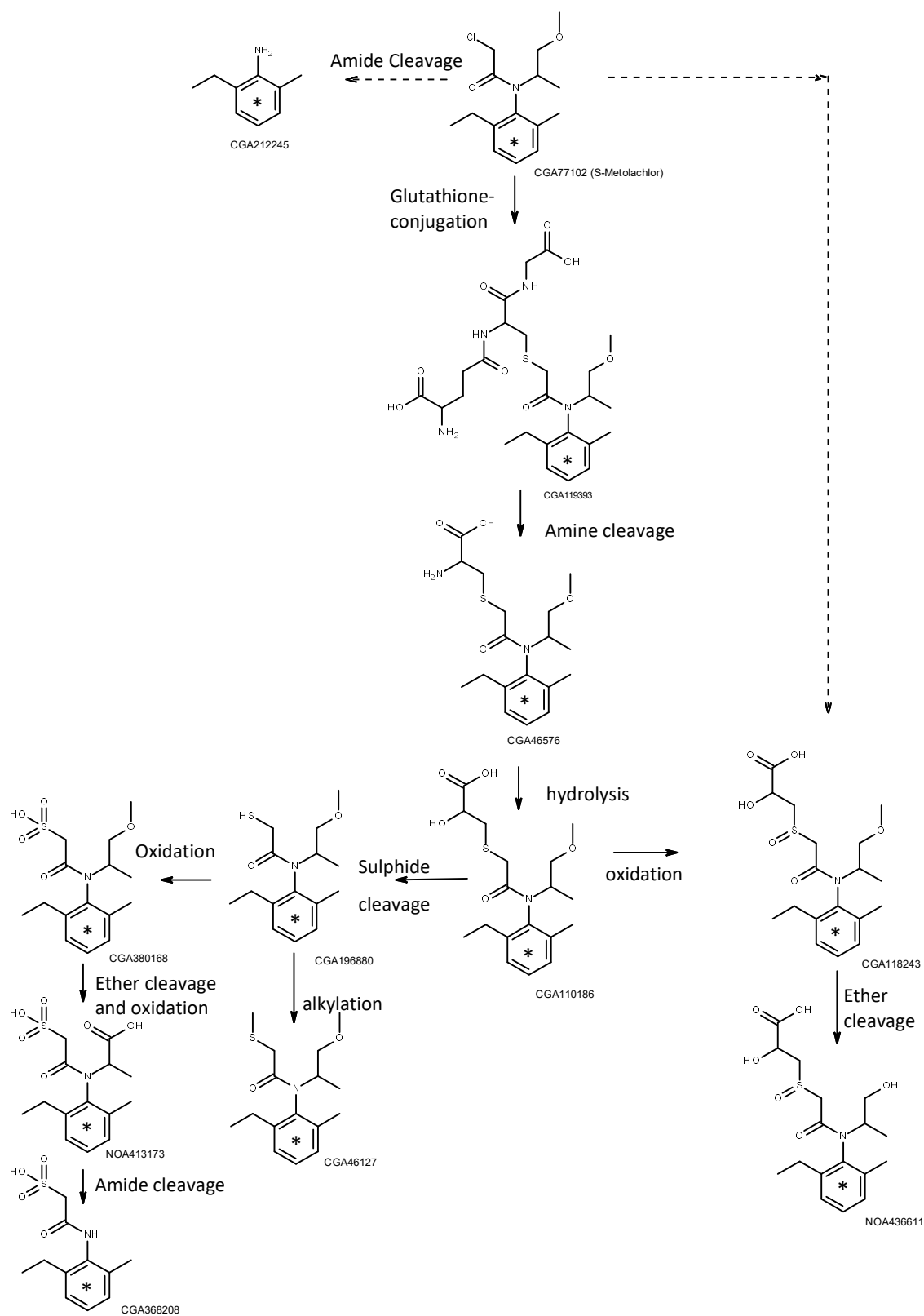


Figure 23: Schematic showing glutathione-mediated metabolism of S-metolachlor.

* denotes the position of ^{14}C . Dashed arrows indicate pathways with possible intermediates. Pathway provided by Syngenta.

The chromatograms of *S*-moc extractions were exposed to radiofilm and measured using a phosphorimager, as shown in Figure S 2. Quantification of this data was performed, as shown in

Figure 24, which describes the metabolism of *S*-moc. This was displayed as either oxidative or glutathionylation metabolism, because, due to the large number of *S*-moc metabolites, it was most practical to combine them as oxidative or glutathione conjugated metabolites. Table S 7 and Table S 8 show summarised data and statistics as to metabolite formation, respectively.

The results show that without the addition of any safener, the metabolism of *S*-moc was extremely rapid, reaching approximately 90% metabolism as early as 4.5 hours after treatment. By 24 hours, metabolism was almost complete. *S*-moc was metabolised to 13% or less by 4.5 hours, and to 2% or less by 48 hours, in all tissues. Rapid *S*-moc uptake, as shown in section 3.2.2.1, has been demonstrated previously, and may play a role in the associated metabolism observed (Al-Khatib et al., 2002). In addition, pre-uptake metabolism of *S*-moc may explain this rapid metabolism, such as has been observed in soil and water (Al-Khatib et al., 2002; Rice, 1996). The observed metabolism was similar for all tissues studied, though metabolism in the stem was slightly slower than in the leaf.

Metabolite formation mirrored this decrease in *S*-moc precisely. The combined glutathione conjugates increased to 40%, 30% and 34% by 24 hours in the leaf, stem and root tissues, respectively, changing little afterwards. The oxidative metabolites showed a lower rate of formation than that of the glutathione metabolites, increasing to approx. 17% by 24 hours in all tissues, changing little afterwards.

Most of the metabolism of *S*-moc occurred through the glutathione pathway, as compared with the oxidative pathway, between 24-72 hours. The leaf and root, however, showed similar levels of both forms of metabolite at 4.5 hours, indicating that metabolism occurred equally through both pathways initially, tending towards glutathionylation after 4.5 hours. Indeed, in the case of stem and root tissues, between 4.5 and 72 hours, the disappearance of parent *S*-moc appeared to match the appearance of glutathione metabolites exactly, while the generation of oxidative metabolites did not change. Since the data reflects percent metabolite extracted, continuous *S*-moc uptake and metabolism may have still been occurring, including to the oxidative metabolites.

The results indicate that benoxacor did not increase the metabolism of *S*-moc, in any tissue or harvest time. It is possible that benoxacor-enhanced metabolism may have happened prior to the first harvest time of 4.5 hours, thereby obscuring any differential metabolism caused by benoxacor. The results also indicated a limited effect of benoxacor on the route of metabolism, with glutathione conjugate and oxidative metabolites showing limited or no changes with the safener, in all tissues. Benoxacor did show a significantly lower amount of oxidative metabolite at 48 h in the stem, though of only 2.32% and on the threshold of significance (adjusted $p = 0.05$).

Metcamifen showed the same lack of effect on *S*-moc metabolism, having no significant effect on the rate of metabolism. The route of metabolism was also barely affected by metcamifen. However a few exceptions were observed. In the leaf tissue, glutathionylation-derived metabolites showed an approximate 10% reduction following metcamifen treatment at 48 and 72 hours, with adjusted p values of 0.00 and 0.03, respectively, the latter close to the threshold of significance. In the stem, the glutathione metabolites showed a 7% increase with metcamifen treatment (adjusted $p = 0.00$), and the oxidative metabolites of the root at 48 hours was 5% lower (adjusted $p = 0.00$). The oxidative metabolites of the leaf at 48 h were also approximately 3% lower, with an adjusted p value of 0.03, again close to the threshold of significance. Since these effects on metabolites were not mirrored by an inverse effect of other metabolites or parent compound, it is unlikely that these effects were physiologically relevant and were most likely due to TLC ROI not assigned accountably to compounds. Considering the modest difference in metabolic profile caused by the safener, this does not appear to signify a differential route of metabolism. Therefore, the only conclusion that can be drawn is that if the safeners have an effect on *S*-moc metabolism, it happens before 4.5 hours.

The lack of observable safener effect on, and rapid metabolism of, *S*-moc may be due to the concentrations of compounds used. It is likely that the concentration of *S*-moc and safeners were different than those used in the field. For example, an Acuron® mixture, sprayed at 4.91 L Ha⁻¹, assuming 36,000-60,000 plants per hectare, would result in over 21 mg *S*-moc delivered per plant; while in this study, after 4.5 hours, only 19.9 µg *S*-moc was taken up ("ACURON® Herbicide Label," accessed 2018; "MAIZE GROWERS GUIDE,"). This low level of herbicide probably accounts for the rapid metabolism of the herbicide, irrespective of treatment.

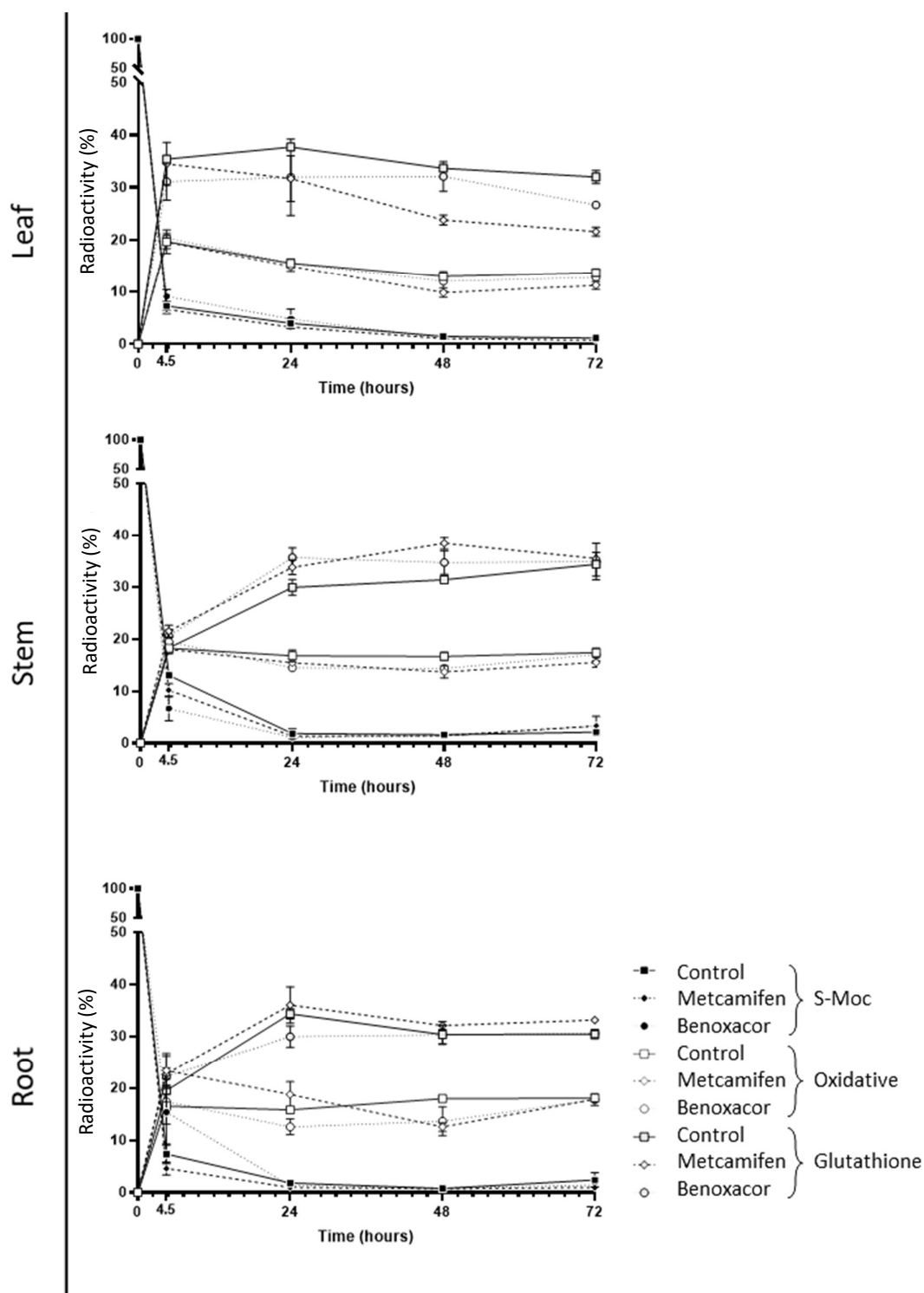


Figure 24: Graphs showing the effect of metcamifen and benoxacor safeners on the metabolism of *S*-metolachlor in different tissues, over time (h).

7 day old maize plants were treated continuously via roots, with 0.1% DMSO (v/v) containing 25 μ M [14 C]-*S*-metolachlor and 25 μ M Safener or no Safener control as described by the legend (bottom right). Plants were harvested 4.5, 24, 48 and 72 h after application. Each compound is shown as a percent of total radioactivity. Results represent means with standard deviations (n = 3).

3.3 Discussion

3.3.1 *Safener effects on herbicides translocation*

It has been hypothesised that safeners may reduce herbicide toxicity in target crops by inhibiting the uptake and translocation of the herbicide. However, a comprehensive analysis of multiple safener-herbicide interactions was carried out by Davies et al. (1999), demonstrating contradiction and providing no general conclusion. It has therefore been suggested that such effects would not contribute significantly to safening (Jablonkai, 2013). In this study, it was shown that metcamifen and benoxacor had no effect on the uptake of mesotrione or S-moc, indicating safening in these cases was not mediated by alterations in translocation.

3.3.2 *Safener translocation*

The selectivity of safeners to metabolise specific herbicides could be hypothesised to result from differential safener uptake and/or translocation. In the current study, a faster uptake and translocation of the safener benoxacor, compared to metcamifen, was observed, giving a possible explanation for the differential effects of each. However, despite benoxacor translocating faster than metcamifen through the plant, its enhancement of mesotrione metabolism was less, suggesting safener efficacy and selectivity was not mediated by the speed of translocation or uptake, in this case. Since no safener effects were observed with S-moc metabolism, safener translocation could not be analysed with respect to the metabolic effect. The translocation effects could be explained in terms of the compounds physicochemical properties, and were due to a differential ability to pass the casparian strip of the root xylem. Another hypothesis for safener selectivity, was that the safeners might localise to specific tissues, thereby having differential effects on tissue-specific herbicides. However, no specific tissue localisation was observed with either safener, which both demonstrated a largely even distribution throughout the plant, with accumulation only in the leaf tips. No long-term tissue localisation was observed, with both safeners fully distributed by two days. When considered together, the effect of translocation rate and localisation may provide a better explanation for the different safener effects. It is plausible that the differences in translocation of benoxacor and metcamifen result in unique time-dependent localisations of each safener, potentially causing unique interactions with herbicides.

3.3.3 *Safener effects on herbicide metabolism*

The current metabolite study indicated that most of the metabolism of mesotrione was due to metabolism to 4-hydroxy-mesotrione, occurring primarily in the aerial tissues. The appearance of this primary metabolite, substantially mirrored the detoxification of mesotrione, indicating it as the major metabolite. The subsequent metabolites in the pathway, MNBA, AMBA and 5-hydroxy-mesotrione showed little variation in content over time in all tissues, irrespective of treatment, contributing no more than 5%, 4% and 2% to the total metabolite composition, respectively. The results identified an increase in the metabolic rate of mesotrione with both safeners. Metcamifen displayed greater enhancement of mesotrione metabolism than benoxacor in leaf and stem tissues, this effect being greatest at 24 and 48 hours. In the leaf tissue, both safener effects had effectively terminated by 48 hours, while in the stem, metcamifen and benoxacor still displayed increased mesotrione metabolism at 48 hours. The observed safener-enhanced metabolism in the stem exceeding that of the leaf, was possibly a function of translocation, assuming the safener was in a higher abundance in the stem due to incomplete translocation. Alternatively, since the leaf appeared to show higher endogenous metabolism, this may have provided less opportunity for safening. The roots, however, displayed only minor effects with either safener. There were no differences observed in the metabolic route. The metabolic enhancement of mesotrione with safeners, metcamifen and benoxacor, has not previously been published and provides an excellent example of chemical selectivity.

The hydroxylation of mesotrione has been described as the basis of maize tolerance to mesotrione, representing the loss of herbicidal activity (Hawkes, 2001; Ma et al., 2013). The downstream metabolites, MNBA and AMBA, also display no pesticidal activity (European Food Safety Authority, 2016). Therefore, the observed metabolic enhancement by the Safeners are likely to confer protective effects against mesotrione in maize.

In addition, the results indicated a rapid detoxification of *S*-moc, in all tissues, with little effect on metabolic rate or route caused by either metcamifen or benoxacor. The results are contradictory to previous studies, which have described an enhanced metabolism of metolachlor with benoxacor application, observing a 65-70% enhancement of metabolism in 1 hour with benoxacor in seedling apical sections (Cottingham et al., 1991), though the experimental conditions differed from those used in this study: Cottingham et al. (1991) germinated maize seeds in a solution containing benoxacor, and after 72 hours, the seedlings

were placed in a solution containing metolachlor. It can therefore be presumed that no safener effects were observed in the current study due to the rapid metabolism of *S*-moc, the early stages of which were missed. While this does not provide any information on chemical selectivity, it does highlight the complex and rapid metabolism of this herbicide. These results partially answer the question of effect longevity, suggesting that if the safeners did increase the metabolism of *S*-moc, they did so before 4.5 hours, and would have no effect on final residue formation at times important for commercial harvest. The findings also suggest that while both pathways may be active, the glutathione-mediated metabolism is favoured over the oxidative pathway.

Taken together the experiments in this chapter indicate that, while selective enhancement of herbicide metabolism by specific safeners does occur in some cases, this is not primarily determined by differences in safener translocation. It is therefore likely that selective enhancement of specific xenobiotic enzymes is responsible for the observed chemical specificity.

3.4 Appendix to Chapter 3

	Time (h)	Metcamifen			Benoxacor			Control		
		Mean	SD	n	Mean	SD	n	Mean	SD	n
mesotrione	4.5	1041.32	90.99	3	786.99	213.98	3	859.32	220.85	3
	24	2023.92	465.34	3	2267.19	314.60	3	2273.72	100.64	3
	48	4026.05	493.03	3	3804.19	354.16	3	4141.72	267.91	3
	72	5262.52	737.68	3	4927.45	843.31	3	5791.79	627.05	3
S-metolachlor	4.5	974.25	77.01	3	830.85	181.22	3	675.92	266.17	3
	24	2897.99	907.15	3	1672.85	377.55	3	2170.39	184.11	3
	48	3260.25	134.83	3	3242.65	94.13	3	3993.05	451.63	3
	72	4944.85	545.00	3	5253.65	573.80	3	5096.12	1517.06	3

Table S 1: Uptake volume data (μL) for Figure 13.

SD; standard deviation. n; number of replicates.

		Time (h)	Significant?	P value	Adjusted P Value
mesotrione	control/metcamifen	4.5	No	0.26	0.70
		24	No	0.41	0.78
		48	No	0.74	0.78
		72	No	0.40	0.78
	control/benoxacor	4.5	No	0.70	0.91
		24	No	0.97	0.97
		48	No	0.26	0.64
		72	No	0.23	0.64
	benoxacor/metcamifen	4.5	No	0.13	0.43
		24	No	0.49	0.87
		48	No	0.56	0.87
		72	No	0.63	0.87
S-metolachlor	control/metcamifen	4.5	No	0.14	0.35
		24	No	0.25	0.43
		48	No	0.05	0.20
		72	No	0.88	0.88
	control/benoxacor	4.5	No	0.45	0.70
		24	No	0.11	0.29
		48	No	0.05	0.18
		72	No	0.87	0.87
	benoxacor/metcamifen	4.5	No	0.28	0.62
		24	No	0.10	0.33
		48	No	0.86	0.86
		72	No	0.54	0.78

Table S 2: Uptake volume statistics for Figure 13.

	Time (h)	Control			Metcamifen			Benoxacor		
		Mean	SD	n	Mean	SD	n	Mean	SD	n
mesotrione	4.5	29.60	21.25	3	7.59	12.32	3	-11.88	28.17	3
	24	6.66	1.66	3	5.56	3.84	3	12.54	11.79	3
	48	10.29	3.46	3	8.42	4.06	3	3.74	1.67	3
	72	13.26	1.09	3	6.53	4.11	3	6.29	4.91	3
S-metolachlor	4.5	63.91	21.57	3	42.11	4.50	3	44.41	14.14	3
	24	25.16	3.29	3	21.30	7.92	3	36.52	4.35	3
	48	14.28	1.38	3	17.49	1.47	3	17.65	2.54	3
	72	11.25	0.71	3	10.55	1.14	3	12.56	1.80	3

Table S 3: Radioactive herbicide uptake data (Bq μL^{-1}) for Figure 14.

SD; standard deviation. n; number of replicates.

		Time (h)	Significant?	P value
mesotrione	Control vs metcamifen	4.5	No	0.20
		24	No	0.67
		48	No	0.58
		72	No	0.05
	Control vs benoxacor	4.5	No	0.11
		24	No	0.44
		48	No	0.04
		72	No	0.07
	benoxacor vs metcamifen	4.5	No	0.33
		24	No	0.38
		48	No	0.14
		72	No	0.95
S-metolachlor	Control vs metcamifen	4.5	No	0.16
		24	No	0.48
		48	No	0.05
		72	No	0.42
	Control vs benoxacor	4.5	No	0.26
		24	No	0.02
		48	No	0.11
		72	No	0.30
	benoxacor vs metcamifen	4.5	No	0.80
		24	No	0.04
		48	No	0.93
		72	No	0.18

Table S 4: Radioactive uptake statistics for Figure 14.

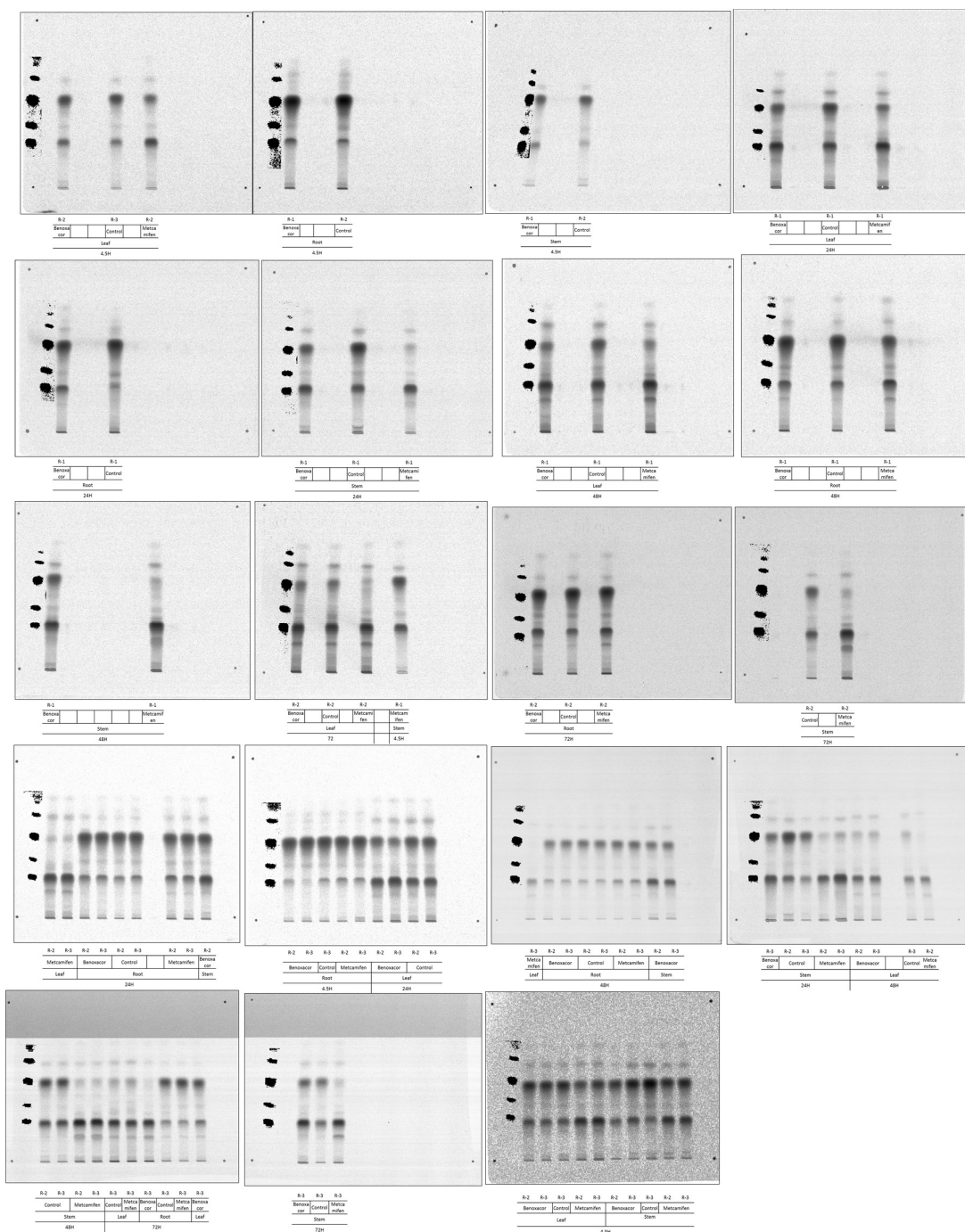


Figure S 1: Phosphorimages of thin layer chromatographs (TLCs) with [^{14}C]-mesotrione-treated plant samples, for Figure 21.

X-axis describes treatment, tissue, harvest time (h) and replicate number. Non-radioactive standards are superimposed on the left of each TLC.

		Control			Metcamifen			Benoxacor			
Tissue	Time (h)	Mean	SD	n	Mean	SD	n	Mean	SD	n	
mesotrione parent	leaf	4.5	56.92	8.08	2	25.70	2.87	3	50.35	6.19	3
		24	47.60	2.91	3	5.79	5.85	3	24.32	9.68	3
		48	20.50	13.38	2	6.41	1.41	3	9.21	2.27	3
		72	10.60	0.54	2	3.20	1.56	2	8.54	1.30	2
	stem	4.5	67.51	2.55	2	41.32	2.60	3	52.21	4.98	3
		24	62.49	7.86	3	4.72	0.51	3	33.55	11.47	3
		48	44.73	1.10	2	3.44	1.29	3	25.24	1.97	3
		72	22.90	19.83	2	4.11	1.42	2	5.17	0.00	1
	root	4.5	87.76	1.54	2	86.63	0.52	2	87.97	3.64	3
		24	81.78	0.72	3	67.26	1.89	2	74.01	4.48	3
		48	56.95	16.44	3	47.20	3.61	3	52.15	17.62	3
		72	67.70	7.45	2	55.20	7.01	2	58.55	5.09	2
4-hydroxy mesotrione	leaf	4.5	14.79	0.64	2	44.26	7.14	3	18.19	2.87	3
		24	36.74	1.74	3	74.97	5.80	3	59.81	8.47	3
		48	41.02	10.96	2	41.96	23.18	3	51.77	5.65	3
		72	54.10	5.23	2	63.15	5.16	2	56.64	2.11	2
	stem	4.5	5.44	0.93	2	31.36	4.93	3	14.50	0.63	3
		24	18.03	0.86	3	70.41	8.51	3	49.30	3.32	3
		48	32.37	0.69	2	73.38	5.90	3	49.96	9.43	3
		72	32.90	1.39	2	68.18	0.84	2	57.03	0.00	1
	root	4.5	3.46	0.11	2	5.33	0.42	2	3.41	2.58	3
		24	6.97	2.92	3	19.12	1.38	2	13.89	2.86	3
		48	9.05	2.08	3	20.71	15.51	3	10.55	1.94	3
		72	9.70	0.59	2	19.43	0.40	2	14.99	3.29	2
AMBA	leaf	4.5	2.33	0.49	2	2.35	0.37	3	2.46	0.60	3
		24	1.55	0.15	3	1.57	0.12	3	1.17	0.36	3
		48	2.96	1.86	2	3.73	2.66	3	2.97	0.95	3
		72	2.25	0.87	2	1.62	0.58	2	1.96	0.85	2
	stem	4.5	2.77	0.88	2	1.89	0.63	3	2.95	0.69	3
		24	1.57	0.61	3	1.90	0.48	3	1.27	0.51	3
		48	2.19	0.19	2	1.54	0.35	3	2.31	1.03	3
		72	2.54	0.74	2	1.76	0.40	2	1.71	0.00	1
	root	4.5	0.46	0.20	2	0.32	0.04	2	0.46	0.18	3
		24	0.76	0.05	3	1.04	0.02	2	0.87	0.08	3
		48	2.90	2.01	3	2.55	1.49	3	2.99	2.10	3
		72	1.49	0.83	2	1.43	0.78	2	1.62	1.10	2

Table S 5: Mesotrione metabolism data expressed in percent radioactivity (%), for Figure 21. SD; standard deviation. n; number of replicates.

	Tissue	Time (h)	Control			Metcamifen			Benoxacor		
			Mean	SD	n	Mean	SD	n	Mean	SD	n
MNBA	leaf	4.5	2.89	0.69	2	2.37	0.28	3	3.11	0.79	3
		24	1.56	0.89	3	1.48	1.56	3	1.36	1.02	3
		48	1.75	2.47	2	2.96	2.83	3	1.38	2.38	3
		72	2.40	3.39	2	1.24	1.75	2	1.01	1.42	2
	stem	4.5	3.09	0.19	2	2.13	0.88	3	3.05	0.18	3
		24	0.60	1.04	3	0.54	0.93	3	1.07	0.92	3
		48	0.00	0.00	2	0.29	0.51	3	2.12	0.70	3
		72	1.91	2.69	2	1.54	2.17	2	0.00	0.00	1
	root	4.5	1.19	0.15	2	1.09	0.04	2	1.29	0.08	3
		24	2.53	0.22	3	2.61	0.16	2	2.26	0.65	3
		48	3.59	0.74	3	3.39	0.30	3	3.96	0.90	3
		72	1.94	2.74	2	1.74	2.46	2	2.08	2.94	2
5-hydroxy mesotrione	leaf	4.5	1.03	1.45	2	1.53	1.34	3	1.50	1.30	3
		24	0.17	0.15	3	0.33	0.29	3	0.22	0.19	3
		48	0.17	0.24	2	0.10	0.17	3	0.11	0.19	3
		72	0.30	0.42	2	0.25	0.35	2	0.27	0.37	2
	stem	4.5	0.51	0.72	2	1.57	0.65	3	1.51	1.40	3
		24	0.00	0.00	3	0.00	0.00	3	0.12	0.21	3
		48	0.00	0.00	2	0.00	0.00	3	0.00	0.00	3
		72	0.00	0.00	2	0.00	0.00	2	0.00	0.00	1
	root	4.5	0.09	0.13	2	0.19	0.00	2	0.12	0.10	3
		24	0.23	0.20	3	0.40	0.05	2	0.21	0.20	3
		48	0.14	0.25	3	0.19	0.33	3	0.12	0.21	3
		72	0.38	0.54	2	0.42	0.59	2	0.39	0.54	2

Table S 5: (Continued).

Treatment	Time (h)	Parent mesotrione			4-hydroxy mesotrione			MNBA			AMBA			5-hydroxymesotrione			
		Significant?	P value	Adjusted P Value	Significant?	P value	Adjusted P Value	Significant?	P value	Adjusted P Value	Significant?	P value	Adjusted P Value	Significant?	P value	Adjusted P Value	
Leaf	control - benoxacor	4.5	No	0.37	0.44	No	0.21	0.51	No	0.77	0.99	No	0.81	0.99	No	0.73	0.99
		24	No	0.02	0.06	Yes	0.01	0.04	No	0.82	0.99	No	0.17	0.53	No	0.74	0.99
		48	No	0.22	0.44	No	0.23	0.51	No	0.88	0.99	No	0.99	0.99	No	0.77	0.99
		72	No	0.17	0.44	No	0.59	0.59	No	0.65	0.98	No	0.77	0.99	No	0.95	0.99
	control - metcamifen	4.5	Yes	0.01	0.02	Yes	0.01	0.03	No	0.30	0.76	No	0.94	0.98	No	0.71	0.98
		24	Yes	0.00	0.00	Yes	0.00	0.00	No	0.94	0.96	No	0.82	0.98	No	0.44	0.90
		48	No	0.14	0.14	No	0.96	0.96	No	0.66	0.96	No	0.75	0.98	No	0.71	0.98
		72	Yes	0.02	0.05	No	0.22	0.40	No	0.71	0.96	No	0.49	0.93	No	0.92	0.98
	metcamifen - benoxacor	4.5	Yes	0.00	0.01	Yes	0.00	0.02	No	0.20	0.59	No	0.81	0.96	No	0.97	1.00
		24	No	0.05	0.13	No	0.06	0.18	No	0.92	0.99	No	0.14	0.46	No	0.61	0.98
		48	No	0.14	0.14	No	0.52	0.52	No	0.50	0.87	No	0.66	0.96	No	0.93	1.00
		72	No	0.07	0.13	No	0.24	0.42	No	0.90	0.99	No	0.69	0.96	No	0.97	1.00
Stem	control - benoxacor	4.5	Yes	0.03	0.04	Yes	0.00	0.00	No	0.86	0.86	No	0.81	0.96	No	0.44	0.61
		24	Yes	0.02	0.04	Yes	0.00	0.00	No	0.59	0.83	No	0.55	0.91	No	0.37	0.61
		48	Yes	0.00	0.00	No	0.09	0.09	No	0.03	0.08	No	0.88	0.96			
		72															

Table S 6: Mesotrione metabolism statistics for Figure 21.

Treatment	Time (h)	parent mesotrione			4-hydroxy mesotrione			MNBA			AMBA			5-hydroxymesotrione			
		Significant?	P value	Adjusted P Value	Significant?	P value	Adjusted P Value	Significant?	P value	Adjusted P Value	Significant?	P value	Adjusted P Value	Significant?	P value	Adjusted P Value	
Stem	control - metcamifen	4.5	Yes	0.00	0.00	Yes	0.01	0.01	No	0.24	0.67	No	0.28	0.62	No	0.18	0.18
		24	Yes	0.00	0.00	Yes	0.00	0.00	No	0.94	0.99	No	0.51	0.62			
		48	Yes	0.00	0.00	Yes	0.00	0.01	No	0.50	0.87	No	0.11	0.37			
		72	No	0.31	0.31	Yes	0.00	0.00	No	0.89	0.99	No	0.32	0.62			
	metcamifen - benoxacor	4.5	Yes	0.03	0.03	Yes	0.00	0.01	No	0.15	0.27	No	0.12	0.32	No	0.95	0.95
		24	Yes	0.01	0.02	Yes	0.02	0.03	No	0.52	0.52	No	0.20	0.36	No	0.37	0.61
		48	Yes	0.00	0.00	Yes	0.02	0.03	No	0.02	0.06	No	0.29	0.36			
		72															
Root	control - benoxacor	4.5	No	0.94	0.94	No	0.98	0.98	No	0.37	0.84	No	>0.999999	>0.999999	No	0.79	1.00
		24	No	0.04	0.16	No	0.04	0.16	No	0.53	0.90	No	0.12	0.41	No	0.92	1.00
		48	No	0.75	0.94	No	0.41	0.66	No	0.61	0.90	No	0.96	1.00	No	0.91	1.00
		72	No	0.29	0.64	No	0.15	0.40	No	0.96	0.96	No	0.91	1.00	No	0.99	1.00
	control - metcamifen	4.5	No	0.43	0.61	No	0.03	0.05	No	0.45	0.91	No	0.42	0.80	No	0.38	0.81
		24	Yes	0.00	0.00	Yes	0.01	0.04	No	0.69	0.97	Yes	0.01	0.02	No	0.34	0.81
		48	No	0.37	0.61	No	0.27	0.27	No	0.68	0.97	No	0.82	0.97	No	0.85	0.98
		72	No	0.23	0.54	Yes	0.00	0.01	No	0.95	0.97	No	0.94	0.97	No	0.96	0.98
	metcamifen - benoxacor	4.5	No	0.66	0.95	No	0.39	0.54	No	0.04	0.16	No	0.36	0.74	No	0.43	0.82
		24	No	0.15	0.47	No	0.10	0.35	No	0.53	0.78	No	0.08	0.27	No	0.30	0.76
		48	No	0.66	0.95	No	0.32	0.54	No	0.35	0.73	No	0.78	0.95	No	0.76	0.94
		72	No	0.64	0.95	No	0.20	0.49	No	0.91	0.91	No	0.86	0.95	No	0.96	0.96

Table S 6: (Continued).

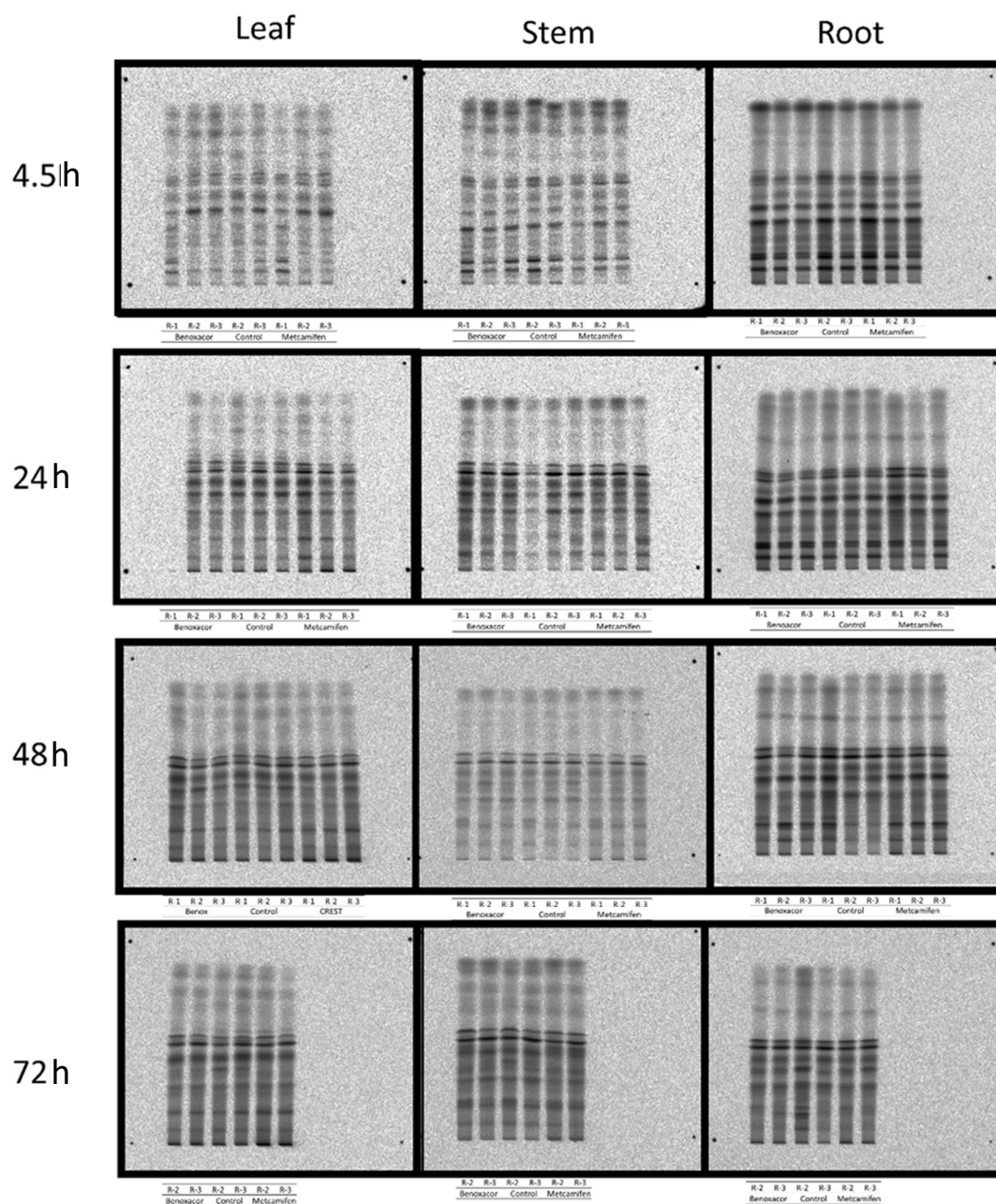


Figure S 2: Phosphorimages of thin layer chromatographs (TLCs) with $[^{14}\text{C}]$ -S-metolachlor-treated plant samples, for Figure 24.

X-axis describes treatment, tissue, and replicate. Y-axis defines harvest time (h). Since the non-radioactive standards were of low visibility, they are not shown here.

compound	Tissue	Time (h)	Benoxacor			Control			Metcamifen		
			Mean	SD	n	Mean	SD	n	Mean	SD	n
S-metolachlor	leaf	0	100.00	0.00	1	100.00	0.00	1	100.00	0.00	1
		4.5	9.12	1.33	3	7.27	0.86	2	6.64	0.85	3
		24	4.81	1.88	3	3.95	1.02	3	3.24	0.32	3
		48	1.11	0.16	3	1.47	0.30	3	1.07	0.25	3
		72	1.20	0.11	2	1.15	0.05	2	0.71	0.18	2
	stem	0	100.00	0.00	1	100.00	0.00	1	100.00	0.00	1
		4.5	6.66	2.35	3	13.02	0.52	2	10.18	1.24	3
		24	1.12	0.38	3	1.87	0.96	3	1.36	0.10	3
		48	1.44	0.08	3	1.64	0.08	3	1.45	0.09	3
		72	3.30	0.54	2	2.12	0.25	2	3.32	1.85	2
	root	0	100.00	0.00	1	100.00	0.00	1	100.00	0.00	1
		4.5	15.37	6.35	3	7.37	1.92	2	4.60	1.23	3
		24	1.29	0.51	3	1.81	0.44	3	0.95	0.59	3
		48	0.86	0.25	3	0.78	0.46	3	0.72	0.09	3
		72	1.42	0.33	2	2.41	1.36	2	0.98	0.23	2
oxidative	leaf	0	0.00	0.00	1	0.00	0.00	1	0.00	0.00	1
		4.5	20.35	0.91	3	19.66	2.28	2	19.56	1.22	3
		24	15.54	0.86	3	15.52	0.53	3	14.93	0.92	3
		48	12.01	1.94	3	12.98	0.68	3	9.84	0.86	3
		72	12.77	1.33	2	13.68	0.80	2	11.23	0.76	2
	stem	0	0.00	0.00	1	0.00	0.00	1	0.00	0.00	1
		4.5	19.45	0.52	3	18.20	0.61	2	18.01	0.85	3
		24	14.46	0.30	3	16.77	1.12	3	15.44	0.34	3
		48	14.33	0.43	3	16.65	0.80	3	13.67	1.19	3
		72	17.02	1.19	2	17.39	0.23	2	15.51	0.96	2
	root	0	0.00	0.00	1	0.00	0.00	1	0.00	0.00	1
		4.5	17.36	1.42	3	16.51	3.48	2	23.32	3.39	3
		24	12.53	1.51	3	15.80	0.58	3	18.72	2.46	3
		48	13.63	2.77	3	17.94	0.43	3	12.56	0.88	3
		72	17.76	1.14	2	18.04	0.06	2	17.83	0.59	2
glutathione	leaf	0	0.00	0.00	1	0.00	0.00	1	0.00	0.00	1
		4.5	31.10	3.54	3	35.41	0.56	2	34.50	4.09	3
		24	31.95	7.26	3	37.71	0.70	3	31.70	4.36	3
		48	32.08	2.83	3	33.66	0.28	3	23.78	0.97	3
		72	26.67	0.65	2	32.01	1.27	2	21.60	0.88	2
	stem	0	0.00	0.00	1	0.00	0.00	1	0.00	0.00	1
		4.5	20.57	1.10	3	18.28	1.00	2	21.48	1.14	3
		24	35.61	1.88	3	29.89	1.51	3	33.75	1.42	3
		48	34.66	2.25	3	31.34	0.21	3	38.36	1.14	3
		72	34.84	3.52	2	34.32	2.31	2	35.43	0.16	2
	root	0	0.00	0.00	1	0.00	0.00	1	0.00	0.00	1
		4.5	22.17	1.62	3	19.50	0.41	2	22.70	3.56	3
		24	29.95	2.05	3	34.32	0.99	3	36.01	3.50	3
		48	30.28	1.75	3	30.35	1.84	3	32.09	0.77	3
		72	30.56	0.55	2	30.45	0.94	2	33.15	0.01	2

Table S 7: S-metolachlor metabolism data in percent radioactivity (%),for Figure 24.

SD; standard deviation. n; number of replicates.

		Time (h)	Significant?	Leaf		Significant?	Stem		Significant?	Root	
				P value	Adjusted P Value		P value	Adjusted P Value		P value	Adjusted P Value
Oxidative	Control - benoxacor	4.5	No	0.65	0.91	No	0.09	0.17	No	0.71	0.92
		24	No	0.97	0.97	No	0.03	0.08	No	0.03	0.10
		48	No	0.46	0.91	Yes	0.01	0.05	No	0.06	0.16
		72	No	0.50	0.91	No	0.71	0.71	No	0.76	0.92
	Control - metcamifen	4.5	No	0.95	0.95	No	0.81	0.81	No	0.12	0.31
		24	No	0.40	0.64	No	0.12	0.31	No	0.12	0.31
		48	Yes	0.01	0.03	No	0.02	0.09	Yes	0.00	0.00
		72	No	0.09	0.24	No	0.12	0.31	No	0.66	0.66
	metcamifen - benoxacor	4.5	No	0.42	0.66	No	0.07	0.19	No	0.05	0.14
		24	No	0.45	0.66	No	0.02	0.08	No	0.02	0.08
		48	No	0.15	0.48	No	0.42	0.51	No	0.56	0.80
		72	No	0.29	0.64	No	0.30	0.51	No	0.95	0.95
Glutathione	Control - benoxacor	4.5	No	0.20	0.50	No	0.10	0.19	No	0.12	0.31
		24	No	0.24	0.50	No	0.01	0.06	No	0.03	0.11
		48	No	0.39	0.50	No	0.06	0.18	No	0.96	0.99
		72	No	0.03	0.13	No	0.88	0.88	No	0.90	0.99
	Control - metcamifen	4.5	No	0.79	0.79	No	0.05	0.10	No	0.32	0.53
		24	No	0.08	0.15	No	0.03	0.09	No	0.47	0.53
		48	Yes	0.00	0.00	Yes	0.00	0.00	No	0.21	0.50
		72	Yes	0.01	0.03	No	0.57	0.57	No	0.06	0.20
	metcamifen - benoxacor	4.5	No	0.34	0.56	No	0.38	0.61	No	0.83	0.83
		24	No	0.96	0.96	No	0.24	0.57	No	0.06	0.17
		48	Yes	0.01	0.03	No	0.06	0.23	No	0.17	0.32
		72	No	0.02	0.07	No	0.84	0.84	No	0.02	0.09
S-moc	Control - benoxacor	4.5	No	0.19	0.46	No	0.04	0.14	No	0.20	0.58
		24	No	0.53	0.78	No	0.28	0.28	No	0.25	0.58
		48	No	0.14	0.46	No	0.04	0.14	No	0.82	0.82
		72	No	0.59	0.78	No	0.11	0.21	No	0.42	0.67
	Control - metcamifen	4.5	No	0.48	0.53	No	0.06	0.19	No	0.13	0.38
		24	No	0.31	0.53	No	0.42	0.66	No	0.11	0.38
		48	No	0.15	0.40	No	0.05	0.19	No	0.84	0.84
		72	No	0.08	0.30	No	0.46	0.66	No	0.28	0.49
	metcamifen - benoxacor	4.5	No	0.05	0.20	No	0.08	0.30	No	0.04	0.17
		24	No	0.23	0.40	No	0.34	0.71	No	0.49	0.68
		48	No	0.83	0.83	No	0.96	1.00	No	0.43	0.68
		72	No	0.08	0.23	No	0.99	1.00	No	0.27	0.60

Table S 8: S-metolachlor metabolism statistics, for Figure 24.

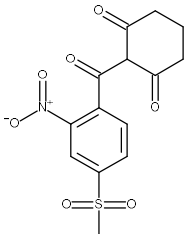
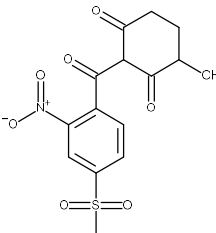
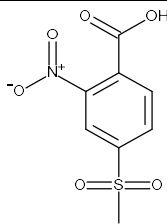
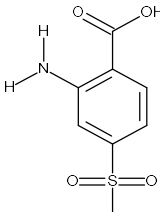
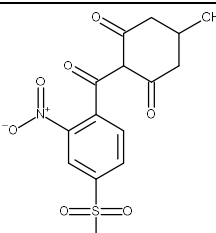
Compound description	Code	Molecular Formula	Structure
mesotrione	ZA1296	C ₁₄ H ₁₃ NO ₇ S	
4-Hydroxy-mesotrione	R282813	C ₁₄ H ₁₃ NO ₈ S	
MNBA	NOA437130	C ₈ H ₇ NO ₆ S	
AMBA	R044276	C ₈ H ₉ NO ₄ S	
5-Hydroxy-mesotrione	R282470	C ₁₄ H ₁₃ NO ₈ S	

Table S 9: Compounds used as identification standards for mesotrione metabolites.
Reference code, molecular formula and structure are shown.

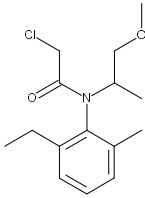
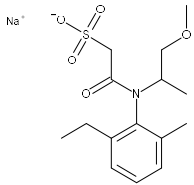
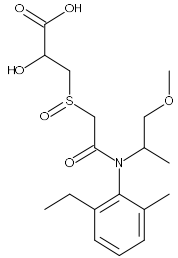
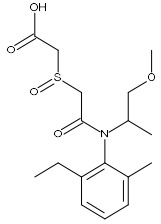
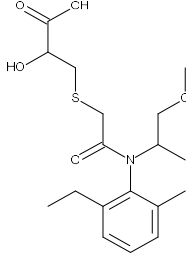
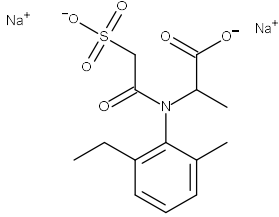
Metabolites type	Compound description	Code	Molecular Formula	Structure
Parent	<i>S</i> -metolachlor	CGA77102	C ₁₅ H ₂₂ ClNO ₂	
	N/A	CGA380168	C ₁₅ H ₂₂ NO ₅ S.Na	
	N/A	CGA118243/ NOA443819	C ₁₈ H ₂₇ NO ₆ S	
Glutathione metabolites	N/A	NOA436611	C ₁₇ H ₂₅ NO ₅ S	
	N/A	CGA110186	C ₁₈ H ₂₇ NO ₅ S	
	N/A	NOA413173	C ₁₄ H ₁₇ NO ₆ S.2Na	

Table S 10: Compounds used as identification standards for *S*-metolachlor metabolites.
Reference code, molecular formula and structure are shown.

Metabolites type	Compound description	Code	Molecular Formula	Structure
	N/A	CGA368208	$C_{11}H_{14}NO_4S.Na$	
	S-metolachlor-cysteine conjugate	CGA46576/ CGA43826	$C_{18}H_{28}N_2O_4S$	
	S-metolachlor-glutathione conjugate	CGA119393	$C_{25}H_{38}N_4O_8S$	
	N/A	CGA196880	$C_{15}H_{23}NO_2S$	
	N/A	CGA46127	$C_{16}H_{25}NO_2S$	

Table S 10: (Continued).

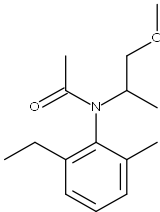
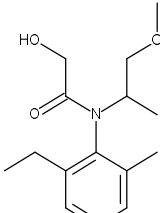
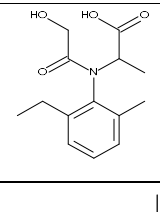
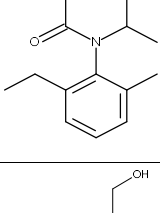
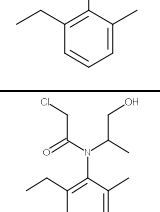
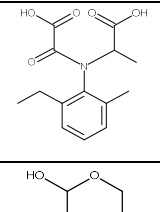
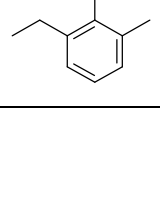

Metabolites type	Compound description	Code	Molecular Formula	Structure
Oxidative metabolites	N/A	CGA41507	$C_{15}H_{23}NO_2$	
	N/A	CGA40172	$C_{15}H_{23}NO_3$	
	N/A	CGA46129	$C_{14}H_{19}NO_4$	
	N/A	CGA351916/ CGA51202	$C_{15}H_{21}NO_4$	
	2-[Amino]-1-propanol	CGA37913	$C_{12}H_{19}NO$	
	N/A	CGA41638	$C_{14}H_{20}ClNO_2$	
	N/A	CGA357704	$C_{14}H_{17}NO_5$	
	N/A	CGA49751	$C_{14}H_{19}NO_3$	

Table S 10: (Continued).

Chapter 4. *In silico* analysis of glutathione-S-transferases

4.1 Introduction

Having investigated the metabolic effects caused by safeners, it was important to understand the enzymes catalysing these reactions. Enzymes of the xenome, the biosystem responsible for xenobiotic metabolism, are known to facilitate safener-induced metabolism, though the precise interactions are still unclear (Davies et al., 1999). Most studies have focused on individual enzymes, rather than whole enzyme families, and genome-wide family analyses would provide greater insight into the involvement of such enzymes in safener effects. It is known that cytochrome p450s (CYPs), ATP binding cassette (ABC)-transporters, UDP-glucosyl transferases (UGTs) and glutathione-S-transferases (GSTs), all play roles in the safener effect, and represent ideal candidates for analysis (Davies et al., 1999; Hatzios, 1991; Pang et al., 2012; Theodoulou, 2000; Theodoulou et al., 2003). The GST family was chosen for in-depth analysis, as this aligned with the expertise of our research group. These analyses were intended to provide generic understanding of safener effects, at the enzyme level, allowing for predictions of individual safener-herbicide interactions, in line with the objectives of the project.

GST enzymes play major roles in secondary metabolism of plants such as flavonoid transport, hydroperoxide reduction, tyrosine catabolism and ascorbate recycling (Dixon et al., 2010b; Edwards et al., 2011). They are also vital elements of the xenome, the main function of GSTs being the conjugation of the tripeptide glutathione to herbicides, resulting in their vacuolar sequestration. This has caused great interest in GSTs as potential determinants of plant tolerance to herbicides and responses to herbicide safeners. Recently, as many as 14 classes of plant GSTs have been described, termed; phi (F, ϕ), tau (U, τ), lambda (L, λ), zeta (Z, ζ), theta (T, θ), dehydroascorbate reductase (DHAR), omega-like or glutathionyl-hydroquinone reductase (GHR), tetrachlorohydroquinone dehalogenase (TCHQD), γ -subunit classes of the eukaryotic translation elongation factor 1B (EF1By), microsomal prostaglandin E-synthase type 2 (mPGES-2), URE2p, iota, metaxin and hemerythrin (H) (Lallement et al., 2015; Liu et al., 2013; Monticcolo et al., 2017). The current study focuses on the main classes; phi, tau, lambda, zeta, theta, DHAR and GHR. These can be divided into those using a serine or cysteine as their catalytic residue, known as serinyl- or cysteinyl- GSTs, respectively. The serinyl-GSTs have been characterised the most extensively and include the phi, tau, zeta, and theta classes, using the serine residue to catalyse the conjugation of the tripeptide glutathione to aromatic,

aliphatic or heterocyclic substrates (Sylvestre-Gonon et al., 2019). The phi and tau classes are responsible for the glutathionylation of xenobiotics in phase II of the xenome (see section 1.6) (Cummins et al., 2011). In addition, the oxidation of glutathione by phi, tau and theta class GSTs may concomitantly cause the reduction of peroxides into alcohols, thereby assigning them peroxidase activity (Sylvestre-Gonon et al., 2019). The zeta class GSTs have also been shown to catalyse the isomerisation of metabolites in the tyrosine metabolic pathway, using GSH as a cofactor (Sylvestre-Gonon et al., 2019). The cysteinyl-GSTs include the DHAR, lambda and GHR classes (Lallement et al., 2014; Sylvestre-Gonon et al., 2019). This cysteine residue generally catalyses the deglutathionylation of substrates, in opposition to the serinyl-GSTs (Lallement et al., 2014). While the physiological roles of these GSTs are not completely understood, there is some information on their activity. Most, if not all, lambda and DHAR GSTs, characterised so far, exhibit thiol-transferase and dehydroascorbate reductase activities but no transferase, peroxidase or isomerase activities (Lallement et al., 2014). The lambda class has been associated with flavonoid recycling, and the DHAR class with the recycling of ascorbate (Dixon et al., 2010a; Lallement et al., 2015; Liu et al., 2013). The GHRs have been mostly characterised in bacteria and fungi, in which they catalyse deglutathionylation reactions in chlorinated quinone catabolism and lignin degradation (Dixon et al., 2010a; Lallement et al., 2014; Lallement et al., 2015; Liu et al., 2013). While GSTs were originally considered cytosolic, some recent evidence indicates GSTs may possess more diverse subcellular localisations. Of the serinyl- GSTs, the phi, tau and zeta classes are still considered cytosolic proteins, while the theta GSTs have been shown to localise to the peroxisome, concomitant with their peroxidase activities (Dixon et al., 2009; Liu et al., 2013; Sylvestre-Gonon et al., 2019). The DHAR and lambda GSTs have been suggested to localise in the chloroplasts of arabidopsis (*Arabidopsis thaliana*) plants, while the localisation of GHR remains unclear (Lallement et al., 2014).

The phylogenetic characterisation of this family has not been comprehensively reviewed in maize since 2000, despite the large number of newly discovered proteins and genes (Mcgonigle et al., 2000). This lack of up to date genetic classification has been recognised in other crops, such as potato, prompting recent GST analyses (Islam et al., 2018). In this study, the maize GSTs were studied by *in silico* methodologies, in order to better understand the role of this enzyme family in safener-induced herbicide metabolism. The sequence relatedness, chromosomal localisation and evolution of these seven classes were first investigated, in order

to classify and characterise the maize GSTs. This information prompted a proposal for an updated and improved nomenclature system. In order to better understand the mechanisms of chemical selectivity, the secondary and tertiary protein structure and residues involved in dimerisation and binding to glutathione and substrates, were analysed. Predictions of subcellular localisation and expression in different tissues and developmental stages, were also made to determine where and when the GSTs were functional.

4.2 Results

4.2.1 Identification and classification of GSTs in maize

The most current maize genome available, the B73 RefGen_v4, published in 2009, is 2.3 gigabases in size, representing over 32,000 genes (Jiao et al., 2017; Schnable et al., 2009). Transposable elements account for almost 85% of the genome, with long terminal repeat transposons considered as the driving force for the drastic increase in genome size (Schnable et al., 2009). Throughout its evolution from its closest ancestor, *Sorghum bicolor*, the maize genome has undergone multiple duplication events, followed by chromosomal breakage and fusions, resulting in a diploid genome, with two copies of ten chromosomes, and an extremely high level of phenotypic and genetic diversity (Schnable et al., 2009).

In order to better understand the maize GST enzyme family, the maize genome (B73 RefGen_v4), available through the NCBI database, was probed for GST genes and proteins, and their sequence similarity analysed by alignment. Seven classes were identified as follows, in descending order of identified sequence number, with protein number and percent shown; tau (38, 58%), phi (16, 25%), lambda (4, 6%), zeta (3, 5%), DHAR (2, 3%), theta (1, 2%) and a unique GST (1, 2%). This unique GST was predicted to be a GHR, based on the results of a BLAST search which identified high similarity to GHR proteins of other species: GSTs sharing over 60% sequence similarity were considered to belong to the same class, with this GST sharing 89% and 83% homology with the respective genes in Heller's rosette grass (*Dichanthelium oligosanthes*) and a member of the rice genus (*Oryza brachyantha*).

In total, 56 genes were identified encoding 65 respective proteins, following potential alternative splicing (Table 15). Maximum likelihood phylogenetic analysis using an LG model of the identified GSTs was performed (Figure 25), to identify sequence relationship, where branch length indicates degree of dissimilarity. The tau and phi classes dominated significantly, with relatively small clades for lambda, zeta and DHAR, and single sequences for theta and

GHR. The family could be divided into three clades. The first clade contained only the zeta class, with individual divergence occurring late in the sequence evolution, after a branch length (BL) of 1.2. The second clade contained the theta and phi classes, which shared an early common ancestry at BL < 0.2. The third clade was split early into the GHR class (BL ~ 0.2), followed by a later divergence into the tau class (BL ~ 0.8) and a further divergence to the DHAR and lambda classes (BL ~ 1). The observed phylogenetic relationship in maize is supported by phylogenetic analyses of the rice (*Oryza sativa*) and arabidopsis GST superfamilies and in a multispecies analysis comparing arabidopsis, rice, barley (*Hordeum vulgare*), spreading earthmoss (*Physcomitrella patens*), manchurian red pine (*Pinus tabulaeformis*), black cottonwood (*Populus trichocarpa*) and tomato (*Solanum lycopersicum*) (Brazier-Hicks et al., 2017; Lallement et al., 2014). An important observation was the organisation of maize GST classes into subclasses showing high sequence similarity. This can be explained by the high degree of gene duplication inherent in maize GST evolution (Schnable et al., 2009; Wei et al., 2007). These subclasses form the basis of a new nomenclature system proposed here.

Table 15 lists the maize GST genes and proteins identified in this study, along with key genomic and proteomic features, following the phylogenetic order shown in Figure 25. It is evident from the 2nd and 10th column that the naming of these GSTs, as shown on NCBI, is inconsistent and sporadic, and fails to follow any unified nomenclature system. Over the years, GSTs have been characterised using a variety of nomenclatures, which are often interchanged, leading to misnaming, duplicate naming, and overall confusion. Sequence relatedness, immunological cross reactivity, kinetic properties and genome organisation have been used to assign classes within this family (Oztetik, 2008). In addition confusion between gene and protein was created as they were classified based upon order of gene sequencing and protein purification, respectively (Edwards et al., 2000). The most recent system follows the format “[source organism binomial]GST[class letter][class number]” where class number is based upon the order of gene discovery in each species and class, for example, *ZmGSTF1* (Edwards et al., 2000). Dimers are shown by displaying both monomer numbers, for example, *ZmGSTF1-2* (Edwards et al., 2000; Frova, 2003; Oztetik, 2008). While this system provides information on species, class and oligomeric state, the use of gene discovery in numbering provides only historical information. Here a new system is proposed intending to include further sequence relationship information in the nomenclature. The lack of adherence to the previously

proposed systems provides a suitable situation for unification and development. The proposed system will use “[*source organism binomial*]*GST*[class letter][subclass].[phylogenetic order]”, for example, *ZmGSTU9.2*. This example would therefore indicate higher sequence similarity to *ZmGSTU9.4* than *ZmGSTU8.1*, by belonging to the same subclass. Dimers would be described by the numbers of both monomers; for example, a dimer of monomers *ZmGSTF1.1* and *ZmGSTF1.3* would be named *ZmGSTF1.1-1.3*. Since no interclass dimers have been discovered, only one prefix would be present in any dimer (Sasan et al., 2011). The proposed nomenclature is used throughout this thesis. Indeed the system should be repeated for each species based on a genome-wide phylogenetic analysis.

	Gene								Protein				
class	NCBI Name	Gene identifiers		Length (bp)	chromosome	Chromosome position	Orientation	Exons	NCBI name	New name	GI accession	Length (A/A)	
Zeta, Z, ζ	gst17	542543	GRMZM2G064255	3858	5	178504869 - 178508727	-	9	GST zeta class	ZmGSTZ1.0	195645582	224	
	N/A	100283891	GRMZM2G124974	3374	10	32563935 - 32567309	-	10	uncharacterized protein LOC100283891	ZmGSTZ1.1	226502416	169	
	N/A	541833	GRMZM2G019090	10837	3	136996861 - 137007698	+	8	GST18	ZmGSTZ1.2	11385487	212	
Theta, T, θ			GRMZM2G077183										
	LOC100285763	100285763		2196	1	306104650 - 306106846	-	6	GST theta-1	ZmGSTT1.0	226504620	249	
Phi, F, φ									GST III(b)	ZmGSTF1.0	4468794	221	
	gst3b	541990	GRMZM2G146246	1562	3	156422305 - 156423867	+	3	unnamed protein product	ZmGSTF1.1	22280	220	
										ZmGSTF1.2	1170090	222	
	gst1	542366	GRMZM2G116273	2455	8	178412108 - 178414563	+	3	GST I	ZmGSTF2.0	168491	214	
	gst8	542740	GRMZM2G156877	1727	3	197152326 - 197154053	+	4	GST 8	ZmGSTF2.1	11385467	224	
	LOC542630	542630	GRMZM2G150474	2541	8	131542340 - 131544881	-	4	GST 15	ZmGSTF2.2	11385481	234	
	gst2	542311	GRMZM2G132093	1245	10	90384434 - 90385679	-	3	GST 4	ZmGSTF2.3	162460024	223	
	gst10	541828	GRMZM2G096153	1234	1	7885528 - 7886762	-	2	GST 10	ZmGSTF3.0	11385471	199	
									GST 10	ZmGSTF3.1	840084403	224	
	gst16	542490	GRMZM5G895383	3532	7	153075999 - 153079531	-	3	GST 16	ZmGSTF4.0	162459378	300	
	gst11	541829	GRMZM2G119499	1303	1	7844425 - 7845728	-	2	GST 11	ZmGSTF4.1	840088348	305	
									GST 11	ZmGSTF4.2	11385473	370	
	gst12	541830	GRMZM2G096269	1414	1	7878478 - 7879892	-	3	GST12	ZmGSTF4.3	11385475	225	
	gst13	541831	GRMZM2G126781	1281	9	154861627 - 154862908	-	3	GST 13	ZmGSTF4.4	11385477	225	
gst9	542629	GRMZM2G126763	1190	9	154871722 - 154872912	-	3	GST 9	ZmGSTF4.5	11385469	226		
csu454(gst)	100282447	GRMZM2G096247	1195	1	7882164 - 7883359	-	3	uncharacterized protein LOC100282447	ZmGSTF4.6	226509775	226		
GHR	LOC100272773	100272773	GRMZM2G102216	2166	4	174746497 - 174748663	-	2	GST	ZmGHR1.0	195652731	387	
DHAR	DHAR4	100382696	GRMZM2G005710	2337	8	137157191 - 137159528	+	6	uncharacterized LOC100382696 precursor	DHAR 4	293334671	265	
	DHAR3	100273125	GRMZM5G855672	2985	8	137153528 - 137156513	+	6	uncharacterized LOC100273125	DHAR 3	226505920	214	
Lambda, L, λ	LOC100282090	100282090	GRMZM2G162486	2289	9	141344108 - 141346397	+	10	IN2-1	ZmGSTL1.0	226532792	242	
	LOC100281225	100281225	GRMZM2G338131	2035	1	43328414 - 43330449	-	10	IN2-1	ZmGSTL1.1	226492152	231	
	pco124824	100282747	GRMZM2G043291	2220	1	43332629 - 43334849	-	10	IN2-1	ZmGSTL1.2	195612768	239	
	saf1	542388	GRMZM2G042639	1766	1	43343299 - 43345065	-	9	IN2-1	ZmGSTL1.3	22347	243	

Table 15: List of Identified maize Glutathione-S-Transferase (GST) genes and proteins.

Data was extracted from NCBI. Bp; base pairs, A/A; amino acids.

class	Gene							Protein					
	NCBI Name	Gene identifiers		Length (bp)	chromosome	Chromosome position	Orientation	Exons	NCBI name	New name	GI accession	Length (A/A)	
Tau, U, τ	gst6	541991	GRMZM2G129357	3581	7	5834880 - 5838461	-	2	GST 6	ZmGSTU1.0	4468796	222	
	gst19	541834	GRMZM2G335618	1076	6	107194718 - 107195794	+	1	GST	ZmGSTU1.1	195639794	229	
	gst5	542734	GRMZM2G308687	1048	1	290470867 - 290471915	-	1	GST parA	ZmGSTU1.2	195635273	224	
	pco061770a	542632	GRMZM2G077206	1062	8	140938758 - 140939820	+	2	GST 27	ZmGSTU2.0	11385505	237	
	LOC542634	542634	GRMZM2G145069 GRMZM2G149182	998	1	82924888 - 82925886	-	2	GST 34	ZmGSTU3.0	11385519	225	
	gst31	541842	GRMZM2G475059	1040	1	8129058 - 8130098	-	2	GST 31	ZmGSTU3.1	1121393426	254	
	gst41	541849	GRMZM2G097989	1367	6	151106734 - 151108101	-	2	GST 41	ZmGSTU4.0	11385533	267	
	LOC100502255	100502255	GRMZM2G016241	1294	1	245013270 - 245014564	-	2	bronze2	ZmGSTU4.1	308080698	259	
	gst23	541845	GRMZM2G416632	1045	7	132447895 - 132448940	+	2	GST 36	ZmGSTU5.0	11385523	222	
	siaf244694b	542633	GRMZM2G127789	982	3	150585123 - 150586105	+	2	GST 29	ZmGSTU5.1	11385509	234	
	LOC541836	541836	GRMZM2G428168	3728	3	150583971 - 150587699	-	4	GST 21	ZmGSTU5.2	11385493	235	
	gst24	541837	GRMZM2G032856	1023	5	216862593 - 216863616	-	2	GST 24	ZmGSTU5.3	13699857	238	
	LOC541840	541840	GRMZM2G146475	864	3	150720671 - 150721535	+	2	GST	ZmGSTU5.4	195649097	232	
	LOC100281369	100281369	GRMZM2G052571	0	N/A	N/A	N/A	N/A	GST	ZmGSTU5.5	226500262	228	
	gst7	542587	GRMZM2G028556	900	3	150759129 - 150760029	-	2	GST	ZmGSTU5.6	195655691	242	
	LOC541839	541839	GRMZM2G363540	881	4	38891421 - 38892302	-	1	GST 26	ZmGSTU6.0	11385503	240	
	LOC100281103	100281103	N/A	0	N/A	N/A	N/A	N/A	GSTU 6	ZmGSTU6.1	226501644	231	
	gpm198	541848	GRMZM2G028821	975	1	83227068 - 83228043	-	2	GST 39	ZmGSTU6.2	11385529	200	
	LOC100193719	100193719	GRMZM2G168229	3515	4	240523216 - 240526731	-	3	GST 33	ZmGSTU6.3	11385517	233	
	LOC100280815	100280815	GRMZM2G146913	10660	3	210250690 - 210261350	+	10	GSTU 6	ZmGSTU7.0	226506704	242	
	LOC100285806	100285806	GRMZM2G146887	1076	3	210237086 - 210238162	+	2	GSTU 6	ZmGSTU7.1	226509086	239	
	LOC100856957	100856957	GRMZM2G056388	997	3	210370615 - 210371612	+	2	GSTU 6	ZmGSTU7.2	363543523	235	
	gst20	541835	N/A	35282	3	206915390 - 206950672		+	2	GST 20	ZmGSTU7.3	11385491	180
			N/A							GSTU 6	ZmGSTU7.4	195637080	232
	LOC542631	542631	GRMZM2G330635	899	10	96969555 - 96970454	-	2	probable GSTU 6	ZmGSTU8.0	806638824	232	
	gst37	541846	GRMZM2G178079	1100	1	83198314 - 83199414		+	2	GST 37	ZmGSTU8.1	11385525	236
										GST 37	ZmGSTU8.2	1143558487	234
	LOC541847	541847	GRMZM2G066369	986	1	83264256 - 83265242		+	2	GST 38	ZmGSTU9.0	162459710	228
										GSTU 6	ZmGSTU9.1	195639848	228
	gst30	541841	GRMZM2G044383	1062	1	83410942 - 83412004	+	1	GST 30	ZmGSTU9.2	11385511	231	
	LOC541838	541838	GRMZM2G161905	1463	9	158666810 - 158668273		-	1	GST25, partial	ZmGSTU9.3	11385501	225
										GSTU 6	ZmGSTU9.4	195642728	240
	gst35	542491	ZEAMMB73_420582	913	9	158676278 - 158677191	-	2	GST 35	ZmGSTU10.0	11385521	235	
	LOC100192043	100192043	GRMZM2G480439	1561	1	83191687 - 83193248	+	3	GSTU 6	ZmGSTU10.1	212275596	245	
	LOC541850	541850	GRMZM2G025190	1138	1	83058521 - 83059659	+	2	GST 42	ZmGSTU10.2	985567325	238	
	gst40	542635	GRMZM2G054653	0	N/A	N/A	N/A	N/A	GST 40	ZmGSTU10.3	11385531	236	
	gst32	541843	GRMZM2G041685	749	1	83119704 - 83120453		+	2	GST 32	ZmGSTU10.4	840083967	138
										GST 32	ZmGSTU10.5	11385515	203

Table 15: (Continued).

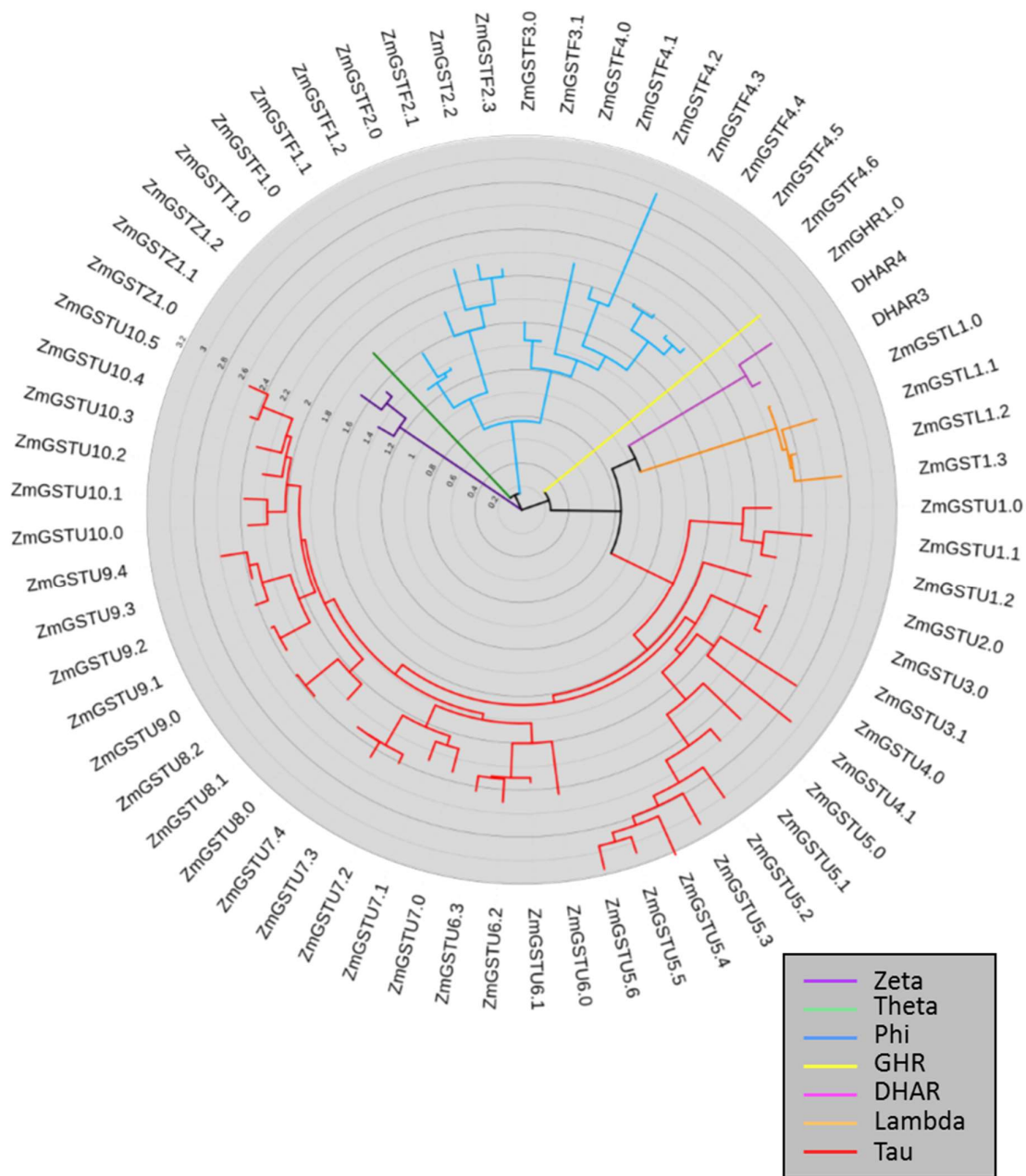


Figure 25: Circular tree of maize Glutathione-S-Transferases (GSTs) based on maximum likelihood phylogenetic analysis using an LG model.

Sequences were aligned and phylogenetic tree produced using seaview software. Tree was annotated using ITOL and Figtree software. Classes are represented by colour as detailed in the legend (bottom right). Internal scale axis (concentric rings) describes branch lengths. Node tip labels show new protein nomenclature as described in Table 15.

4.2.2 Functions of maize GSTs

Through a search of literature, the herbicide substrate activity of maize GSTs were reviewed in order to better understand the specific roles of each GST in safener effects (Table 16). As expected the zeta and lambda class GSTs showed no glutathione conjugating activity (Frova, 2003). The phi and tau classes showed varying degrees of activity, displaying specificity towards individual substrates. In all cases, the activity to the model substrate 1-chloro-2,4-dinitrobenzene (CDNB) was higher than that of the other herbicides. CDNB is used as a model substrate to test the general glutathione conjugation ability of GSTs, and displays a high degree of variation between individual phi and tau class members. Very low activities were observed for *ZmGSTF2.1-2.1*, *ZmGSTF2.3-2.3*, *ZmGSTF3.0-3.0*, *ZmGSTF4.5-4.5*, and *ZmGSTU4.1-4.1*, with all substrates, indicating these enzymes likely do not function in endogenous metabolism of the analysed herbicides. They may have other roles in cell function or may be safener-inducible. It has been determined that under normal conditions, the dominant GST in maize foliage is *ZmGSTF2.0-2.0* (previously *ZmGSTF1-1/ZmGSTI-I*), displaying the most glutathione conjugating activity, with Dixon (1998) identifying a CDNB activity of 1693 nkat mg⁻¹, and presumably responsible for endogenous herbicide metabolism in tolerant plants (Dixon et al., 1997). However it is relatively unaffected by safeners (Dixon et al., 1997).

In contrast, safeners such as dichlormid and benoxacor increase the expression of the *ZmGSTF2.3* subunit, which binds the constitutive *ZmGSTF2.0* subunit, forming the heterodimer *ZmGST2.0-2.3* (previously *ZmGSTF1-2/ZmGSTI-II*) (Dixon et al., 1997; Holt et al., 1995; Irzyk et al., 1993). This isoenzyme has the third largest glutathionylation activity of the analysed GSTs, with Dixon (1998) identifying a CDNB activity of 1125 nkat mg⁻¹, and forms one of the major isoenzymes responsible for safener-induced herbicide metabolism (Dixon et al., 1997; Dixon et al., 2002b). It has been demonstrated that GSTs containing the subunits *ZmGSTF1.0* and *ZmGSTF2.3* are active towards chloroacetanilides, and are induced by safeners, though only *ZmGSTF1.0* is constitutively expressed (Dixon et al., 1998a; Prade et al., 1998). Thus *ZmGSTF2.0-1.0*, which displays the second largest CDNB activity of 1240 nkat mg⁻¹ (Dixon, 1998), exists constitutively and is increased upon certain Safener treatments.

Of the Tau class GSTs, *ZmGSTU1.2-1.0*, *ZmGSTU1.1-1.1*, *ZmGSTU1.2-1.2*, and *ZmGSTU7.3-7.3* represent the most active isoenzymes, with respect to glutathione conjugation to CDNB, with *ZmGSTU4.1-4.1* (previously BZ2/Bronze2) showing minimal activity. Protein studies also

indicate that ZmGSTU1.2 is constitutively expressed, though less abundantly than ZmGSTF2.3 (Dixon, 1998; Dixon et al., 1999; Rao, 2014).

Though not all combinations of herbicide have previously been tested, it is apparent that the phi class GSTs show high activities towards the herbicides alachlor and metolachlor, chloroacetanilide inhibitors of VLCFA synthesis, while the tau class GSTs show high activity towards the fluorodifen herbicide, a diphenylether inhibiting PPO (see section 1.2). This indicates possible class-specific herbicide substrate preferences, with phi class GSTs conjugating chloroacetanilides and tau class GSTs conjugating diphenyl-ethers. This observation is supported by previous indications that phi class enzymes are highly active towards chloroacetanilide and thiocarbamate herbicides, which both share an amide group, while tau class enzymes are active against diphenylether and aryloxyphenoxypropionate herbicides, which both share a diphenyl ether group (Jepson et al., 1994; Rao, 2014; Thom et al., 2002). This has been observed in crops such as rice (Cho et al., 2007). The high activity of tau class GSTs in conjugating fluorodifen has been observed in red shepherd's purse (*Capsella rubella*) and soybean (*Glycine max*) (Axarli et al., 2009b; He et al., 2016).

Previously known as	New name	Specific activities against substrates						
		CDNB	Atrazine	Alachlor	Fluorodifen	Metolachlor	Acetochlor	Chlorimuron-ethyl
ZmGST 17	ZmGSTZ1.0-1.0	0.75 ^{b 8}	0 ⁸	0 ⁸				0.0017 ^{b 8}
ZmGST III-III/ZmGST III	ZmGSTF1.0-1.0			3.0 ^{a 6}		1.1 ^{a 6}		
GSTIII	ZmGSTF1.1-1.1	30.05 ^{b 8}	0.00083 ^{b 8}	0.05 ^{b 8}				0.005 ^{b 8}
ZmGST I-III	ZmGSTF2.0-1.0	1240 ^{b 1}	0.07 ^{b 1}	1.25 ^{b 1}	0.19 ^{b 1}	1.93 ^{b 1}		
ZmGSTF1/ZmGSTI-I/ZmGSTI	ZmGSTF2.0-2.0	1233.33 ^{b 2}	Unk ⁴	0.38 ^{b 2}				0.067 ^{b 8}
		375 ^{c 3}	0 ⁵	0.06 ^{b 5}	0.00067 ^{b 5}	0.04 ^{b 1}		
		235 ^{b 5}	0.11 ^{b 1}	1.47 ^{b 1}	0.01 ^{b 1}			
		1693 ^{b 1}	0.01 ^{b 8}	1.28 ^{b 8}				
		774.75 ^{b 8}						
ZmGSTII/ZmGST I-II	ZmGSTF2.0-2.3	433.33 ^{b 2}	0 ⁵	0.63 ^{b 2}	0.0033 ^{b 5}	1.72 ^{b 1}		
		106.67 ^{b 5}	0.07 ^{b 1}	0.40 ^{b 5}	0.26 ^{b 1}			
		1125 ^{b 1}		3.20 ^{b 1}				
ZmGST 8	ZmGSTF2.1-2.1	0.25 ^{b 8}	0 ⁸	0 ⁸				0.0033 ^{b 8}
ZmGST II-II/GST IV/ZmGSTF2	ZmGSTF2.3-2.3	0.25 ^{b 8}	0.0033 ^{b 7}	0.043 ^{b 7}		0.035 ^{b 7}	0.047 ^{b 7}	0.005 ^{b 8}
			0 ⁸	0.017 ^{b 8}				
ZmGST 10	ZmGSTF3.0-3.0	0.25 ^{b 8}	0 ⁸	0 ⁸				0.0017 ^{b 8}
ZmGST 9	ZmGSTF4.5-4.5	0.5 ^{b 8}	0 ⁸	0 ⁸				0.0017 ^{b 8}
in2-1	ZmGSTL1.3	0.25 ^{b 8}		0 ⁸				0 ⁸
ZmGST V-VI	ZmGSTU1.2-1.0	597 ^{b 1}	0 ¹		0.49 ^{b 1}	0.88 ^{b 1}		
ZmGST 19	ZmGSTU1.1-1.1	35.6 ^{b 8}	0.0013 ^{b 8}	0.45 ^{b 8}				0.032 ^{b 8}
ZmGST V-V	ZmGSTU1.2-1.2	216 ^{b 1}	0 ¹		0.47 ^{b 1}	0.49 ^{b 1}		0.0067 ^{b 8}
		65.65 ^{b 8}	0.00017 ^{b 8}	0.3 ^{b 8}	0.518 ^{b 9}	0.253 ^{b 9}		
		90.7 ^{b 9}						
BZ2	ZmGSTU4.1-4.1	0.25 ^{b 8}	0 ⁸	0 ⁸				0.0033 ^{b 8}
ZmGST20	ZmGSTU7.3- 7.3	22.47 ^{b 8}	0.00033 ^{b 8}	0.13 ^{b 8}				0.0017 ^{b 8}

Table 16: Known maize Glutathione-S-Transferase (GST) activity against herbicide substrates.

Data collated from literature survey. Superscript numbers define sources: 1; Dixon, 1998 , 2; Mozer et al., 1983 , 3; Wiegand et al., 1986 , 4; Wosnick et al., 1989 , 5; Holt et al., 1995 , 6; O'connell et al., 1988 , 7; Irzyk et al., 1993 , 8; Mcgonigle et al., 2000 , 9; Dixon et al., 1998a . Superscript letters define specific activity units: a; $\mu\text{g mg}^{-1} \text{h}^{-1}$, b; nkat mg^{-1} , c; $\Delta\text{A}_{340} \text{min}^{-1} \text{mg}^{-1}$. CDNB; 1-Chloro-2,4-dinitrobenzene.

4.2.3 *Evolution of GSTs*

Despite the numerous studies focusing on GSTs, it is still unclear how the GST superfamily has evolved. A better understanding of the GSTs evolutionary relationships could shed light on the understanding of the multiple functions performed by this family. Figure 26 represents a proposed scheme of GSTs evolution, performed by literature search of the presence of GST classes in distinct domains, kingdoms and orders. The GHR class is present in photosynthetic organisms, Metazoa, Archae and Halobacteriaceae, indicating it as likely the first GST class that evolved from the thioredoxin-like ancestor enzyme (Lallement et al., 2014; Sasan et al., 2011). The indication that a catalytic cysteine was the original residue, supports this finding (Sylvestre-Gonon et al., 2019). A monophyletic origin for the zeta and theta classes has been suggested, preceding the plant-animal split (Dixon et al., 1998b; Thom et al., 2002), and indeed they are present in both animals and plants, likely following divergence with GHR (Frova, 2003). Since zeta and theta classes show such high similarity and presence in the same kingdoms, it is hard to know when the divergence between the classes occurred, and which came first. As such, they are considered together in Figure 26. However, it has been suggested that the theta class is the closest to the original progenitor of all eukaryotic GSTs, and therefore may be considered to precede the zeta class (Edwards et al., 2000; Frova, 2003; Sylvestre-Gonon et al., 2019). The DHAR class exists in both algae and terrestrial plants, whilst the remaining classes GSTs are found only in terrestrial plants, suggesting DHAR as the next class to appear. The information obtained from the phylogenetic analysis (section 4.2.1), confirmed that DHAR and lambda classes evolved from a common ancestor related to GHR, indicating a split into two major ancestries (Lallement et al., 2014). The phylogeny indicates lambda class GSTs evolved from a common ancestor of DHAR. Phi and tau class GSTs are found only in plants, and the phylogenetic analysis would suggest that they evolved from an ancestor shared with the theta class, and DHAR and lambda classes, respectively (Dixon et al., 2002b; Thom et al., 2002). Interestingly, the use of serine as the catalytic residue appears to have evolved in a convergent manner. The use of a catalytic serine, instead of the cysteine used by the original GHR, appears in the tau class, and the ancestrally distinct theta class, indicating convergent evolution towards this active residue, required for GSH conjugation (Sylvestre-Gonon et al., 2019). As such, the tau and phi classes are considerably distinct in overall sequence, yet share similar functions in xenobiotic detoxification (Dixon et al., 2002a). This indicates an evolutionary selection pressure towards having a large range of enzymes capable of detoxifying xenobiotics through GSH conjugation. This is not surprising since single amino acid

changes are very common, and in this case cause an increase in the number of metabolic substrates. The alpha, pi and mu GSTs in mammals evolved the use of a catalytic tyrosine residue for glutathionylation, while the beta GSTs retained the original cysteine, indicating the catalytic residue is adapted for a variety of catalytic function (Dixon et al., 2002b).

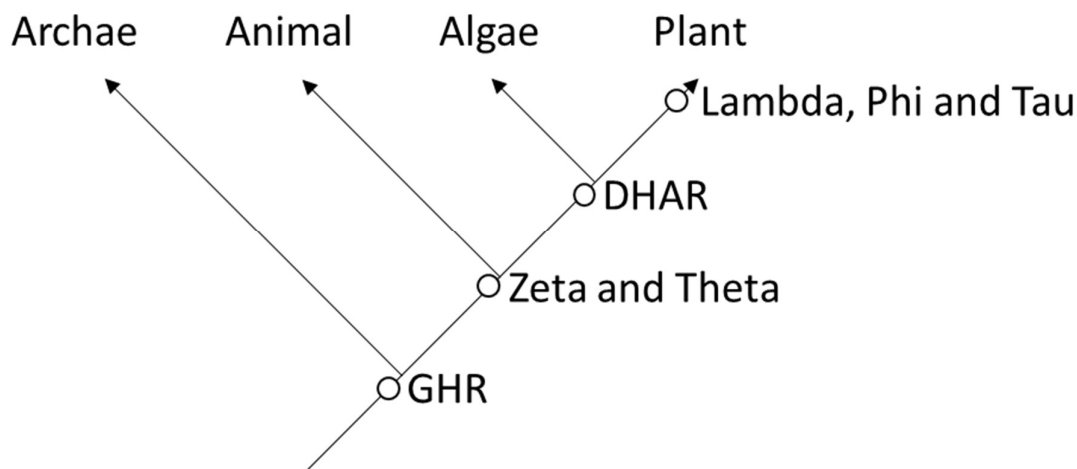


Figure 26: Schematic indicating proposed evolution of Glutathione-S-Transferases (GSTs) based on the literature and the information obtained in section 4.2.1.

GST classes are denoted by circles.

4.2.4 Chromosome distribution of maize GSTs

The chromosome distribution of plant GSTs was discovered to be non-random as early as 1999, which may provide information about the evolution of the large family of GSTs in maize (Frova, 2003). The *in-silico* chromosomal positioning of the identified maize GST genes was analysed and is shown in Figure 27. The genes are found on all chromosomes, except chromosome 2, and in the mitochondrial and plastidial genomes. The highest number of sequences (19 genes) was observed on chromosome 1, a pattern also observed in arabidopsis (Frova, 2003). Chromosome 3 possessed 11 GST genes, and chromosomes 4-10 all contained 5 or less genes. The large size of the family with diverse chromosomal positioning is suggestive of numerous gene duplication events and transpositions, as has been described for the domestication of maize (Kramer et al., 2007; Oztetik, 2008). Indeed maize domestication from its ancestor, *Andropogoneae*, is believed to include genetic divergence and subsequent convergence, resulting in a large chromosome size, while simultaneously causing a high degree of gene duplication and transposition (Wei et al., 2007). This early event likely caused the large phi and tau classes, which showed two to four clusters on multiple chromosomes. The individual genes, not present within clusters have most likely arisen through duplication and

conventional transposition. In fact, the high diversity of the GST family has been attributed to a combination of chromosome gene duplication, unequal crossing over, alternative splicing, swapping and mutagenesis (Sasan et al., 2011).

A high degree of clustering occurred within each class, with individual patterns observed for each. The tau class GSTs presented in four clusters on chromosomes 1, 3 & 9, with individual genes on almost all other chromosomes. The phi class GSTs presented in clusters on chromosomes 1 & 9, with individuals on four other chromosomes. The high numbers and localisations of these two GSTs classes indicates they have undergone the highest degree of duplication and transposition, a trend also observed in rice (Frova, 2003). DHAR class GSTs possessed a single cluster on chromosome 8, while lambda class GSTs showed a cluster on chromosome 1 and an individual on chromosome 9. The low number and tight chromosomal clustering of DHAR and lambda GSTs indicates recent duplication events. Zeta, theta and GHR class GSTs presented no clustering. These classes presented low gene numbers and localisation, indicating a low degree of duplication and transposition.

This clustering of classes has been documented previously, but it is interesting to note that the sequence similarity-based subclass predictions (section 4.2.1) match this clustering relatively closely (Frova, 2003). For example, members of the *ZmGSTF1* subclass are clustered together on chromosome 3. It may be supposed that individual class members duplicated and transposed, creating clustered subclasses with similar sequences on different chromosomes.

4.2.5 *Domain organisation and interface interactions of maize GST proteins*

In order to further understand the differences inherent in the GST superfamily, the domain organisation and the residues involved in dimerisation, known as interface residues, of maize GSTs were analysed by compiling available data from NCBI (Figure 28). GSTs are usually defined by two domains, on the basis of secondary structure and function. The N-terminal domain contains the thioredoxin superfamily fold, which remains relatively consistent in all GST classes, and a C-terminal domain known to be involved in substrate specificity, which shows more variation between classes (Frova, 2003). These domains are flanked by N-terminal and C-terminal extensions and surround a central linker sequence. As shown in Figure 28, this pattern was observed for all GSTs except *ZmGSTU10.4* and *ZmGHR1.0* possessing no N-terminal domain and *ZmGSTF4.0* possessing no C-terminal domain. Since GSTs are characterised by both domains, these cases are likely due to incorrect assignment in the genome, or sequence truncation in the case of *ZmGSTU10.4* (Axarli et al., 2009a). The overall structure of the GSTs, with respect to N-terminal and C-terminal domain length and overall length, was similar for the whole GST family. The N-terminal region was typically around 70 to 90 amino acids, though the DHAR proteins showed a lower size of 57 residues. The C-terminal region showed higher variation, from 59 to 166 amino acids. The N-terminal extension was typically 0 to 25 amino acids in length, though DHAR4 presented a larger extension of 59 residues. The N-C linker region was consistently between 10 and 20 amino acids in length. The C-terminal extension was highly variable ranging from 5 to 89 residues. These observations support previous finding that the C-terminal regions of GSTs are more variable than the N-terminal regions (Frova, 2003).

Each GST monomer may form a dimer through electrostatic, hydrophobic ball and socket, or hydrophilic interactions, except for the DHAR and Lambda classes, which exist only as monomers (Dixon et al., 2005; Lallement et al., 2014). These enzymes can exist as homo- or hetero- dimers, with the interaction occurring between the N-terminal domain of one monomer and the C-terminal domain of the partner monomer. Hetero-dimers may only form between members of the same class, due to differences in specific interface residues used (Dixon et al., 2005).

As shown in Figure 28, interface residues are positioned at close to the N-terminal/C-terminal boundary, highlighting conservation of the dimerisation system in GSTs. Interestingly, the theta class, most of the tau class (92%) and some of the phi class (13%) GSTs possessed

interface residues on both C- and N- terminal domains, while zeta class GSTs showed interface residues on only one (67%), or on no (33%), terminal domain. Most lambda (75%) and DHAR (50%) GSTs presented no interface residues, consistent with their monomeric oligomerisation. Thus, some incongruent results were shown, possibly due to miss-annotations of the genome, including the identification of interface residues in DHAR4 and *ZmGSTL1.1* and a lack of interface residues in all zeta class GSTs, *ZmGHR1.0*, *ZmGSTF- 1.0*, *1.1*, *1.2*, *2.1*, *2.2*, *3.0*, *3.1*, *4.0*, *4. 1*, *4.2*, *4.3*, *4.4*, *4.5*, *4.6*, and *ZmGSTU-1.1*, *5.1* and *10.4*.

Figure 29 highlights the specific interface residues that are involved in the dimer interface reactions of each class. This indicated a high use of both hydrophilic and hydrophobic residues. The larger classes, phi and tau, displayed 68% and 79% hydrophilic residues, respectively. Zeta and theta classes, possessed 9% more hydrophobic residues than hydrophilic and GHR displayed 67% hydrophilic residues. Thus, most dimerising GST classes used more hydrophilic than hydrophobic interactions to achieve dimerisation. This is contradictory to previous descriptions of interface residues as primarily hydrophobic (Dixon et al., 2005). Some studies have also indicated the use of hydrophobic residues for phi class GSTs, and hydrophilic residues for theta and tau classes, of which only the trend in tau has been observed here (Frova, 2003).

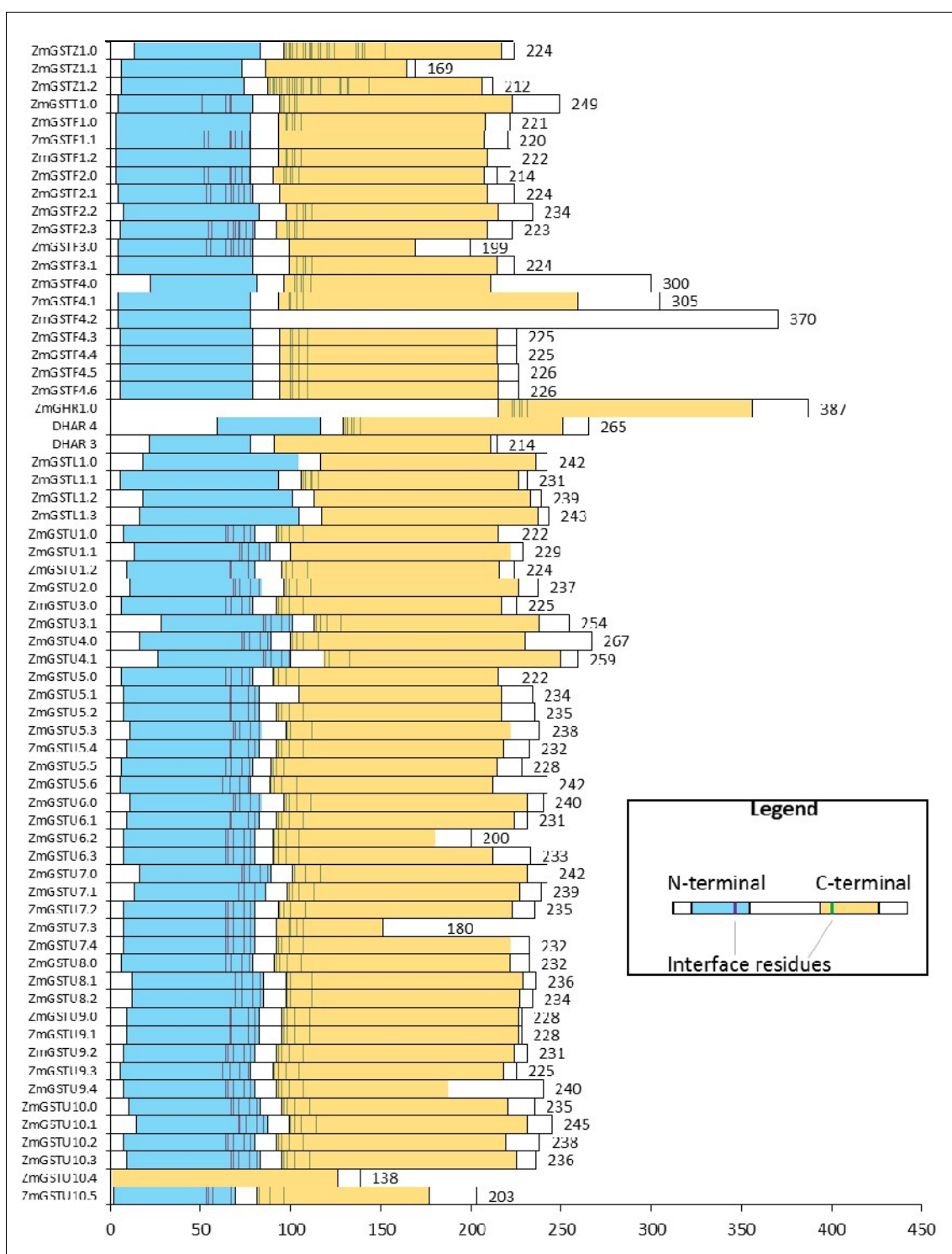


Figure 28: *In-silico* domain and interface residue localisations of maize Glutathione-S-transferase (GST) proteins.

Data on GST protein domains and interface residues were extracted from NCBI and mapped using Excel. X-axis indicates amino acid length. Y-axis indicates GST protein, according to new nomenclature. Legend (right) indicates N-terminal and C-terminal domains and interface residues. Data labels (bar tips) denote protein length in amino acid number.

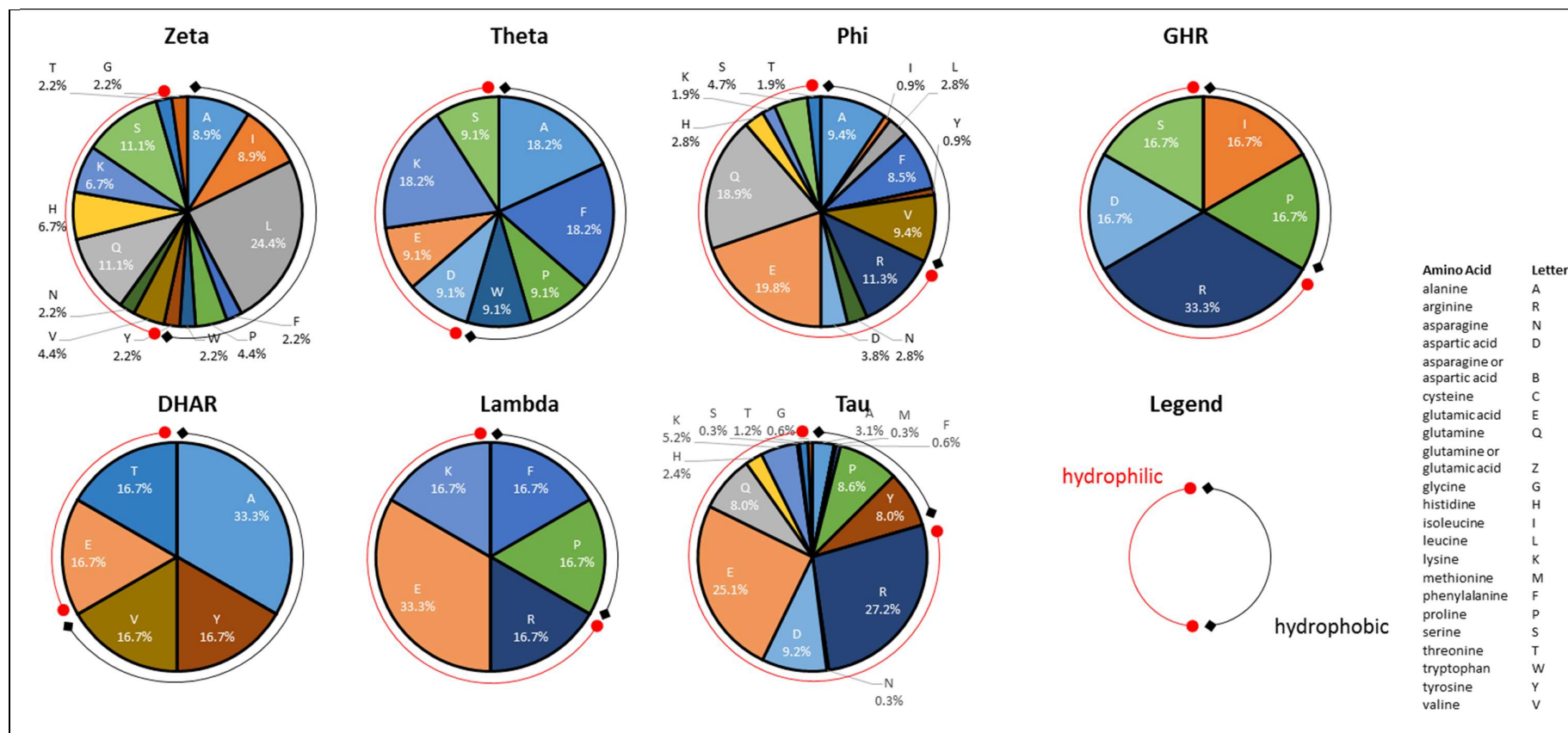


Figure 29: Pie charts describing percentage ratios of amino acid residues involved in dimer interface interactions of Glutathione-S-transferase (GST) classes.

Data on dimer interface residues were extracted from NCBI and plotted using Excel. The number of times each amino acid was involved in interface reactions was taken as a percentage of the total number of interface reactions for each class. Legend (bottom right) describes hydrophilic and hydrophobic residues. Amino acids described by IUPAC letters (shown on the right). Amino acid properties taken from "A Review of Amino Acids," Accessed 2019 .

4.2.6 G-site of maize GSTs

To understand the conserved interaction of GSTs with GSH, the glutathione-binding site (G-site) was investigated, through alignment of maize GST protein sequences, with G-site annotations from the genome included (Figure 30). In general, the *in silico* analysis of the G-site residues showed high inter-class and higher intra-class position and residue conservation, indicating strong selection towards retaining these sequences for glutathione-binding function.

The analysis showed seven potential G-site residues, described by the alignment positions 122, 124, 169, 182, 187, 204, 205 (Figure 30). However, alignment number 124 presented only a 9% family similarity and therefore may not be a vital G-site residue and in consequence only the alignment numbers 122, 169, 182, 187, 204, 205 may be considered G-site residues. In addition, there is some incongruence caused by the lack of G-site residues in the GHR and lambda class, and some phi (44%), zeta (66%) and tau (8%) class enzymes, which may represent a lack of glutathione binding but more likely is due to a lack of annotation in the genome.

To avoid reliance on databases that may have misidentified residues, hydrogen bond (H-bond) interactions of the G-site were investigated by analysis of GST X-ray and NMR structures, with GSH as the ligand (Figure 31). The models used for this schematic are detailed in Table S 11. Comparison of the alignment and H-bond interactions provides clear determination of important G-site residues.

Focusing on the different positions determined by the alignment as potential G-site residues, the position 205 (Figure 30) presented a serine in all sequences, except *ZmGSTU10.4* which had no G-site annotated, and displayed an 89% family similarity. This was confirmed by the H-bond analysis, in which nine out of ten investigated structures presented a serine residue stabilising the glutamyl-carboxylic acid group of glutathione; the exception, DHAR from rice (*Oryza sativa*), using lysine for this function. The position 204, showing a 72% sequence similarity in the family, presented glutamic acid as the most common residue (80% of GSTs), with aspartic acid representing the alternative. In addition, eight out of ten structures used glutamic acid to stabilise the glutamyl-ammonium group of glutathione, the DHAR structures instead using a lysine (DHAR from rice) or aspartic acid (DHAR 3A from black cottonwood (*Populus trichocarpa*)) for this function. In those cases, aspartic acid was not annotated as a G-site residue, though its use in the DHAR structure suggests these may function as G-site

residues. While no zeta or theta X-ray structures were found, the alignment suggested they may use aspartic acid and glutamic acid to bind this moiety, respectively. The position 187, displaying a family sequence alignment of 49%, presented isoleucine or valine in annotated sites of all classes. The H-bond analysis confirmed this, with the nitrogen and carbonyl groups of the glutathione cysteinyl-region being co-stabilised by valine (5/10 cases), or isoleucine (4/10 cases); the exception, GHR (GST X1-1/GHR1 from black cottonwood), using a tryptophan to stabilise only the carbonyl group. Alternate residues include glutamine and alanine which are not annotated. Finally, the position 122 corresponds to the catalytically active residue of the GSTs. The sequence similarity was shown to be 43%, which reflects the use of two different residues depending on class. The phi, tau, theta, and zeta classes all presented a serine in this catalytic site, as has been demonstrated in the literature (Sylvestre-Gonon et al., 2019). This residue activates the glutathione cysteinyl-sulfur group, which is considered to be the activation step of glutathione for conjugation to xenobiotics (Axarli et al., 2010; Lallement et al., 2014). The DHAR, lambda and GHR classes, however, all possessed a cysteine at this location, as seen in the literature (Lallement et al., 2014; Sylvestre-Gonon et al., 2019). Unlike serine, this residue catalyses the deglutathionylation of substrates (Lallement et al., 2014). As such, the replacement of an active serine at alignment position 122 with a cysteinyl residue causes loss of glutathione conjugation activity, and often causes the reverse reaction, deglutathionylation, to occur (Lallement et al., 2014). Despite the widely understood importance of this catalytic serine, only one structure (GSTU30 from black cottonwood) showed this H-bond interaction. Therefore, it is likely that some annotations have been incorrectly assigned in the genome.

These analyses have identified the key residues and positions for GSH binding in GSTs. While certain classes have evolved the use of different residues, the G-site positions remain similar and the residues perform the same hydrogen bond interactions required for GSH binding. However, the catalytic serine or cysteine used by different classes creates a binding chemistry responsible for different reactions, namely glutathione conjugation or de-conjugation (Lallement et al., 2014).

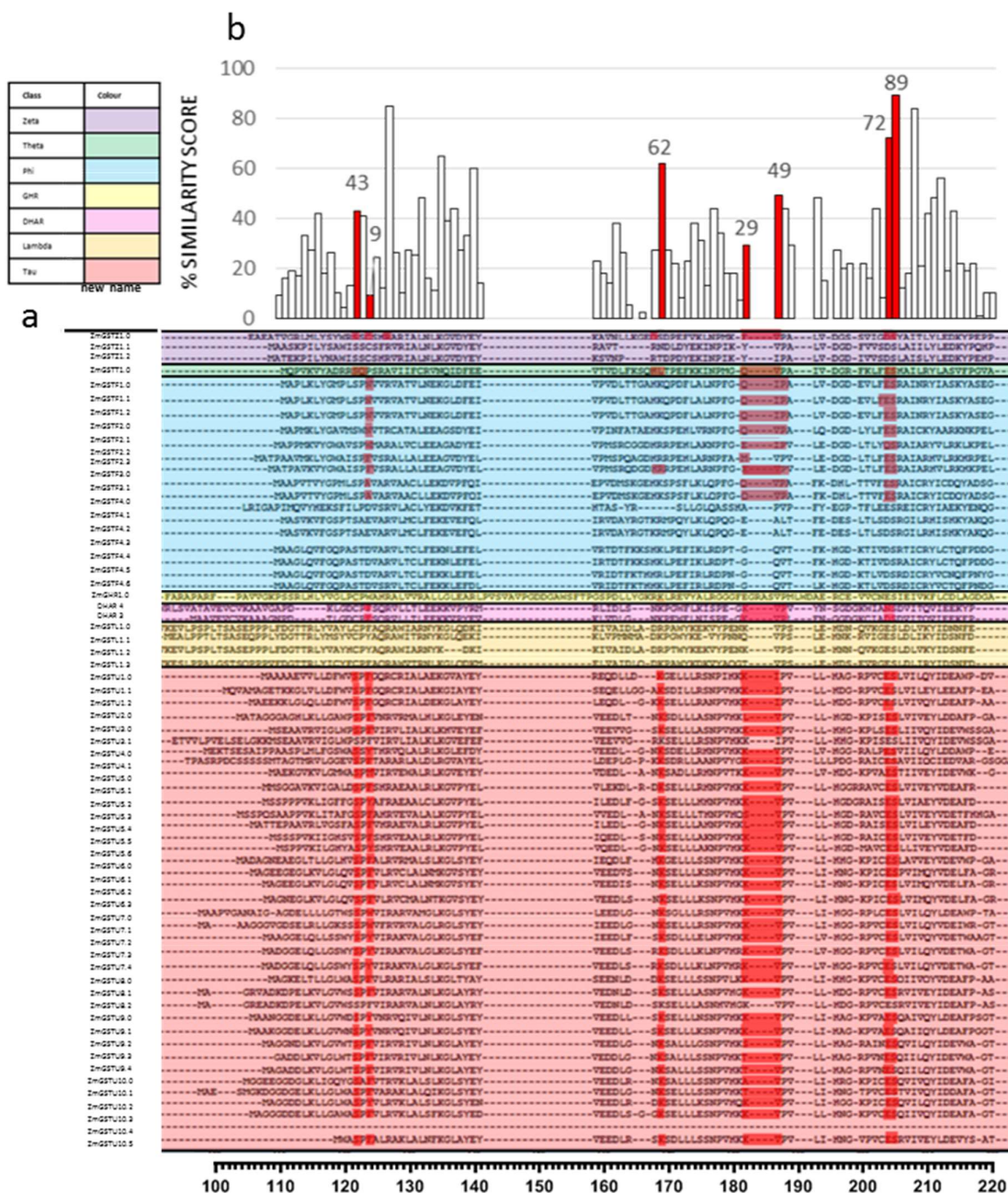


Figure 30: a; Aligned maize Glutathione-S-Transferase (GST) sequences with identified Glutathione-binding (G-) sites displayed in red. **b;** Graph showing percent similarity of residues between positions 110-220 of the alignment, with important sites highlighted in red with data values.

Alignment of GST sequences performed using seaview software. X-axis describes alignment positions. Colour Key of GST class is shown (top left).

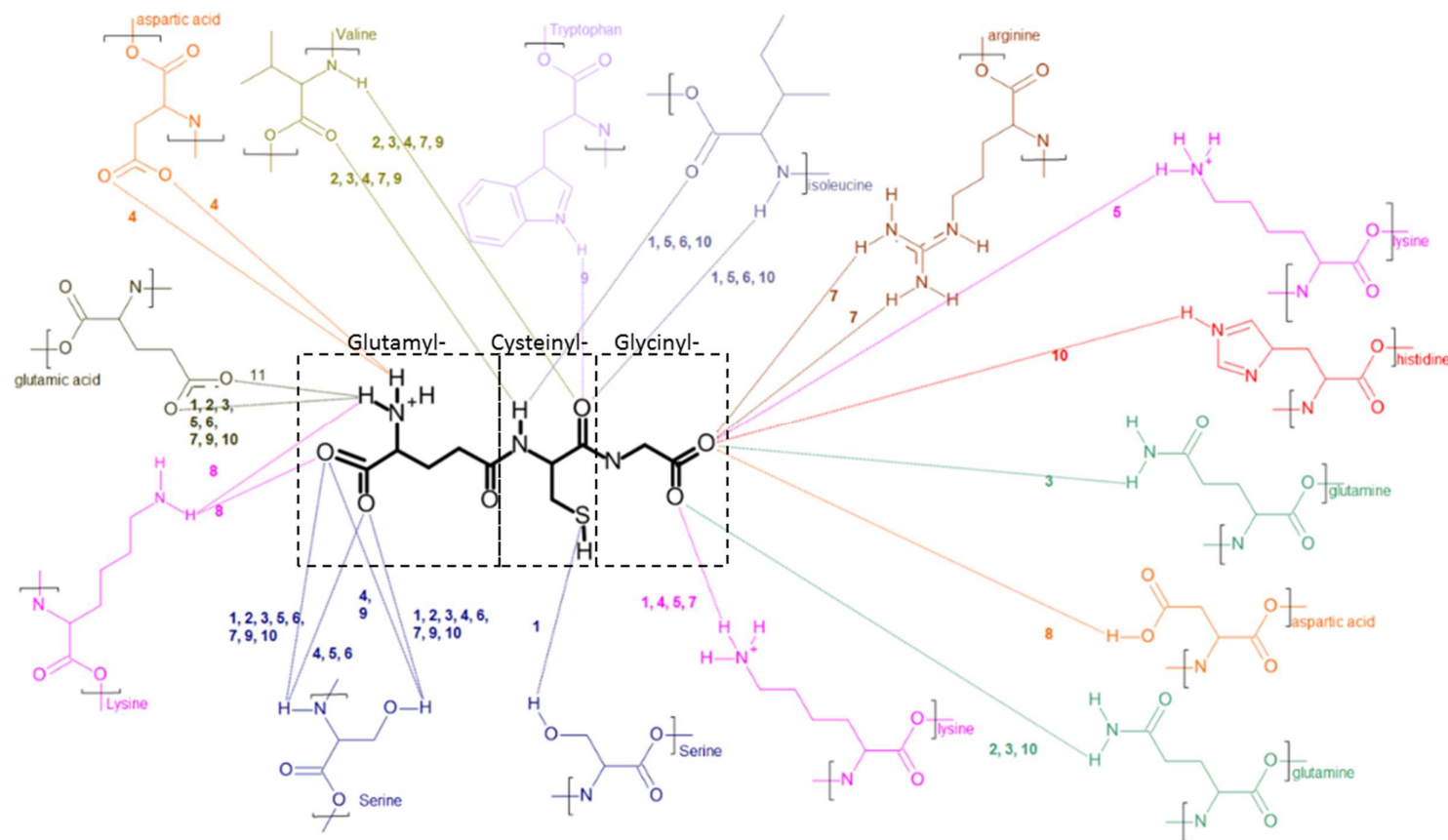


Figure 31: 2-Dimensional hydrogen-bond schematic of Glutathione-binding (G-) site interactions of resolved Glutathione-S-Transferase (GST) structures.

- 1 Data on hydrogen-bonding interactions were taken from X-ray crystallography and NMR structures and mapped using Biovia draw. Glutathione is shown in the centre with peptides labelled in dashed boxes. Hydrogen bonds are shown with dotted lines. Colours distinguish different amino acids.
- 2 Numbers indicate the structures with the respective interactions as detailed in Table S 11. Basic amino acid motifs (N-C-(C=O)-O) are surrounded by square brackets.
- 3
- 4

4.2.7 *H-site of maize GSTs*

As well as the G-sites, the substrate-binding sites (H-sites) of the GSTs, as annotated in the genome, were investigated to understand the basis of differences in substrate specificity (Figure 32). Based on overall sequence similarity, three common motifs were identified which could be used as predictors of H-site position and general substrate binding; F/L/Y-X-X-W, L/V-X-X-F/Y, and P-X-X-X-X-V-F/V-X-X-X-F/V where X represents any amino acid. The use of chemically similar residues at each predicted H-site indicates that while substitutions of amino acids may occur, it must be to those with similar chemical or structural properties.

The *in silico* analysis (Figure 32) identified eleven H-site positions for phi class enzymes, as follows (including class sequence similarities); 266 (37%), 270 (16%), 271 (40%), 274 (14%), 275 (28%), 277 (22%), 278 (16%), 282 (13%), 285 (10%), 446 (9%) and 453 (8%). The specific residues used in the H-sites (Figure 33) indicated phi class GSTs utilised a large percentage of phenylalanine, tyrosine and valine, all containing hydrophobic side chains, two of which have aromatic rings. Proline, which contains a pyrrolidine ring, was also heavily used in this class. Alanine was also used, though displays little similarity to the other amino acids. Though not recognised as an H-site residue of phi class GSTs, position 456 (26%) showed significant sequence conservation and therefore may be involved in the binding site, possibly for structural reasons.

In tau class enzymes, the *in silico* analysis indicates fifteen H-site positions, as follows (including class sequence similarities); 266 (79%), 270 (7%), 271 (21%), 274 (6%), 275 (13%), 277 (0%), 278 (11%), 279 (6%), 280 (19%), 446 (12%), 453 (48%), 538 (27%), 540 (27%), 543 (14%) and 547 (9%). The most commonly used residues in tau class GSTs were leucine, phenylalanine, tryptophan, and tyrosine, all possessing hydrophobic side chains, three of which have aromatic rings. Interestingly, tau and phi class GSTs shared similar usage of phenylalanine and tyrosine residues for substrate binding, though also used a variety of different residues. This observation supports the theory that these differences may mediate GST class specificity towards different herbicide classes (see section 4.2.2).

Similarly, the intra-class substrate specificity may be explained by the variety of residues used. Zeta class GSTs displayed H-sites (including class sequence similarities) at 70 (100%), 73 (43%), 75 (24%), 453 (100%) and 460 (9%), while theta class GSTs displayed H-sites at 266, 270, 271, 274, 275, 277, 278, 282, 446 and 462. Zeta and theta class GSTs displayed very similar profiles, using identical proportions of arginine, tyrosine, methionine and leucine. Glutamine and

alanine were also used by both, with theta also using histidine and valine. The similar profiles of zeta and theta is consistent with predictions that these classes share common functional roles in primary cell metabolism (Frova, 2003). Analysis of the lambda class, identified seven H-site positions as follows (including class sequence similarities); 259 (69%), 262 (40%), 263 (26%), 266 (62%), 268 (100%), 446 (33%) and 453 (31%). The H-site positions (including class sequence similarities) in the DHAR class were 254 (100%), 268 (100%), 269 (100%), 446 (100%) and 453 (100%). In the GHR class the H-site positions were 254, 268, 269, 446 and 453. DHAR, Lambda and GHR class GSTs all used very different residue for substrate binding, consistent with their differing functions and substrates.

Globally, the regions of these residues were reasonably conserved within classes, and between classes to a lesser degree, indicating the H-site cleft is structurally conserved. Interestingly, tau class enzymes displayed an extra region at alignment positions 538-547. In contrast, the specific residues involved in binding were very poorly conserved, which is likely responsible for the enzyme-substrate specificity. There was some conservation of residue within classes, with 9-40%, 7-48% and 31-100% conservation in phi, tau and lambda class enzymes, respectively. It is likely that, since binding depends on all interacting residues, the least conserved residues are responsible for individual enzyme-substrate specificity while the more conserved residues are important for class-specific binding, as described in section 4.2.2.

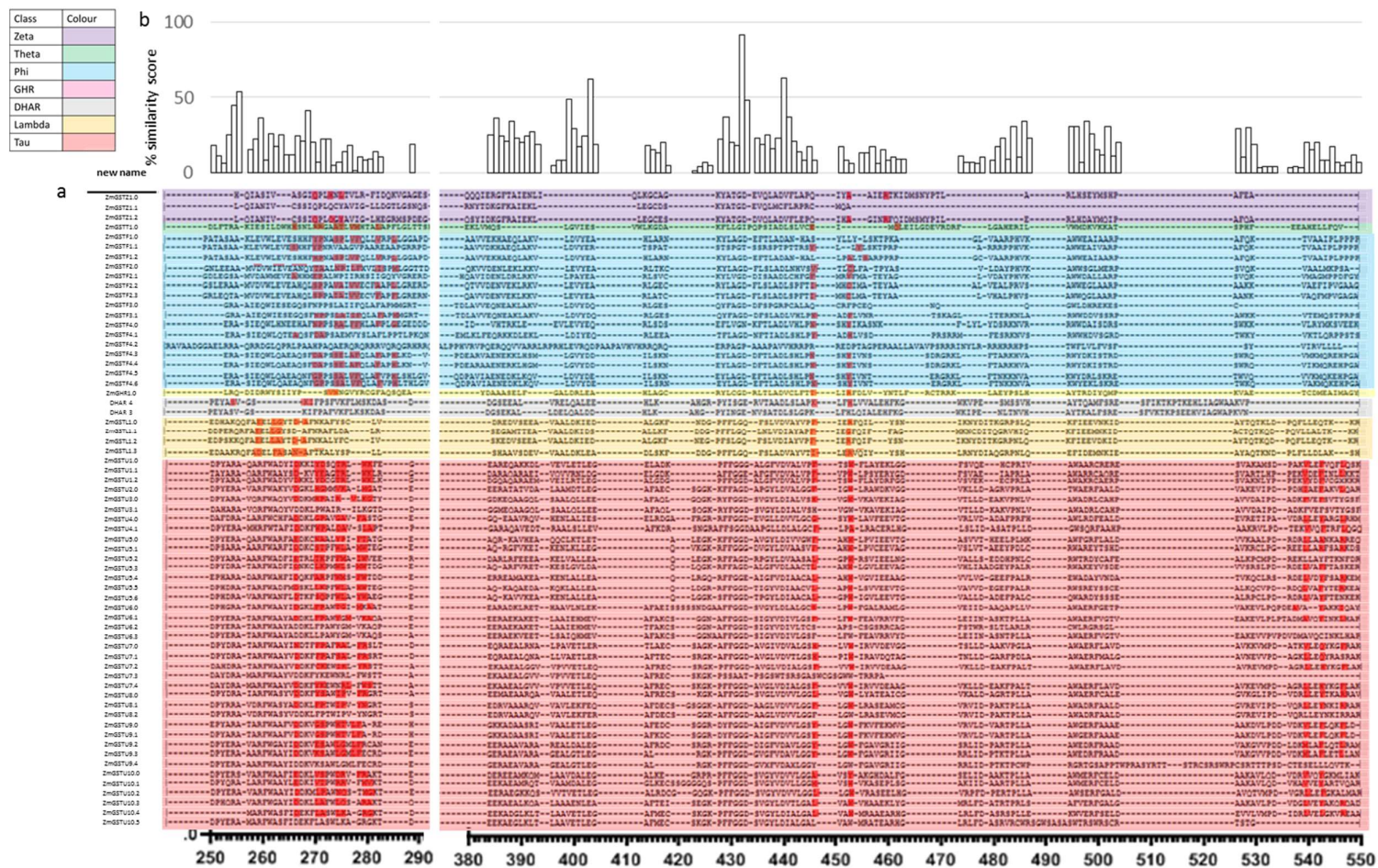


Figure 32: a; Aligned maize Glutathione-S-Transferase (GST) sequences with identified substrate binding (H-) sites displayed in red. b; Graph showing percent similarity of residues from alignment positions 250 to 290 and 380 to 550.

Alignment of GST sequences performed using seaview software. GST class legend is shown (top left). X-axis describes alignment positions.

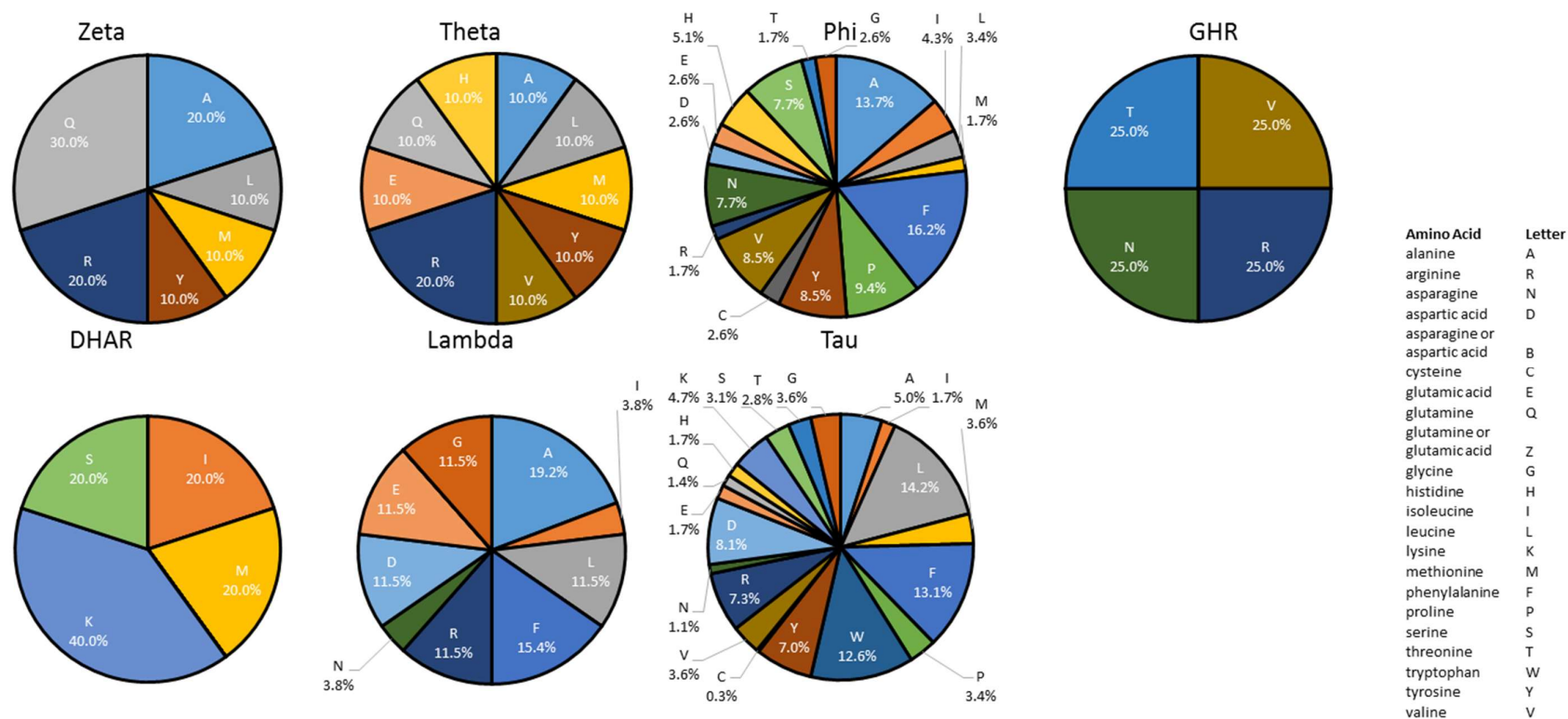


Figure 33: Pie charts showing percentage ratio of amino acid residues involved in substrate binding.

Data on residues involved in substrate binding were extracted from NCBI and plotted using Excel. The number of times each amino acid was involved in substrate binding was taken as a percentage of the total number of substrate binding residues for each class. Amino acids described by IUPAC letters (shown on the right). Amino acid properties taken from "A Review of Amino Acids," Accessed 2019 .

4.2.8 3D structure of maize GSTs

To investigate the three dimensional structures of the GSTs, homology models of the GSTs identified in this study were created based on X-ray crystal structures. The GST structures are shown in Figure 34, in which members of each class have been superimposed to show the general class structures and to identify similarities. The secondary structures of each class, as determined by structure based alignment of the homology models, are shown in Figure S 4, while a clear visualisation of the theta class GST is shown in Figure 35 for reference.

Existing X-ray crystal structures of GSTs were identified and used as templates for the homology modelling (Table S 12). These were chosen on the basis of sequence identity, atomic resolution, and restricted to show glutathione binding, to ensure reliable templates were used. The atomic resolutions of templates ranged from 1.25 Å to 2.8 Å, allowing for determination of secondary structure and gross features of functionally important regions, such as active sites (Mazzone, 1998). 30% sequence identity is generally considered the minimum threshold for homology modelling, whereby a known structure can be predicted with accuracy equivalent to low resolution x-ray structure (Xiang, 2006). All structures exceeded this threshold, except for ZmGSTF4.0, ZmGSTF4.1 and ZmGSTF4.2. The quality of produced homology models were analysed to determine their reliability in predicting structure. Figure S 3 shows example data for the homology model of ZmGSTL1.0. Figure S 3. a demonstrates a Ramachandran plot, in which the dihedral angles of the protein backbone are plotted, and compared with energetically favoured areas (Ramachandran et al., 1963). For topological studies, secondary structure prediction and atomic interaction analysis, structures are required to present $\geq 55\%$, $\geq 65\%$ and $\geq 75\%$ of residues within the core regions, respectively, as represented by the red areas in Figure S 3. a (Morris et al., 1992). All homology models displayed over 84% of residues in this core region. Figure S 3. b demonstrates the QMEAN scores calculated by Swiss-model, which estimates the global model quality and assigns a numerical value, where negative and positive values indicate properties worse and better than experimental structures, respectively. In general structures with QMEAN above -4.0 are considered acceptable, which was satisfied by 94% of sequences. This value is a composite score of four parameters; C β , All atom, Solvation and Torsion, which describe the interaction potential between beta carbon atoms, all atoms, the solvation potential, and torsion angle potential, respectively (Bienert et al., 2017). Therefore, all models generated in this thesis were assessed by the aforementioned criteria and showed acceptable quality except ZmGSTF-

1.1, -4.0, -4.1 and -4.2. Homology models could not be made for ZmGSTF2.0, ZmGSTU1.2 and ZmGSTU9.4, due to unidentified residues in the sequences.

Visual assessment identified high structural conservation within and between classes, aside from the oligomeric states and orientations. This is suggestive of a strong evolutionary pressure for retention of certain structural motifs at the active sites (Frova, 2003; Horton et al., 2007). The general secondary structure in all classes was consistent with that of other species, showing the typical two-domain fold (Sasan et al., 2011). This fold is characterised by an N-terminal domain containing part of the thioredoxin superfamily fold, characterised by a $\beta\alpha\beta\alpha\beta\alpha$ motif (Sasan et al., 2011). This general structure was identified in the homology models based on X-ray crystallography, in all GST classes, though there existed some splitting of α -helices (Figure S 4). The β -strands are oriented with three antiparallel β -strands ($\beta 1$, $\beta 3$ and $\beta 4$), and a parallel β -strand ($\beta 2$) creating a structure combining aspects of a β -sheet and a β -psi loop and is positioned between two α -helices (Sasan et al., 2011). On the other hand, the C-terminal domain is comprised solely of α -helices, which show more variation between classes and are known to contain the determinants for substrate specificity (Frova, 2003). Each class, and indeed members of each class showed a diverse range of α -helix numbers in this region, potentially providing differences in substrate specificity (Figure S 4).

The dimer interface has large V-shape cleft, with a buried surface area of 2,700-3,400 Å². This cleft is considered to have an auxiliary role in the functional specificities of GSTs. For all classes, except DHAR, lambda and GHR, the G- and H-sites exist in the dimer interface. In addition, their dimerisation plane showed high similarity in all dimerising classes, except the GHR class. The monomers of all dimerised classes are orientated such that each monomer is translated 180° in the X-plane and 180° in the Y-plane relative to each other, known as two-fold symmetry (Dixon et al., 2002b). This symmetry, shown in theta, phi, zeta and tau class GSTs, is caused by dimerisation using interactions that include $\beta 4$. However, GHR dimerises using α -helices, exposing the typical active site to the environment, and causing the monomers of GHR to separate vertically, instead of the usual horizontal separation, as seen in the orientations shown in Figure 34. This strange GHR dimerisation orientation is supported by the different location of dimerisation residues discussed in section 4.2.5. While this is based on a crystal structure of a GHR from bacteria (*Escherichia coli*), it was also observed in black cottonwood (*Populus trichocarpa*) and a fungus (*Phanerochaete chrysosporium*) and has been defined as the Xi structural class (Lallement et al., 2015). As such, the GHR glutathione and substrate

binding sites are between N- and C-terminal regions, and not within the dimer interface (Lallement et al., 2015).

It is important to note that homology modelling only provides predictions of sequence structure, which may vary from experimentally elucidated structures. For example, unique regions in a protein sequence, not present in the crystal structure template, cannot be accurately modelled and oligomeric states may differ between the template and target protein (Bordoli et al., 2009; Gupta et al., 2014). In addition, large structural changes caused by small differences in primary structure are unlikely to be modelled accurately (Bordoli et al., 2009). Fortunately, GSTs have been extensively characterised in many species, and crystal structures were available for each class, with oligomeric states resolved. Therefore, the results of this homology modelling study should be analysed with caution. The oligomer states may not be accurately reflected in the predictions.

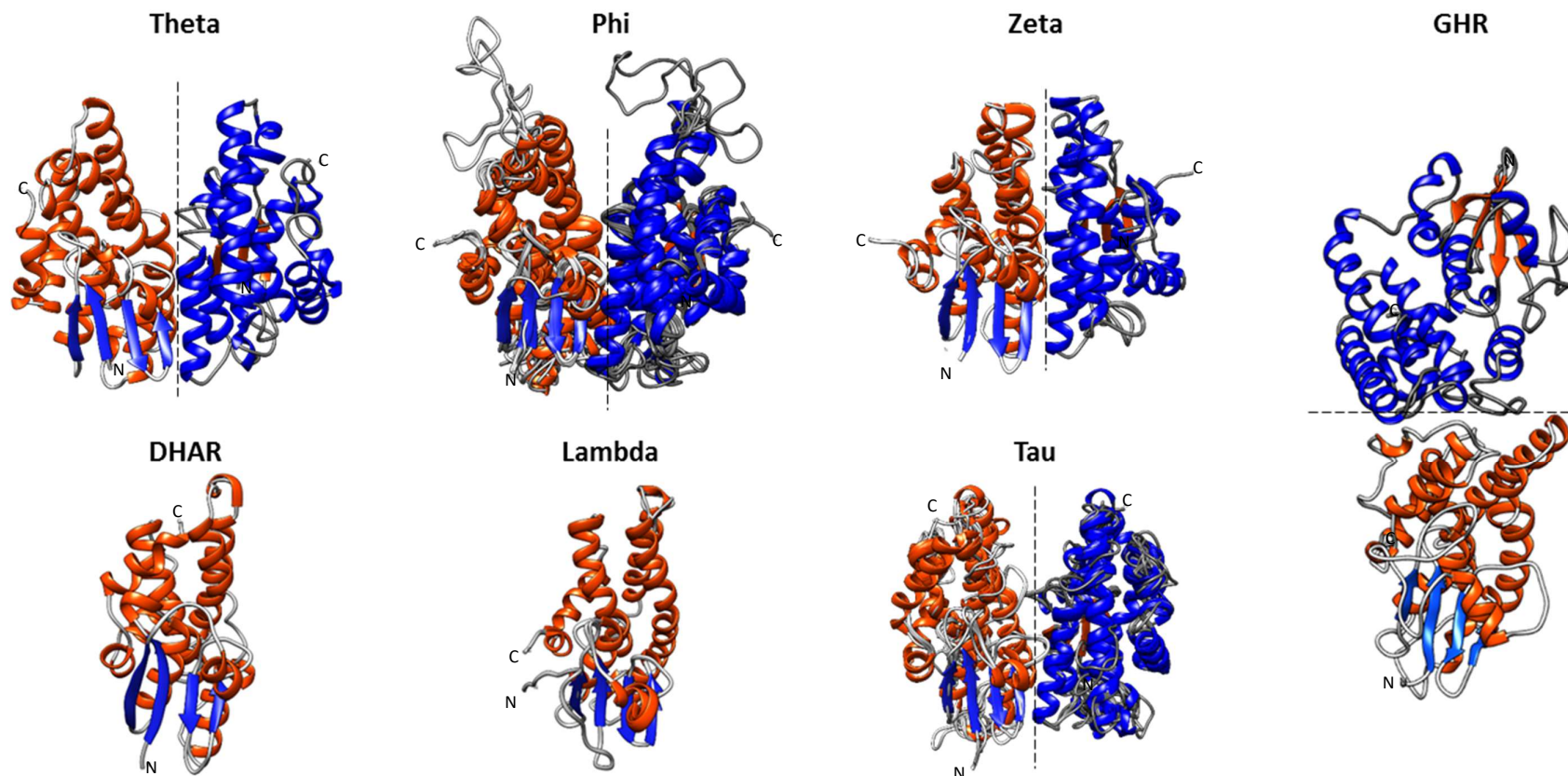


Figure 34: Glutathione-S-Transferase (GST) homology structures, superimposed in ribbon format.

Homology models of all GST proteins were made by inputting protein sequences into Swiss-model software, and superimposed using Chimera. α -helices and β -strands are distinguished by colour. Monomers of dimers have opposing colouring. N- and C- terminals are denoted by N and C, respectively. Dotted lines indicate planes of dimerisation.

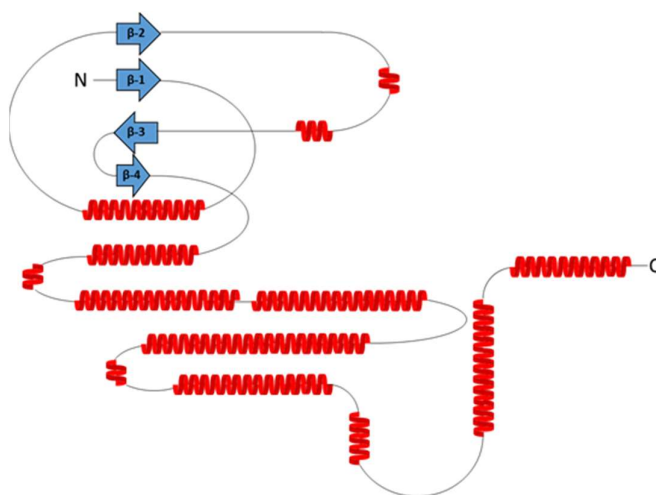


Figure 35: Schematic of theta class Glutathione-S-Transferase (GST) fold.

Secondary structure of theta class GST homology structure was plotted as a 2-dimensional image using Powerpoint. Sizes of α -helices and β -strands are to scale of theta GSTs used in this study. Blue arrows; β -strands, red helices; α -helices. N; N-terminal, C; C-terminal.

4.2.9 Targeting sequences of maize GSTs

GSTs have primarily been considered cytosolic proteins, though new evidence of differential localisation of specific GSTs, such as has been identified in proteomic studies of arabidopsis, has prompted a search for GST localisation, which may provide insight into function (Dixon et al., 2009; Sasan et al., 2011). To further understand the role of GSTs, the subcellular localisation of GSTs was investigated, using a search of the known N- and C- terminal targeting sequences (TS) in the GST protein sequences (Table 17). Four programs were used in TS identification to ensure robust analysis, though there was little correlation observed between the programs. This can be assigned in part to different capacities of each program: Wolf psort and Cello are able to identify TS for the nucleus, mitochondria, cytosol, plasma membrane, extracellular matrix, chloroplast, vacuole and peroxisome, while LocSigDB can identify TS for the nucleus, mitochondria, extracellular matrix, peroxisome, and plasma membrane, and TargetP can identify only chloroplast, mitochondria or secretory TS (see section 2.2 for program information). TS that predict localisation to the endoplasmic reticulum (ER), and golgi apparatus were excluded from analysis, as these likely reflect basic protein folding, and TS for lysosomal and cytoskeletal targeting were not considered, as these are likely involved in protein turnover. Localisation of the theta class GST to the peroxisome was used a positive control, since peroxisomal TS have been identified in theta GSTs in rice, soybean and barrelclover (*Medicago truncatula*) and this localisation has been confirmed in arabidopsis

(Dixon et al., 2009). Wolf pSort and LocsigDB programs correctly predicted this localisation, while Cello and TargetP did not.

The typical cytoplasmic localisation of GST was supported by the presence of at least one cytoplasmic localisation prediction in 80% of sequences (Table 17), though only 12% exclusively predicted cytoplasmic TS, specifically *ZmGSTF4.5*, *ZmGSTF4.6*, DHAR 3, *ZmGSTL1.1*, *ZmGSTU1.1*, *ZmGSTU1.2*, *ZmGSTU5.1*, and *ZmGSTU8.2*. Since cytoplasmic localisation does not require targeting sequences, and is the default localisation, this analysis may underestimate the cytoplasmic localisation of the GSTs. 23% of the protein sequences indicated secretion to the extracellular matrix, though no cases exclusively predicted this subcellular localisation. Some evidence of apoplastic GSTs has been published, usually for those displaying peroxidase activity, associated with theta and some phi class GSTs (Dixon et al., 2002b; Flury et al., 1996; Foyer et al., 2001). However, the current prediction indicated members of the theta, phi, DHAR and zeta class, not correlating well with previous literature. However, the phi class members showing secretory TS comprise the *ZmGSTF3* subclass and three of the four *ZmGSTF2* subclass members, indicating a degree of subclass localisation. Nuclear localisation signals were detected on 42% of proteins including zeta, phi, GHR and tau classes, though exclusively only in *ZmGSTF4.1*. While only a few accounts of nuclear GST localisation have been documented, new studies are increasing support for such localisation (Dixon et al., 2002b; Takahashi et al., 1995). In arabidopsis, a tau class GST was found to localise primarily in the nucleus, and was thought to be involved in redox-sensitive transcriptional regulation or nucleic acid repair (Dixon et al., 2009). Once again, the localisation is restricted to specific subclasses, existing in all F3, five of the six F4, three of the four U6, all of the U7, three of the five U9, and five of the six U10 *ZmGST* subclass members. As mentioned previously, the theta class GST, *ZmGSTT1.0*, was the only example of a peroxisomal TS. Theta GST peroxisomal localisation has been observed in arabidopsis, where its glutathione peroxidase (GPOX) activity prevented membrane damage caused by fatty acid oxidation, and targeting sequences for peroxisomal localisation have been identified in rice, soybean and barrelclover (Dixon et al., 2009). This prediction is therefore supported by previous findings. Mitochondrial TS were identified in 9% of proteins, though not exclusively in any case. These TS were not present in any subclass or class trend, and may occur in specific cases. However, the presence of a TS in two of the three zeta class, and the GHR class, indicates these as likely classes to show mitochondrial localisation. No DHAR sequences

displayed mitochondrial TS, despite previous findings that DHAR proteins are chloroplast or mitochondrion targeted (Frova, 2003). Chloroplast TS were identified in 58% of the sequences, though exclusively in only *ZmGSTF1.0*, *ZmGSTF1.1*, *ZmGSTU4.1* and *ZmGSTU10.4*. These TS were present in all classes except the theta class, and showed some subclass specificity. Those subclass members displaying chloroplast TS include the F1, F2 and F3 and U2, U3, U4, six of seven U5, and U6 *ZmGST* subclasses, indicating these subclasses may have evolved this localisation. The indication that subclasses may conserve these targeting sequences provides an interesting hypothesis; that subclasses evolved for different subcellular localisations, and were further specialised for function. As such, the GST superfamily could be further categorised by localisation. For example, the *ZmGSTF1* subclass could be described as the chloroplast-localised phi subclass, though a lack of uniformity in the predictions makes this difficult.

For comparison, the available data on the subcellular localisations of GSTs from arabidopsis (*Arabidopsis thaliana*) were collated (Table 18), as this proteome has been most extensively researched. A combination of literature survey and proteome analysis using ProteomicsDB (section 2.2) were used to identify experimentally determined localisations, which were comprised of confocal microscopy coupled with fluorescent protein fusions, such as green fluorescent protein (GFP), or proteomic assays. No arabidopsis zeta GSTs were identified in the search, and thus the predictions could not be validated. The theta GSTs of arabidopsis, *AtGSTT1-3*, all localised to the peroxisome in at least one experiment, by virtue of SKI or SKM targeting signals (Dixon et al., 2009). The prediction that *ZmGSTT1.0* localises to the peroxisome, is based on the identification of an SKL targeting peptide. Together this information indicates this prediction is likely correct. The phi GSTs of maize were predicted to localise mainly to chloroplasts or remain in the cytoplasm. The arabidopsis experiments indicated a large degree of cytoplasmic localisation, with some chloroplastidial targeting, supporting this theory. The maize GHR was predicted to have chloroplastidial, nuclear and mitochondrial targeting sequences. The arabidopsis GHRs, GHR1 and GHR4, both localised to the chloroplast, which supports the prediction that *ZmGHR1.0* is chloroplast localised. The maize DHAR GSTs were predicted to localise to the chloroplast, cytosol or be secreted. Analysis of the experiments with arabidopsis identified all of these localisations and many more, making the predictions hard to validate. The arabidopsis lambda class GSTs were identified as localised in the cytosol, plasma membrane, chloroplast and peroxisome, supporting the

chloroplast and cytosol predictions for the maize lambda GSTs. The maize tau class GSTs were mostly predicted as cytosolic, chloroplastic or nuclear localised, which is mirrored in the results of the arabidopsis GST experiments.

new names	Localisation
ZmGSTZ1.0	Cyto ^{ab} , Mito ^c
ZmGSTZ1.1	Chlo ^b , Sect ^c , Mito ^a
ZmGSTZ1.2	Cyto ^a , Chlo ^b , Nucl ^d
ZmGSTT1.0	Cyto ^a , Prxs ^{bd}
ZmGSTF1.0	Chlo ^{ab}
ZmGSTF1.1	Chlo ^{ab}
ZmGSTF1.2	Cyto ^a , Chlo ^b
ZmGSTF2.0	Cyto ^a , Chlo ^b
ZmGSTF2.1	Cyto ^a , Chlo ^b , Sect ^c
ZmGSTF2.2	Cyto ^a , Chlo ^b , Sect ^c
ZmGSTF2.3	Cyto ^a , Chlo ^b , Sect ^c
ZmGSTF3.0	Chlo ^b , Nucl ^d , Sect ^{ac}
ZmGSTF3.1	Cyto ^a , Chlo ^b , Nucl ^d , Sect ^c
ZmGSTF4.0	Cyto ^a , Nucl ^b
ZmGSTF4.1	Nucl ^{ab}
ZmGSTF4.2	Cyto ^b , Nucl ^{ad}
ZmGSTF4.3	Cyto ^a , Nucl ^b
ZmGSTF4.4	Cyto ^a , Nucl ^b
ZmGSTF4.5	Cyto ^{ab}
ZmGSTF4.6	Cyto ^{ab}
ZmGHR1.0	Chlo ^{bc} , Nucl ^d , Mito ^a
DHAR 4	Chlo ^{ab} , Sect ^c
DHAR 3	Cyto ^{ab}
ZmGSTL1.0	Cyto ^a , Chlo ^{bc}
ZmGSTL1.1	Cyto ^{ab}
ZmGSTL1.2	Cyto ^{ab} , Chlo ^b
ZmGSTL1.3	Chlo ^{ac} , Mito ^b
ZmGSTU1.0	Cyto ^{ab} , Sect ^c
ZmGSTU1.1	Cyto ^{ab}
ZmGSTU1.2	Cyto ^{ab}
ZmGSTU2.0	Cyto ^a , Chlo ^b , Nucl ^d , Mito ^c
ZmGSTU3.0	Cyto ^a , Chlo ^b , Sect ^c
ZmGSTU3.1	Cyto ^a , Chlo ^b

new names	Localisation
ZmGSTU4.0	Cyto ^a , Chlo ^b , Nucl ^d
ZmGSTU4.1	Chlo ^{abc}
ZmGSTU5.0	Cyto ^a , Chlo ^b
ZmGSTU5.1	Cyto ^{ab}
ZmGSTU5.2	Cyto ^a , Chlo ^b , Sect ^c
ZmGSTU5.3	Cyto ^a , Chlo ^b , Sect ^c
ZmGSTU5.4	Cyto ^a , Chlo ^b
ZmGSTU5.5	Cyto ^a , Chlo ^{bc}
ZmGSTU5.6	Cyto ^a , Chlo ^b , Mito ^c
ZmGSTU6.0	Cyto ^b , Chlo ^a
ZmGSTU6.1	Cyto ^a , Chlo ^b , Nucl ^d
ZmGSTU6.2	Chlo ^{ab} , Nucl ^d , Sect ^c
ZmGSTU6.3	Cyto ^b , Chlo ^a , Nucl ^d , Sect ^c
ZmGSTU7.0	Cyto ^b , Chlo ^a , Nucl ^d
ZmGSTU7.1	Cyto ^{ab} , Nucl ^d
ZmGSTU7.2	Cyto ^{ab} , Nucl ^d , Mito ^c
ZmGSTU7.3	Cyto ^{ab} , Nucl ^d
ZmGSTU7.4	Cyto ^{ab} , Nucl ^d
ZmGSTU8.0	Cyto ^a , Chlo ^b , Sect ^c
ZmGSTU8.1	Cyto ^a , Chlo ^b
ZmGSTU8.2	Cyto ^{ab}
ZmGSTU9.0	Cyto ^{ab} , Nucl ^d
ZmGSTU9.1	Cyto ^{ab} , Nucl ^d
ZmGSTU9.2	Chlo ^{ab} , Nucl ^d
ZmGSTU9.3	Cyto ^{ab} , Sect ^c
ZmGSTU9.4	Cyto ^b , Chlo ^a
ZmGSTU10.0	Cyto ^{ab} , Nucl ^d
ZmGSTU10.1	Cyto ^a , Chlo ^b , Nucl ^d
ZmGSTU10.2	Cyto ^{ab} , Nucl ^d
ZmGSTU10.3	Cyto ^{ab} , Nucl ^d
ZmGSTU10.4	Chlo ^{ab}
ZmGSTU10.5	Chlo ^{ab} , Nucl ^d

Table 17: C- and N- terminal targeting sequences of Glutathione-S-Transferases (GSTs).

Protein sequences analysed for targeting sequences using multiple programs. Superscripts define program (and source): a; Cello (Yu et al., 2006), b; Wolf pSort (Horton et al., 2007), c; TargetP (Emanuelsson et al., 2000), d; LocsigDB (Negi et al., 2015). Cyto; cytoplasm, Chlo; chloroplast, Prxs; peroxisome, Nucl; nucleus, Sect; secretory, Mito; mitochondrion. 'ER', 'golgi', 'lysosome', 'cytoskeleton' and 'other' were removed from analysis.

GST	Subcellular localisation	Source (and experimental method)
GSTT1	Peroxisomes ^{nb}	a (FP)
	Plastid and Peroxisome	b (PA)
GSTT2	Peroxisomes ^{nb}	a (FP)
GSTT3	Peroxisomes ^{nb}	a (FP)
	Plastid	b (PA)
GHR1	Cytosol	c (PA)
	Chloroplast	d (PA)
GHR4	Chloroplast	e (PA)
DHAR1	Apoplast, Chloroplast, Plasma membrane, Peroxisome, Vacuole, Nucleus and Mitochondrion	b (PA)
	Cytosol	f (FP)
	Peroxisome	e (FP)
	Mitochondrion	h (PA)
	Cytosol	c (PA)
	Plasma membrane	i (PA)
DHAR2	Chloroplast	j (PA)
	Plasma membrane and Mitochondrion	b (PA)
	Cytosol	c (PA)
DHAR3	Plasma membrane	i (PA)
	Chloroplast and Plastid	b (PA)
GSTL2	Chloroplast	k (PA)
	Cytosol and Peroxisomes ^{Nb}	a (FP)
	Chloroplast and Peroxisome	b (PA)
	Peroxisome	a (FP)
GSTL3	Chloroplast	k, j, e (PA)
	Plasma membrane	b (PA)
GSTF2	Cytosol	c (PA)
	Cytosol ^{nb}	a (FP)
GSTF3	Plasma membrane, Chloroplast, Apoplast and Vacuole	b (PA)
	Plasma membrane and Mitochondrion	b (PA)
GSTF5	Mitochondrion	b (PA)
GSTF6	Cytosol ^{nb}	a (FP)
	Extracellular region, Vacuole and Cell wall	b (PA)
GSTF7	Vacuole, Extracellular region, Cytoplasm and Nucleus	b (PA)
GSTF8	Cytosol ^{nb}	a (FP)
	Nucleus, Chloroplast and Thylakoid	b (PA)
GSTF9	Cytosol ^{nb}	a (FP)
	Plasma membrane, Peroxisome, Chloroplast, Vacuole, Apoplast and Thylakoid	b (PA)
GSTF10	Apoplast, Peroxisome, Chloroplast, Plasma membrane, Vacuole and Cell wall	b (PA)
GSTF12	Cytosol ^{nb}	a (FP)
	Nucleus, Cytoplasm	b (PA)
GSTU2	Cytosol ^{nb}	a (FP)
GSTU5	Plasma membrane and Peroxisome	b (PA)
GSTU6	Peroxisome	b (PA)
GSTU7	Cytosol ^{nb}	a (FP)
GSTU9	Cytosol ^{nb}	a (FP)
GSTU11	Cytosol ^{nb}	a (FP)
GSTU12	Nucleus ^{nb}	a (FP)
GSTU13	Nucleus	b (PA)
GSTU16	Nucleus	b (PA)
GSTU17	Chloroplast	b (PA)
GSTU19	Cytosol ^{nb}	a (FP)
	Plasma membrane, Mitochondrion and Chloroplast	b (PA)
GSTU20	Nucleus, Mitochondrion, Cytoplasm, Chloroplast and Apoplast	b (PA)
GSTU23	Mitochondrion	b (PA)
GSTU28	Cytosol ^{nb}	a (FP)

Table 18: Experimentally determined subcellular localisation of *Arabidopsis thaliana* GSTs, compiled from literature survey and using ProteomicsDB.

a; Dixon et al., 2009 , b; ProteomicsDB, c; Ito et al., 2011 , d; Klodmann et al., 2011 , e; Ferro et al., 2010 , f; Grefen et al., 2010 , g; Reumann et al., 2009 , h; Chew et al., 2003 , i; Marmagne et al., 2007 , j; Peltier et al., 2006 , k; Zybailov et al., 2008 . (FP); fluorescent protein fusion, (PA); proteomic assay. Superscripted Nb; Expressed in tobacco (*Nicotiana benthamiana*).

4.2.10 *GST expression throughout development and in different tissues of maize plants*

Endogenous regulation of GSTs can provide a greater understanding of GST roles, and thus the effect of plant growth and development on endogenous GST expression was determined by a combined analysis of various experiments available through the software, Genevestigator (section 2.2). In addition, the expression levels in different maize tissues was analysed, to investigate tissue specificity. This software integrates public microarray and RNA-seq experiments, allowing for analysis of gene expression in different biological contexts. Here, the available database of mRNA-seq data in maize (ref: AGPv4) was investigated with respect to the GST genes identified in this thesis. The expression levels given for each gene and condition represent the mean of at least 12 samples. The data is presented as \log_2 gene expression in Figure 36, which represents the relative expression of each gene, in a logarithmic manner. Three gene IDs could not be identified in the studies, and are displayed by blank cells. No significant class or subclass trends were observable in the development stages, and only a few class or subclass trends were observed in the tissues, with members of each class showing considerable variation in expression profile.

The expression levels in the developmental analysis ranged from $\log_2 = 0$ (no expression) to $\log_2 = 10.8$ (highest expression), though in most cases did not exceed $\log_2 = 6$. In cases where significant expression was observed, it was apparent that expression was higher in early developmental stages, such as germination. *ZmGSTF2.0*, *ZmGSTF1.0*, *ZmGSTF1.1*, *ZmGSTF1.2* and *DHAR3* represent the GSTs most highly induced in all developmental stages. Some GSTs were expressed differentially in certain developmental stages, indicating functions important for these phases. For example *ZmGSTF2.3* was expressed statistically higher during germination ($\log_2 = 7.4 \pm 0.2$) than any other stage ($\log_2 \leq 3.6$) ($p < 0.0001$), and therefore is likely to possess a functional role important for germination only.

Since a large range of tissues were available for investigation, five important tissues were chosen for the analysis: The whole shoot, the culm (main stem) of the shoot, the blade (lamina) of the foliar leaf, and the shoot apex (Sekhon et al., 2011). In the tissue analysis, the expression ranged from $\log_2 = 0$ (no expression) to $\log_2 = 10.05$ (highest expression), though in most cases did not exceed $\log_2 = 7$. As with the developmental analysis, *ZmGSTF2.0*, *ZmGSTF1.0*, *ZmGSTF1.1* and *ZmGSTF1.2* and *DHAR3* represent the GSTs most highly induced in all tissues. Some GSTs were expressed differentially in certain tissues, indicating functions important for these tissues. For example, *ZmGSTU4.0* was expressed higher in the shoot apex ($\log_2 = 3.39 \pm$

0.13) than any other tissue ($\log_2 \leq 0.86$) ($P < 0.001$), while *ZmGSTU1.2* was expressed higher in the blade (lamina) ($\log_2 = 7.71 \pm 0.45$) than any other tissue ($\log_2 < 5.94$) ($p < 0.0011$).

As mentioned, there was only a slight degree of class correlation observed, with a number of tau class GSTs displaying expression primarily in the blade (59%) while many phi class GSTs displayed most expression in the shoot apex (67%). A lack of class correlation has also been observed in potato (*Solanum tuberosum* L.) and Cambodian dragon tree (*Dracaena cambodiana*), though the latter did display a slightly positive expression ratio of stem to leaf in phi class GSTs (Islam et al., 2018; Zhu et al., 2016). This trend was also seen by Frova (2003) in rice GSTs, though the extent of variation was not published until Soranzo et al. (2004) observed the trend in both rice tau and phi classes. In most cases, GST expression was consistent in all tissues.

Of course, transcript expression can only predict protein expression and enzymatic activity, which does not always follow a proportional relationship. It has been determined that while individual translation from mRNA to protein is a complex relationship, that categorising groups of genes leads to a more linear relationship between transcription and translation (Greenbaum et al., 2002). However, since this experiment was designed to highlight important trends in the expression of GST genes, this is not of major concern.

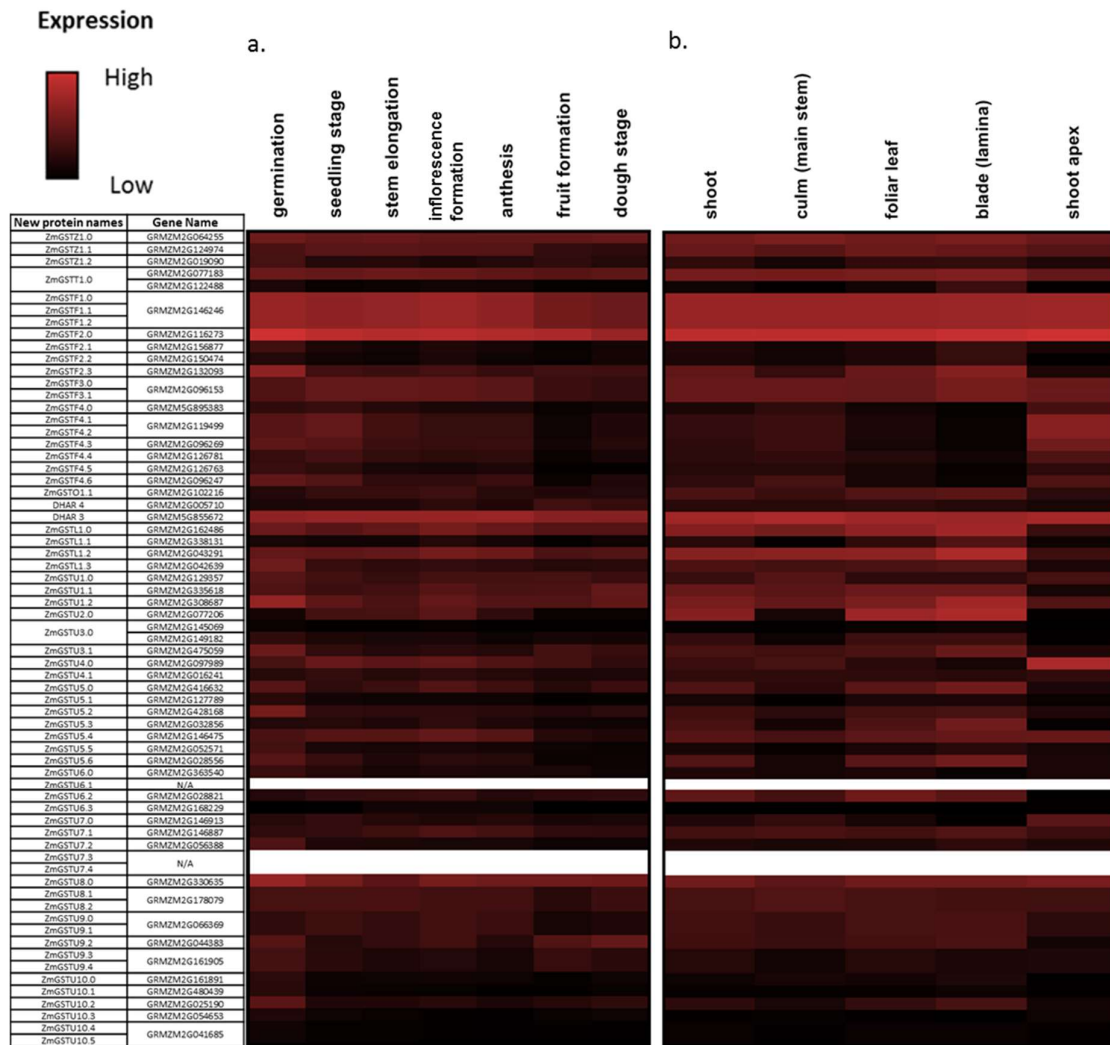


Figure 36: Heat map showing expression of Glutathione-S-Transferases (GSTs) a; throughout development of maize plant and b; in different tissues.

Expression data extracted from Genevestigator software and mapped using Graphpad software. Colour chart (top left) indicates relative level of expression, where low is $\log_2 = 0$ and high is the highest value (a; $\log_2 = 10.8$, b; $\log_2 = 10.05$). White cells describe unidentified genes.

4.3 Discussion

In this chapter, the *in silico* analyses provided a clearer characterisation of the evolution, structures and expression of each GST class. The tau and phi classes, present only in plants, are thought to have appeared late in GST evolution, through distinct ancestries, though their large size indicates extensive duplication and divergence in maize (Frova, 2003). Their clustering on many chromosomes indicates transposition with significant divergence into new subclasses. The phi and tau class GSTs have independently evolved an active serine residue, and show similar functions in xenobiotic detoxification, except with respect to substrate. Their differences in substrate-binding residues may account for their different herbicide class targets. The typical secondary and tertiary structure are also conserved: they share similar interface residues, despite their distinct lineage, again indicating convergent evolution. A variety of localisation sequences were observed and may indicate subclass specialisation to certain organelles, though the high rate of cytoplasmic predictions leaves uncertainty in these classes.

Theta GSTs are predicted as early classes in the family, which was confirmed by the phylogenetic analysis, chromosomal position and sequence (Edwards et al., 2000; Frova, 2003; Sylvestre-Gonon et al., 2019). The zeta class GSTs likely evolved from the theta class, as indicated by the phylogenetic analysis. The low abundance of theta and zeta genes indicates few gene duplications or subsequent gene losses, supported by previous observations (Frova, 2003). Their similarity in sequence, and predicted use of similar residues for substrate binding, is in accordance with their similar functions in cell metabolism (Dixon et al., 1998b; Frova, 2003). They have retained the typical secondary and tertiary structure, and developed the use of an active serine. The substrate binding residues used, differ significantly from the tau and phi class, explaining their differing functions. The main difference between the zeta and theta classes appears to be their subcellular targeting sequences. While the peroxisomal targeting sequence of theta GSTs is consistent with the known function of theta GSTs in GPOX activity, the zeta class displays a range of possible localisations, though comparison with other species may indicate a cytoplasmic localisation (Dixon et al., 2002b).

The results revealed a close relationship between DHAR and lambda GSTs, with DHAR preceding lambda in GST evolution. They are the only GSTs to function as monomers and they retain the original use of cysteine as their catalytic residue, required for deglutathionylation activity (Frova, 2003; Lallement et al., 2014; Lallement et al., 2015; Sasan et al., 2011). Their

clustering on different chromosomes indicates transposition and further evolution to form the classes. They display very different substrate-binding residues, explaining their differences in function: DHARs are known to catalyse the reduction of dehydroascorbate to ascorbate (Frova, 2003; Lallement et al., 2014), while lambda GSTs may be involved in flavonoid metabolism or trafficking (Dixon et al., 2010a). The predicted localisation of these classes indicates both may be chloroplastidial.

An unknown GST was identified as a member of the GHR class, which appears to be the most primitive class (Lallement et al., 2015). Like the lambda and DHAR GSTs, they are known to use a catalytic cysteine, which is thus likely the original active residue (Lallement et al., 2014; Lallement et al., 2015). Therefore, it can be proposed that the serinyl-GSTs evolved from GHR, through two distinct ancestries, one path leading to the zeta, theta and phi classes, and another to the tau class. The unique substrate-binding residues of GHRs is consistent with their exclusive role in the deglutathionylation of glutathionylated quinones, though the targeting sequence prediction indicates GHR may function in the nucleus, chloroplast or mitochondria (Lallement et al., 2015). Their dimerisation orientation is also unique in the GST family, presenting with a Xi-orientation. Therefore, evolution to the zeta, theta, phi classes, introduced the typical dimerisation pattern. Conversely, evolution to the lambda and DHAR classes, introduced active monomeric GSTs, though subsequently introduced the typical dimerisation in the tau class, in yet another example of convergent evolution.

From the GST expression analyses a number of highly endogenously expressed GSTs were identified. *ZmGST- F1.0, F1.1, F1.2, F2.0* and *DHAR 3*, were all highly expressed in all tissues at all developmental stages and may be considered constitutively expressed GSTs. These GSTs likely play vital roles in basic cell function.

4.4 Conclusions

In this study, the GSTs identified in maize have been classified and characterised, and investigated with respect to chromosome location, protein domains, binding sites, 3D-structure, localisation and expression. The phylogenetic analysis has revealed the sequence relationship between and within each class. This has allowed for classification of unidentified GSTs, and subclasses have been proposed. These subclasses have proved useful in improving the nomenclature system for GSTs to include sequence similarity. The evolutionary progression of GSTs to their now large enzyme class, has been described on the basis of appearance in distinct kingdoms, in a novel prediction. Determining the chromosomal

localisation of GST genes, and comparing with the phylogeny and literature, has indicated the steps involved in the growth and divergence of the family; the large duplication and transposition likely being an evolutionary mechanism to generate a broad range of genes, with redundant and specific functions. The protein domain investigation has shown the similarity of N-terminal, C-terminal and domain interface regions between all GST family members, while the investigation of G-and H-sites identified more variation. The G-sites, responsible for GSH-binding, showed high intra- and inter- class similarity with respect to region and residue, explaining the conserved function of glutathione binding. The main variation was the amino acid residues used for the H-bonding interactions, though similar residues were used. The H-sites, responsible for substrate binding, showed larger inter-class variation of region and residue, revealing a potential system for substrate specificity. Higher intra-class conservation of H-sites may explain class-specific substrate interactions, or may imply conservation of some residues for structural reasons. This study has found some evidence of mis-annotated or unannotated sequences, with respect to domains, interface regions, and G/H-sites in the maize genome, highlighting a need for more comprehensive annotation and experimental validation when publishing new sequences. The homology structure comparisons revealed high similarity of secondary to quaternary structure within and between classes, aside from the monomeric states of lambda and DHAR enzymes, and the GHR Xi-dimerisation. The subcellular localisation predictions indicated a range of novel organelle targets, suggesting GSTs may not simply be cytosolic proteins, but may localise to the chloroplast, mitochondria, peroxisome, and even be secreted into the extracellular matrix.

An interesting phenomenon highlighted in this study is the convergent evolution of the catalytic serine and the typical dimerisation pattern. While tau class GSTs evolved through a distinct ancestry to the other serine-GSTs, they have been selected towards the same structure and catalytic role.

4.5 Appendix to Chapter 4

Number	PDB ID	GST Class	Name	Species	Common Names	Method	Resolution (Å)
1	5j4u	Tau	GSTU30	<i>Populus trichocarpa</i>	black cottonwood western balsam-poplar California poplar	X-ray diffraction	1.249
2	5f07	Phi	GSTF8	<i>Populus trichocarpa</i>	black cottonwood western balsam-poplar California poplar	X-ray diffraction	1.5
3	4ri6	Phi	GSTF1	<i>Populus trichocarpa</i>	black cottonwood western balsam-poplar California poplar	X-ray diffraction	1.523
4	5n9u	DHAR	Dehydro-ascorbate reductase 3A	<i>Populus trichocarpa</i>	black cottonwood western balsam-poplar California poplar	Solution NMR	-
5	5g5a	Tau	GSTU25	<i>Arabidopsis thaliana</i>	thale cress mouse-ear cress arabidopsis	X-ray diffraction	1.95
6	4top	Tau	GST	<i>Glycine max</i>	Soybean Soya bean	X-ray diffraction	2.351
7	4pqi	Lambda	GSTL3	<i>Populus trichocarpa</i>	black cottonwood western balsam-poplar California poplar	X-ray diffraction	1.95
8	5d9x	DHAR	Dehydro-ascorbate reductase	<i>Oryza sativa</i>	Asian rice	X-ray diffraction	1.68
9	4uss	GHR	GST X1-1 (GHR1)	<i>Populus trichocarpa</i>	black cottonwood western balsam-poplar California poplar	X-ray diffraction	2.5
10	5f06	Phi	GSTF7	<i>Populus trichocarpa</i>	black cottonwood western balsam-poplar California poplar	X-ray diffraction	1.8

Table S 11: Table describing details of Glutathione-S-Transferase (GST) models used in Figure 31.

Protein databank (PDB) ID included. -; no data given.

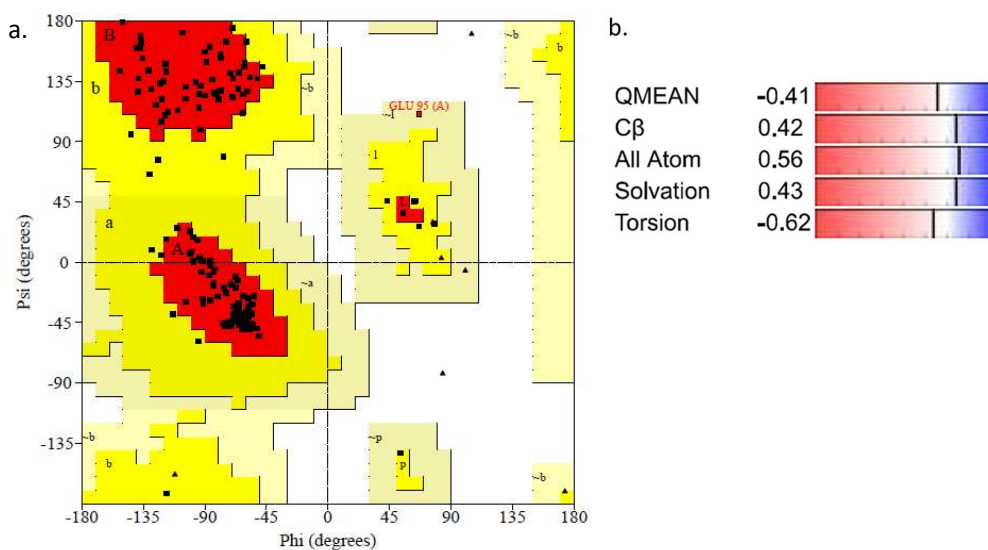


Figure S 3: Example data used to validate homology model quality. a; Ramachandran plot, b; global quality estimate,

Data of ZmGSTL1.0 homology model, produced by Procheck (a) and Swiss-Model (b). Scoring function of quality; average (QMEAN), for the interaction potential between beta carbon atoms (C β), for the interaction potential between all atoms (All atom), for the solvation potential (solvation), and for the torsion angle potential (torsion).

New name	QMean	Template	Resolution (Å)	Sequence identity (%)	Ramachandran plot (% residues in regions)			
					Favoured (A, B, L)	Additionally allowed (a, b, l, p)	Generously allowed (~a, ~b, ~l, ~p)	Disallowed (no letter)
ZmGSTZ1.0	-0.84	1FW1	1.90	48.54	94.1	4.9	1.1	0.0
ZmGSTZ1.1	-2.68	1FW1	1.90	43.51	94.5	3.3	2.2	0.0
ZmGSTZ1.2	-3.08	1FW1	1.90	39.81	91.9	7.0	0.6	0.6
ZmGSTT1.0	-2.75	2C3T	2.40	40.19	90.5	7.3	0.8	1.5
ZmGSTF1.0	-2.85	1BYE	2.80	49.28	87.8	10.5	0.9	0.7
ZmGSTF1.1	-5.54	1BYE	2.80	40.10	87.2	11.0	1.0	0.8
ZmGSTF1.2	-2.23	1BYE	2.80	49.76	91.9	7.5	0.1	0.4
ZmGSTF2.1	-2.18	1BYE	2.80	55.92	91.3	7.9	0.5	0.3
ZmGSTF2.2	-2.20	1BYE	2.80	55.66	92.2	7.0	0.4	0.4
ZmGSTF2.3	-2.00	1BYE	2.80	57.49	91.8	7.7	0.0	0.5
ZmGSTF3.0	-3.86	1BYE	2.80	36.78	85.3	12.3	1.3	1.1
ZmGSTF3.1	-3.62	1BYE	2.80	36.67	86.8	10.9	1.4	0.9
ZmGSTF4.0	-4.23	1BYE	2.80	27.04	90.9	7.7	0.7	0.8
ZmGSTF4.1	-4.81	1BYE	2.80	23.56	84.4	12.9	1.9	0.8
ZmGSTF4.2	-4.06	1BYE	2.80	19.44	85.2	11.8	2.0	1.0
ZmGSTF4.3	-3.28	1BYE	2.80	32.21	88.5	9.4	1.3	0.8
ZmGSTF4.4	-3.28	1BYE	2.80	31.73	89.5	8.7	1.2	0.6
ZmGSTF4.5	-3.34	1BYE	2.80	31.55	90.5	8.8	0.5	0.3
ZmGSTF4.6	-3.33	1BYE	2.80	32.04	89.2	10.2	0.4	0.3
ZmGHR1.0	-3.39	3R3E	2.21	45.15	87.8	11.5	0.7	0.0
DHAR 4	-0.53	5LOL	2.30	68.57	95.0	4.4	0.6	0.0
DHAR 3	-0.37	5LOL	2.30	66.82	95.4	4.0	0.6	0.0
ZmGSTL1.0	-0.16	4PQH	1.40	66.96	90.6	8.9	0.5	0.0
ZmGSTL1.1	-0.06	4PQH	1.40	61.33	94.7	4.7	0.5	0.0
ZmGSTL1.2	-0.49	4PQH	1.40	65.79	87.9	10.5	1.6	0.0
ZmGSTL1.3	0.32	4PQH	1.40	62.10	92.7	6.7	0.5	0.0
ZmGSTU1.0	0.21	5J4U	1.25	59.45	96.3	2.6	1.0	0.0
ZmGSTU1.1	-1.05	5J4U	1.25	47.93	93.7	5.8	0.5	0.0
ZmGSTU2.0	-1.69	5J4U	1.25	40.00	93.9	5.0	1.1	0.0
ZmGSTU3.0	-1.53	5J4U	1.25	45.93	93.6	5.3	1.1	0.0
ZmGSTU3.1	-1.59	5J4U	1.25	43.69	94.6	4.3	1.1	0.0
ZmGSTU4.0	-1.60	5J4U	1.25	35.65	93.2	5.8	1.0	0.0
ZmGSTU4.1	-3.30	5J4U	1.25	33.64	90.0	8.5	0.5	1.0
ZmGSTU5.0	-0.07	5J4U	1.25	47.75	95.9	3.0	1.2	0.0
ZmGSTU5.1	0.02	5J4U	1.25	41.41	93.1	5.8	1.2	0.0
ZmGSTU5.2	-1.01	5J4U	1.25	36.00	94.4	4.5	1.1	0.0
ZmGSTU5.3	-1.53	5J4U	1.25	40.58	93.5	4.9	1.1	0.5
ZmGSTU5.4	-0.95	5J4U	1.25	39.41	95.0	3.3	1.7	0.0
ZmGSTU5.5	-0.51	5J4U	1.25	38.60	94.8	4.2	1.0	0.0
ZmGSTU5.6	0.01	5J4U	1.25	39.81	95.5	4.0	0.6	0.0
ZmGSTU6.0	-1.46	5J4U	1.25	39.42	92.6	6.3	1.1	0.0
ZmGSTU6.1	-1.95	5J4U	1.25	42.63	92.4	4.7	2.3	0.6
ZmGSTU6.2	-1.39	5J4U	1.25	39.68	93.5	4.7	1.8	0.0
ZmGSTU6.3	-1.59	5J4U	1.25	44.68	91.6	4.9	2.3	1.2
ZmGSTU7.0	-1.70	5J4U	1.25	41.55	94.0	5.5	0.5	0.0
ZmGSTU7.1	-0.92	5J4U	1.25	40.38	94.0	5.5	0.0	0.5
ZmGSTU7.2	-1.58	5J4U	1.25	41.55	92.5	5.9	1.3	0.3
ZmGSTU7.3	-2.60	5J4U	1.25	39.26	93.8	4.1	1.4	0.7
ZmGSTU7.4	-1.80	5J4U	1.25	41.18	93.0	5.4	1.6	0.0
ZmGSTU8.0	-2.36	5J4U	1.25	42.20	92.9	6.6	0.5	0.0
ZmGSTU8.1	-0.92	5J4U	1.25	37.04	94.8	3.6	1.6	0.0
ZmGSTU8.2	-0.61	5J4U	1.25	36.36	92.8	6.7	0.5	0.0
ZmGSTU9.0	-1.05	5J4U	1.25	44.97	95.0	4.3	0.7	0.0
ZmGSTU9.1	-0.81	5J4U	1.25	44.97	94.0	4.7	1.3	0.0
ZmGSTU9.2	-2.47	5J4U	1.25	43.28	90.6	7.1	2.3	0.0
ZmGSTU9.3	-2.26	5J4U	1.25	42.13	91.9	5.9	1.6	0.5
ZmGSTU10.0	-1.49	5J4U	1.25	42.79	93.7	5.2	1.0	0.0
ZmGSTU10.1	-1.65	5J4U	1.25	44.44	92.8	6.1	1.1	0.0
ZmGSTU10.2	-1.63	5J4U	1.25	40.93	93.3	5.9	0.3	0.5
ZmGSTU10.3	-0.88	5J4U	1.25	39.53	94.6	4.9	0.5	0.0
ZmGSTU10.4	-1.32	5J4U	1.25	40.85	89.7	10.3	0.0	0.0
ZmGSTU10.5	-0.35	5J4U	1.25	52.26	94.4	4.9	0.7	0.0

Table S 12: Homology model characteristics, for Figure 34.

PDB accessions given for each model template. Ramachandran analysis is given as percentage of residues in regions, as defined by the letters in Figure S 3. a.

[illegible][illegible]

147

Chapter 5. The effect of safeners and stresses on xenome enzyme induction

5.1 Introduction

The mode of action of safeners has been investigated in several crops, and although the specific interactions between safeners and their targets remain elusive, there is a consensus that safeners reduced herbicide damage in crops by enhancing the metabolism of the herbicide (Davies et al., 1999; Kraehmer et al., 2014). This is achieved through enhancement of certain enzymes involved in xenobiotic detoxification such as glutathione-S-transferases (GSTs) and cytochrome P450s (CYPs) (Hatzios, 1991; Hatzios et al., 2004; Skipsey et al., 2011). The levels of the tripeptide antioxidant glutathione (GSH), are also often increased, though the contribution of this to the safening effect is not confirmed (Davies et al., 1999; Hatzios et al., 2004; Riechers et al., 2010). An interesting and yet poorly understood phenomena of safeners is their selectivity for which crop and herbicide they safen, known as botanical and chemical selectivity, respectively.

It has been hypothesised that different xenobiotic enzymes might be affected by different safeners and detoxify different herbicides, providing a possible explanation for how chemical selectivity of safeners is achieved (Hatzios, 1991; Hatzios et al., 2004; Komives, 1992). This is discussed in Section 1.7, in which some examples of this selective enzyme usage are compiled from the literature, highlighting how different herbicides are detoxified by different enzymatic processes. The first experiments in the current chapter sought to identify important xenobiotic enzymes of safening effects and to test the hypothesis that safeners with chemical specificity towards different herbicides would have differential effects on the expression of these important enzymes. The results of this study aimed to elucidate the general mechanism of safener chemical selectivity, and to provide a basis for predictions of such selectivity.

While these enzymes are most commonly associated with xenobiotic detoxification, they chronologically precede the use of artificial pesticides and must therefore have evolved for other physiologically important functions, likely in electrophile detoxification reactions associated with secondary metabolism (Coleman et al., 1997; Edwards et al., 2011; Frova, 2003). The range of effects of these enzymes on xenobiotic detoxification likely results from their large family sizes and structural and functional diversity, leading to a versatility of their action on multiple substrates. GSTs have been implicated in reducing oxidative stress damage via alkenal detoxification, and show some class-specific functions (Cummins et al., 1997; Frova,

2003; Gronwald et al., 1998). Phi and tau class GSTs have demonstrated ligand-binding (ligandin) roles; binding flavonoids, auxins and cytokinins (Frova, 2003; Gonneau et al., 1998; Marrs, 1996; Mueller et al., 2000). Phi, tau and theta class GSTs have also displayed peroxidase activity (Cummins et al., 1999; Edwards et al., 2000; Frova, 2003; Scalla et al., 2002). Zeta class GSTs are known to catalyse the isomerisation of maleylacetoacetate to fumarylacetoacetate in tyrosine degradation (Frova, 2003). DHAR and lambda GSTs cannot conjugate GSH to substrates, and instead may act as thiol transferases, or catalyse deglutathione reactions, and DHAR may catalyse GSH-dependent dehydroascorbate reduction reactions (Frova, 2003; Lallement et al., 2014). Many members of these latter classes have been shown to be induced by oxidative stress, and appear to act as antioxidant enzymes (Dixon et al., 2002a; Frova, 2003). However, enzyme class cannot always infer function, which should be determined individually (Frova, 2003). CYPs have roles in the biosynthesis of phenylpropanoids, terpenoids, and alkaloids (Bolwell et al., 1994; Ohkawa et al., 1999). In addition, CYPs catalyse the hydroxylation of fatty acids and epoxidation of lauric acid (Bolwell et al., 1994). It is likely that the ability of GSTs and CYPs to detoxify herbicides evolved from these other catalytic functions, and it is plausible that these enzymes are regulated by signalling pathways linked to controlling natural product metabolism. Therefore, the relationship between the effects of safeners, abiotic stresses and plant hormones on the regulation of GSTs was investigated to identify similarities that might indicate similar signalling pathways.

To allow comparison with metabolic data from Chapter 3, the same safeners, metcamifen and benoxacor, were investigated. Chapter 3 identified a difference in the ability of these safeners to metabolise the herbicide mesotrione, making these safeners perfect candidates to test the hypotheses.

5.2 Results

5.2.1 *Safener effects on GST transcript expression in maize cell culture*

To determine differential safening effects on the entire family of maize GSTs, and to identify safener-inducible genes, a previously generated next generation sequencing study was analysed. The study had been performed by Melissa Brazier-Hicks (Syngenta, UK) and Johnathan Cohn (Syngenta, USA), on Black Mexican Sweetcorn (BMS) cell culture treated with metcamifen or benoxacor and then sampled at 30, 90 and 240 min. The full set of unigenes were analysed with respect to the induction of GSTs, as identified in Chapter 4. The effects of metcamifen and benoxacor on GST expression at all time points, in each class, were compared

(Figure 37) (Table 19). Regression analysis was used to identify any safener-specific effects on gene induction, where the gradients (Y) indicated the differences between safener effects and the trendline coefficients of determination (R^2) indicated the variation between individual GSTs. Correlation analysis was used to identify statistical differences between safener effects, where the p values described significance and the Pearson correlation values (r) described the linearity of the relationship; with $r = 0$ indicating no relationship and $r = 1$ indicating complete relationship, between safener effects. The linear regression of all GSTs, at all times, displayed a gradient of $1.0139X - 0.0637$ with an R^2 of 0.7141 indicating a positive, approximately 1:1, linear relationship as to the effects of each safener. The Pearson correlation of this analysis produced an r of 0.845 ($p = 0.000$) which indicated a strong, statistically significant, correlation. When each class was analysed individually, all classes except for the GHR class showed a positive, statistically significant correlation, with r between 0.681 and 0.994 ($p \leq 0.005$). All classes except GHR and theta had a trend gradient between 0.77 and 1.02 indicating a relatively similar response of the genes to both safeners, with R^2 values between 0.4641 and 0.9884 indicating a range of variation. The zeta, DHAR and tau classes displayed the least difference between safener effects, with gradients between 0.7728 and 1.0168, and correlation over 0.897 ($P < 0.001$). These classes also displayed low variation ($R^2 > 0.8038$). The lambda and phi classes displayed more difference between safener effects, with gradients of 0.8212 and 0.8976, respectively, indicating greater induction resulting from metcamifen than benoxacor. The low correlations, 0.747 and 0.681, and R^2 values, 0.5580 and 0.4641, for lambda and phi classes, respectively, indicated a large degree of variation between individual GSTs or times, though the correlations were still statistically significant ($p < 0.005$). GHR presented a gradient of 1.8860, indicating benoxacor caused a larger effect on induction of the GHR gene than metcamifen. The high R^2 (0.8585) and r (0.927) values, indicated a low degree of variation between the times analysed, though the correlation was not significant ($p = 0.246$), likely on account of only one gene being analysed. The low gradient of the theta class (0.6037) indicated a larger inductive effect was caused by metcamifen than benoxacor. The high R^2 (0.9298) and r (0.964) values indicated a low degree of variation, with the class also showing a significant correlation ($p = 0.002$). The small gene numbers of these latter two classes made the analysis tenuous, and should not be over-analysed.

The data showed a number of genes that were responsive only to one safener, as indicated by points on either axis, which were identified and analysed later. It was also evident that

upregulation by the safeners is more prevalent than downregulation, indicated by the larger number of positive values.

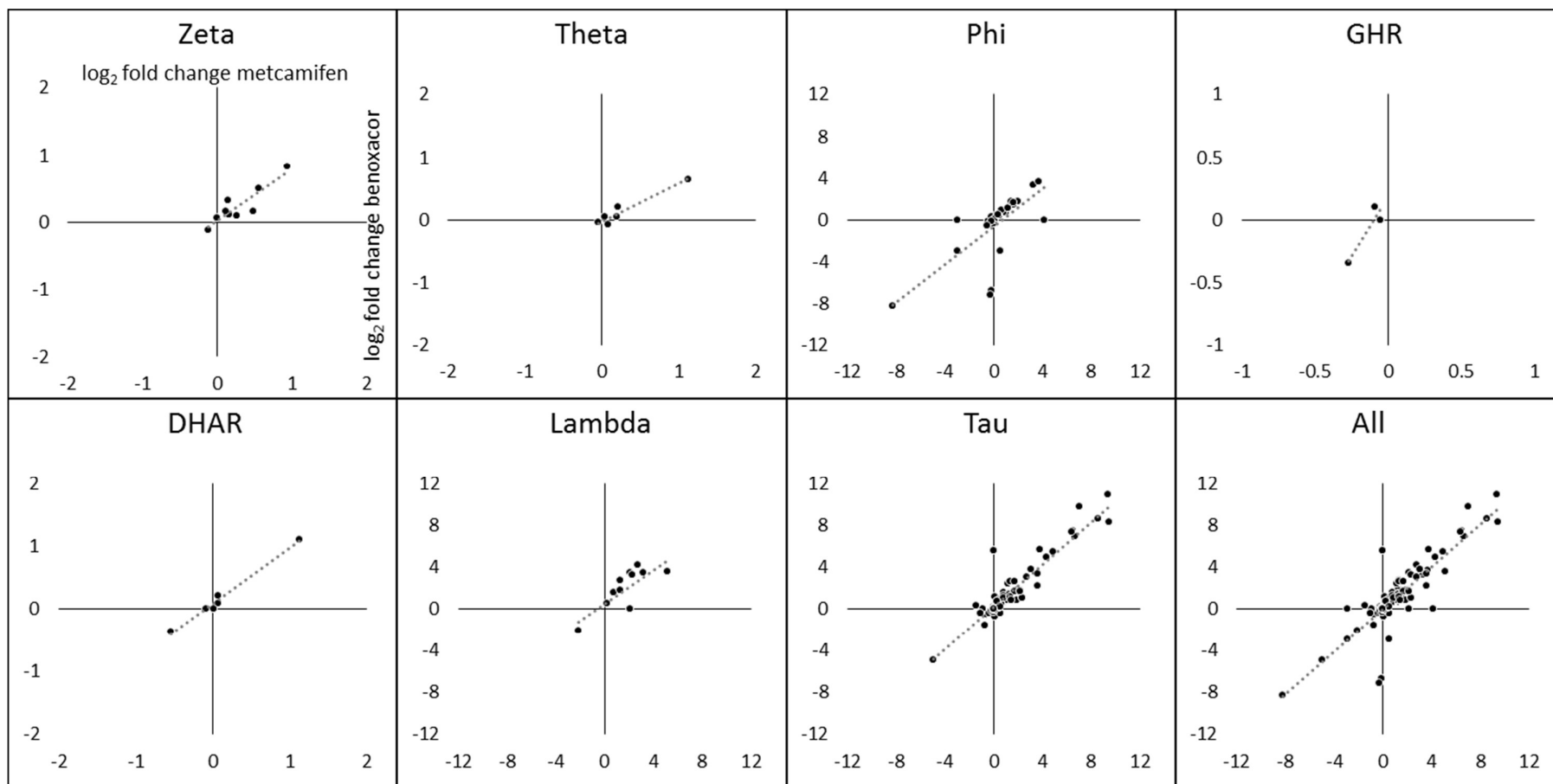


Figure 37: Regression analysis showing the effect of safeners, metcamifen and benoxacor, on induction of Glutathione-S-Transferase (GST) classes. Black Mexican Sweetcorn cell cultures were treated with 5 μ m Safener or control, and sampled at 30, 90 and 240 min, followed by next generation sequencing analysis. The data was analysed using Excel and Graphpad. Data are displayed as \log_2 fold change values at 30, 90 and 240 minutes. Axes labels are shown in zeta graph only (top left). Dotted grey lines represent linear regressions.

Class	Pearson correlation (r)	P-Value	Gradient (Y =)	R ²
Zeta	0.897	0.001	0.7728X + 0.0192	0.8038
Theta	0.964	0.002	0.6037X - 0.0226	0.9298
Phi	0.681	0.000	0.8976X - 0.6420	0.4641
GHR	0.927	0.246	1.8860X + 0.1730	0.8585
DHAR	0.994	0.000	0.8989X + 0.0747	0.9884
Lambda	0.747	0.005	0.8212X + 0.4251	0.5580
Tau	0.919	0.000	1.0168X + 0.1962	0.8442
All	0.845	0.000	1.0139X - 0.0637	0.7141

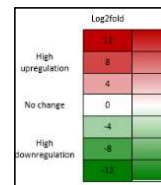
Table 19: Correlation and regression analysis of next generation sequencing data of Glutathione-S-Transferase (GST) classes (Figure 37).

Table 20 details the effects of each safener on individual GST genes at each time point, displayed in the phylogenetic order defined in Chapter 4. Zeta, theta, DHAR and GHR gene expression was relatively unaffected ($-1.5 < \log_2 < 1.5$) by either safener, with most genes showing non-significant effects. Phi, lambda and tau class genes showed both up and down regulation by the two safeners, with no apparent class trends. A high degree of similarity between the effects of both safener was observable, if not in magnitude in whether regulation was positive or negative. Moderate induction ($\log_2 > 1.5$, $\log_2 < -1.5$) occurred as early as 30 minutes, and in most cases where significant effects were observed. When gene induction was observed, it did not abate by 240 minutes. In fact, phi class genes showed a constant increase over time. Lambda and tau class genes showed either consistent increases or parabolic trends. Fifteen genes showing moderate induction ($\log_2 > 1.5$) by safeners were identified as potential biomarkers for safening in section 5.2.2.2. These were two phi, three lambda, and ten tau class genes (Table 20 *). Nine genes showing differential regulation by benoxacor and metcamifen were characterised on the basis of observing significant induction with only one safener at a given time. This group consisted of one zeta, two phi, one lambda and five tau class genes (Table 20 Δ).

Class	Name	gene ID	Gene accession	Metcamifen			Benoxacor				
				30 min	90 min	240 min	30 min	90 min	240 min		
Zeta	ZmGSTZ1.0	542543	GRMZM2G064255	0.26	-0.01	0.48	0.10	0.06	0.16	Δ	
	ZmGSTZ1.1	100283891	GRMZM2G124974	0.16	-0.11	0.14	0.11	-0.11	0.33		
	ZmGSTZ1.2	541833	GRMZM2G019090	0.12	0.55	0.93	0.15	0.50	0.82		
Theta	ZmGSTT1.0	100285763	GRMZM2G077183	0.08	-0.05	0.21	-0.07	-0.04	0.21		
			GRMZM2G122488	0.20	0.04	1.12	0.04	0.04	0.65		
Phi	ZmGSTF1.0	541990	GRMZM2G146246	0.04	0.03	0.37	0.06	-0.08	0.35		
	ZmGSTF1.1										
	ZmGSTF1.2										
	ZmGSTF2.0	542366	GRMZM2G116273	0.25	0.69	1.03	0.38	0.73	0.75		
	ZmGSTF2.1	542740	GRMZM2G156877	0.82	1.63	2.03	0.75	1.43	1.77		
	ZmGSTF2.2	542630	GRMZM2G150474	0.42	0.66	1.20	0.52	0.96	1.16		
	ZmGSTF2.3	542311	GRMZM2G132093	1.49	3.30	3.66	1.78	3.30	3.66		*
	ZmGSTF3.0	541828	GRMZM2G096153	0.18	-0.42	-0.10	0.35	-0.15	-0.01		
	ZmGSTF3.1										
	ZmGSTF4.0	542490	GRMZM5G895383	-0.03	1.64	-0.20	-0.34	1.64	0.24		Δ
	ZmGSTF4.1	541829	GRMZM2G119499	-0.14	-8.27	-0.29	-6.75	-8.27	-7.17		
	ZmGSTF4.2										
	ZmGSTF4.3	541830	GRMZM2G096269	0.00	0.00	4.14	0.00	0.00	0.00		
	ZmGSTF4.4	541831	GRMZM2G126781	0.11	0.19	-0.19	-0.07	0.16	-0.14		
	ZmGSTF4.5	542629	GRMZM2G126763	0.50	0.35	-0.56	0.35	0.50	-0.56		
	ZmGSTF4.6	100282447	GRMZM2G096247	0.52	-2.94	-2.94	-2.94	0.00	-2.94		
	GHR	ZmGHR1.0	100272773	GRMZM2G102216	-0.05	-0.27	-0.09	0.00	-0.35		0.10
		DHAR 4	100382696	GRMZM2G005710	-0.54	-0.08	1.12	-0.37	0.00		1.10
DHAR	DHAR 3	100273125	GRMZM5G855672	0.07	0.01	0.07	0.09	0.01	0.22		
Lambda	ZmGSTL1.0	100282090	GRMZM2G162486	0.20	0.76	1.32	0.48	1.58	2.78	*Δ	
	ZmGSTL1.1	100281225	GRMZM2G338131	-2.12	2.12	2.12	-2.12	0.00	0.00	*	
	ZmGSTL1.2	100282747	GRMZM2G043291	2.15	2.75	2.29	3.51	4.15	3.30	*	
	ZmGSTL1.3	542388	GRMZM2G042639	1.29	3.21	5.13	1.80	3.46	3.58	*	
Tau	ZmGSTU1.0	541991	GRMZM2G129357	0.91	2.74	3.58	1.36	3.04	3.35	*	
	ZmGSTU1.1	541834	GRMZM2G335618	0.09	0.13	0.30	-0.02	-0.24	0.12	Δ	
	ZmGSTU1.2	542734	GRMZM2G308687	0.78	1.17	1.32	1.61	2.42	2.60	*	
	ZmGSTU2.0	542632	GRMZM2G077206	n/a	n/a	n/a	n/a	n/a	n/a		
	ZmGSTU3.0	542634	GRMZM2G145069	7.03	9.40	4.92	9.79	10.89	5.50	*Δ	
			GRMZM2G149182	7.07	9.40	4.92	9.79	10.90	5.49	*Δ	
	ZmGSTU3.1	541842	GRMZM2G475059	3.78	6.47	6.67	5.64	7.47	6.95	*	
	ZmGSTU4.0	541849	GRMZM2G097989	-0.13	-0.39	-0.70	-0.22	-0.43	-0.66		
	ZmGSTU4.1	100502255	GRMZM2G016241	0.06	-0.91	-0.70	-0.47	-0.55	-0.54		
	ZmGSTU5.0	541845	GRMZM2G416632	0.00	-0.02	0.66	0.01	0.08	0.53		
	ZmGSTU5.1	542633	GRMZM2G127789	0.07	-0.36	-0.20	0.05	-0.39	-0.21		
	ZmGSTU5.2	541836	GRMZM2G428168	1.27	1.90	2.14	1.49	1.73	1.78	*	
	ZmGSTU5.3	541837	GRMZM2G032856	-0.92	0.07	0.57	-0.04	-0.73	-0.42		
	ZmGSTU5.4	541840	GRMZM2G146475	0.01	0.02	0.04	0.03	-0.01	0.18		
	ZmGSTU5.5	100281369	GRMZM2G052571	0.17	-0.02	0.18	0.34	-0.31	0.21		
	ZmGSTU5.6	542587	GRMZM2G028556	1.68	3.09	4.31	2.63	3.79	4.97	*	
	ZmGSTU6.0	541839	GRMZM2G363540	0.00	0.13	1.89	0.00	1.18	0.84		
	ZmGSTU6.1	100281103	n/a	n/a	n/a	n/a	n/a	n/a	n/a		
	ZmGSTU6.2	541848	GRMZM2G028821	0.45	0.71	1.27	0.05	0.54	1.08		
	ZmGSTU6.3	100193719	GRMZM2G168229	n/a	n/a	n/a	n/a	n/a	n/a		
	ZmGSTU7.0	100280815	GRMZM2G146913	0.32	0.06	0.11	0.30	0.08	0.14		
	ZmGSTU7.1	100285806	GRMZM2G146887	0.08	0.20	0.36	0.00	0.11	0.34		
ZmGSTU7.2	100856957	GRMZM2G056388	0.66	0.82	1.04	0.68	0.63	0.83			
ZmGSTU7.3	541835	n/a	n/a	n/a	n/a	n/a	n/a	n/a			
ZmGSTU7.4											
ZmGSTU8.0	542631	GRMZM2G330635	0.68	1.25	1.70	1.02	1.32	1.68	*		
ZmGSTU8.1	541846	GRMZM2G178079	0.58	1.08	0.66	0.70	0.86	0.50			
ZmGSTU8.2											
ZmGSTU9.0	541847	GRMZM2G066369	-1.03	-1.42	2.37	-0.39	0.30	1.03			
ZmGSTU9.1											
ZmGSTU9.2	541841	GRMZM2G044383	0.54	0.81	0.86	0.92	1.28	1.03			
ZmGSTU9.3	541838	GRMZM2G161905	0.29	1.35	2.16	0.70	1.12	1.69	*		
ZmGSTU9.4											
ZmGSTU10.0	542491	GRMZM2G161891	-0.19	0.22	0.68	-0.12	-0.10	0.31	Δ		
ZmGSTU10.1	100192043	GRMZM2G480439	6.40	8.29	5.44	7.36	5.56	8.11			
ZmGSTU10.2	541850	GRMZM2G025190	0.04	0.06	0.52	-0.08	-0.14	0.20	Δ		
ZmGSTU10.3	542635	GRMZM2G054653	1.44	-0.74	3.58	0.80	-1.54	2.17	*Δ		
ZmGSTU10.4	541843	GRMZM2G041685	0.00	-4.95	0.00	5.57	-4.95	0.00			
ZmGSTU10.5											

Table 20: Perturbation of maize Glutathione-S-Transferase (GST) genes by safeners, metcamifen and benoxacor, determined through next generation sequencing.

Black Mexican Sweetcorn cell cultures were treated with 5 μ m Safener or control, and sampled at 30, 90 and 240 min, followed by next generation sequencing analysis. The data was analysed using Excel and Graphpad. Values represent log₂ fold change compared to a control. Legend (bottom right) describes heat map colours. Values in blue are not significant ($p \geq 0.05$). Values in black are significant ($p < 0.05$). * denotes genes with significant log₂ values > 1.5. Δ denotes genes with significant values with only one safener at a given time.



5.2.2 *Safener effects on GST and CYP transcript expression in whole plants*

To determine the effect of the safeners on xenome gene induction in whole plants, quantitative real-time polymerase chain reaction (qPCR) was performed on maize plants, treated with benoxacor or metcamifen, over the course of three days. The gene induction was analysed first by relative quantification, a method used to compare the levels of 'gene of interest' transcripts in treated samples with control samples, after normalisation to a reference gene.

5.2.2.1 *Reference primer design and validation*

A reference gene was required to normalise the data between qPCR runs: by comparing all genes of interest to this reference gene, any variations in samples, efficiencies and errors could be accounted for. This reference gene was chosen on the basis of being unaffected by the treatments investigated, while demonstrating consistency in expression throughout the growth of the plant. As such, common reference genes are often those involved in basic cellular function, which are constitutively expressed at a steady level. Five reference genes were tested on the basis of replication efficiency, melting efficiency, product size and stability. Based upon the work by Lin et al. (2014), and also using well-known reference genes, DPP9, NAC, DUF, CDK and Actin 1 were investigated as potential reference genes (Table 21). Details of the primers for these prospective reference genes are shown in Table 21.

Gene Primer	NCBI code	Forward				Reverse				Product Length (bp)
		Sequence (5-3')	T _m (°C)	GC%	Start	Sequence (5-3')	T _m (°C)	GC%	Start	
DPP9	NM_0011744 61.1	GAAGGGCCTT GCAAAACCTG	59.97	55.00	656	ACCATCCCATGC TGTTACCG	60.11	55.0 0	794	139
NAC	NM_0011590 59.2	ACATGCCGTT GAACTTTGCC	59.97	50.00	1605	TTGCTTCCGGAA CCTCAGAG	59.68	55.0 0	1685	81
DUF	NM_0011482 17.1	GGCCTCGACC TTTCCAGAAA	59.96	55.00	447	GTGGAGCTTGCA TCTCTGGT	60.04	55.0 0	569	123
CDK	NM_0011472 29.1	CACCAGGTCT TTGCACGTTG	59.97	55.00	753	AATACATCCAGC GGCCCAAA	60.03	50.0 0	848	96
ACTIN 1	NM_0011551 79.1	GCCGATCGTA TGAGCAAGGA	59.97	55.00	1198	TAGAGCCACCGA TCCAGACA	60.03	55.0 0	1303	106

Table 21; Reference gene primer sequences.

Sequence, melting temperature (T_m) (°C), Guanine/Cytosine content (GC%), start position, and product length in base pairs (bp) are shown for each forward and reverse primer.

The primers were tested for replication efficiency, melting quality, expression stability and product size. In order to test efficiency, a dilution curve of cDNA concentration was performed using each primer (Table 22). An efficiency criteria of 2.00 ± 0.2 was used to identify primers that precisely duplicate the DNA per qPCR cycle, as previously suggested (Svec et al., 2015; Taylor et al., 2017). A criteria for the standard dilution curve coefficient of determination (R^2) of 0.95 - 1.00 was used to determine efficient dilution. This test also produced melting curves which were tested visually based upon the normality of their curves (Table 23), restricting for single normally distributed curves, consistent in each dilution. To validate whether the correct sequence was being replicated, the actual size of the replicated DNA was compared to the designed product size. This was performed using agarose gel electrophoresis of qPCR amplified DNA samples, including untreated and benoxacor treated samples, to identify any differences accrued from treatment (Figure S 5, Figure 38 and Figure 39). Differences of 15% between the measured and predicted size, and of 10% between the treated and untreated samples, were considered acceptable. The expression of the reference genes were compared in untreated and benoxacor treated maize plants (Figure 40), to determine expression stability. Statistical analysis was performed, and primers displaying statistical variation between treatments were considered unsuitable (Table S 13). The validation experiments indicated DPP9 and CDK as the only reference gene primers within suitable limits for the four tested parameters. DPP9, having a far better efficiency than CDK, was therefore used as the reference gene in all subsequent qPCR experiments.

Parameter	DPP9	NAC	Gene DUF	CDK	Actin 1
Slope	-3.1026	-3.3493	-2.6017	-2.9671	-3.8348
Efficiency	2.1 ^a	1.99 ^a	2.42 ^b	2.17 ^a	1.82 ^a
Error	0.14	0.19	0.59	0.21	0.19
R ²	0.99 ^a	0.99 ^a	0.87 ^b	0.99 ^a	0.99 ^a
Y-Intercept	27.87	27.68	30.5	30.14	27.88

Table 22: Reference gene primer efficiency data.

Superscripts defined values: a; suitable, b; unsuitable.

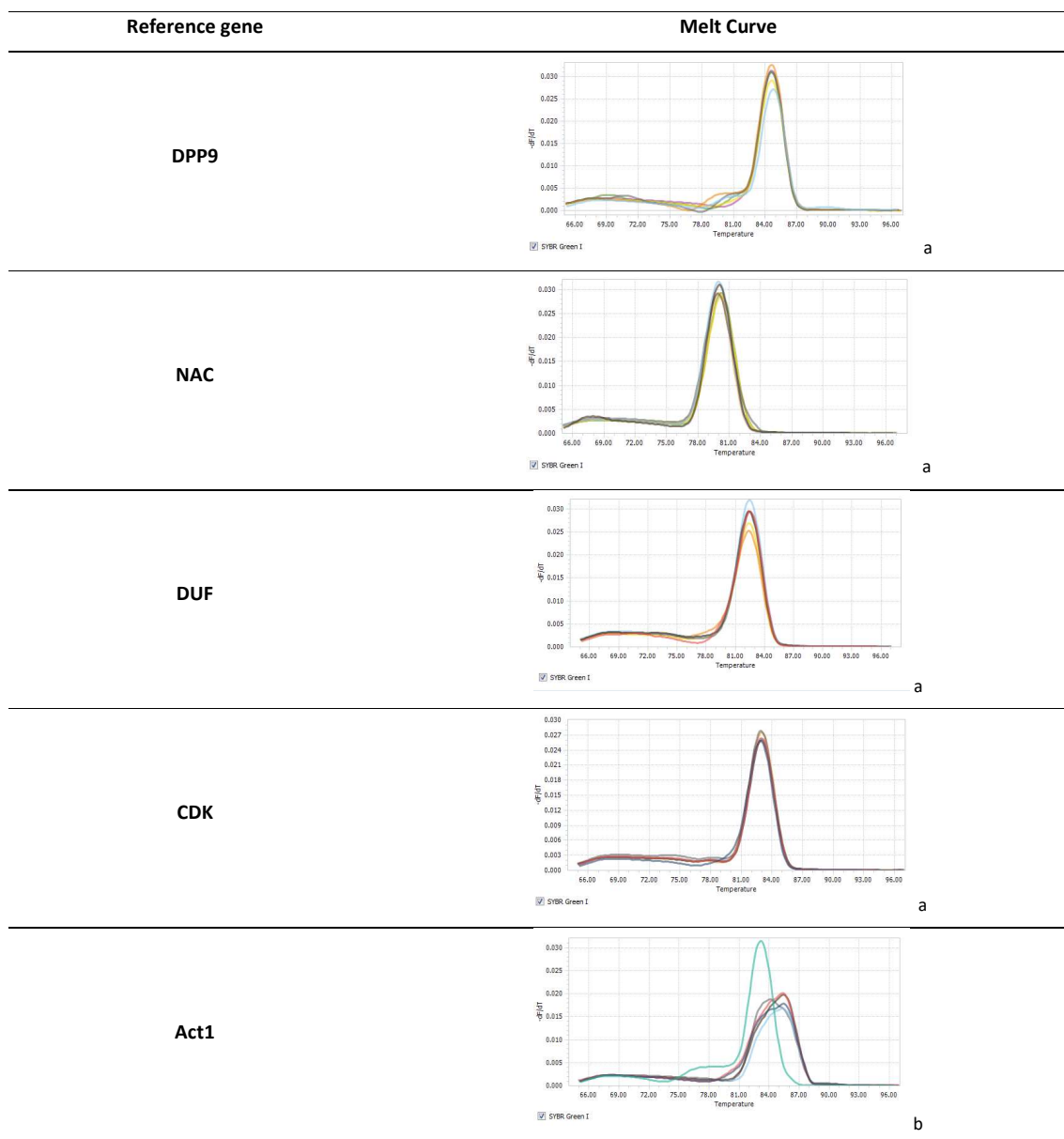


Table 23: Melting curves for reference gene primers.

Temperatures of 66-96 °C are plotted against $-dF/dT$ (rate of change of fluorescence relative to temperature). Letters define curves: a; suitable. b; non-suitable

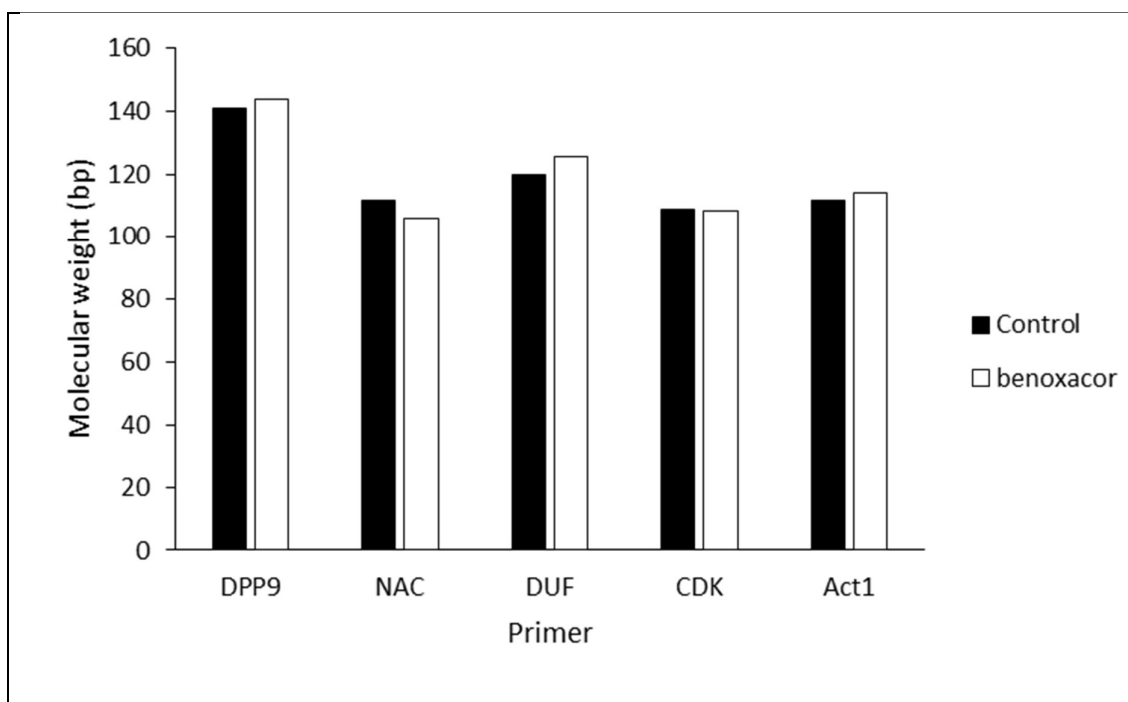


Figure 38: Bar chart showing calculated molecular weights of reference gene replicated region of treated and untreated samples as defined by the legend (right).

Calculated molecular weights were determined through agarose gel electrophoresis, which are shown in base pairs (bp). All differences between treated and non-treated samples were considered acceptable.

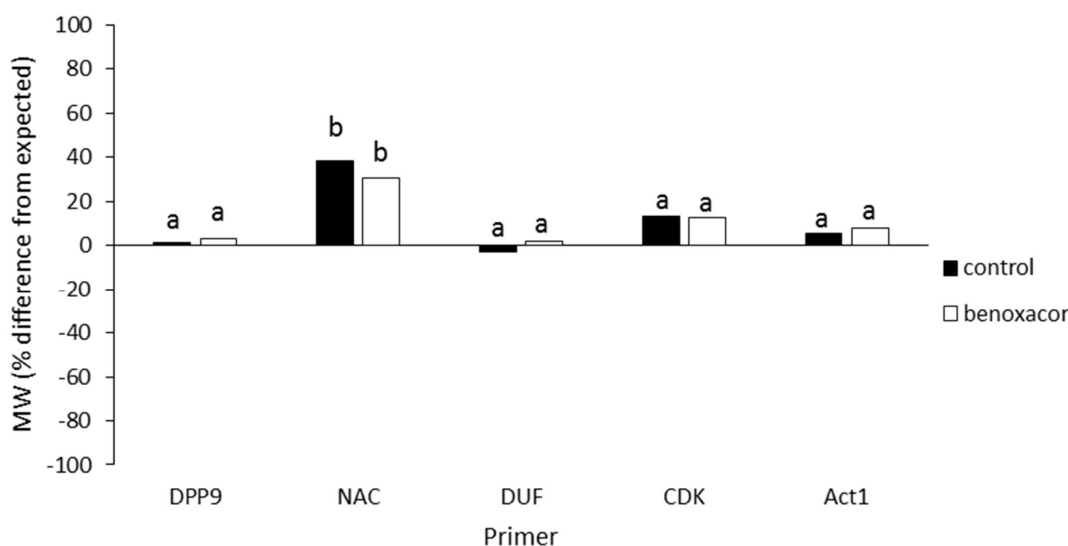


Figure 39: Bar chart showing percentage difference in molecular weight of calculated compared to expected product sizes of reference genes.

Calculated molecular weights were determined through agarose gel electrophoresis. Legend (right) shows treatment. Letters define differences between measured and expected product size: a; suitable and b; non-suitable.

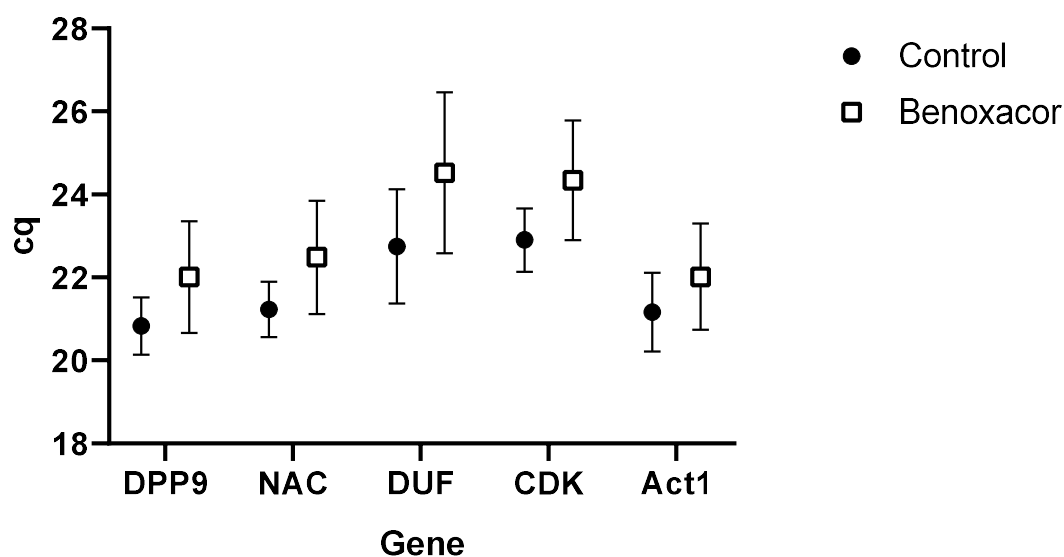


Figure 40: Quantification cycle (Cq) of reference gene primers with benoxacor treatment compared to control treatment.

Legend (top right) defines treatment. Data plotted as means with standard deviation. 3 biological and 3 technical replicates were used for each data point.

5.2.2.2 Gene of interest primer design and validation

Primers were designed to amplify sequences of xenobiotic detoxification enzymes belonging to the GST and CYP superfamilies. Due to the large size of these families, three members of each were chosen for study. One member from each of the phi and tau class GSTs were chosen, since these are known to be involved in safener-mediated xenobiotic detoxification (Andrews et al., 2005). A lambda class GST was also included as, although not involved in xenobiotic detoxification, this class is known to be strongly induced by safeners and abiotic stresses (Dixon et al., 2002a; Skipsey et al., 2011). The individual members of each class were chosen on the basis of safener inducibility as informed by the literature and analysis of the data presented in section 5.2.1. These GSTs were first restricted to fifteen genes being at least moderately induced ($\log_2 > 1.5$) in the next generation sequencing (NGS) analysis, corresponding to the three classes. The NGS indicated *ZmGSTF2.3* (previously *ZmGSTF2/GSTIV*) as the most safener inducible phi class GST. It has also been well documented that *ZmGSTF2* expression is induced by benoxacor (Fuerst et al., 1993; Irzyk et al., 1993). *ZmGSTL1.3* (previously *ZmGSTL1/saf1/ln2-1*) was one of the most safener inducible lambda class GSTs in the NGS, and has been demonstrated as safener inducible by the benzenesulfonamide safener N-(aminocarbonyl)-2-chlorobenzene-sulfonamide (2-CBSU) in maize (Hershey et al., 1991). *ZmGSTU1.2* (previously *ZmGSTU1/GSTV*), while not the most safener inducible in the NGS, has

been previously characterised and described as dichlormid safener inducible (Dixon et al., 1998a) and has been shown to play a key role in the metabolism of nitrodiphenyl ether herbicides (Cole D. J., 1997). While the NGS data was not interrogated for CYP genes, the literature contained enough information to identify safener-inducible genes of interest. CYP72A5 was shown to be induced by the safener 1,8-naphthalic anhydride (1,8-NA) and the sulfonylurea herbicide triasulfuron in maize seedlings (Persans et al., 2001). CYP81A9 has been shown to be involved in the metabolism of multiple herbicides in maize (Brazier-Hicks et al., 2017; Pataky et al., 2008). CYP81A4 was selected based on unpublished work derived from our lab. The primer sequences for all six genes of interest are shown in Table 24. The sequence and primer positions of *ZmGSTU1* are shown in Figure 41 as an example. The primers for the genes of interest were tested with respect to replication efficiency, melting quality and product size.

Gene Primers	NCBI Code	forward				reverse				Product length (bp)
		Sequence (5-3')	Tm (°C)	GC%	start	Sequence (5-3')	Tm (°C)	GC%	start	
ZmGSTU1.2	NM_001112 244.1	GTGCGCAAGAA CCTCTACCC	60.11	60.00	633	GGATGCTCTACT CGATGCCC	60.04	60.00	717	85
ZmGSTF2.3	NM_001111 896.2	CAGGAGCGGAG CAGAACTAA	60.67	55.00	61	GATACGAACGG CGAGATAGC	59.84	55.00	151	91
ZmGSTL1.3	NM_001111 963.1	ATCTGCTACTTC TGCCCGTTC	60.78	52.38	129	CCTGTGCGTAA ACCTTGTC	60.55	55.00	264	136
CYP81A4	NM_001175 353.2	CTATGCTTGCC GTCCTCAAG	55.80	55.00	1579	CGGCTCACTCC AGGAAGAA	56.50	55.00	1709	150
CYP81A9	NM_001319 705.1	GGTGTATGACG TAGCTTCCG	55.20	55.00	1675	CCATTCCATACA CTCGGCGA	57.10	55.00	1738	83
CYP72A5	NM_001147 214.1	AACTGCACCCT CAACATGG	57.90	55.00	1555	GTAGTGTCCGG TAGCAGCAT	56.80	55.00	1619	84

Table 24: Gene of interest primer sequences.

Sequence, melting temperature (Tm) (°C), Guanine/Cytosine content (GC%), start position, and product length base pairs (bp) are shown for each forward and reverse primer.

The replication efficiency and R^2 criteria was satisfied for all primers tested (Table S 14). The melting curves for all primers were of satisfactory quality (Figure S 6). The calculated product sizes of the qPCR products (Figure S 7) were within the 15% criteria of the expected product size (Figure S 8) for all gene of interest primers. Therefore, all primers were considered suitable for use. Two primers were removed from study due to unacceptable primer qualities or lack of induction by safeners. These primers, for *ZmGSTU1.0* and *CYP89B19*, are described in Table S 15.

CTAACGCCGAGGCGAGAACAAAGAAAAGCTCGACATGGCCGAGGAGAAGAAGCAGGGCCTGCAGCTGCTGGACTTCTGGGTGAGCCCATTTCGGGCAG
CGTGCCGCATCGCATGATGAGCAGAAAGGGCTGGCTACGAGTACCTGGAGCAGGACCTGGGGAACAAGAGCGAGCTGCTCTCCGCGCAACCCGGT
GCATAAGAAGATCCCGTGCTGCTGCACGACGGCCGCCCTGTCGAGTCCCTCGTCATCGTGCAGTACCTCGACGAGGCGTTCCCGGCGGCGGCGCG
GCGTGCTCCCCCGGACCCCTACGCGCGCGCAGGCCGCTTCTGGGCGGACTACGTCGACAAGAAGCTCTACGACTGCGGCACCCGGCTGTGGAAG
CTCAAGGGGGACGGCCAGGCGCAGGCGCGCGCCGAGATGGTCGAGATCCTCCGCACGCTGGAGGGCGGCTCGGCGACGGGCCCTTCTTCGGCGGCGA
CGCCCTCGGCTTCGTCGACGTCGCGCTCGTGCCCTCACGTCTGGTTCTCGCTACGACCGCTTCGGGCGGCTCAGCGTGGAAGAAGGAGTGCCCGAGG
CTGGCCGCTGGGCCAAGCGCTGCGCCGAGCGCCCCAGCGTGGCCCAAGAACCTCTACCCGCGGAGAGGTCTACGACTTCGTCTGCGGGATGAAGAAG
GTGCGCCAAGAACCTCTACCC
AGGCTGGGCATCGAGTAGAGCATCCATCGGTGCGCGGTGGCTGGCCGGGAGTAATAATGACGAACCAATTATCTAGTTTTGGTTTGAGTGTCTCAGCA
CCGTAGCTCATCTCGTAGG
GAGCAGTTCGTTCATGAGTTCGTGCTGTTGATTTTCTATTGTCAGCGGTGGCAGCGCCGTACGTGTTGCCTCGTACACCACAACCGAATAAGGGGGT
GTTTGGTTTGCCCTCCTAAAAATTTAGCCCTATCAAAAAAAAAAAAAAAAAA

Figure 41: *ZmGSTU1.2* gene sequence with primer positions.

Bold grey text; Forward primer annealing to complementary stand. Bold black text; reverse primer annealing to strand. Replicated sequence shown in grey highlight.

5.2.2.3 *Relative quantification*

The relative expressions of the three GST and three CYP genes, in response to the safeners, metcamifen and benoxacor, are shown in Figure 42 and Figure 43, respectively. The summarised data and statistical analyses are shown in Table S 16. The safener effects on gene induction were analysed with respect to time, tissue and gene. Over the time course, metcamifen induced the transcripts in a parabolic trend, with peak induction at 48 h, though in some cases a biphasic induction pattern was observed with peaks at 3 h and 48 h. In most cases, benoxacor induced transcripts maximally at 3 h, declining steadily with time, though in some cases also causing biphasic induction, with a smaller second peak at 48 h.

In the majority of cases, benoxacor caused a greater induction of genes at 3 h than metcamifen, indicating a faster effect on transcriptional regulation. Metcamifen, however, gave a greater induction than benoxacor at the later time points, indicating a longer lasting effect on gene regulation. This was especially evident in the leaves for GSTs and in the stems for the CYPs. The effect of the safeners also varied between tissues, with metcamifen causing the highest induction of *ZmGSTF2.3*, *ZmGSTL1.3* and *CYP71A5* genes in the leaf, followed by the stem, with the lowest induction seen in the roots. However, *ZmGSTU1*, *CYP81A9* and *CYP81A4* all maintained similar induction rates over all tissues. In contrast, benoxacor caused the greatest induction of genes in the stems, followed by the roots and leaves. Metcamifen generally caused a higher induction than benoxacor in the leaves, except in the case of *ZmGSTU1.2*, where they showed similarly low levels. Metcamifen and benoxacor showed similar induction

levels in the stems and roots, again excluding *ZmGSTU1.2*, where benoxacor caused far higher induction. The effects of the safeners also varied between gene targets. Among the GST genes, metcamifen caused the greatest induction in *ZmGSTL1.3* and *ZmGSTF2.3* with the lowest in *ZmGSTU1.2*. Benoxacor caused a similar degree of induction of the GSTs, save for *ZmGSTF2.3* in the stem which was relatively lower. Among the CYP genes, metcamifen caused a similar degree of induction between genes, though displaying a greater effect on CYP72A5 in the leaf. Benoxacor gave a similar induction of all CYP genes.

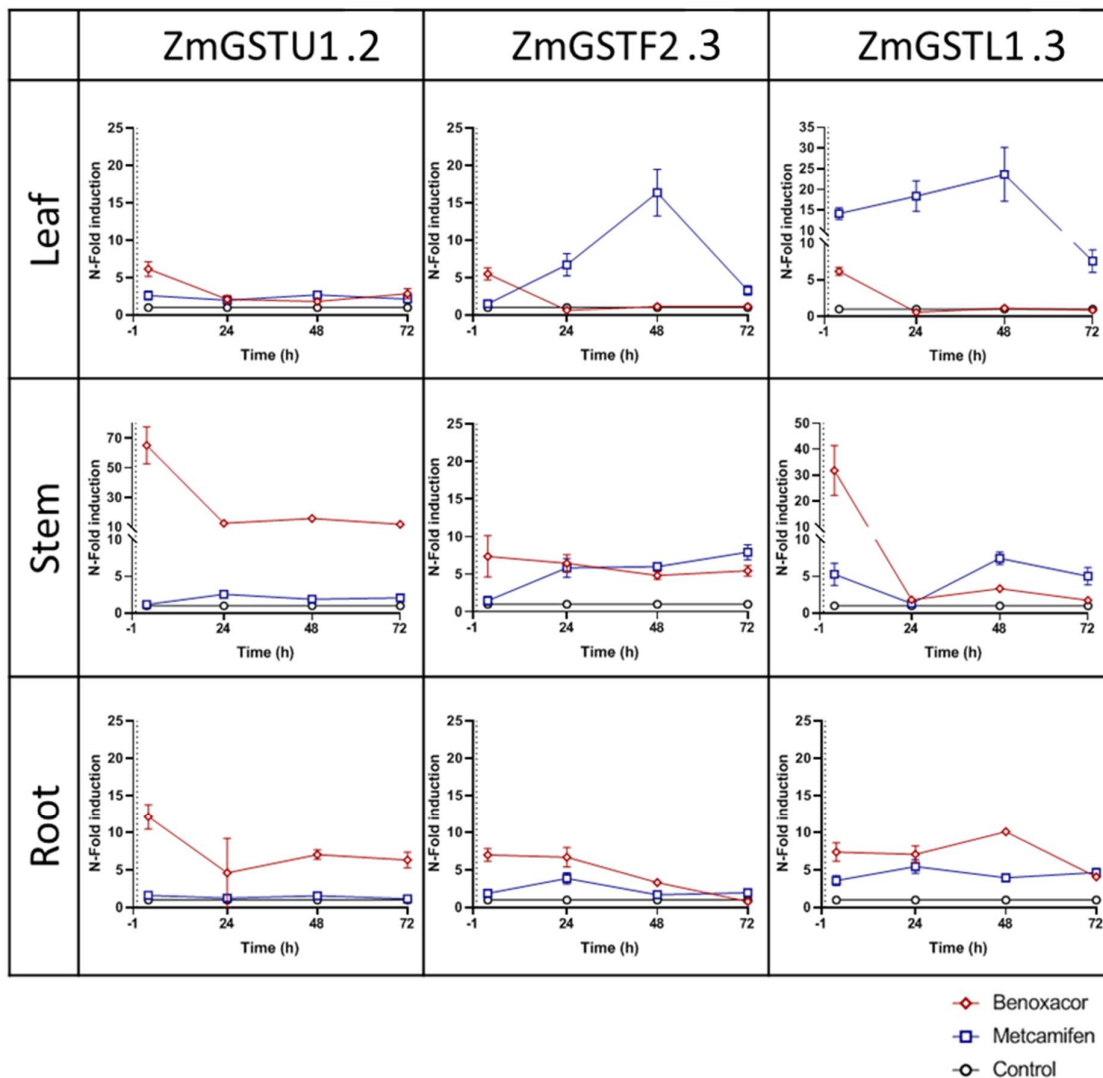


Figure 42: Relative quantification of Glutathione-S-Transferase (GST) enzyme induction with safeners, metcamifen and benoxacor, showing N-fold induction against time (h).

7 day old maize plants were treated for 1 hour (between -1 and 0 hours (dotted line)) with 0.1% (v/v) DMSO containing 25 μ M Safener or no safener control as defined by legend (bottom right). Plants were harvested at 3 h, 24 h, 48 h, and 72 h. Results represent means with standard deviations. 3 biological and 3 technical replicates were used for each data point.

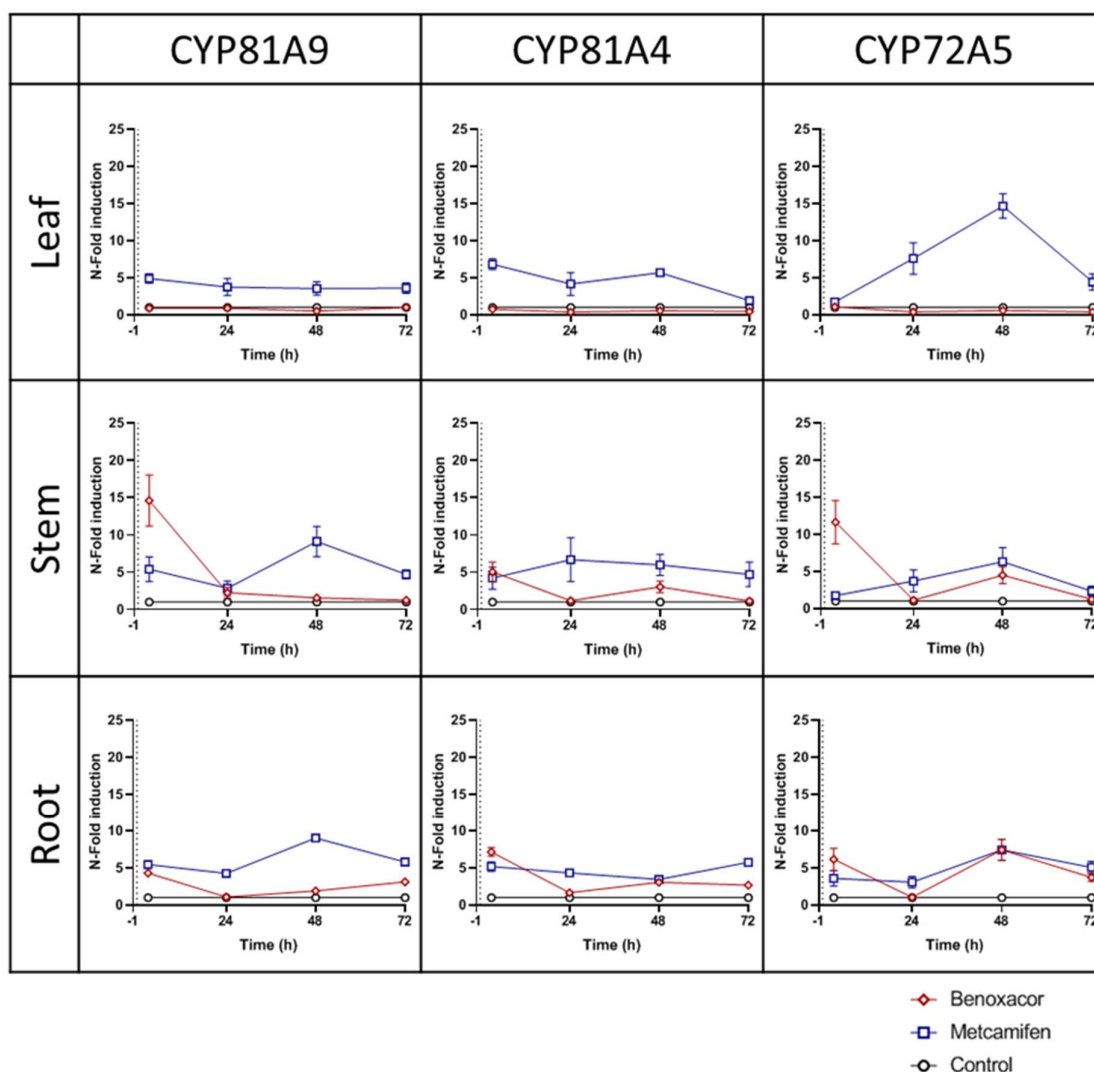


Figure 43: Relative quantification of Cytochrome P450 (CYP) enzyme induction with safeners, metcamifen and benoxacor, showing N-fold induction against time (h).

7 day old maize plants were treated for 1 hour (between -1 and 0 hours (dotted line)) with 0.1% (v/v) DMSO containing 25 μ M Safener or no safener control as defined by legend (bottom right). Plants were harvested at 3 h, 24 h, 48 h, and 72 h. Results represent means with standard deviations. 3 biological and 3 technical replicates were used for each data point.

These results describe the relative induction of genes with safeners, as compared to untreated plants, normalised to a reference gene, and thus do not indicate absolute transcript numbers. While this effectively shows the effects of safeners on gene regulation, it does not provide insight on endogenous gene expression. Understanding the magnitude of each gene's expression would provide a better understanding of their involvement in safening effects. To allow comparisons of endogenous gene expression, the data was converted into quantitative values using gBlocks® (Integrate DNA Technologies). gBlocks® are synthetic, double stranded

DNA fragments ordered to a specific sequence. They are designed to be bound by the primers used in relatively quantified experiments, imitating the cDNA used. As their initial concentration is known, they can be used to create standard curves of Cq against DNA copy number, which can then be used to quantify existing qPCR data. This is useful in comparing expression levels of different genes, which cannot be done with relative quantification. However, absolute quantification has its own limitations. Since the gBlocks® specifically quantify individual genes, the reference gene is not considered, and thus normalisation cannot be performed. As such, experimental variation cannot be controlled. Their accuracy of quantification is also hard to validate. Thus, care should be taken not to over-analyse the data.

5.2.2.4 gBlock® design and validation

Two gBlocks® were designed with three gene fragments on each, in order to limit the size of the gBlocks®. Multiple gene fragments can be used on the same gBlock®, as only one primer pair will be used at a time, and therefore only the desired sequence will be replicated. Since only the replicated part of the gene is needed, the fragments were designed from five bases before, to five bases after, the replicated sequence, to ensure full primer annealing. In addition, 5 bases from the middle of each fragment were removed to alter the size of the PCR product in case size validation was needed. In the case of the CYP81A4 sequence, due to some internal replication, a single base was removed at position 42. Figure 44 and Figure 45 show the design of the gBlocks® for GSTs and CYPs respectively.

```

CCAGCGTCGCCAAGAACCTCTACCCGCCCGAGAAGGTCTACGAC[TTTCGTCTGCGGGATGAAGAAGA]
GGCTGGGCATCGAGTAGAGCATCCATCGG[ACTTGCAGGAGCGGAGCAGAACTAAGTGCAGAGAAC]
AGGACATATGG[CTACG]CCGGCGGTGAAGGTTTACGGGTGGGCTATCTCGCCGTTTCGTATCGCGGGT
GTACATCTGCTACTTCTGCCCCTTCGCTCAGCGCGCCTGGGTCACCAGGAACTTGAAGGGTTTGCAG
GACAAGATGGAGCTGGTGGCCATCGATCTGCAGGACAAACCGGCTTGGTACAAGGACAAGGTTTAC
GCACAGGGCACG

```

Legend: ZmGSTU1.2, ZmGSTF2.3, ZmGSTL1.3, Primer position, removed, Final length: 327bp

Figure 44: gBlock® design for Glutathione-S-Transferase (GST) quantitative/real time polymerase chain reaction (qPCR) quantification.

Full sequence of gBlock® DNA used to quantify GST qPCR data. The legend below the sequence identifies sequence origins, primer positions, internal sequences removed and final base length in bp.

CCATGCTATGCTTGGCGTCCTCAAGGGACTGTGAGCGCCATGCTATGCCTTGATACATAAGTAAGCT
 TTTTCTTTAGTAAAGCAGTCATCTTGCCTCTCAAGCAGTTGCTTGCTTTATTGCTTGAAACTCACTTT
 CTCCTGGAGTGTAGCCGCCGCA TGAAGGGTGTATGACGTAGCTCCGAGTTCCGAGCATATATATT
 CACTTGCCTTGTACTAGTTGATTTTCGCCGAGTGTATGGAATGGATTTTGATAAACTGCACCCTCA
 ACATGGTGCTCAGATAAGGCTCAAAAAGCTTCTCCGTGATGCTCCTTCTATGCTGCTACCGGACACT
 ACTTTCG

Legend: CYP81A4, CYP81A9, CYP72A5, Primer position, removed, Final Length: 331bp

Figure 45: gBlock® design for Cytochrome P450 (CYP) quantitative/real time polymerase chain reaction (qPCR) quantification.

Full sequence of gBlock® DNA used to quantify CYP qPCR data. The legend below the sequence identifies sequence origins, primer positions, internal sequences removed and final base length in bp.

The standard curves are shown in Figure 46 using logarithmic X-axes, since the relationship between Cq and DNA copy number is logarithmic (Svec et al., 2015). Each standard curve presented a uniform linear trend ($R^2 > 0.99$), indicating a successful quantitation of the intended sequences.

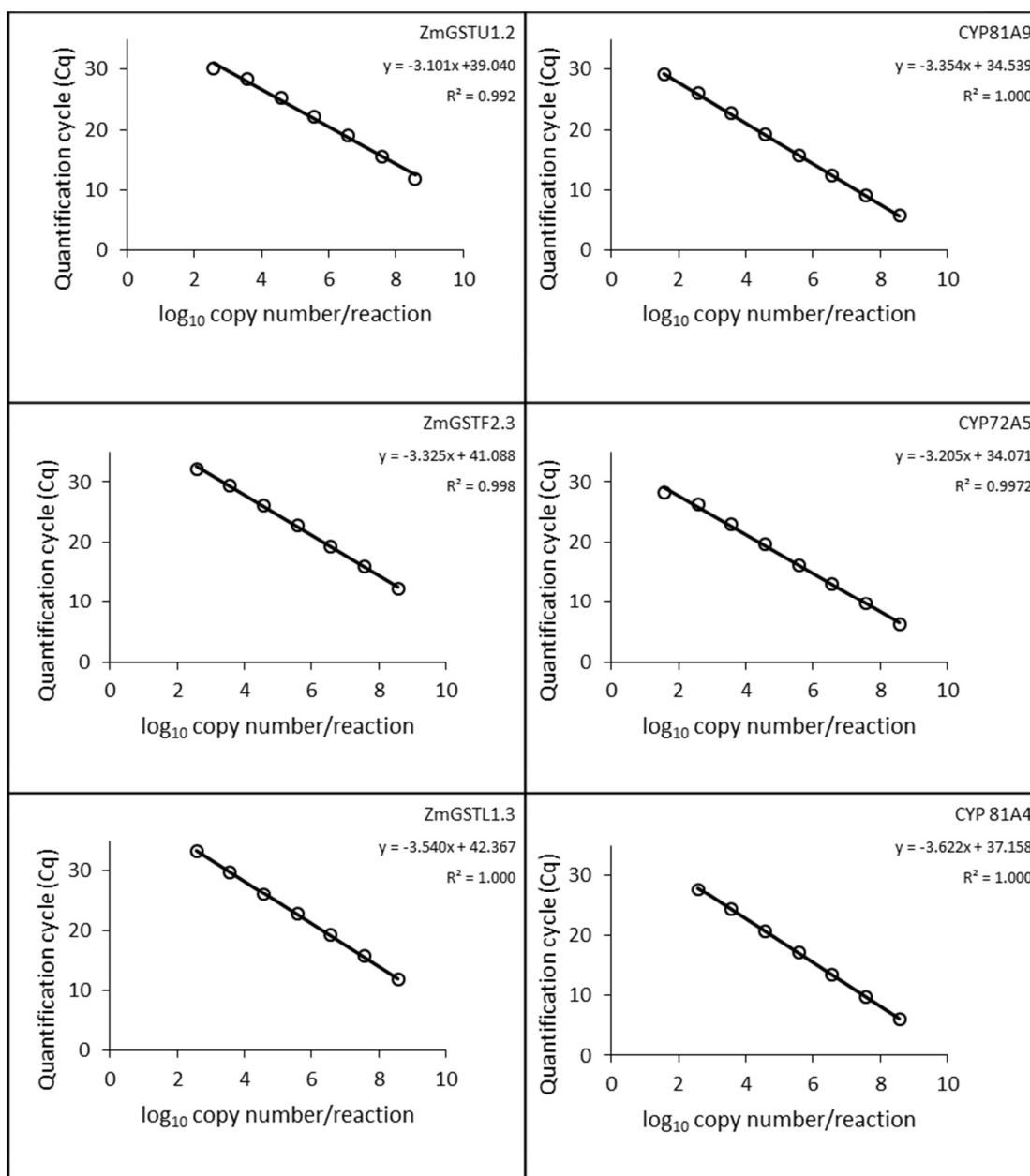


Figure 46: gBlock® standard curves showing relationship between \log_{10} complementary DNA (cDNA) copy number per reaction and quantification cycle (Cq).

Gene titles, trendline equations and coefficients of determination (R^2) are shown (top right) in each box. Linear trendlines are shown as black lines.

5.2.2.5 Absolute quantification

Using the gBlock® standard curves, the Cq values generated from the control groups of the relative quantification (section 5.2.2.3) were converted into DNA copy number/reaction, and replotted as absolute quantification (Figure 47). The endogenous expression of the six genes were analysed with respect to time, tissue, and gene. Summarised data is shown in Table S 17.

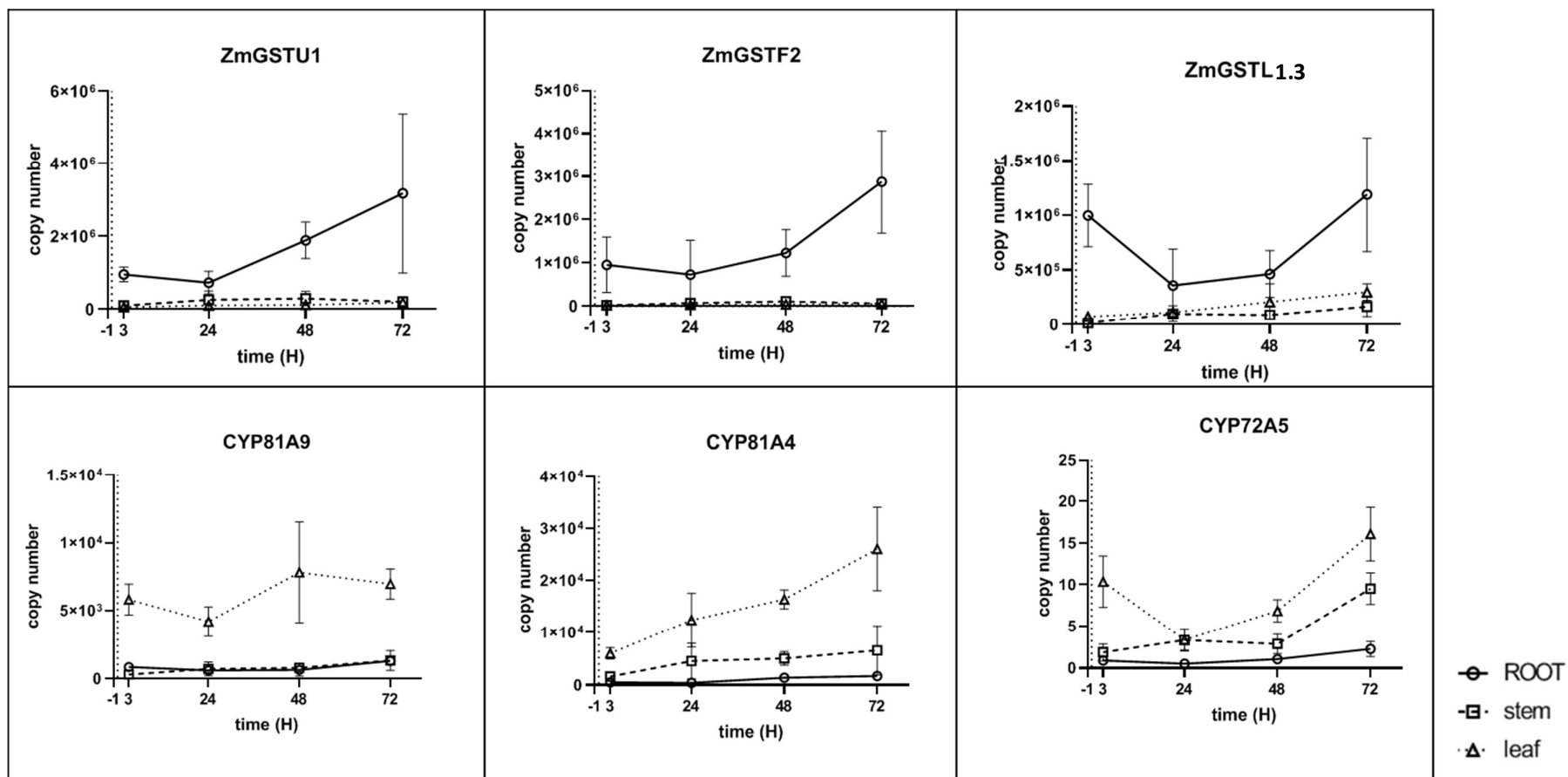


Figure 47: Absolute quantification of endogenous gene transcription showing complementary DNA (cDNA) copy numbers against time (h). 7 day old controls plants were treated for 1 hour (between -1 and 0 hours (dotted line)) with 0.1% (v/v) DMSO. Plants were harvested at 3 h, 24 h, 48 h, and 72 h. Results represent means with standard deviations. 3 biological and 3 technical replicates were used for each data point. Legend (bottom right) describes tissue.

The endogenous expression of the GST enzymes was greatest in the roots in all cases, with the stem and leaf displaying little expression. The CYPs, however, display the opposite trend, with the highest endogenous expression in the leaves. Again the expression in the other tissues was lower, though CYP81A4 and CYP72A5 were expressed notably more in the stem than the root. The expression of the GSTs generally increased over time in the root, with little change in the stem and leaf tissues. One exception was seen in *ZmGSTL1.3*, which increased in expression over time in the stem and leaf, but showed an inverse parabolic trend in the root. The expression of the CYPs in the leaf showed a net increase, with biphasic, linear or inverse parabolic trends for CYP81A9, CYP81A4 and CYP72A5, respectively. The expression of CYPs in the other tissues showed a more gradual linear increase over time.

All GSTs, in all tissues expressed at least 50,000 transcript copies per reaction at their maxima, while the CYPs showed less expression. CYP81A9 expressed at least 1,000 transcripts per reaction in all tissues, while CYP81A4 expressed at least 1,500 transcripts per reaction and CYP72A5 expressed only 2 transcripts per reaction.

5.2.3 *Effect of safeners on the expression of GST proteins in maize plants*

As mentioned in section 4.2.10, transcript induction may not be mirrored exactly by protein expression. Thus the effects of each Safener on the expression of GST proteins was also determined. Proteomic analyses have the benefit of being able to predict changes to enzyme activity and metabolism with fewer assumptions than transcriptomic analyses, since differences in mRNA translation efficiency can be disregarded. However, proteomics by western blot requires the cloning, expression and purification of recombinant proteins for validation, which is more time consuming, expensive, and often problematic than designing simple primers required for transcript analysis by qPCR. Therefore, if the transcript analysis of GST expression accurately reflected the protein analysis, this would allow rapid, inexpensive and simple qPCR to be used in place of western blotting. To determine if the observed effect of safeners on GST transcript induction would translate into effects on GST protein induction, western blot analysis was carried out on hydroponically grown maize plants, treated with metcamifen and benoxacor, over the course of a week. Plants were treated with Safener for 1 hour, then harvested 0 hours, 1 day, 3 days, 5 days and 7 days after. Proteins containing the subunits of *ZmGSTF2.3* (previously *ZmGSTF2/GSTIV*) and *ZmGSTU1.2* (previously *ZmGSTU1/GST V*), were analysed, in order to compare with the transcript expression analysis (section 5.2.2.3). *ZmGSTF2.0* (previously *ZmGSTF1/GST I*) was also included as a non-inducible

GST, known to dimerise with *ZmGST2.3*. In order to quantify the western blot data, purified versions of these proteins were required for comparison. Recombinant *ZmGSTF2.0*, *ZmGSTF2.3* and *ZmGSTU1.2* were expressed in *Escherichia coli*, and purified for this purpose. In addition, the GSH conjugating activity of these proteins were investigated by assays with 1-chloro-2,4-dinitrobenzene (CDNB), and compared in order to validate their function.

5.2.3.1 Cloning, expression and purification of recombinant GST proteins

Plasmids designed to express the proteins *ZmGSTU1.2* and *ZmGSTF2.0* were previously generated in our research group (Dixon, 1998; Dixon et al., 1998a), and the resultant protein sequences are shown in Figure 48 and Figure 49 respectively. Since no plasmid was available for *ZmGSTF2.3*, an insert sequence was designed and cloned into the pET-Strp3 expression vector (Figure S 9). The insert sequence and resultant protein sequence are shown in Figure 50, a and b, respectively. The *ZmGSTF2.3* insert sequence was confirmed by sequencing.

MAEEKKQGLQLLDFWVSPFGQRCRIAMDEKGLAYEYLEQDLGNKSELLLRANPVHKKIPVLLHGRPVCESLVIVQYLDEAFPAAPALLPADP
YARAQARFWADYVDKKLYDCGTRLWKLKGDGQAQARAEMVEILRTLEGALDGPFFGGDALGFVDVALVPFTSWFLAYDRFGGVSVEKECP
RLAAWAKRCAERPSVAKNLYPPEKVYDFVCGMKKRLGIE

Figure 48: *ZmGSTU1.2* protein sequence.

MAPMKLYGAVMSWNLTRCATALEEAGSDYEIVPINFATAEHKSPEHLVRNPFQVQVPALQDGDLYLFESRAICKYAARKNKPELLREGNLEEAA
MVDVWIEVEANQYTAALNPILFQVLISPMLGTTDQKVVDENLEKLVLEVYEARLTCKYLAGDFLSLADLNHVSVTLCFLATPYASVLDAYP
HVKAWWSGLMERPSVQKVAALMKPSA

Figure 49: *ZmGSTF2.0* protein sequence.

- a. AGGCTTAATTAACCATATGGCGACTCCAGCAGTGAAGGTTACGGTTGGGCTATCTACCATTGTTCTCGCGCATTACTGGCCC
TTGAGGAGGCGGGAGTGGACTACGAATTAGTACCGATGTCTCGTCAAGATGGCGATCATCGCCGTCCGAGCACCTGGCTCGCA
ATCCATTGGAAAAGTCCCCGTGCTGGAGGATGGCGACCTTACGTTATTGCAATCTCGCGCTATTGCTCGCCATGTACTTCGCAAG
CACAAGCCTGAATTATTGGGGGGTGGTCGTCTGGAACAGACTGCCATGGTGGATGTCTGGTTGGAGGTGGAGGCACACCAACTT
AGTCCTCCTGCTATTGCAATTGTTGTAGAGTGTGTGTTGCGCCTTCTTAGGCCCGCAACGCAATCAGGCAGTGGTAGACGAGA
ACGTAGAGAAGCTTAAAAAGGTACTGGAAGTCTACGAGGCTCGTCTGGCTACTTGTACTTATTAGCGGGTGATTCTTAAGCTTA
GCTGACTTGTCTCCGTTACCATATGCATTGCTTAATGGCAACCGAGTACGCAGCCTTGGTACACGCACTGCCTCACGTATCTGCG
TGGTGGCAAGGATTAGCGGCACGCCCGCGCTAATAAGGTGGCGCAATTTATGCCCGTAGGGGCGGGGGCTCTAAAGAACA
GAATAGGTCGACCTGCAGGCCA
- b. MATPAVKVYGWAISPFVSRALLALEEAGVDYELVPMRQDGDHRRPEHLARNPFGKVPVLEDGDLTLFESRAIARHVLKHKPELLGG
GRLEQTAMVDVWLEVEAHQLSPPAIAIVVECVFAPFLGRERNQAVVDENVEKLVLEVYEARLATCTYLAGDFLSLADLSPFTIMHCL
MATEYAALVHALPHVSAWWQGLAARPAANKVAQFMPVGAGAPKEQE

Figure 50: a; *ZmGSTF2.3* DNA insert sequence. b; *ZmGSTF2.3* protein sequence.

Regions are defined by formatting as follows; Partial Strep tag vector Nde1 restriction site
insert sequence stop codon Sal1 restriction site

The recombinant proteins were expressed in Tunetta *E. coli* cells, using Isopropyl β -D-1-thiogalactopyranoside (IPTG) as an induction agent (Dixon et al., 2009). Purification of the expressed proteins was performed using an affinity column, which binds the strep II-tag (WSHPQFEKG) added to each sequence by the expression vector (Dixon et al., 2009). Purification spectra, and protein concentration profiles are shown for *ZmGSTU1.2*, *ZmGSTF2.0* and *ZmGSTF2.3* in Figure 51, Figure 52, and Figure 53, respectively.

Due to the low yield obtained for *ZmGSTF2.3*, the purification step was performed twice, and thus both purification steps are shown in Figure 53, 1 and 2. The large peak at 0-10 mL, and the double peak at 0-20 mL in Figure 53, a2, reflects the loading phase, where the protein is applied to the column. The peak after 12 mL, or after 25 mL in Figure 53, a2, reflects the elution phase, where the purified protein is eluted after column washing. These elution peaks correspond closely with the protein concentration of each fraction. Aberrant peaks such as those seen at 21mL in Figure 51, a, correspond to air bubbles passing the UV sensor, and can be disregarded.

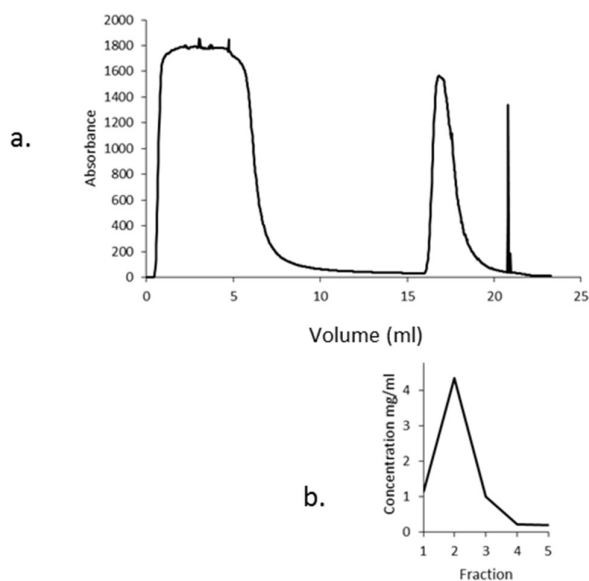


Figure 51: a; Ultraviolet (UV) spectrum displaying purification of *ZmGSTU1.2* recombinant protein showing absorbance against volume eluted (mL). b; Concentration (mg mL⁻¹) of *ZmGSTU1.2* recombinant protein in purified fractions.

The fractions are aligned with their elution volume.

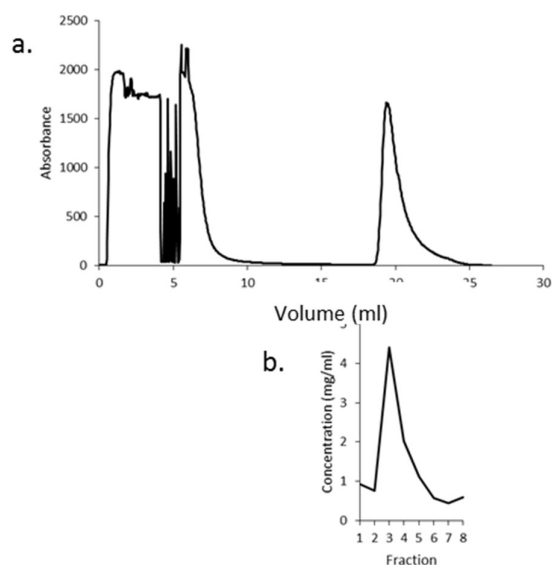


Figure 52: a; Ultraviolet (UV) spectrum displaying purification of *ZmGSTF2.0* recombinant protein showing absorbance against volume eluted (mL). b; Concentration (mg mL⁻¹) of *ZmGSTF2.0* recombinant protein in purified fractions.

The fractions are aligned with their elution volume.

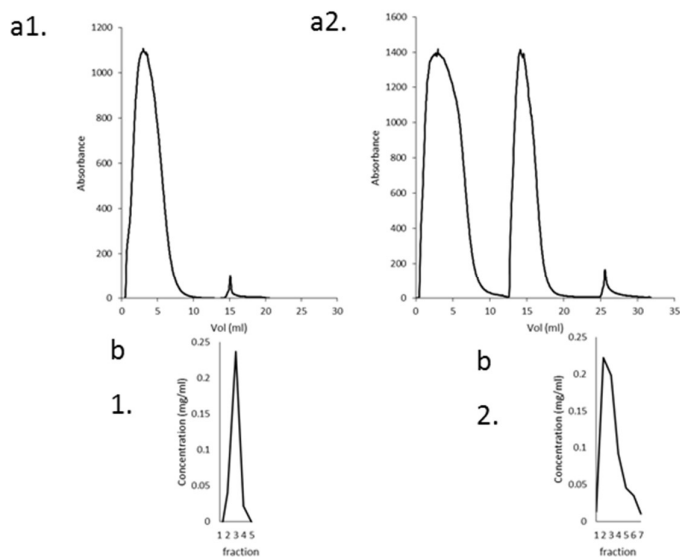


Figure 53: a; Ultraviolet (UV) spectra displaying purification of *ZmGSTF2.3* recombinant protein showing absorbance against volume eluted (mL). b; Concentrations (mg mL⁻¹) of *ZmGSTF2.3* recombinant protein in purified fractions.

The fractions are aligned with their elution volume. 1 and 2 refer to individual purifications.

The purified recombinant proteins were quantified by UV spectrophotometry using molecular mass and extinction coefficient predictions, shown in Table 25.

Protein	Molecular mass (g mol ⁻¹)	Extinction coefficient (M ⁻¹ cm ⁻¹)
ZmGSTF2.0	25685.813	39970
ZmGSTF2.3	26434.52	35012.5
ZmGSTU1.2	26983.295	45660

Table 25: Properties of recombinant proteins.

Molecular mass and extinction coefficients are shown for strepII-tagged proteins. Molecular mass and extinction coefficient predictions were generated by ExPASy software (Table 9).

To verify and characterise the glutathione conjugating activity of the recombinant proteins, GST assays were performed with 1-chloro-2,4-dinitrobenzene (CDNB) (Figure 54). The results indicated that all recombinant proteins possess statistically significant GST activity, with ZmGSTF2.0 displaying the most activity of 3323.0±76.1 nkat mg⁻¹. Previous reports have demonstrated activities of 1693 nkat mg⁻¹ and 775 nkat mg⁻¹ (Table 16). ZmGSTU1.2 displayed the next highest activity 439.8±15.5 nkat mg⁻¹. Previous reports have indicated an activity of 216 nkat mg⁻¹, 66 nkat mg⁻¹, and 90.7 nkat mg⁻¹ (Table 16). ZmGSTF2.3 possessed the least activity of 27.3±4.9 nkat mg⁻¹, GST activity. Previous reports have indicated an activity of 0.25 nkat mg⁻¹ (Table 16). Despite the wide variation of these results in the literature, likely due to differences in assay procedure or purification efficiency, the recombinant proteins in this study showed greater activity than in the literature, indicating efficient GST activity.

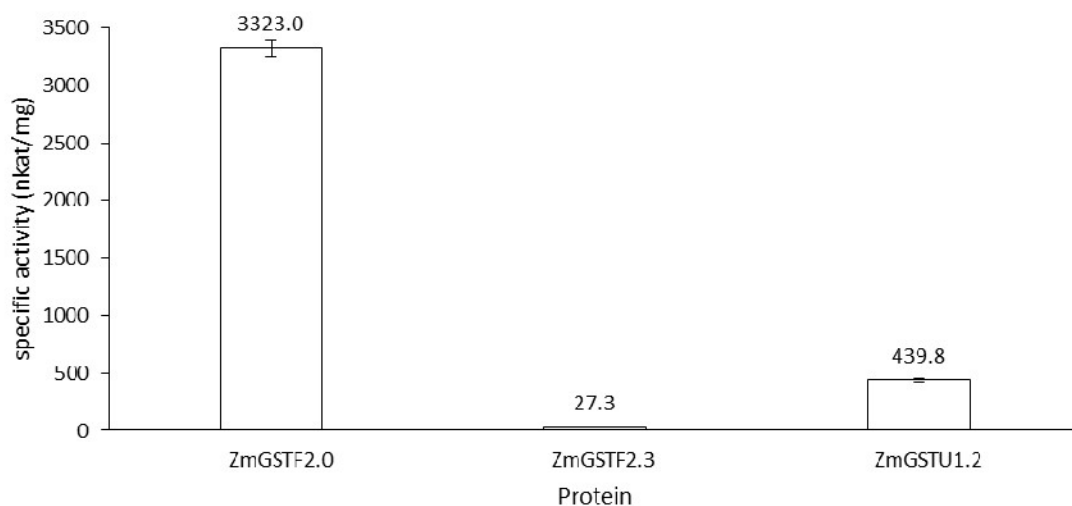


Figure 54: Recombinant protein activity towards 1-chloro-2,4-dinitrobenzene (CDNB) (nkat mg⁻¹).

Results represent means with standard deviation (n = 3). Data labels indicate means.

5.2.3.2 Antibodies

Antibodies, generated in our research group, were tested with the recombinant proteins, to determine their specificity for use in quantification of the western blot analysis. An antibody

raised to the homodimer of a wheat GST, *TaGSTU1-1*, was shown to cross react with *ZmGSTU1.2* recombinant protein (Cummins et al., 1997) (Figure 55). Single bands were observed for the recombinant *ZmGSTU1.2* and in plant samples, at 26 kDa, close to the expected mass of 27.0 kDa. Since only one band was recognised, the protein recognised by this antibody in plant material will herein be referred to as *ZmGSTU1.2-1.2*

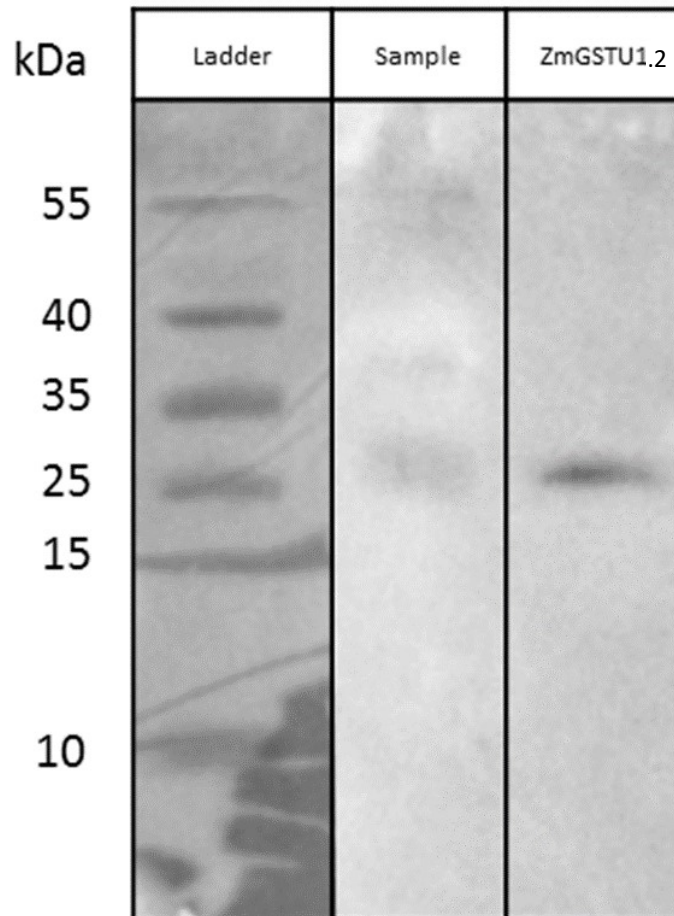


Figure 55: Western blot showing cross reactivity of *TaGSTU1-1* antibody with recombinant *ZmGSTU1.2* protein and crude protein from leaves of untreated maize plants (sample). Molecular weights of ladder markers are shown (left) (kDa). All protein is applied at 5 ng.

The antibody raised to the heterodimer *ZmGSTF2.0-2.3*, was shown to react with both *ZmGSTF2.0* and *ZmGSTF2.3* recombinant proteins (Figure 56) (Dixon et al., 1998a). *ZmGSTF2.0* displayed a mass of 25 kDa, close to the expected 25.7 kDa, while *ZmGSTF2.3* displayed a mass of 26 kDa, close to the expected 26.4 kDa. The maize tissue sample displayed a broader band spanning both these masses, indicating the presence of both proteins. A range of SDS-PAGE gels were used to try to resolve these bands (data not shown) without success. Therefore, the protein recognised in plant material will herein be referred to as *ZmGSTF2.0-2.3*.

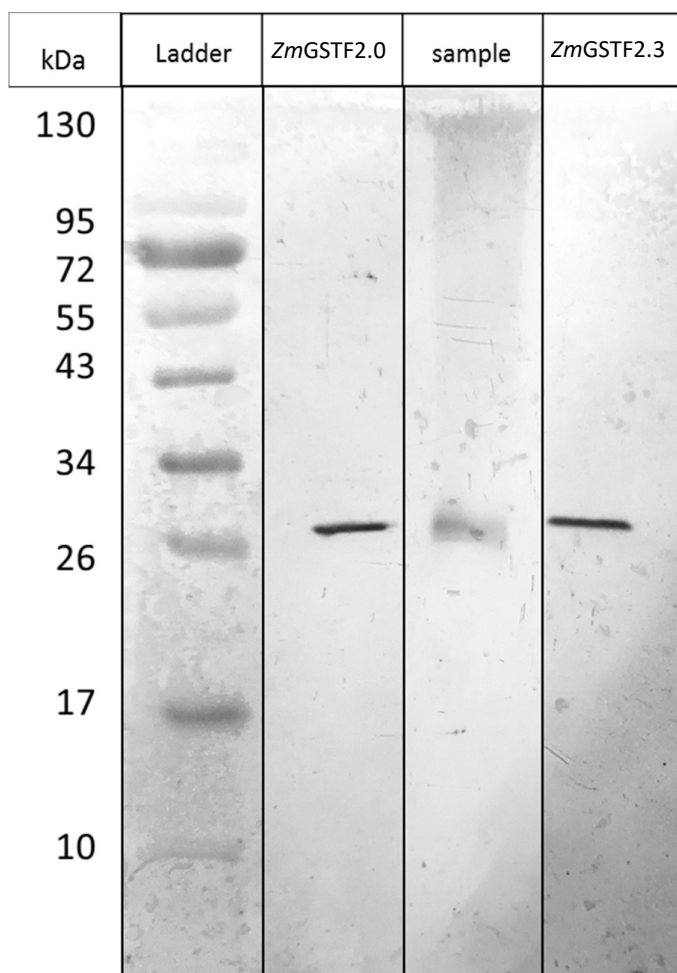


Figure 56: Western Blot showing cross reactivity of *ZmGSTF2.0-2.3* antibody with recombinant *ZmGSTF2.0* and *ZmGSTF2.3* proteins and crude protein from stems of metcamifen (25 μ M) treated maize plants (sample).

Molecular weights of ladder markers are shown (left) (kDa). All protein is applied at 10 ng.

To validate their use as western blot quantification markers, dilution curves of the recombinant proteins were analysed. This would also establish the range of effective quantification. Since *ZmGSTF2.0* and *ZmGSTF2.3* subunits could not be resolved, only *ZmGSTF2.0* was used as a recombinant protein marker. The data is shown in Figure 57 and Figure 58 for the *ZmGSTU1.2* and *ZmGSTF2.0* proteins, respectively. Single bands were observed for both *ZmGSTF2.0* and *ZmGSTU1.2* (Figure 57.a and Figure 58.a) indicating purity of recombinant protein sample. The dilution curves (Figure 57.b-c and Figure 58.b-c) showed a high linearity in the ranges of 1.25 ng to 20 ng for *ZmGSTU1.2* and 0.6125 ng to 10 ng for *ZmGSTF2.0*, both displaying coefficients of determination (R^2) over 0.99. Thus the recombinant proteins were considered appropriate for use as western blot quantification markers within these specified ranges.

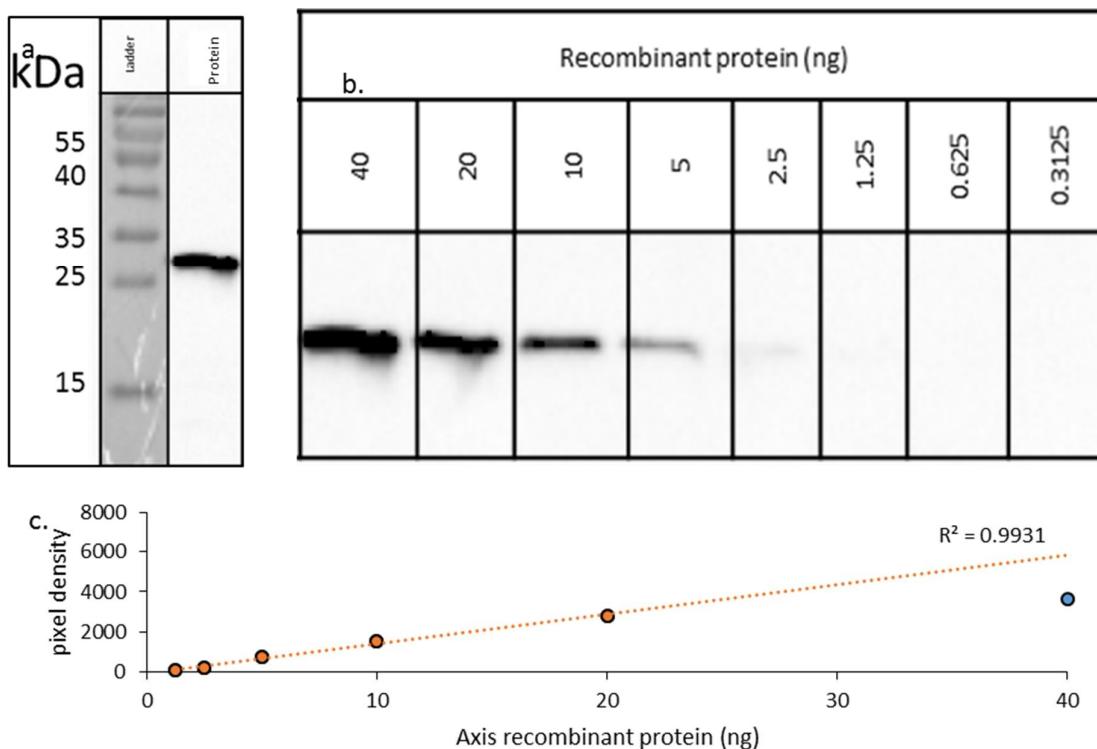


Figure 57: a; Western blot of *TaGSTU1-1* antibody with 40 ng *ZmGSTU1.2* recombinant protein. Molecular weight ladder shows mass of markers (kDa). b; western blot of dilution curve of *TaGSTU1-1* antibody with *ZmGSTU1.2* recombinant protein. c; Graph of data in b, showing density of western blot bands against amount of recombinant proteins (ng). Orange markers indicate protein amounts within the range of effective quantification. Blue markers indicate protein amounts outside the range of effective quantification. The dotted line represents a linear trendline for the orange markers, with associated R^2 .

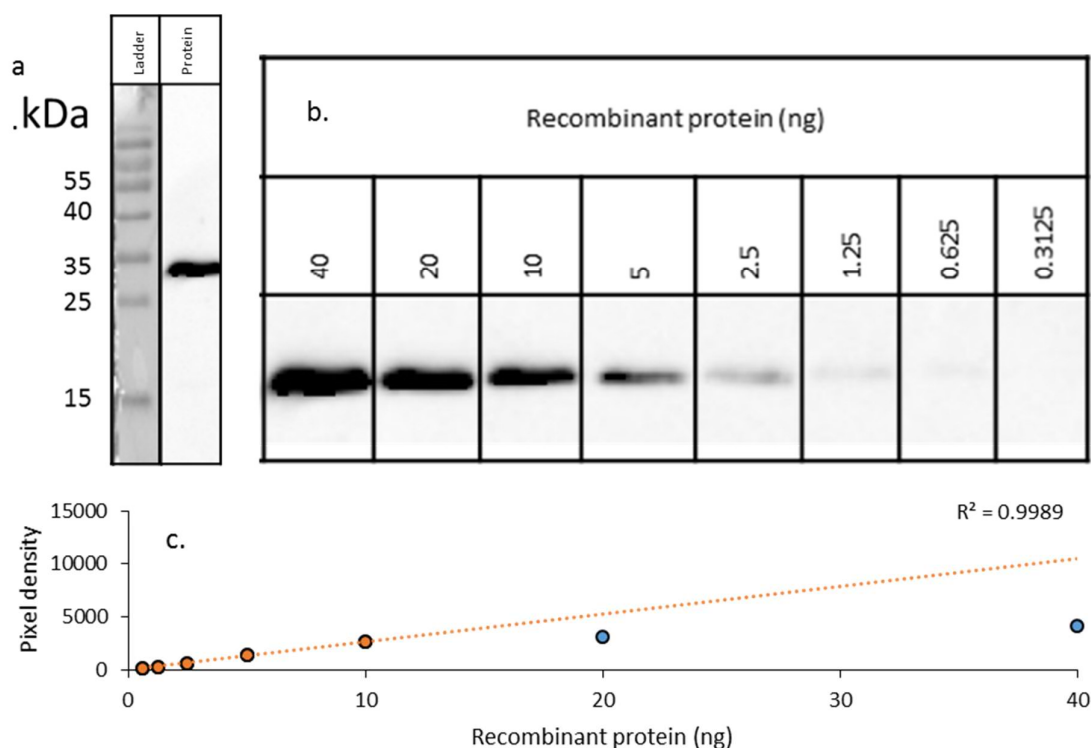


Figure 58: a; Western blot of *ZmGSTF2.0-2.3* antibody with 40 ng *ZmGSTF2.0* recombinant protein. Molecular weight ladder shows mass of markers (kDa). b; Western blot of dilution curve of *ZmGSTF2.0-2.3* antibody with *ZmGSTF2.0* recombinant protein. c; Graph of data in b, showing density of western blot bands against amount of recombinant proteins (ng).

Orange markers indicate protein amounts within the range of effective quantification. Blue markers indicate protein amounts outside the range of effective quantification. The dotted line represents a linear trendline for the orange markers, with associated R^2 .

5.2.3.3 Absolute quantification

The results of the absolute quantification are shown in Figure 59. In the leaf tissue, the safeners caused little change to the content of *ZmGSTF2.0-2.3* or *ZmGSTU1.2-1.2*. The most substantial effect was seen with benoxacor at 0 hours, reaching 0.045% of total protein content, indicating a very rapid enhancement of induction. Benoxacor caused slightly greater enhancement of *ZmGSTF2.0-2.3* content than metcamifen over the first 72 hours. In the stem much larger effects were seen. The safeners enhanced the generation of *ZmGSTF2.0-2.3* considerably, with benoxacor causing the greatest stimulation. Benoxacor also caused an induction effect at 0 hours, unlike metcamifen, indicating a more rapid effect. After 7 days, the effects of both safeners were very similar, with approximately 0.05% protein content. This suggests the safener effects had not terminated within one week, though the safener-specificity had. Similarly, both safeners caused a parabolic increased production of *ZmGSTU1.2-1.2* in the stem tissues, with the greatest effect caused by benoxacor. With both

safeners the effect was low at 0 and 7 days, indicating a transient effect. The effect of the safeners was remarkably similar with the different proteins, except for the slightly lessened effect of metcamifen on *ZmGSTU1.2-1.2* compared to *ZmGSTF2.0-2.3* in the stem.

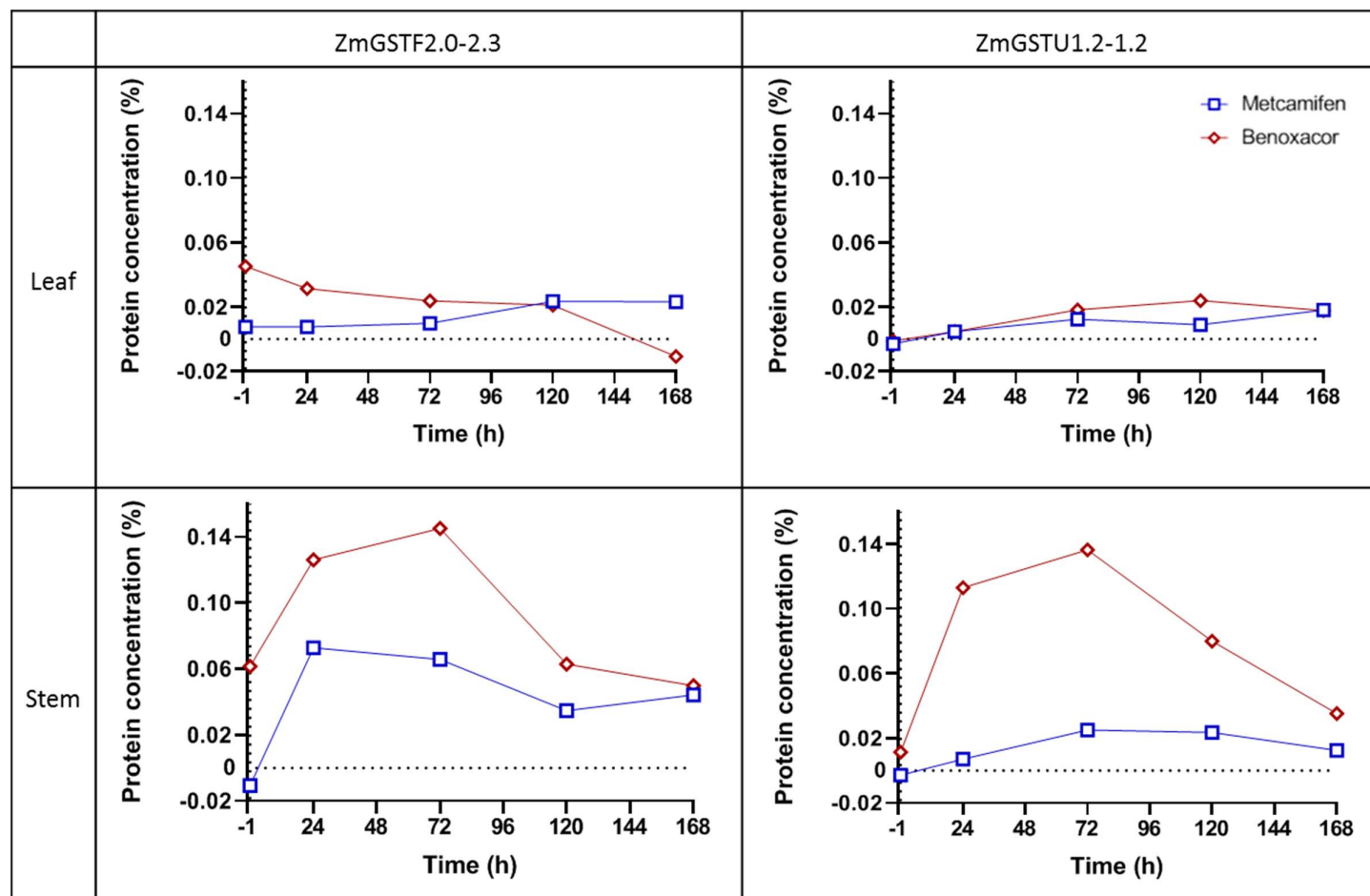


Figure 59: Expression of Glutathione-S-Transferase (GST) proteins in leaf and stem tissues, plotted as percentage of total protein (after normalisation to control) against time (h).

7 day old maize plants treated for 1 hour (between -1 and 0 hours (dotted line)) with 0.1% (v/v) DMSO containing 25 μ M Safener or no Safener control as defined by legend (top right). Plants were harvested at 0 h, 1 d, 3 d, 5 d and 7 d. Sample number (n) = 1.

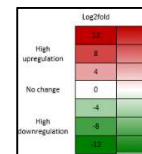
5.2.4 *Effect of abiotic stress on maize GST transcripts*

In order to understand the signalling pathways involved in safener effects, the relationship between safener and abiotic stress responses was analysed. The effects of seven stresses on maize GST expression were investigated using Genevestigator software (section 2.2), and compared with the next generation sequencing (NGS) analysis (section 5.2.1). Table 26 details the effect of various abiotic stresses on GST expression, specifically; cold, dehydration, drought, simulated drought, heat, submergence and 12-OPDA (a jasmonate growth regulator). The regulation of only the tau, lambda and phi class GSTs were altered considerably ($\log_2 > 1.5$, $\log_2 < -1.5$). Submergence and 12-OPDA caused the greatest number of genes to be upregulated or downregulated ($\log_2 > 1.5$, $\log_2 < -1.5$). Interestingly, these stresses caused similar induction profiles with each other and both safeners (Table 26 includes safener NGS data for comparison). A Pearsons correlation was performed on the \log_2 data of the abiotic stresses and 90 minute safener effects, in order to accurately determine the co-expression caused by certain treatments (Table 27). The data indicated a positive and statistically significant correlation between the effects of metcamifen and benoxacor on the GSTs at 90 min ($r = 0.9719$, $p = 0.0000$). Submergence and 12-OPDA possessed the highest degree of correlation with the safeners ($r = 0.5$, $p < 0.0003$), in which the correlation was positive. The data also indicated a slightly lower, yet significant, positive correlation between the safeners, metcamifen and benoxacor, and cold stress ($r = 0.4454$, $p = 0.0007$, and $r = 0.4324$, $p = 0.0011$, respectively). The data also indicated a significant correlation between the safeners, metcamifen and benoxacor, and drought ($r = -0.3451$, $p = 0.0106$, and $r = -0.3858$, $p = 0.0040$, respectively), though less significant, and negatively correlated. Dehydration, heat and simulated drought showed no significant correlation with the safeners ($p > 0.05$).

Class	Name	Gene accession	Cold	Dehyd- ration	Drought	Heat	Simulate drought	Submer- gence	12-OPDA	Metcamifen			Benoxacor		
										30 min	90 min	240 min	30 min	90 min	240 min
Zeta	ZmGSTZ1.0	GRMZM2G064255	0.16	0.74	0.32	-0.39	1.05	0.83	-0.03	0.26	-0.01	0.48	0.10	0.06	0.16
	ZmGSTZ1.1	GRMZM2G124974	-0.50	0.22	0.36	-0.46	0.04	0.09	-0.08	0.16	-0.11	0.14	0.11	-0.11	0.33
	ZmGSTZ1.2	GRMZM2G019090	0.02	-0.36	-0.39	-0.17	-0.48	1.26	-0.56	0.12	0.55	0.93	0.15	0.50	0.82
Theta	ZmGSTT1.0	GRMZM2G077183	0.12	0.97	0.04	0.07	1.06	0.95	0.40	0.08	-0.05	0.21	-0.07	-0.04	0.21
		GRMZM2G122488	0.12	0.97	0.04	0.07	1.06	0.95	0.40	0.20	0.04	1.12	0.04	0.04	0.65
Phi	ZmGSTF1.0	GRMZM2G146246	0.35	0.05	0.18	-1.39	0.50	0.59	0.00	0.04	0.03	0.37	0.06	-0.08	0.35
	ZmGSTF1.1														
	ZmGSTF1.2														
	ZmGSTF2.0	GRMZM2G116273	-0.10	-0.10	-0.45	1.06	-0.40	0.27	2.21	0.25	0.69	1.03	0.38	0.73	0.75
	ZmGSTF2.1	GRMZM2G156877	0.27	-0.12	-0.78	0.00	-0.31	6.00	1.85	0.82	1.63	2.03	0.75	1.43	1.77
	ZmGSTF2.2	GRMZM2G150474	-0.33	0.54	-1.11	0.14	0.11	4.72	2.49	0.42	0.66	1.20	0.52	0.96	1.16
	ZmGSTF2.3	GRMZM2G132093	0.47	0.01	-0.52	1.50	-0.35	6.55	4.00	1.49	3.30	3.66	1.78	3.30	3.66
	ZmGSTF3.0	GRMZM2G096153	-0.29	-0.96	0.33	-2.38	-0.17	0.05	-0.92	0.18	-0.42	-0.10	0.35	-0.15	-0.01
	ZmGSTF3.1														
	ZmGSTF4.0	GRMZM5G895383	-1.30	0.10	-0.18	-1.51	-0.18	-0.48	-0.14	-0.03	1.64	-0.20	-0.34	1.64	0.24
	ZmGSTF4.1	GRMZM2G119499	-0.72	0.08	-0.08	-2.33	-0.33	-1.25	-0.05	-0.14	-8.27	-0.29	-6.75	-8.27	-7.17
	ZmGSTF4.2														
	ZmGSTF4.3	GRMZM2G096269	-0.78	0.00	-0.29	-1.81	0.19	-0.98	0.00	0.00	0.00	4.14	0.00	0.00	0.00
	ZmGSTF4.4	GRMZM2G126781	-0.62	0.00	-0.05	-4.07	-0.71	-0.89	0.00	0.11	0.19	-0.19	-0.07	0.16	-0.14
	ZmGSTF4.5	GRMZM2G126763	-0.17	0.03	-0.15	-2.85	-0.02	-0.99	1.05	0.50	0.35	-0.56	0.35	0.50	-0.56
	ZmGSTF4.6	GRMZM2G096247	-0.55	0.53	-0.44	-3.11	0.37	-0.80	0.00	0.52	-2.94	-2.94	-2.94	0.00	-2.94
GHR	ZmGHR1.0	GRMZM2G102216	0.10	-0.37	0.05	-0.05	0.35	-0.59	-0.83	-0.05	-0.27	-0.09	0.00	-0.35	0.10
DHAR	DHAR 4	GRMZM2G005710	-0.29	-0.04	0.01	-0.66	0.36	-0.16	-0.17	-0.54	-0.08	1.12	-0.37	0.00	1.10
	DHAR 3	GRMZM5G855672	-0.15	-0.31	0.30	0.36	0.84	-0.08	-0.29	0.07	0.01	0.07	0.09	0.01	0.22
Lambda	ZmGSTL1.0	GRMZM2G162486	1.02	1.10	0.33	-0.14	0.30	3.67	1.01	0.20	0.76	1.32	0.48	1.58	2.78
	ZmGSTL1.1	GRMZM2G338131	0.63	2.01	0.54	-0.63	1.56	0.63	1.22	-2.12	2.12	2.12	-2.12	0.00	0.00
	ZmGSTL1.2	GRMZM2G043291	0.63	2.01	0.54	-0.63	1.56	0.63	1.22	2.15	2.75	2.29	3.51	4.15	3.30
	ZmGSTL1.3	GRMZM2G042639	1.29	1.42	0.58	0.92	1.13	4.95	2.48	1.29	3.21	5.13	1.80	3.46	3.58
	ZmGSTU1.0	GRMZM2G129357	-0.57	0.44	0.47	-1.83	0.04	2.74	3.26	0.91	2.74	3.58	1.36	3.04	3.35
	ZmGSTU1.1	GRMZM2G335618	-0.83	4.93	1.19	-1.66	0.65	-0.10	-0.42	0.09	0.13	0.30	-0.02	-0.24	0.12
	ZmGSTU1.2	GRMZM2G308687	-0.29	2.97	-0.29	4.45	1.00	3.84	4.31	0.78	1.17	1.32	1.61	2.42	2.60
	ZmGSTU2.0	GRMZM2G077206	0.22	-0.36	-0.08	-0.46	-0.02	-1.40	-1.21	n/a	n/a	n/a	n/a	n/a	n/a
	ZmGSTU3.0	GRMZM2G145069	0.44	1.23	-1.83	-0.37	-0.13	4.79	4.36	7.03	9.40	4.92	9.79	10.89	5.50
		GRMZM2G149182	0.44	1.23	-1.83	-0.37	-0.13	4.79	4.36	7.07	9.40	4.92	9.79	10.90	5.49
Tau	ZmGSTU3.1	GRMZM2G475059	3.44	1.71	-0.88	-0.96	0.24	5.38	3.54	3.78	6.47	6.67	5.64	7.47	6.95
	ZmGSTU4.0	GRMZM2G097989	-0.71	0.54	0.33	-1.25	0.25	-2.72	0.00	-0.13	-0.39	-0.70	-0.22	-0.43	-0.66
	ZmGSTU4.1	GRMZM2G016241	-1.77	0.00	-0.80	-1.53	-1.70	-1.82	0.03	0.06	-0.91	-0.70	-0.47	-0.55	-0.54
	ZmGSTU5.0	GRMZM2G416632	0.54	1.24	-0.27	0.14	1.25	4.44	1.42	0.00	-0.02	0.66	0.01	0.08	0.53
	ZmGSTU5.1	GRMZM2G127789	-0.76	-0.31	-0.21	-0.67	0.21	0.67	0.00	0.07	-0.36	-0.20	0.05	-0.39	-0.21
	ZmGSTU5.2	GRMZM2G428168	0.83	0.19	-1.10	-0.75	0.08	2.39	2.39	1.27	1.90	2.14	1.49	1.73	1.78
	ZmGSTU5.3	GRMZM2G032856	-0.91	0.23	-0.91	-1.44	0.19	5.20	-0.38	-0.92	0.07	0.57	-0.04	-0.73	-0.42
	ZmGSTU5.4	GRMZM2G146475	-0.60	0.46	-1.45	-0.84	-0.41	-0.62	0.11	0.01	0.02	0.04	0.03	-0.01	0.18
	ZmGSTU5.5	GRMZM2G052571	0.10	0.04	-1.12	-0.01	-0.04	4.64	-0.12	0.17	-0.02	0.18	0.34	-0.31	0.21
	ZmGSTU5.6	GRMZM2G028556	0.84	-0.80	-1.80	-1.20	0.45	8.29	2.80	1.68	3.09	4.31	2.63	3.79	4.97
	ZmGSTU6.0	GRMZM2G363540	-1.39	0.01	-0.04	-2.70	0.40	-0.41	0.21	0.00	0.13	1.89	0.00	1.18	0.84
	ZmGSTU6.1	n/a	n/a	n/a	n/a	n/a	n/a	n/a	n/a	n/a	n/a	n/a	n/a	n/a	n/a
	ZmGSTU6.2	GRMZM2G028821	-0.91	1.23	-0.36	-0.32	0.66	0.89	-0.33	0.45	0.71	1.27	0.05	0.54	1.08
	ZmGSTU6.3	GRMZM2G168229	0.04	0.00	0.02	-0.06	0.00	0.00	0.00	n/a	n/a	n/a	n/a	n/a	n/a
	ZmGSTU7.0	GRMZM2G146913	-0.31	0.96	0.36	-0.43	2.34	-0.10	0.18	0.32	0.06	0.11	0.30	0.08	0.14
	ZmGSTU7.1	GRMZM2G146887	-1.19	0.28	-0.29	-0.28	0.26	0.17	0.34	0.08	0.20	0.36	0.00	0.11	0.34
	ZmGSTU7.2	GRMZM2G056388	0.22	3.94	0.34	2.10	0.41	3.54	3.65	0.66	0.82	1.04	0.68	0.63	0.83
	ZmGSTU7.3	n/a	n/a	n/a	n/a	n/a	n/a	n/a	n/a	n/a	n/a	n/a	n/a	n/a	n/a
	ZmGSTU7.4														
	ZmGSTU8.0	GRMZM2G330635	-0.44	2.86	-0.49	-0.11	0.56	2.43	2.35	0.68	1.25	1.70	1.02	1.32	1.68
	ZmGSTU8.1	GRMZM2G178079	-1.44	1.03	-0.62	-0.54	0.02	1.38	1.00	0.58	1.08	0.66	0.70	0.86	0.50
	ZmGSTU8.2														
	ZmGSTU9.0	GRMZM2G066369	-1.13	0.93	0.11	-0.07	-0.28	-1.15	0.32	-1.03	-1.42	2.37	-0.39	0.30	1.03
	ZmGSTU9.1														
	ZmGSTU9.2	GRMZM2G044383	4.07	1.67	-1.49	-0.22	-0.72	6.47	1.14	0.54	0.81	0.86	0.92	1.28	1.03
	ZmGSTU9.3	GRMZM2G161905	0.97	0.16	1.68	-0.89	-0.31	1.58	2.62	0.29	1.35	2.16	0.70	1.12	1.69
	ZmGSTU9.4														
	ZmGSTU10.0	GRMZM2G161891	-0.65	0.35	0.09	2.36	0.16	0.12	-0.11	-0.19	0.22	0.68	-0.12	-0.10	0.31
	ZmGSTU10.1	GRMZM2G480439	1.91	0.00	-0.26	0.23	-0.98	1.38	1.44	6.40	8.59	8.44	7.36	8.56	8.31
	ZmGSTU10.2	GRMZM2G025190	-0.20	1.88	0.48	1.04	1.16	5.19	1.56	0.04	0.06	0.52	-0.08	-0.14	0.20
	ZmGSTU10.3	GRMZM2G054653	0.00	0.00	0.00	0.00	-0.75	0.00	0.00	1.44	-0.74	3.58	0.80	-1.54	2.17
	ZmGSTU10.4	GRMZM2G041685	0.02	-0.26	0.08	-0.01	-0.04	0.42	4.54	0.00	-4.95	0.00	5.57	-4.95	0.00
	ZmGSTU10.5														

Table 26: Perturbation of maize Glutathione-S-Transferase (GST) genes by abiotic stresses.

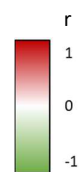
Perturbation expression data extracted from Genevestigator software. Values represent log₂ fold change compared to a control. Legend (bottom right) describes heat map. Values in blue are not significant (p≥0.05). Values in black are significant (p<0.05). Data from Table 20 included for reference.



		Cold	Dehydration	Drought	Heat	Simulate drought	submergence	12-OPDA	Metcamifen	Benoxacor
Pearson (r)	Cold	1.0000								
	Dehydration	0.1379	1.0000							
	Drought	-0.1688	0.1863	1.0000						
	Heat	0.1994	0.3231	-0.0040	1.0000					
	Simulate drought	0.0212	0.4171	0.3547	0.2187	1.0000				
	submergence	0.5463	0.2155	-0.4541	0.3759	0.0854	1.0000			
	12-OPDA	0.3845	0.3080	-0.2691	0.3939	0.0121	0.6283	1.0000		
	Metcamifen	0.4454	0.1721	-0.3451	0.1870	-0.0306	0.4876	0.4987	1.0000	
	Benoxacor	0.4324	0.1720	-0.3858	0.1515	-0.0392	0.4740	0.5235	0.9719	1.0000
P	Cold	0.0000								
	Dehydration	0.3110	0.0000							
	Drought	0.2136	0.1692	0.0000						
	Heat	0.1406	0.0152	0.9767	0.0000					
	Simulate drought	0.8769	0.0014	0.0073	0.1054	0.0000				
	submergence	0.0000	0.1107	0.0004	0.0043	0.5313	0.0000			
	12-OPDA	0.0034	0.0209	0.0449	0.0027	0.9292	0.0000	0.0000		
	Metcamifen	0.0007	0.2134	0.0106	0.1758	0.8261	0.0002	0.0001	0.0000	
	Benoxacor	0.0011	0.2137	0.0040	0.2741	0.7785	0.0003	0.0000	0.0000	0.0000

Table 27: Pearsons correlation of abiotic stress and safener perturbation.

Correlation analysis of expression results from Table 26, were performed using graphpad. Metcamifen and benoxacor data chosen from 90 min. Pearsons values (r) and P-values (P) are shown. Significant p-values (< 0.05) are identified in bold. Legend (bottom right) indicates r-values for heat map.



5.3 Discussion

5.3.1 Safener effects on GST and CYP transcript regulation

The next generation sequencing study data (section 5.2.1) identified a number of GST genes induced by the safeners, benoxacor and metcamifen. These occurred in all classes, though not significantly in the GHR class. Since only phi and tau class enzymes are involved in safener-induced metabolism, the others induced may be involved in responses to general stress, since safeners themselves have been shown to cause toxicity at certain concentrations (Andrews et al., 2005; Day et al., 1996; Deridder et al., 2006). They may also be involved in the safening effect through a mechanism other than herbicide detoxification, such as increased transport of ligands for sequestration by vacuolar transporters (Gaillard et al., 1994). However, as expected, the most abundant and highly induced classes were phi, tau and lambda (Jablonkai, 2013). Benoxacor and metcamifen showed some differential effects on gene regulation in two phi, one lambda, five tau class GSTs and one zeta class GST. Therefore it could be deduced from this experiment that safener chemical specificity, mediated through GST herbicide detoxification, appears to rely mainly on tau class GST induction. An important observation was the high induction of *ZmGSTF2.3* in response to safeners, when compared to the low induction of *ZmGSTF2.0*, which supports previous findings (Jablonkai, 2013). Three important

genes, *ZmGSTF2.3*, *ZmGSTU1.2* and *ZmGSTL1.3* were identified from this study as safener-inducible and used for further investigation.

The results of the relative quantification study (section 5.2.2.3) identified a clear differential induction profile of important GSTs and CYPs, following treatment with metcamifen or benoxacor, with respect to gene, tissue and time. It was hypothesised that while the induction effects might be similar with respect to time, a differential subset of genes and tissue localisation might occur for the safeners. The timing of induction, however, showed a significant difference between each safener, metcamifen acting later than benoxacor. This fits with the observation by Skipsey et al. (2011) that safeners may induce rapid xenobiotic responses (RXR) or slow xenobiotic responses (SXR), indicated by maximal induction by 4 hours or 24 hours respectively, though a limited number of times was used in the aforementioned study. Using this system, benoxacor would fall into the RXR while metcamifen would fall into the SXR. A three-phase safener response has also been proposed, indicating 90 minutes as the phase in which xenobiotic genes are induced by metcamifen in rice cultures (Brazier-Hicks et al., 2020). However, in the current study, the xenobiotic genes were upregulated by metcamifen mostly at 24-48 hours. Benoxacor, however, may have been most highly induced in this early time frame. It is likely that differences in biological system, species, or experimental design, have caused this differential timing of response. The induction profiles also demonstrated an interesting phenomenon; that the induction of genes was either linear, parabolic or biphasic. A parabolic trend can be understood as the temporary increase in transcripts due to gene induction, followed by a decrease in transcripts due to degradation. This transience of effect has been demonstrated following safener treatment, often showing similarly rapid decreases in induction (Skipsey et al., 2011). The biphasic pattern is not uncommon for gene induction, and likely represents positive feedback loops of control of transcription factors (Kocsy et al., 2001). A linear response indicates that the full range of safener effects is not observed, and a parabolic or biphasic trend might occur if later times were investigated. Unfortunately, while unlikely to last considerably longer than three days, the full range of safener induction was not observed at the times sampled, especially with the early benoxacor effects. This problem has been reported previously, with respect to RXR being overlooked, and the data reported in this chapter supports this claim that safener responses should be investigated before 3 hours and later than 24 hours, if the whole effect is to be observed (Skipsey et al., 2011).

The differential induction pattern may play a role in mediating safener chemical selectivity. A good example of this is that benoxacor stimulated transcriptional induction primarily in the stems, while metcamifen did so primarily in the leaves. Assuming the magnitude of induction is related to metabolic activity, it could be supposed that the safeners cause differential activity in different tissues. This observed tissue specificity of induction, combined with a differential active site of specific herbicides, may together provide an explanation for chemical selectivity. Previous studies have suggested that tissue-specific GST expression is important for safener-induced herbicide tolerance (Deridder et al., 2006). As such, herbicides applied aerially or that act primarily on leaves, may be metabolised most efficiently by enzymes that are induced most markedly in the leaves when exposed to the compatible safener partner. Similarly, herbicides that target the stem or apical meristem, may be metabolised most efficiently by enzymes that are induced by safeners in the stem. For example, it has been hypothesised that safeners for chloroacetanilides exert their main effect on herbicide metabolism by inducing GST in the coleoptile to prevent the herbicide from reaching the meristematic tissue (Riechers et al., 2010). The large induction by benoxacor, designed to work with the chloroacetanilide metolachlor, in the stem supports this hypothesis. Similarly, HPPD inhibitors such as mesotrione are known to work primarily in the meristematic leaf tissue and new leaves where carotenoids and tocopherols are needed (Ma et al., 2013; Mitchell et al., 2001). The large induction observed with metcamifen, known to work with mesotrione, in the leaves, supports this hypothesis. In addition, the roots are affected much less than the aerial parts of the plant, indicating that the roots have less of a role in safening.

It can be surmised that those genes induced the most are more likely to be involved in the safening process, with CYP81A4 likely to have the least involvement. Overall, the two safeners have demonstrated differential induction of xenobiotic detoxification genes, in different tissues and over a relatively short time frame, providing support for the hypothesis that chemical selectivity may be mediated by specific xenome gene regulation.

The results of the absolute quantification (section 5.2.2.5) demonstrated a clear difference between endogenous GST and CYP expression levels, with less difference between individuals of each family. The high endogenous expression of GST enzymes in the root may indicate an important functional role. It is likely this role is in functions other than xenobiotic detoxification, with GSTs implicated in antioxidant defences critical for nitrogen fixation in root tissues (Dalton et al., 2009). The high endogenous expression of CYP enzymes in the

leaves is also likely due to endogenous functions besides xenobiotic metabolism. Considering the roles of CYPs in electron transport chains, abundant in the chloroplasts of leaves, the high expression in this tissue is not unexpected. The net increase in expression of all genes over time, in at least one tissue, indicates increased demands for these enzymes with plant development.

The high transcript numbers seen with the GSTs indicates physiological relevance, and thus the dramatic increase with safeners is likely associated with a biological effect. The same can be assumed with CYP81A9 and CYP81A4, though perhaps their lower expression levels may indicate less of an effect of their induction with safeners. The extremely low transcript numbers seen with CYP72A5 may not translate into a significant biological effect. Previous studies have identified that transcripts of this gene are not detectable in maize root tissues (Persans et al., 2001). Even though the expression increased with safeners, the resultant number of enzymes would still be extremely low and may not have any effect on xenobiotic detoxification. The higher expression of GSTs than CYPs may be due to localisation, enzymatic rate or secondary metabolism.

Some of these results are consistent with previous findings. For example, Dixon et al. (1997) found that *ZmGSTF2.3* was endogenously expressed only in the roots, but appeared in the foliage after safener treatment, as has been shown here. As with *ZmGSTU1.2* observed here, various tau class GSTs of a wheat species (*Triticum tauschii*) were induced most by safeners, cloquintocet-mexyl and fluxofenim, in the coleoptiles (Riechers et al., 2003). As the results of the current study indicated, most GST genes in maize have been demonstrated to be higher in the roots than the shoots, endogenously (Li et al., 2017). The dichloromethyl-ketal safener, MG-191 has been shown to induce the expression of *ZmGSTU1.2* in the root and shoot after one day of treatment, matching closely the effect of benoxacor shown here, in contrast to the low enhancement caused by metcamifen (Jablonkai, 2013; Jablonkai et al., 2001). The similarity of the structures of MG-191 and benoxacor (see section 1.10), as compared with metcamifen, indicates a possible structural trend. Indeed it has been demonstrated that *ZmGSTU1.2* is induced more selectively than *ZmGSTF2.3*, the former responding to dichloroacetanilides (Jablonkai, 2013). Since benoxacor and MG-191 have been shown to safen maize against chloroacetanilide herbicides, *ZmGSTU1.2* may be important for this specificity (Jablonkai, 2013; Kramer et al., 2007).

5.3.2 *Effect of safeners on GST protein regulation*

The results of section 5.2.3 identified an enhanced expression of the *ZmGSTU1.2-1.2* protein with application of metcamifen and benoxacor, with the greatest effect in the stem, and with benoxacor. This observation supports the transcript analysis (section 5.2.2.3), which displayed the same pattern. A time delay was observed between the transcriptional and translational effects, with the greatest inductions at 3 hours and 72 hours, respectively. This likely reflects the time required for basic translation of mRNA into protein, and protein folding. While the antibody raised to *ZmGSTF2.0-2.3* could not differentiate between *ZmGSTF2.0* and *ZmGSTF2.3* recombinant protein, and thus was likely recognising both subunits, predictions can be made as to which protein was produced in response to the safeners. The next generation sequencing data (section 5.2.1) and endogenous expression data (Chapter 4), indicated *ZmGSTF2.0* as a constitutively expressed protein with little enhancement of transcript by either safener, as supported by previous observations (Dixon et al., 1997). Conversely, *ZmGSTF2.3* showed low levels of endogenous expression, and high stimulation of transcription from both safeners (Dixon et al., 1997; Holt et al., 1995; Irzyk et al., 1993). The effect of safeners, therefore, often leads to a greater content of the heterodimer *ZmGST2.0-2.3* (Dixon et al., 1997; Holt et al., 1995; Irzyk et al., 1993). Thus, the safener effects observed with *ZmGSTF2.0-2.3* were likely reflecting the increased transcription of *ZmGSTF2.3*. An increased transcription of *ZmGSTF2.3* was observed with application of metcamifen and benoxacor in both tissues, with a greater effect in the stem, and with benoxacor, such that the trends showed only mild similarity to the transcript data (section 5.2.2.3). The large effect of metcamifen and low effect of benoxacor on *ZmGSTF2.3* transcript induction in the leaf was not reflected in the protein regulation, with both safeners causing a similar mild enhancement of protein levels. In the stem, the *ZmGSTF2.3* transcript demonstrated an early induction with benoxacor and a later induction with metcamifen, while the *ZmGSTF2.3* protein was expressed with both safeners at similar times, with metcamifen causing a greater effect. The dissimilarity between safener-induced transcript and protein induction of *ZmGSTF2.3* indicates some effect was preventing the transcript enhancement from translating into an associated protein enhancement. Another, less likely, explanation may be that *ZmGSTF2.0* protein levels were enhanced, confusing the results. The different trends observed with the transcript and protein expression systems means transcript levels cannot be used in isolation to infer the effect of Safeners on protein expression.

5.3.3 *Effect of abiotic stresses on GST transcript induction*

The abiotic stresses caused a range of effects on the regulation of GST genes (section 5.2.4). This was most likely because GSTs not only detoxify xenobiotics, but have functions in stress responses. For example certain GSTs have been shown to increase in expression as a result of salt stress (Mittova et al., 2003). Each stress elicited a unique induction profile of the GST family, implying different signalling pathways, involving different individual GSTs to respond to the stresses. This is understandable, since the physiological responses to each stress would have to be different. In each case, the stress caused altered regulation of multiple GSTs indicating multiple functions and/or redundancy of function. As with xenobiotic detoxification, zeta, theta, DHAR and GHR classes were barely affected by the stresses. This may suggest that these classes have little role in stress response or xenobiotic detoxification, but it may simply be that they have an endogenously high expression and can function without altered regulation of transcription. The stresses causing the greatest effect on GST induction were submergence and 12-OPDA, indicating GSTs have an important role in dealing with these stresses. These two stresses also caused a remarkably similar regulation profile as each other and the safeners, metcamifen and benoxacor. It may therefore be hypothesised that the signalling pathway mediating the safener effect on GSTs shares some commonality with that of submergence and jasmonates. Submergence causes multiple stresses, including reduced oxygen uptake, reduced light availability, and reduced transpiration. The signalling pathway mediating the response includes the increase in ethylene, and altered levels of giberellins (Tamang et al., 2015). The regulation of some GSTs by ethylene provides a possible explanation for the enhancement of GST expression by submergence, and a possible link with the Safener response (Smith et al., 2003). The link between jasmonate and Safener signalling has been previously proposed, with OPDA and safeners acting on GST gene expression via TGA transcription factors (Riechers et al., 2010). Methyl-jasmonate has also been shown to co-express certain genes with metcamifen in rice, though the effects were considered to be mediated through different pathways (Brazier-Hicks et al., 2020). Of course, the overall effects on the respective transcriptomes would be very different with each stress or treatment, but it appears that a similar set of GSTs are expressed within the larger complex signalling system.

5.4 Conclusions

This chapter has investigated the effects of two safeners on the induction of genes encoding enzymes important for herbicide detoxification. A comprehensive analysis of the effect of

these safeners on the maize GST superfamily in cell culture was performed and led to a focus on important members of GST and CYP families in hydroponically grown maize. The induction effects of the safener metcamifen have not previously been published, and these results provide a novel understanding of the mechanism of action of this safener. While the effects of benoxacor on the induction of some GST genes have been demonstrated previously, this is the first instance whereby these specific genes have been investigated, in hydroponic maize. As such, the behaviours of individual GSTs in the early safener response have been determined. In addition, the question of the longevity of safener effects has been partially answered, with the results indicating that most induction of the xenobiotic detoxification enzymes is completed by three days after transient dosage. The hypothesis that chemical selectivity of herbicide safeners is mediated by differential induction of xenome enzymes has been given support by the current findings. Differential induction profiles of important xenobiotic detoxifications enzymes have been observed for the two safeners, at the transcript and protein level, indicating selectivity based on enhancement of enzyme synthesis. With the increased levels of these enzymes related to increased detoxification ability, and the enzymes displaying selectivity to herbicide substrates, this hypothesis for safener selectivity appears likely. To confirm this theory, the roles of each enzyme in the protection against the two herbicides would have to be tested. Enzyme knockouts could help determine the importance of each enzyme, though redundancy of function may hinder this. Over-expression studies could also provide information on the protective capacity of each enzyme.

The effects of abiotic stresses and hormones on GST expression was also demonstrated, identifying enzymes potentially involved in the associated responses. Interestingly, it was found that the induction profiles caused by safeners closely matched those of submergence stress and 12-OPDA treatment. The genes co-expressed by these treatments are therefore likely to be involved in the associated responses. This provides support for the hypothesis that safening effects are mediated through signalling pathways originally used for responses to certain abiotic stresses or involved in specialised hormone signalling, which may help to elucidate the safener mode of action.

5.5 Appendix to Chapter 5

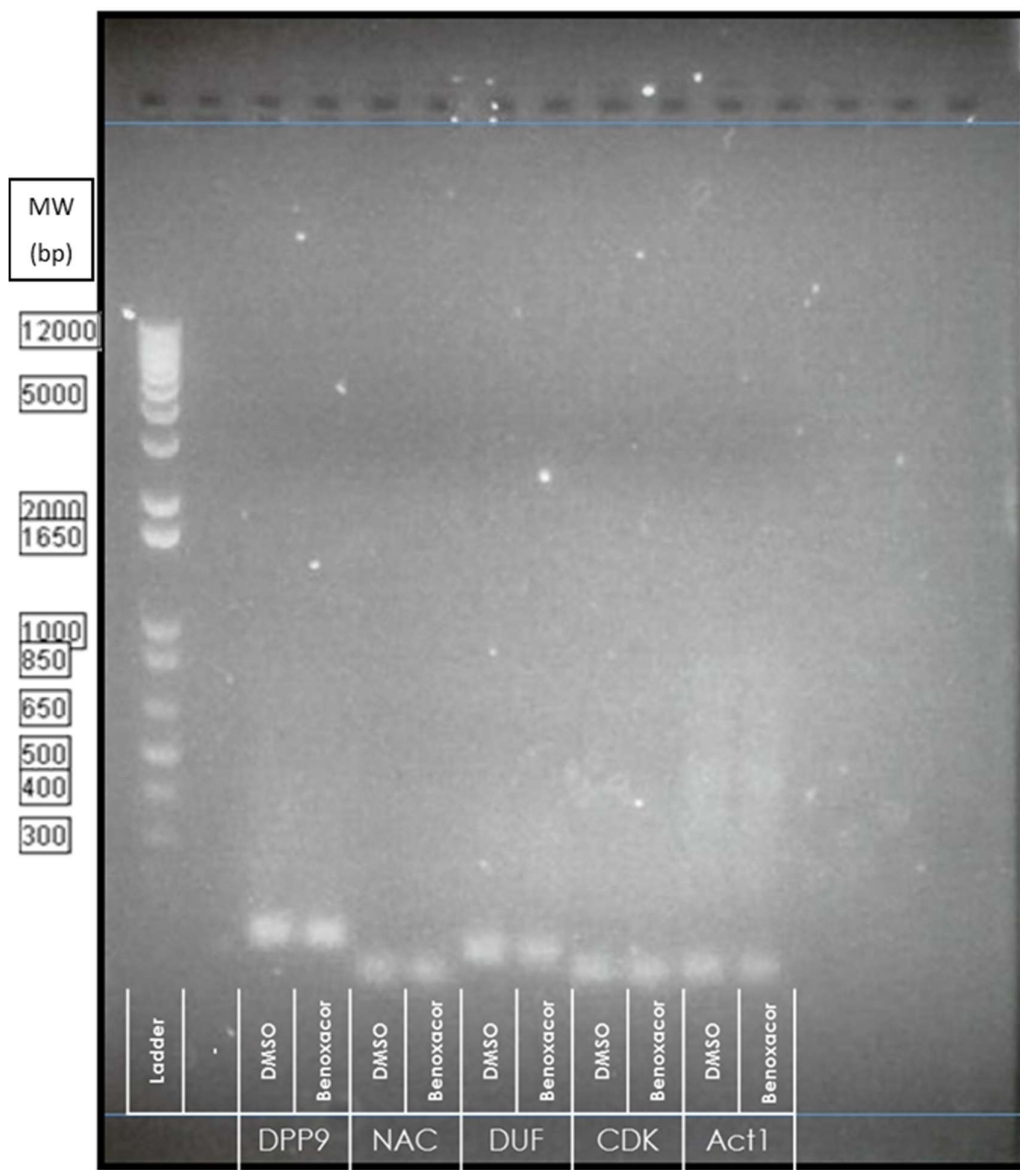


Figure S 5: Agarose gel electrophoresis of reference gene replicated region, for Figure 38 and Figure 39.

Samples applied at 5 μ l. Ladder (left) indicates molecular weight markers in base pairs (bp). Blue lines indicate region of electrophoresis.

	Significance	P value	Mean of benoxacor	Mean of Control	Difference	SE of difference	t ratio	df
DPP9	No	0.25	22.01	20.83	1.18	0.87	1.36	4.00
NAC	No	0.23	22.48	21.23	1.25	0.87	1.43	4.00
DUF	No	0.27	24.52	22.75	1.77	1.37	1.29	4.00
CDK	No	0.20	24.34	22.90	1.44	0.94	1.53	4.00
Act1	No	0.41	22.02	21.16	0.85	0.92	0.93	4.00

Table S 13: Statistical analysis of reference gene Cq values in stability test, for Figure 40.

p values < 0.05 were considered significant.

	Gene Name							
	ZmGSTU1.2	ZmGSTU1.0	ZmGSTF2.3	ZmGSTL1.3	CYP81A9	CYP81A4	CYP72A5	CYP89B19
Slope	-3.322	-3.2507	-3.3856	-3.73	-3.2438	-3.5777	-3.1292	-3.1683
Efficiency	2.00 ^a	2.03 ^a	1.97 ^a	1.85 ^a	2.03 ^a	1.90 ^a	2.09 ^a	2.07 ^a
Error	0.12	0.15	0.15	0.53	0.34	0.21	0.33	0.11
R²	1 ^a	0.99 ^a	0.99 ^a	0.95 ^a	0.97 ^a	0.99 ^a	0.97 ^a	1 ^a
Y-Intercept	22.19	23.18	24.62	20.76	21.18	22.89	30.34	26.57

Table S 14; Primer efficiencies for genes of interest (Table 24).

Superscripts denote result acceptability: a; acceptable.

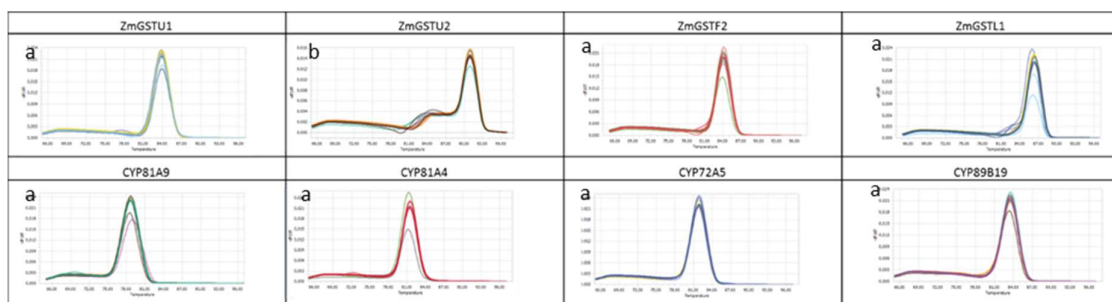


Figure S 6; Melting peaks for genes of interest (Table 24).

Temperatures of 66–96 °C are plotted against $-dF/dT$ (rate of change of fluorescence relative to temperature). Superscripts denote result acceptability: a; acceptable, b; unacceptable.

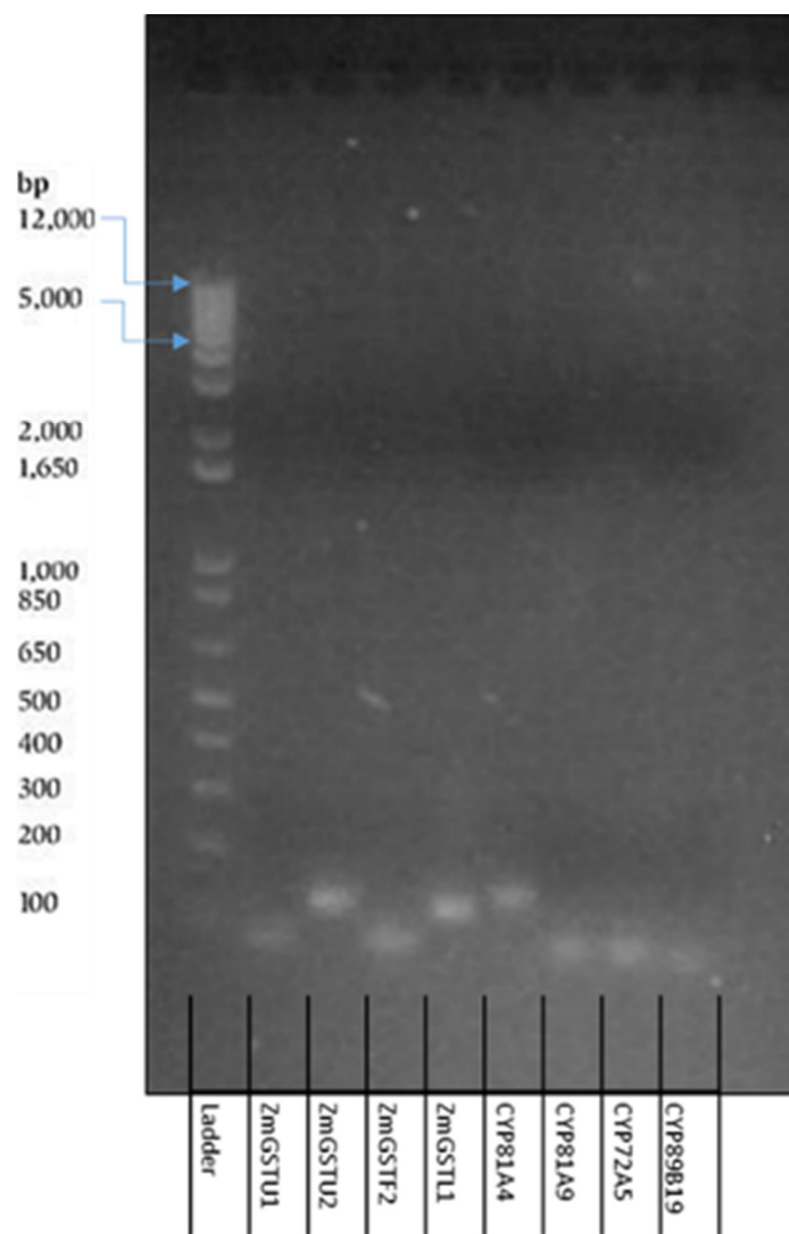


Figure S 7; Agarose gel electrophoresis of gene of interest primers (Table 24). Samples applied at 5 μ L. Ladder (left) shows molecular weights in base pairs (bp).

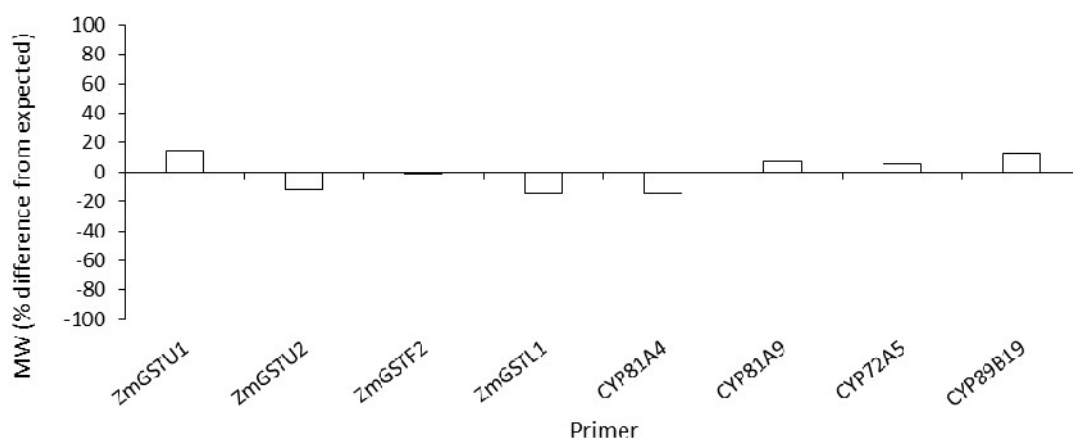


Figure S 8: Bar chart showing difference of in molecular weight of calculated compared to expected product sizes of genes of interest.

Calculated molecular weights determined by agarose gel electrophoresis. All molecular weight differences were considered acceptable.

Gene	NCBI Code	forward				reverse				Product Size
		Seque nce (5-3')	Tm (°C)	GC%	start	Seque nce (5-3')	Tm (°C)	GC%	start	
ZmGSTU1.0	NM_001111642.1	CGCTCG	59.97	60.00	289	GCCGA	60.25	60.00	429	141
		TCATCC TCCAGT AC				GTCTG GCTGTC ATAG				
CYP89B19	NM_001152595.1	CCCAGC	63.10	61.10	1045	TGACAC	64.20	52.40	1094	70
		CATCCA GGAGA A				CCCTTC CTTGTT GTC				

Table S 15: Obsolete gene of interest primers.

Sequence, melting temperature (Tm) (°C), Guanine/Cytosine content (GC%), start position, and product length in base pairs (bp) are shown for each forward and reverse primer.

	Time (h)	3			24			48			72		
Treatment	Gene	DMSO	metcamifen	benoxacor	DMSO	metcamifen	benoxacor	DMSO	metcamifen	benoxacor	DMSO	metcamifen	benoxacor
Root	ZmGSTU 1.2	1.00 ± 0.10 ^a	1.62 ± 0.12 ^b	12.08 ± 1.68 ^c	1.00 ± 0.12 ^a	1.26 ± 0.21 ^a	4.59 ± 1.02 ^a	1.00 ± 0.12 ^a	1.56 ± 0.14 ^b	7.03 ± 0.63 ^c	1.00 ± 0.22 ^a	1.17 ± 0.20 ^a	6.30 ± 1.06 ^b
	ZmGSTF 2.3	1.00 ± 0.09 ^a	1.88 ± 0.14 ^b	6.99 ± 0.86 ^c	1.00 ± 0.15 ^a	3.86 ± 0.74 ^b	6.68 ± 1.28 ^c	1.00 ± 0.03 ^a	1.70 ± 0.05 ^b	3.32 ± 0.10 ^c	1.00 ± 0.13 ^a	1.95 ± 0.29 ^c	0.81 ± 0.08 ^a
	ZmGSTL 1.3	1.00 ± 0.11 ^a	3.59 ± 0.66 ^b	7.36 ± 1.25 ^c	1.00 ± 0.12 ^a	5.44 ± 0.90 ^b	7.07 ± 1.12 ^b	1.00 ± 0.02 ^a	3.96 ± 0.10 ^b	10.07 ± 0.25 ^c	1.00 ± 0.05 ^a	4.65 ± 0.53 ^b	4.08 ± 0.16 ^b
	CYP81A9	1.00 ± 0.04 ^a	5.43 ± 0.19 ^b	4.29 ± 0.37 ^b	1.00 ± 0.04 ^a	4.26 ± 0.21 ^b	1.09 ± 0.05 ^a	1.00 ± 0.05 ^a	8.99 ± 0.41 ^c	1.91 ± 0.09 ^b	1.00 ± 0.04 ^a	5.78 ± 0.26 ^c	3.12 ± 0.10 ^b
	CYP81A4	1.00 ± 0.10 ^a	5.17 ± 0.63 ^b	7.13 ± 0.57 ^c	1.00 ± 0.08 ^a	4.33 ± 0.35 ^b	1.66 ± 0.13 ^b	1.00 ± 0.06 ^a	3.45 ± 0.21 ^b	3.06 ± 0.19 ^b	1.00 ± 0.07 ^a	5.74 ± 0.29 ^c	2.67 ± 0.20 ^b
	CYP72A5	1.00 ± 0.33 ^a	3.59 ± 1.03 ^b	6.15 ± 1.48 ^b	1.00 ± 0.34 ^a	3.09 ± 0.77 ^b	1.04 ± 0.34 ^a	1.00 ± 0.21 ^a	7.40 ± 1.40 ^b	7.42 ± 1.44 ^b	1.00 ± 0.18 ^a	5.05 ± 0.81 ^b	3.71 ± 0.54 ^b
Stem	ZmGSTU 1.2	1.00 ± 0.20 ^a	1.18 ± 0.36 ^a	65.19 ± 12.50 ^b	1.00 ± 0.06 ^a	2.57 ± 0.24 ^b	12.67 ± 1.70 ^c	1.00 ± 0.05 ^a	1.91 ± 0.08 ^b	15.85 ± 0.91 ^c	1.00 ± 0.10 ^a	2.09 ± 0.27 ^b	11.94 ± 1.30 ^c
	ZmGSTF 2.3	1.00 ± 0.43 ^a	1.48 ± 0.57 ^a	7.37 ± 2.76 ^b	1.00 ± 0.05 ^a	5.84 ± 1.26 ^b	6.45 ± 1.13 ^b	1.00 ± 0.11 ^a	6.00 ± 0.50 ^b	4.82 ± 0.52 ^b	1.00 ± 0.10 ^a	7.94 ± 0.99 ^b	5.45 ± 0.72 ^b
	ZmGSTL 1.3	1.00 ± 0.32 ^a	5.29 ± 1.51 ^b	31.80 ± 9.53 ^c	1.00 ± 0.08 ^a	1.31 ± 0.28 ^a	1.82 ± 0.28 ^a	1.00 ± 0.11 ^a	7.47 ± 0.83 ^a	3.34 ± 0.36 ^b	1.00 ± 0.24 ^a	5.04 ± 1.19 ^b	1.75 ± 0.44 ^a
	CYP81A9	1.00 ± 0.27 ^a	5.41 ± 1.68 ^b	14.60 ± 3.41 ^c	1.00 ± 0.34 ^a	2.86 ± 0.97 ^b	2.25 ± 0.71 ^a	1.00 ± 0.05 ^a	9.12 ± 2.04 ^c	1.56 ± 0.10 ^b	1.00 ± 0.16 ^a	4.71 ± 0.59 ^b	1.25 ± 0.22 ^a
	CYP81A4	1.00 ± 0.31 ^a	1.62 ± 0.12 ^a	12.08 ± 1.68 ^b	1.00 ± 0.30 ^a	1.26 ± 0.21 ^a	4.59 ± 1.02 ^a	1.00 ± 0.20 ^a	1.56 ± 0.14 ^b	7.03 ± 0.63 ^c	1.00 ± 0.36 ^a	1.17 ± 0.20 ^a	6.30 ± 1.06 ^b
	CYP72A5	1.00 ± 0.27 ^a	1.75 ± 0.47 ^a	11.64 ± 2.91 ^b	1.00 ± 0.33 ^a	3.71 ± 1.48 ^b	1.13 ± 0.45 ^a	1.00 ± 0.26 ^a	6.31 ± 1.90 ^b	4.51 ± 1.15 ^b	1.00 ± 0.26 ^a	2.34 ± 0.66 ^a	1.25 ± 0.33 ^a
leaf	ZmGSTU 1.2	1.00 ± 0.20 ^a	2.61 ± 0.59 ^b	6.15 ± 0.98 ^c	1.00 ± 0.18 ^a	1.98 ± 0.32 ^b	2.11 ± 0.54 ^b	1.00 ± 0.13 ^a	2.70 ± 0.43 ^b	1.81 ± 0.21 ^b	1.00 ± 0.23 ^a	2.13 ± 0.40 ^b	2.85 ± 0.68 ^b
	ZmGSTF 2.3	1.00 ± 0.21 ^a	1.48 ± 0.23 ^a	5.50 ± 0.80 ^b	1.00 ± 0.14 ^a	6.72 ± 1.48 ^b	0.65 ± 0.07 ^a	1.00 ± 0.25 ^a	16.36 ± 3.12 ^b	1.12 ± 0.22 ^a	1.00 ± 0.23 ^a	3.29 ± 0.65 ^b	1.12 ± 0.21 ^a
	ZmGSTL 1.3	1.00 ± 0.12 ^a	14.17 ± 1.43 ^c	6.16 ± 0.56 ^b	1.00 ± 0.17 ^a	15.39 ± 3.68 ^b	0.58 ± 0.09 ^a	1.00 ± 0.36 ^a	23.62 ± 6.51 ^b	1.12 ± 0.31 ^a	1.00 ± 0.17 ^a	7.56 ± 1.55 ^b	0.87 ± 0.16 ^a
	CYP81A9	1.00 ± 0.18 ^a	4.88 ± 0.63 ^b	0.90 ± 0.12 ^a	1.00 ± 0.19 ^a	3.75 ± 1.14 ^b	0.90 ± 0.19 ^a	1.00 ± 0.26 ^a	3.56 ± 0.90 ^b	0.51 ± 0.11 ^a	1.00 ± 0.13 ^a	3.60 ± 0.72 ^b	1.01 ± 0.35 ^a
	CYP81A4	1.00 ± 0.14 ^a	6.81 ± 0.72 ^b	0.76 ± 0.08 ^a	1.00 ± 0.29 ^a	4.16 ± 1.53 ^b	0.38 ± 0.11 ^a	1.00 ± 0.06 ^a	5.67 ± 0.30 ^a	0.56 ± 0.03 ^a	1.00 ± 0.23 ^a	1.92 ± 0.49 ^b	0.46 ± 0.10 ^a
	CYP72A5	1.00 ± 0.22 ^a	1.73 ± 0.33 ^b	1.09 ± 0.18 ^a	1.00 ± 0.27 ^a	7.59 ± 2.11 ^c	0.39 ± 0.13 ^a	1.00 ± 0.14 ^a	14.64 ± 1.66 ^c	0.61 ± 0.10 ^a	1.00 ± 0.15 ^a	4.41 ± 1.08 ^b	0.39 ± 0.07 ^a

Table S 16: Heat map of quantitative/real time polymerase chain reaction (qPCR) data (Figure 42 and Figure 43).

Colours indicate degree of up/down-regulation indicated by the legend (bottom right). Data shown as expression fold ± standard deviation. 3 biological and 3 technical replicates were used for each data point. Colour based upon log₂(expression fold). Values within white squares (each tissue, gene and time) that do not share a common letter are significant (p < 0.05)



gene	Time (h)	Root		Stem		Leaf	
		mean	SD	mean	SD	mean	SD
ZmGSTU1.2	3	957085.60	199465.30	103393.50	33655.12	64316.81	25929.81
	24	731384.40	312012.20	262105.50	239898.90	108704.70	40749.27
	48	1890196.00	499879.20	299774.40	198613.40	120211.20	23134.99
	72	3184036.00	2190294.00	208545.70	127152.00	185386.80	37044.04
ZmGSTF2.3	3	957177.20	643605.10	20991.01	11790.42	24186.10	5699.55
	24	733130.10	793502.20	71284.77	26696.84	30946.97	15954.17
	48	1229994.00	538969.50	111434.00	78051.42	45822.97	16447.22
	72	2875402.00	1187628.00	60963.80	35604.70	52213.87	9206.58
ZmGSTL1.3	3	997019.70	285231.70	14427.98	3448.81	73681.81	11432.65
	24	358790.60	332536.60	98426.51	36136.74	112594.20	61218.28
	48	464536.80	213767.60	89274.85	29609.01	208787.80	165667.80
	72	1189958.00	521231.10	165702.20	90239.85	299990.40	75665.49
CYP81A9	3	860.24	176.91	302.61	105.77	5819.74	1142.82
	24	610.92	138.31	724.99	508.59	4195.29	1076.07
	48	648.55	460.24	795.23	185.51	7815.90	3714.15
	72	1293.81	221.25	1327.23	729.39	6966.73	1115.19
CYP81A4	3	519.63	80.91	1601.60	756.37	6028.82	1083.79
	24	422.07	209.00	4541.07	3359.21	12387.02	5176.07
	48	1389.20	348.41	5035.72	1320.74	16369.80	1805.69
	72	1721.28	727.07	6573.01	4682.66	26059.53	8009.10
CYP72A5	3	0.90	0.51	1.89	1.00	10.37	3.10
	24	0.53	0.26	3.34	1.34	3.36	1.21
	48	1.08	0.43	2.88	1.17	6.85	1.35
	72	2.28	0.90	9.53	1.90	16.06	3.22

Table S 17: gBlock® absolute quantification summarised data (Figure 47)

SD; standard deviation

TGGCGAATGGGACGCGCCCTGTAGCGGCGCATTAAAGCGGGCGGGTGTGGTGGTTACGCGCAGCGTGACCGCTACACTTGCCAGCGCCCTAGCGCCGCTCCTTTCGCTTTCTTC
CCTTCTTCTCGCCACGTTGCGCGCTTCCCGCTCAAGCTCTAAATCGGGGGCTCCCTTATAGGGTTCGATTAGTGCTTTACGGCACCTCGACCCAAAAAACTGATTAGGGT
GATGTTACAGTAGTGGCCATCGCCCTGATAGACGGTTTTTCGCCCTTGACGTTGGAGTCCAGCTTTTAAATAGTGGAAGTCTGTTCCAACTGGAACAACTCAACCTATC
TCGGTCTATTCTTTGATTATAAGGGATTTTCCGATTTCGGCTATTGTTTAAAAAATGAGCTGATTAACAAAAATTAACGCGAATTTTAAACAAATATTAACGTTTACAATTT
CAGGTGGCACTTTTCGGGAAATGTGCGCGGAACCCCTATTGTTATTTTCTAAATACATTCAATATGTATCCGCTCATGAATTAATCTTAGAAAACTCATCGAGCATCAAT
GAAACTGCAATTTATTATATCAGGATTATCAATACCATATTTTAAAAAGCCGTTTCTGAATGAAGGAGAAAACTCACCGAGGCAGTTCATAGGATGGCAAGATCCTGGTAT
CGGTCTCGATTCCGACTCGTCCAACATCAATACAACCTATTAATTTCCCTCGTCAAAAAATAGGTTATCAAGTGAGAAATCACCATGAGTGACGACTGAATCCGGTGAGAATGG
CAAAAGTTTATGCATTTCTTCCAGACTTGTTAACAGGCCAGCCATTACGCTCGTCATCAAAATCACTCGCATCAACCAAAACCGTTATTCACTCGTATTGCGCCTGAGCGAGACG
AAATACGCGATCGCTGTTAAAGGACAATTACAACAGGAATCGAATGAACCGCGCAGGAACACTGCCAGCGCATCAACAATATTTTACCTGAATCAGGATATTCTTCTAATA
CCTGGAATGCTGTTTTCCCGGGGATCGCAGTGGTGAGTAACCATGCATCATCAGGAGTACGGATAAAATGCTTGATGGTGGGAAGAGGCATAAAATCCGTCAGCCAGTTTAGTCT
GACCATCTCATCTGAATCATATTGGCAACGCTACCTTTGCCATGTTTCAAGAACTCTGCGGCATCGGGCTTCCATACAATCGATAGATTGTGCGACCTGATTGCCCGACATT
ATCGCGAGCCATTATACCATATAAATCAGCATCCATGTTGGAATTTAATCGCGGCTAGAGCAAGACGTTTCCGTTGAATATGGCTATAACACCCCTGTATTACTGTTTATG
TAAGCAGACAGTTTTATTGTTATGACCAAAATCCCTTAACGTGAGTTTTCTGCTCACTGAGCGTCAGACCCGTAAGAAAGATCAAGGATCTTCTGAGATCCTTTTTTCTGCGC
GTAATCTGCTGTTGCAAAACAAAAACCCGCTACCAGCGGTGTTGTTTTCGGGATCAAGAGTACCAACTCTTTTCCGAAGGTAAGTGGCTCAGCAGAGCGCAGATACC
AAATACTGCTCTTAGTGAGCGTAGTTAGGCCACCACTCAAGAACTCTGTAGCACCGCTACATACCTCGCTGCTAATCTGTTACAGTGGCTGCTGCGAGTGGCGATAA
GTCGTGCTTACCGGGTGGACTCAAGACGATAGTTACCGATAAGGCGCAGCGTGGGCTGAACGGGGGGTTCGTGCACACAGCCAGCTTGGAGCGAACGACCTACACCG
AACTGAGATACCTACAGCGTAGCTATGAGAAAGCGCCAGCTTCCGAAGGGAGAAAGGCGGACAGGTATCCGGTAAGCGGCAGGGTCGGAACAGGAGAGCGCAGCAGGGGA
GCTTCCAGGGGAAACGCTGGTATCTTATAGTCTGCGGGTTTCCGACCTCTGACTGAGCGTCGATTTTGTGATGCTGTCAGGGGGCGGAGCCTATGAAAAACGCC
AGCAACGCGGCTTTTACGGTCTTGGCTTTTGTGCGCTTTTGTCTACATGTTCTTCTGCTTATCCCTGATTCTGTGGATAACCGTATTACCGCTTTGAGTGAGCTGATAC
CGCTCGCGCAGCCGAACGACCGAGCGCAGCTAGTGAAGCAGTATACACTCCGCTATCGTACGTGAGTGGTCTGCTGCGCCCGACCCGCCAACCCGCTGACG
GGTGCACTCTCAGTACAATCTGCTCTGATGCGCATAGTTAAGCCAGTATACACTCCGCTATCGTACGTGAGTGGTCTGCTGCGCCCGACCCGCCAACCCGCTGACG
CGCCCTGACGGGCTTGTCTGCTCCCGCATCCGCTTACAGACAAGCTGTGACCGTCTCCGGGAGCTGATGTGTCAGAGGTTTTACCGTCAACCGAAACGCGCAGGAGCT
GCGGTAAAGCTCATCAGCTGGTGGTGAAGCGATTACAGATGTCTGCTGTTTCTCCGCTCCAGCTCGTTGAGTTTCTCAGAAAGCGTTAATGTCTGGCTTCTGATAAAGCGGG
CCATGTTAAGGGCGGTTTTTCTGTTGGTCACTGATGCTCGCTGAAGGGGATTTCTGTTATGGGGGTAATGATACCGATGAACGAGAGAGGATGCTCACGATACGGGT
TACTGATGATGAACATGCCGGTTACTGGAACGTTGTGAGGGTAACAACTGGCGGTATGGATGCGCGGGACAGAGAAAACTCACTCAGGGTCAATGCCAGCGCTTCTGTTAA
TACAGATGATGGTGTTCACAGGGTAGCCAGCAGCATCTGCGATGCAGATCCGGAACATAATGGTGACGGGCGCTGACTTCCGCTTCCAGACTTACGAAACCGGAAACCG
AAGACCATTATGTTGTTGCTCAGGTGCGACAGCTTTTGACGAGCAGTGCCTTACGTTGCTGCGTATCGGTGATTCTGCTAACCAGTAAGGCAACCCGCCAGCCTAG
CCGGTCTCAACGACAGGAGCAGCATCATGCGCACCCGTGGGGCCGCTATGCCGGGATAATGGCTGCTTCTGCGGAAACGTTTGGTGGCGGGACAGTGACGAAGGCTTG
AGCGAGGGCGTCAAGATTCCGAATACCGCAAGCGACAGGCCGATCATGTCGCGCTCCAGCGAAAGCGTCTCGCCGAAATGACCCAGAGCGCTCGCGGACCTGCTCTAC
GAGTTGATGATAAAGAGACAGTCATAAGTGCGGCGACGATAGTCATGCCCCGCGCCACCGGAAGGAGCTGACTGGGTTGAAGGCTCTCAAGGGCATCGGTGAGATCCCG
GTGCTAATGAGTGAGCTAACTACATTAATTGCGTGGCTCACTGCCGCTTCCAGTCCGGGAAACCTGCTGTCAGCTGCATTAAATGAATCGGCCAACGCGCGGGGAGAGG
CGGTTTGCATTATGGCGCGCAGGGTGGTTTTTCTTTACAGTGAGACGGGCAACGCTGATTGCCCTTACCGCTGCGCTGAGAGAGTTGAGCAAGCGGTCCAGCTGGT
TTGCCCCAGCAGGCGAAATCTGTTTGATGGTGGTTAACGGCGGGATATAACATGAGCTGCTTCGATGATCGTGTATCCCACTACCGAGATATCCGACCAACGCGCAGCCCG
GACTCGGTAATGGCGCGCATTGCGCCAGCGCCATCTGATGTTGGCAACGACATCGCAGTGGGAACGATGCCCTCATTACGATTTGATGTTTGTAAAAACCGACATGG
CACTCCAGTGCCTTCCGTTCCGATATCGGCTGAATTTGATTGCGAGTGAGATATTTATCCAGCCAGCCAGACGACGCGCCGAGACAGAACTTAAATGGGCCGCTAACAG
CGCATTTGCTGGTAGCCAAATGCGACGAGATGCTCCAGCCAGTCCGCTACCGTCTTATGGGAGAAAAATAACTGTTGATGGGTGCTGCTCAGAGACATCAAGAAATAAC
GCCGGAACATTAGTGACGAGCAGTTCACAGCAATGGCATCTGCTCATCCAGCGGATAGTTAATGATCAGCCACTGACGCGTTGCGCGAGAAGATTGTGACCCGCCGCTTTAC
AGGCTTGCAGCCGCTTCTGTTCTACCATGCACACCAACGCTGGCACCCAGTTGATCGCGCGGAGATTAATCGCCGCGACAATTTGCGACGGCGGTGCGAGGCCAGACTGGA
GGTGGCAACGCCAATCAGCAACGACTGTTTCCCGCCAGTTGTTGTGCCACGCGGTGGGAATGTAATTACGCTCCGCCATCGCGCTTCCACTTTTCCCGGTTTTTCGAGAAA
CGTGGCTGGCTGTTTACCACGCGGGAAAGGTTTTCGCCATTGATGGTGTCCGGGATCTCGACGCTCTCCCTATGCGACTCTGCATTAGGAAGCAGCCAGTAGTAGTTGAGG
CCGTTGAGCAGCGCGCGCAAGGAATGGTCATGCAAGGAGATGGCGCCCAACGCTCCCGGCCACGGGCTGCCACCATAACCGCCGAACAGCGCTCATGAGCCCG
AAGTGGGAGCCGATCTTCCCATCGGTGATGTCGGCGATATAGCGCCAGCAACCGCACTGTGGCGCCGGTATGCCGGCCAGTATGCGTCCGGCTAGAGGATCGAGATC
TCGATCCCGCAAAATTAACGACTCACTATAGGGGAATTGTGAGCGGATAACAATCCCTCTAGAAATAATTTGTTAACTTTAAGAAGGAGATATACATGGCTAGCTGGAG
CCACCCGAGTTCGAGAAAGGCTTAATATAACCAATATGTCATGTCGATGCTGCAAGGCCACCGATAGGCTGAGCACCACCAACCACTGAGATCCGGCTGCTAACA
AAGCCGAAAGGAGCTAGTTGGTGTGCCACCGCTGAGCAATAACTAGCATAAACCCCTGGGGCTCTAAACGGGTCTTGAGGGGTTTTTGTGAAGGAGGAATATATC
CGGAT

Figure S 9: pET-STRP3 expression vector sequence.

Important sequences; STREP-TAG NdeI SalI. ^ represents exact restriction sites.

Chapter 6. Conclusions and future Work

6.1 Conclusions

Herbicides, while necessary to ensure the high crop yields required to satisfy modern food demand, have one major limitation; they are often not selective enough and may damage crops (Green, 2014; Scarponi et al., 2009b). Safeners, first discovered in the late 1940's, are extremely important agrochemicals, conferring additional selectivity to herbicide products (Cataneo et al., 2013; Kraehmer et al., 2014; Matola et al., 2007; Scarponi et al., 2009a; Scarponi et al., 2009b; Scarponi et al., 2006). It is widely believed that safeners increase selectivity by enhancing herbicide detoxification in the crop but not the weed, through increased expression of xenobiotic detoxifying enzymes (Cataneo et al., 2013; Del Buono et al., 2007; Scarponi et al., 2009a; Scarponi et al., 2009b; Scarponi et al., 2006). Through extensive research and development, over twenty safeners have been developed, with many used extensively in herbicide products (Scarponi et al., 2006; Sivey et al., 2015). Interestingly, safeners have demonstrated botanical and chemical selectivity, conferring protection only in certain crops or to certain herbicides, respectively (Hatzios, 1991). Despite their widespread use, and extensive development, their mechanism of selectivity is largely unknown.

Due to the ever-increasing demands of regulatory authorities regarding new product development, including safener registration, it was important to gain a clearer understanding of safener effects, both specific and generic. The project was designed with the intention of understanding safener effects on herbicide metabolism and residue formation more clearly, with a specific focus on herbicide selectivity. The project aimed to determine:

- A. Does the presence of a safener causes a significant and long term change in metabolic/profile residue by;
 - 1. Leading to quantifiable changes in the metabolic profile of the herbicide?
 - 2. Generation of different metabolite(s) due to a change in the route of metabolism and/or;
 - 3. Increased levels of known metabolite(s) due to enhanced rate of metabolism?
- B. Can xenobiotic metabolism be better understood through *in silico* approaches?
- C. Can safener selectivity be understood and predicted by analyses of xenome gene and protein induction?

Here the outcomes of the research will be summarised, and related to the aims and hypotheses. The pipeline of studies is shown in Figure 60, for reference.

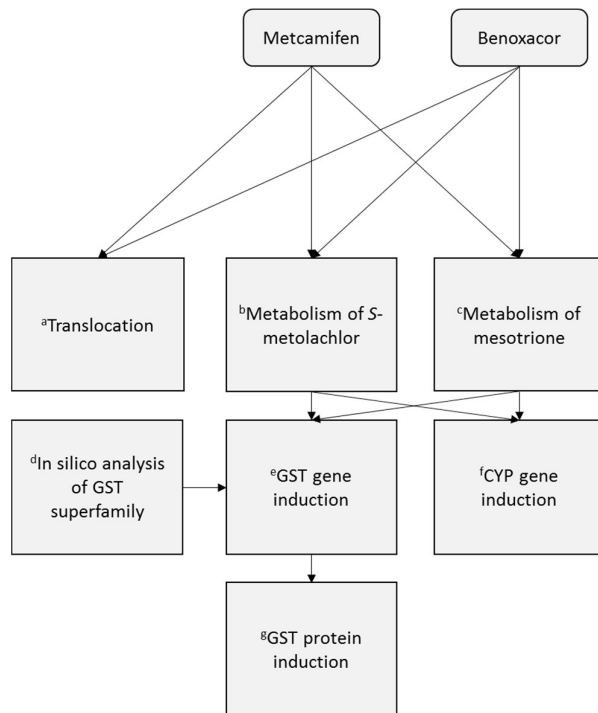


Figure 60: Study pipeline.

Superscript letters (a-g) are given for in-text reference.

A metabolic study (Figure 60. b-c) was designed to determine safener effects on residue profile, to analyse the longevity of metabolic effects, and by using multiple safener-herbicide combination, to identify safener selectivity, thereby addressing the project questions A, 1-3. This study utilised radio-labelled herbicides that could track the formation of metabolites using thin layer chromatography (TLC). Safeners and herbicides were chosen such that some combinations were expected to work more effectively than others and thus provide a system to investigate selectivity. The newly developed safener, metcamifen, was predicted to be more effective at metabolising mesotrione than benoxacor, and benoxacor was expected to metabolise *S*-metolachlor (*S*-moc) most efficiently. Cross combinations of these chemistries were used with the intention of providing information on chemical specificity. Metabolic effect longevity, with and without safeners, was analysed by following metabolite generation over several days. This also allowed the metabolic rate and route to be determined. Tissues were analysed independently, providing information that could indicate whether specific localisation provided a basis for selectivity.

The results of the study indicated that metcamifen caused a significantly higher enhancement of mesotrione metabolism than benoxacor, as expected on the basis of their known partner herbicides. Both metcamifen and benoxacor caused an increase in the metabolic rate of mesotrione, and showed no alteration to metabolic route: Mesotrione demonstrated only one route of catabolism, via an oxidative hydrolysis, and in all cases, the conversion to 4-hydroxy-mesotrione was the major step. Thus, it was determined that these safeners did not cause an alteration to the metabolic pathway of mesotrione, and they enhanced detoxification through an increased rate of the endogenous pathway. The longevity of the safener effects was determined, with each safener causing no significant effect on metabolism by 72 hours after application. Thus, no long term metabolic effects were observed. The metabolism of mesotrione, with and without safeners, occurred primarily in the leaf and stem tissues, with little observed in the roots. Therefore, since no safener-specific tissue localisation was observed, this was not considered to be a mechanism for conferring selectivity.

The unsafened metabolism of *S*-moc was so rapid that no safener effects could be observed. This meant that questions regarding safener effects on the *S*-moc metabolic profile could not be directly answered. Also comparisons with mesotrione could not be made, and thus the selectivity of the safeners could not be fully cross-checked. However, the metabolism of *S*-moc was observed, and many conclusions could be made. The safeners did not cause a long term alteration to metabolic profile, with the metabolite levels unaffected at the times investigated. If herbicide metabolism was enhanced by the safeners, this must have occurred before 4.5 hours. *S*-moc was known from previous studies to be catabolised by one of two pathways, oxidative or via glutathionylation (Syngenta personal comm.). It was determined that the glutathionylation-based metabolism of *S*-moc was more active than the oxidative metabolism, and no effects were observed with the safeners. The metabolic rate of *S*-moc appeared identical in all tissues, including the root, which was in contrast to mesotrione. Therefore, no tissue specificity was observed, and was not considered to be a mechanism for selectivity.

A possible explanation for the high metabolism of *S*-moc compared to mesotrione is that the high constitutive activity of GST enzymes would metabolise *S*-moc but not the exclusively oxidised mesotrione. Considering the root metabolism of *S*-moc exceeded that of mesotrione, it could be predicted that these GSTs would localise in the root. It was hypothesised that root exudated enzymes may have contributed to pre-uptake metabolism. This hypothesis was

based on the knowledge that oxidoreductases and peroxidases, major phase I enzymes, have been detected in root exudates (Gramss et al., 1999; Rani et al., 2015). GSTs and the GSH cofactor, involved in phase II metabolism, have also been detected in root exudates (Rani et al., 2015; Rani et al., 2016). In addition the applied levels of S-moc may have been insufficient for observation of metabolism. Interestingly, the uptake of each herbicide occurred differently, with mesotrione showing a consistent uptake rate, and S-moc showing an early concentrating effect; S-moc was initially taken into the plant at a higher concentration than applied, followed by a reduction to the application dose. Analysis of the physicochemical properties of each herbicide provided a suitable explanation for this effect; that S-moc had properties more suitable for uptake through the plant roots than mesotrione.

In addition to the hypothesis testing, a system for rapid and accurate analysis of herbicide metabolism, and safener effects thereupon, has been developed. This could prove very useful in safener screening, prior to expensive, large scale metabolic studies.

To determine whether the selectivity of the Safeners towards the herbicides could be explained by differences in safener uptake or translocation, the movement of the safeners was investigated using radiolabelling (Figure 60.a). This study was also designed to indicate whether safeners localised to specific tissues, which could explain their selectivity. It was determined that benoxacor was taken up and distributed throughout the plant at a higher rate than metcamifen. Since metcamifen caused the greater enhancement to mesotrione metabolism, this result indicated that safener translocation was unlikely to be responsible for safener selectivity. In addition, no specific safener localisation was observed, with metcamifen and benoxacor distributing evenly throughout the plant tissues. The only accumulation of safeners was in the leaf tips, consistent with an aerial movement of compounds (Deboer et al., 2014). The differential translocation rate of the safeners was attributed to the physicochemical properties of the compounds. Such parameters could therefore be used as predictors of safener mobility, though not providing information on efficacy.

Following the results of the metabolic study, a close investigation of the GST superfamily was performed (Figure 60.d). The role of this xenome enzyme family in safener-induced metabolism has been verified in many crops and compound combinations, and offered an opportunity to gain a deeper insight of the systems governing safening. The aim was to understand which GSTs were involved in the specific safener effects, and to determine if these effects could be understood by *in silico* analysis, thereby addressing the project question B.

Considering their importance in safening, it was important to fully understand the whole enzyme family, which has not been fully analysed for nearly two decades in the maize crop (Mcgonigle et al., 2000).

Firstly, the GSTs sequences from maize were isolated from the B73 RefGen_v4 maize genome, through NCBI, producing a comprehensive list of the superfamily, and the phylogenetic relationship of the enzymes was determined. Since the current nomenclature system for this enzyme class was identified as sporadic and based, in part, on order of discovery, a new system was proposed, including information on sequence similarity for a better understanding of individual enzymes. A new decimal number was introduced to the nomenclature, based on subclasses with similar sequences, as determined by the phylogenetic analysis. The proposed system uses “[*source organism binomial*]*GST*[class letter][subclass]. [phylogenetic order]”. For example the well characterised dimer, ZmGSTF1-1, would be named ZmGSTF2.0-2.0. It is hoped that this system will be implemented, leading to a unified classification in the field. A chromosomal analysis was performed, supporting the findings of sequence relationship, and providing an understanding of maize GST evolution to its now large and diverse collection. Investigation of the protein domain structure determined that general class structure was shared between all GSTs, with the most variation observed in the terminal extensions. The interface residue analysis revealed that, contrary to previous findings (Dixon et al., 2005), hydrophilic residues are used more often at the predicted dimer interfaces. By comparing all of the annotated G-sites, common alignment positions and residues were identified. In many cases a variety of different residues were used in the hydrogen-bonding of glutathione, however these residues possessed similar properties. The H-sites showed a higher degree of variation in alignment position, and residues used, forming a likely basis of substrate selectivity. Motifs have been identified that will make H-site identification much easier in the future. The predicted 3D structures of each GST, as determined through homology modelling, highlighted the similarity of GST structure within and between classes. Only the oligomerisation pattern was noticeably different, with lambda and DHAR classes showing no dimerisation and GHR showing a unique Xi dimer orientation, in contrast to the typical GST dimerisation. However, one limitation of homology modelling is that tertiary structure prediction may not be accurate. A range of targeting sequences were identified on each GST enzyme by predictive software, providing an insight into their potential subcellular localisation. While it would have to be verified *in vivo* or *in vitro*, it was predicted that a number of GSTs

may localise to various organelles including the chloroplast and mitochondria, and there may be some extracellular role for certain GSTs. So far, there is little evidence of GSTs functioning in such diverse subcellular locations, and this should be investigated more closely to ensure the roles of GSTs are not incorrectly assigned by assuming cytosolic localisation. Investigation of literature and a proteome database in section 4.2.9 supported the likelihood of GSTs localising to diverse subcellular organelles in arabidopsis. To determine which GSTs were endogenously expressed, their expression throughout maize development was determined through analysis of experimental databases. From this it was determined that few changes in GST expression occurred over time, and many GSTs genes were inactive. *ZmGSTF2.0*, *ZmGSTF1.0*, *ZmGSTF1.1* and *ZmGSTF1.2* and DHAR3 represented the GSTs most highly expressed in all developmental stages. The same analysis was carried out in different maize tissues, which discovered a low degree of localised expression. The same five GST genes, highly expressed in development, were also the greatest expressed in the tissue analysis. The *in silico* analysis therefore provided a basis for understanding generic and specific roles of this important enzyme family in xenobiotic detoxification.

In order to understand the roles of individual GST superfamily members in safening, thereby addressing project question C, next generation sequencing data was analysed, providing insight into safener selectivity and allowing determination of safener-induced GSTs. It was observed that metcamifen and benoxacor caused very similar effects on GST expression. The tau, zeta and DHAR classes were affected equally by the safeners while theta, phi and lambda classes showed a slightly higher effect upon metcamifen treatment than benoxacor treatment. The GHR class showed a lack of statistical correlation between the treatments, likely as a result of low sample size. The safeners caused a high induction of fifteen transcripts; *ZmGST- F2.1*, *F2.3*, *L1.0*, *L1.2*, *L1.3*, *U1.0*, *U1.2*, *U3.0*, *U3.1*, *U5.2*, *U5.6*, *U8.0*, *U9.3/9.4*, and *U10.3*. By further focusing on highly induced GSTs and including relevant CYPs, and by investigating whole maize plants at more physiologically relevant times, a greater understanding of the safener effects on xenome enzymes was provided (Figure 60.e-f). qPCR analysis identified differential induction of *ZmGSTU1.2*, *ZmGSTF2.3* and *ZmGSTL1.3* in different maize tissues. Most of the safener effects were observed in the aerial tissues. *ZmGSTU1.2* showed a higher induction with benoxacor than metcamifen, especially in the stem. *ZmGSTF2.3* was induced preferentially by metcamifen, rather than benoxacor, especially from 24 hours. *ZmGSTL1.3* expression was enhanced with benoxacor at early times and metcamifen at later times, mostly

observed in the aerial tissues. Also, the time dependence of the gene induction, with benoxacor causing inductive effects earlier than metcamifen, can be explained by the translocation rates of the safeners, which demonstrated the same trend. Despite the exclusively oxidation-based metabolism of mesotrione, the Safener-induced expression of these GSTs showed some correlation with the Safener-induced metabolism of mesotrione. The Safener effects on metabolism and on expression were seen mostly in the aerial tissues. In addition, the Safener-induced expression of *ZmGSTF2.3* and *ZmGSTL1.3* correlated well with the observed Safener-induced metabolic effects with mesotrione.

Absolute quantification using g-blocks as standards was performed to determine the tissue specificity and biological relevance of the xenome enzyme expression. As suggested earlier, a high root GST content may explain the higher metabolism of *S*-moc than mesotrione. Indeed, the results indicated that the most GST expression occurred in the roots, representing over 85% of the GST expression in the three tissues at 3 hours. Therefore, the rapid *S*-moc metabolism may be attributed to this high endogenous GST expression. Similarly, the tissue expression pattern of rice GSTs indicated a higher shoot expression than root and leaf (Frova, 2003). Thus a high root GST expression cannot be assumed to be universal, and may be specific to a subset of genes.

The protein levels of *ZmGSTF2.0-2.3* and *ZmGSTU1.2-1.2* were also assessed (Figure 60.g), and showed that the safener-induced transcript expression pattern of *ZmGSTU1.2* was mirrored in protein levels. The pattern observed for *ZmGSTF2.0-2.3* was more complex, and showed less similarity to the transcript induction. This may be as a result of the complexity in investigating a heterodimer, or could reflect a translational effect.

The CYP genes investigated, CYP81A9, CYP81A4, and CYP72A5 displayed less extreme inductive responses to the safeners, than the GSTs. Metcamifen caused induction of all three genes in all tissues, in most cases greater than that conferred by benoxacor. Benoxacor caused large induction mainly at 3 hours in the stem. Thus the same time dependency of effect as the GSTs was observed. The effect of the Safeners on expression of the CYPs showed some similarity to the effects on mesotrione metabolism. Metcamifen had a greater impact on mesotrione metabolism, and the largest impact on CYP expression. Similarly the greatest metabolic and expression effects were observed in the aerial tissues.

The G-block analysis indicated that CYP72A5 was present in extremely low abundance, possibly too low for significant function in metabolism. In contrast to the GSTs, the expression of all CYPs was greatest in the leaves. This high expression of CYPs in the leaves has been attributed to involvement in leaf initiation and senescence, though this may be attributed to a specific subset of genes (Christ et al., 2013; Miyoshi et al., 2004).

The identified differential tissue expression of GSTs and CYPs, in the roots and leaves, respectively, may be important for the detoxification of herbicides applied in different manners. Certain herbicides may be metabolised primarily by GSTs in the roots, while other herbicides are metabolised primarily by CYPs in the leaves. This theory is supported by the metabolic data, in which *S*-moc was metabolised extensively in the roots via glutathionylation, while mesotrione was metabolised oxidatively in the aerial tissues.

To investigate the possible signalling pathways through which Safeners exert their effect on GST expression, a range of abiotic stress experiments were analysed. It was observed that both submergence stress and 12-OPDA application caused similar GST expression profiles as the safeners. Thus it is possible that safeners enhance certain GSTs through the same or similar pathways as those used for such stresses. The submergence stress is known to cause a response through a signalling pathway involving ethylene, while the 12-OPDA effect is known to occur through a specialised TGA transcription factor pathway. Thus safeners may tap into existing specialised pathways to elicit the GST expression responses. The known similarity of safener signalling with salicylic acid signalling supports this hypothesis (Behringer et al., 2011). However, the software only allowed for analysis of a limited number of stresses, potentially overlooking other signalling pathways involved.

By combining all analyses in this thesis, the method of chemical selectivity observed in safeners, can be proposed (Figure 61). The ability of metcamifen and benoxacor to induce the expression of xenome enzymes has been demonstrated, with metcamifen having a greater effect on phi class GSTs and benoxacor having a greater effect on tau class GSTs. It has also been observed that safeners inducing phi class GST expression may be more effective at metabolising chloroacetanilide and thiocarbamate herbicides, while those inducing tau class GSTs may be more effective at metabolising diphenylether and aryloxyphenoxypropionate herbicides. In addition, knowledge on how each herbicide is metabolised, can be combined with information on whether safeners induce CYPs or GSTs, to provide predictions on the effective safener-herbicide combinations. The observed tissue specificity of gene induction

may also provide clues to chemical selectivity. It is proposed that stem active herbicides such as *S*-moc and other chloroacetanilides, are metabolised faster when treated with safeners, such as benoxacor, which upregulate stem xenome enzymes. Conversely, it is proposed that leaf active herbicides such as mesotrione and other HPPD-inhibitors, are metabolised more effectively when treated with safeners, such as metcamifen, which upregulate xenome enzymes in the leaves. Due to the complexity of this proposal, the tissue specificity is not included in Figure 61. If this system can be confirmed, then effective safener-herbicide partners could be predicted.

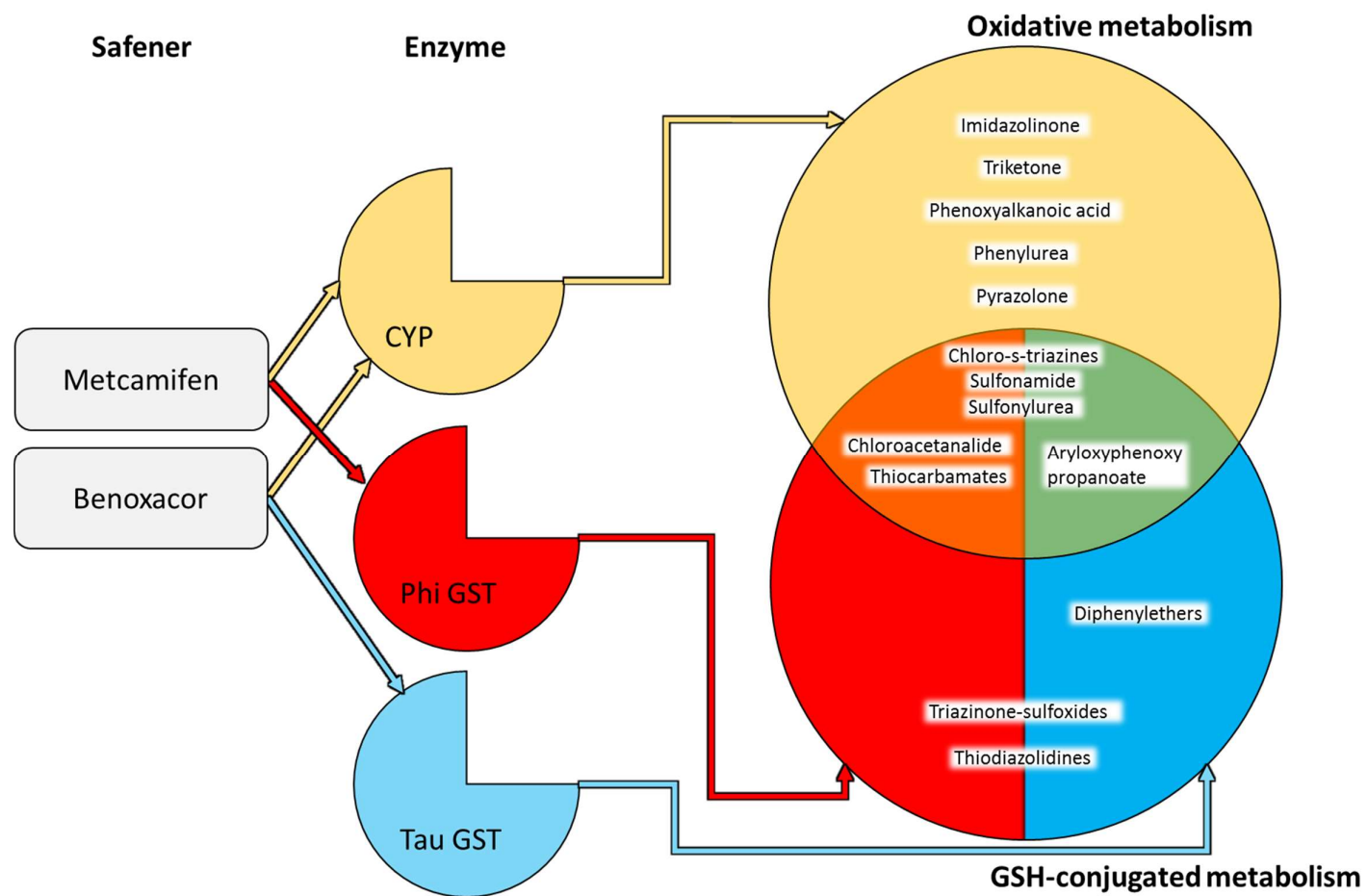


Figure 61: Proposed system of safener selectivity.
Colours represent interactions.

This thesis has determined that the metabolism of herbicides in maize plants is a rapid step, not lasting more than a few days. The safening process occurs through an enhancement of metabolic rate, with no alteration to the catabolic pathways. This rate alteration is also very transient, effectively terminating within three days, indicating safeners cause no long term effects or alterations to final residue profile, and do not pose a concern for regulatory authorities.

It has been determined that safeners are selective towards enhancing the metabolism of specific herbicide substrates, and that metcamifen causes the most potent enhancement of mesotrione metabolism, compared to benoxacor. It has been determined that safener mobility does not play a primary role in the mechanism of this selectivity, and that safeners do not accumulate in specific tissues. Glutathionylated herbicides such as S-moc may be metabolised even more rapidly due to high root GST levels.

The GST enzyme family has been studied extensively, and it is clear that by possessing a diverse range of sequences in defined classes and subclasses, with specific and redundant functions and substrate specificities, a huge range of xenome responses are available to plants. This *in silico* analysis is an important step in understanding the mechanisms of Safeners, and may provide a basis for future work using computer-based analysis to predict safener efficacy. The methods used here may be applied to other enzyme families with roles in the xenome, to create greater understanding of Safener action.

The complex regulation of specific enzymes mediates the unique effects of each safener. While genes such as *ZmGSTL1.3* may be upregulated by safeners, their role in safening is unclear, as they are not associated with xenobiotic detoxification. Since the safener-specific induction of *ZmGSTU1.2* contrasts that of mesotrione metabolism, this enzyme likely has no involvement in mesotrione metabolism. With a transcript regulation matching the metabolic effects on mesotrione, *ZmGSTF2.3* may be involved in mediating the safener action upon mesotrione, though this must be indirect, since mesotrione is not metabolised directly by the action of GSTs. This could be through involvement in signalling pathways, and indeed GSTs have been shown to regulate redox signalling pathways that transcriptionally activate defense genes (Cummins et al., 2013).

GSTs have also demonstrated protective responses through functions other than glutathione-conjugation. For example, herbicide Safeners have been shown to induce GSTs in blackgrass

which enhanced tolerance to paraquat, through GPOX activity reducing oxidative injury, rather than glutathione conjugation (Cummins et al., 1999). Similarly multiple herbicide resistance (MHR) in blackgrass and annual rye grass, was associated with increased expression of a GST with limited ability to metabolise herbicides, through accumulation of protective flavonoids via ligandin function (Cummins et al., 2013). This included protection against chlortoluron, a herbicide not metabolised by GSTs (Cummins et al., 2013). However, this would not explain the effect upon mesotrione metabolism.

Other candidate genes for involvement in safening are those highly upregulated by the safeners; *ZmGST-F2.1*, *L1.0*, *L1.2*, *U1.0*, *U3.0*, *U3.1*, *U5.2*, *U5.6*, *U8.0*, *U9.3/9.4*, and *U10.3*. A number of GSTs have been observed as endogenously expressed, with little stimulation by safener, and thus likely play roles in basic cell function. *ZmGSTF2.0*, *ZmGSTF1.0*, *ZmGSTF1.1*, *ZmGSTF1.2* and *DHAR3* should therefore be considered non-safener responsive GSTs, and are likely vital for the healthy development of maize plants.

The data presented in this thesis not only provide specific results for the compounds investigated, but also provide a methodology for small scale analyses of safener efficacy, and metabolic, transcriptomic and proteomic effects. Such methodologies could be adapted to industrial use, to avoid or precede large scale field trials.

The data presented in this thesis highlights the complexity of agrochemical interactions on plant metabolism. While many trends can be observed, it is difficult to fully understand the entire biosystem. Safeners act upon a huge variety of enzymes, each with unique transcriptional and translational effects. These enzymes may be directly involved in metabolism or may function in general stress response or as part of a signalling pathway. The substrate-specificity of such enzymes is dependent on subtle changes in their protein sequences, affecting active site interactions with xenobiotics, which are not clear. While the movement of Safeners can be explained by physicochemical properties, the method of Safener effects on gene expression are still elusive. It is important for a full understanding of Safener effects to identify the way in which Safeners elicit their effects, whether this is through interactions with transcriptional regulators, or a modification of plant defenses.

6.2 Future work

The lack of safener effects observed with *S*-moc metabolism prevented the cross comparison of safener selectivity. It was hypothesised that metcamifen would preferentially enhance the metabolism of mesotrione, while benoxacor would preferentially enhance the metabolism of *S*-moc. The cross comparison would have provided an excellent example of safener chemical selectivity, and provided a clear basis for understanding such selective protection. Unfortunately, the metabolism of *S*-moc was far more rapid than anticipated, and any safener effects were unobservable as a result. Due to the nature of the experiment, which relied on specialised facilities at the Syngenta international research centre (Jealott's Hill, UK) preliminary tests to determine metabolic rate, and therefore optimise the times investigated, were impossible. Therefore, further investigation of the safener effects on *S*-moc, focusing on earlier times, and possibly with altered chemical concentrations, would be valuable. It is possible that metabolism of the herbicide began before uptake into the plant, by root exudate enzymes, and this should be taken into consideration when performing this experiment. The dose solution not taken up by the plant and the root wash were not tested for metabolites, as this consideration had not been made at the time. This additional step could provide evidence of pre-plant metabolism. Future studies should focus on the enzyme profiles and enhanced metabolic effects of root associated material. It is also possible that the high metabolic rate was related in some way to the concentrating effect observed with *S*-moc uptake, which should be investigated further.

The system developed during this project for rapid testing of metabolic effects caused by safeners in whole plants, using hydroponics and radiolabelled herbicides, could be used during the screening process of safener development. It could also be used to test existing safener-herbicide partners, on a more comprehensive scale. This would certainly provide a wealth of information on safener selectivity, efficacy and the nature of metabolic enhancement.

The benefit of superfamily *in silico* analyses cannot be emphasised enough, and should be performed far more often than they currently are. With the rapid growth of publicly available genomes, there is no reason why important enzyme classes should not be investigated comprehensively. It would be advisable, for an even greater understanding of safener action, to perform comprehensive, genome-wide, *in silico* analyses, on other xenome enzymes involved in safening. The CYP enzyme superfamily would be a good candidate for such analysis, as has not been performed comprehensively in maize. One *in silico* study attempted in this

project that proved unsuccessful was the use of computer software to predict binding affinities of GSTs with herbicide substrates. This was tested using the Autodock Vina plugin of Chimera, with homology models of each GST family member, and a variety of substrates. The hypothesis was that this software could predict binding affinities, which may be proportional to enzyme activity to specific substrates, and could be used as a predictor of herbicide targets. However, preliminary testing with control enzymes and substrates, the affinities of which were already known, demonstrated no relationship between predicted and actual affinity. Thus the system could not be validated. If further work was directed to optimising the system, such that binding affinity could be accurately predicted, it could act as an early phase in the screening of new safeners, or even in determining the direction of new product development. It could also determine important residues involved in substrate binding, and allow artificial manipulation of existing xenome enzymes towards higher metabolic activity, through site-directed mutagenesis (Perperopoulou et al., 2018). Also, the *in silico* analysis provided predictions on GST subcellular localisations, and further study should focus on validating these predictions. Being able to predict the precise subcellular localisation of maize GSTs *in silico*, would ensure their function is not misinterpreted.

While studying the safener effects on xenome enzyme protein regulation, a few problems occurred. The main problem was the specificity of the available antibodies. The antibody raised to ZmGSTF2.0-2.3 was able to recognise both ZmGSTF2.0 and ZmGSTF2.3, the masses of which were separated by only 0.1 kDa, far too low for resolution by SDS-PAGE. Since this study had the potential to verify that no translational effects were evident in the safener-induction of ZmGSTF2.3, it would be beneficial to resolve the issues mentioned. Time constraints rendered the development of new, more specific antibodies, impractical. Future work should be directed towards determining if the transcript analysis is matched to the protein analysis, which would allow quick, accurate, and relatively cheap, qPCR to be used instead of western blotting.

Another study which was not completed due to technical problems was the analysis of recombinant protein activity against an array of substrates. The aim of the experiment was to link the safener-induced expression of GSTs to their activity upon specific substrates. This would have allowed testing of the hypothesis that safener selectivity is based on specific regulation of xenome enzymes with specific substrate activities. The recombinant proteins, expressed for the purpose of western blot quantification, were to be exposed to various

herbicide substrates, *in vitro*, and the resulting rate of metabolism analysed by mass spectrometry. However, problems with the mass spectrometry method occurred, specifically that reference standards of tested compounds could not be quantified accurately. It appeared that the ionisation spectra of certain herbicides contained unrecognised, aberrant peaks. In addition, the sensitivity of the apparatus was not sufficient to produce clear, significant results from the *in vitro* system used. Future work should focus on optimising the mass spectrometric analysis of the *in vitro* system. In addition it would be interesting to perform an *in vitro* study, analysing the GST activities of safener-treated maize. To generate a full understanding of the involvement of GSTs in safening, with respect to specificity, the regulation of the enzymes and their activities on relevant substrates should be carried out in tandem, though the huge number of combinations would make this very difficult and time consuming.

As mentioned in section 5.4, to confirm that selectivity of xenome enzymes contributes to Safener selectivity, the role of each enzyme in crop protection would have to be verified. Enzyme knockouts and overexpression studies would provide valuable information on the importance of each enzyme in the Safener effect.

A potential future study could analyse the effects of Safeners on herbicide metabolism at the field scale. This would allow application of the agrochemicals under commercial conditions, allowing for a more accurate understanding of the effects of Safeners in the field. In addition, the results could be compared to those in this thesis, which would determine the validity of small scale studies in predicting large scale studies.

Personally, it appears that systems biology offers the greatest hope of understanding the extremely complex systems involved in safener action. Only through a complete understanding of how all xenome enzymes coordinate the safener response, and how the signalling pathways are mediated, can the process be directed towards producing ever more effective and reliable products. The rapid advancement of technology, especially in 'omic' sciences, is likely going to lead this frontier. Already meta-analyses are increasing in frequency and reliability, and their usefulness cannot be overstated. The use of experimental databases in section 4.2.10 and 5.2.4 is a perfect example of how publicly available data can be used in countless ways. Modelling of data such as is presented in this thesis, will prove invaluable in generating comprehensive systems understanding, especially with respect to external perturbation.

Abbreviations

Abbreviations	Word(s)
A	Absorbance
b	Pathlength
bp	Base pairs
*g	Relative centrifugal force
c	Concentration
[¹² C]	Carbon-12 (non-radioactive isotope)
[¹⁴ C]	Carbon-14 (radioactive isotope)
°C	Degrees Celsius
cDNA	Complementary DNA
CDNB	1-chloro-2,4-dinitrobenzene
cm	Centimetre
Cq	Quantification cycle
Ct	Threshold cycle
cv.	Cultivar
CYP	Cytochrome P450 mixed-function oxidase
d	Day
DHAR	Dehydroascorbate reductase
DNA	Deoxyribonucleic acid
DMSO	Dimethyl sulfoxide
EDTA	Ethylenediaminetetraacetic acid
F	Phi class GST
g	Gram
GHR	Glutathionyl-hydroquinone reductase
GSH	Glutathione
GST	Glutathione-S-Transferase
h	Hour
HCl	Hydrochloric acid
HPLC	High-performance liquid chromatography
kb	Kilobase-pairs
kDa	Kilodalton
L	Litre
	Lambda class GST
M	Molar
mg	Milligram
min	Minute
mL	Millilitre
mM	Millomolar
mmol	Millimole
nkat	Nanokatal
pc	Personal communication
qPCR	Quantitative Polymerase chain reaction
RNA	Ribonucleic acid
RPM	Revolutions per minute
s	Second

Abbreviations	Word(s)
SD	Standard Deviation
SDS	Sodium dodecyl sulfate
SDS-PAGE	SDS-polyacrylamide gel electrophoresis
T	Theta class GST
TLC	Thin layer chromatography
U	Tau class GST
UV	Ultraviolet
v/v	Volume to volume
v/w	Volume to weight
w/v	Weight to volume
w/w	Weight to weight
Z	Zeta class GST
Greek abbreviations	
Δ	Delta (change)
ε	Molar extinction coefficient
μg	Microgram
μL	Microlitre
μM	Micromolar
Latin abbreviations	
<i>At</i>	<i>Amaranthus tuberculatus</i> (Waterhemp)
	<i>Arabidopsis thaliana</i> (Arabidopsis)
<i>As</i>	<i>Avena sativa</i> (Oat)
<i>Dc</i>	<i>Dracaena cambodiana</i> (Cambodian dragon tree)
<i>E. coli</i>	<i>Escherichia coli</i>
<i>Ev</i>	<i>Eriochloa villosa</i> (Woolly cupgrass)
<i>Gm</i>	<i>Glycine max</i> (Soybean)
<i>Gsp.</i>	<i>Gossypium sp.</i> (Cotton)
<i>Ht</i>	<i>Helianthus tuberosus</i> (Jerusalem artichoke)
<i>Hv</i>	<i>Hordeum vulgare</i> (Barley)
<i>Nsp.</i>	<i>Nicotinia. sp</i> (Tobacco)
<i>Os</i>	<i>Oryza sativa</i> (Rice)
<i>Sb</i>	<i>Sorghum bicolor</i> (Sorghum)
<i>Sc</i>	<i>Secale cereale</i> (Rye)
<i>So</i>	<i>Saccharum officinarum</i> (Sugarcane)
<i>St</i>	<i>Solanum tuberosum</i> (Potato)
<i>Ta</i>	<i>Triticum aestivum</i> (Wheat)
<i>Tsp.</i>	<i>Tulipa sp.</i> (Tulip)
<i>Vr</i>	<i>Vigna radiate</i> (Mung bean)
<i>xT</i>	<i>x-Triticosecale</i> (Triticale)
<i>Zm</i>	<i>Zea mays</i> (Corn)

Bibliography

- Abrol, D. P., & Shankar, U. (2014). Pesticides, Food Safety and Integrated Pest Management. 167-199.
- ACURON® Herbicide Label. (accessed 2018). Retrieved from <https://www.syngenta.ca/pdf/labels/>
- Ahrens, W. (1994). *Herbicide Handbook* (7th ed.). Champaign, IL: Weed Science Society of America.
- Al-Khatib, K., Unland, J. B., Olson, B. L. S., & Graham, D. W. (2002). Alachlor and metolachlor transformation pattern in corn and soil. *Weed Science*, 50(5), 581-586.
- Alferness, P., & Wiebe, L. (2002). Determination of mesotrione residues and metabolites in crops, soil, and water by liquid chromatography with fluorescence detection. *Journal of Agricultural and Food Chemistry*, 50(14), 3926-3934.
- Andrews, C. J., Cummins, I., Skipsey, M., Grundy, N. M., et al. (2005). Purification and characterisation of a family of glutathione transferases with roles in herbicide detoxification in soybean (*Glycine max* L.); selective enhancement by herbicides and herbicide safeners. *Pesticide Biochemistry and Physiology*, 82(3), 205-219.
- Axarli, I., Dhavala, P., Papageorgiou, A. C., & Labrou, N. E. (2009a). Crystal structure of Glycine max glutathione transferase in complex with glutathione: investigation of the mechanism operating by the Tau class glutathione transferases. *Biochemical Journal*, 422(2), 247-256.
- Axarli, I., Dhavala, P., Papageorgiou, A. C., & Labrou, N. E. (2009b). Crystallographic and functional characterization of the fluorodifen-inducible glutathione transferase from *Glycine max* reveals an active site topography suited for diphenylether herbicides and a novel L-site. *Journal of Molecular Biology*, 385(3), 984-1002.
- Axarli, I., Georgiadou, C., Dhavala, P., Papageorgiou, A. C., et al. (2010). Investigation of the role of conserved residues Ser13, Asn48 and Pro49 in the catalytic mechanism of the tau class glutathione transferase from *Glycine max*. *Biochimica et Biophysica Acta*, 1804(4), 662-667.
- Bartholomew, D. M., Van Dyk, D. E., Lau, S. M., O'Keefe, D. P., et al. (2002). Alternate energy-dependent pathways for the vacuolar uptake of glucose and glutathione conjugates. *Plant Physiology*, 130(3), 1562-1572.
- Behringer, C., Bartsch, K., & Schaller, A. (2011). Safeners recruit multiple signalling pathways for the orchestrated induction of the cellular xenobiotic detoxification machinery in *Arabidopsis*. *Plant Cell & Environment*, 34(11), 1970-1985.
- Benkert, P., Biasini, M., & Schwede, T. (2011). Toward the estimation of the absolute quality of individual protein structure models. *Bioinformatics*, 27(3), 343-350.
- Bienert, S., Waterhouse, A., de Beer, T. A., Tauriello, G., et al. (2017). The SWISS-MODEL Repository-new features and functionality. *Nucleic Acids Research*, 45(D1), D313-D319.
- Bijman, J., & Tait, J. (2002). Public policies influencing innovation in the agrochemical, biotechnology and seed industries. *Science and Public Policy*, 29(4), 245-251.
- Blum, R., Beck, A., Korte, A., Stengel, A., et al. (2007). Function of phytochelatin synthase in catabolism of glutathione-conjugates. *The Plant Journal*, 49(4), 740-749.
- Bolwell, P. G., Bozak, K., & Zimmerlin, A. (1994). Plant cytochrome p450. *Phytochemistry*, 37(6), 1491-1506.

- Bordoli, L., Kiefer, F., Arnold, K., Benkert, P., et al. (2009). Protein structure homology modeling using SWISS-MODEL workspace. *Nature Protocols*, 4(1), 1-13.
- Brazier-Hicks, M., Evans, K. M., Cunningham, O. D., Hodgson, D. R., et al. (2008). Catabolism of glutathione conjugates in *Arabidopsis thaliana*. Role in metabolic reactivation of the herbicide safener fenclorim. *Journal of Biological Chemistry*, 283(30), 21102-21112.
- Brazier-Hicks, M., Gershater, M., Dixon, D., & Edwards, R. (2017). Substrate specificity and safener inducibility of the plant UDP-glucose-dependent family 1 glycosyltransferase super-family. *Plant Biotechnology Journal*, 16(1), 337 - 348.
- Brazier-Hicks, M., Howell, A., Cohn, J., Hawkes, T., et al. (2020). Chemically induced herbicide tolerance in rice by the safener metcamifen is associated with a phased stress response. *Journal of Experimental Botany*, 71(1), 411-421.
- Brown, H. M. (1990). Mode of Action, Crop Selectivity, and Soil Relations of the Sulfonylurea Herbicides. *Pesticide Science*, 29(3), 263-281.
- Campe, R., Hollenbach, E., Kammerer, L., Hendriks, J., et al. (2018). A new herbicidal site of action: Cinmethylin binds to acyl-ACP thioesterase and inhibits plant fatty acid biosynthesis. *Pesticide Biochemistry and Physiology*, 148, 116-125.
- Carringer, R. D., Rieck, C. E., & Bush, L. P. (1978). Metabolism of EPTC in Corn (*Zea mays*). *Weed Science*, 26(2), 157-160.
- Carvalho, S. J. P. d., Nicolai, M., Ferreira, R. R., Figueira, A. V. d. O., et al. (2009). Herbicide selectivity by differential metabolism: considerations for reducing crop damages. *Scientia Agricola*, 66(1), 136-142.
- Cataneo, A. C., Ferreira, L. C., Mischak, M. M., Velini, E. D., et al. (2013). Mefenpyr-diethyl action on fenoxaprop-p-ethyl detoxification in wheat varieties. *Planta Daninha*, 31(2), 387-393.
- Chew, O., Whelan, J., & Millar, A. H. (2003). Molecular definition of the ascorbate-glutathione cycle in *Arabidopsis* mitochondria reveals dual targeting of antioxidant defenses in plants. *Journal of Biological Chemistry*, 278(47), 46869-46877.
- Cho, H. Y., & Kong, K. H. (2007). Study on the biochemical characterization of herbicide detoxification enzyme, glutathione S-transferase. *BioFactors*, 30(4), 281-287.
- Christ, B., Sussenbacher, I., Moser, S., Bichsel, N., et al. (2013). Cytochrome P450 CYP89A9 is involved in the formation of major chlorophyll catabolites during leaf senescence in *Arabidopsis*. *Plant Cell*, 25(5), 1868-1880.
- Cobb, A. H., & Reade, J. P. H. (2011). *Herbicides and Plant Physiology* (Vol. 7.1): John Wiley & Sons.
- Cole D. J., C. I., Hatton P. J., Dixon D., Edwards R. . (1997). *Glutathione transferases in crops and weeds*: Wiley, Chichester, UK.
- Cole, D. J., & Edwards, R. (2000). *Secondary metabolism of agrochemicals in plants*.: John Wiley & Sons.
- Coleman, J., Blake-Kalff, M., & Davies, E. (1997). Detoxification of xenobiotics by plants: chemical modification and vacuolar compartmentation. *TRENDS in Plant Science*, 2(4), 144-151.
- Colovic, M. B., Krstic, D. Z., Lazarevic-Pasti, T. D., Bondzic, A. M., et al. (2013). Acetylcholinesterase inhibitors: pharmacology and toxicology. *Current Neuropharmacology*, 11(3), 315-335.
- Cottingham, C. K., & Hatzios, K. K. (1991). Influence of the Safener Benoxacor on the Metabolism of Metolachlor in Corn. *Zeitschrift Fur Naturforschung C-a Journal of Biosciences*, 46(9-10), 846-849.

- Cummins, I., Burnet, M., & Edwards, R. (2001). Biochemical characterisation of esterases active in hydrolysing xenobiotics in wheat and competing weeds. *Physiologia Plantarum*, 113(4), 477-485.
- Cummins, I., Cole, D. J., & Edwards, R. (1997). Purification of multiple glutathione transferases involved in herbicide detoxification from wheat (*Triticum aestivum* L.) treated with the safener fenchlorazole-ethyl. *Pesticide Biochemistry and Physiology*, 59(1), 35-49.
- Cummins, I., Cole, D. J., & Edwards, R. (1999). A role for glutathione transferases functioning as glutathione peroxidases in resistance to multiple herbicides in black-grass. *The Plant Journal*, 18(3), 285-292.
- Cummins, I., Dixon, D. P., Freitag-Pohl, S., Skipsey, M., et al. (2011). Multiple roles for plant glutathione transferases in xenobiotic detoxification. *Drug Metabolism Reviews*, 43(2), 266-280.
- Cummins, I., Wortley, D. J., Sabbadin, F., He, Z., et al. (2013). Key role for a glutathione transferase in multiple-herbicide resistance in grass weeds. *Proceedings of the National Academy of Sciences of the U.S.A.*, 110(15), 5812-5817.
- Dalton, D. A., Boniface, C., Turner, Z., Lindahl, A., et al. (2009). Physiological roles of glutathione s-transferases in soybean root nodules. *Plant Physiology*, 150(1), 521-530.
- Davies, J., & Caseley, J. C. (1999). Herbicide safeners: a review. *Pesticide Science*, 55(11), 1043-1058.
- Day, K. E., & Hodge, V. (1996). Toxicity of the Herbicide Metolachlor, some Transformation Products and a Commercial Safener to an Alga (*Selenastrum capricornutum*), a Cyanophyte (*Anabaena cylindrica*) and a Macrophyte (*Lemna gibba*). *Water Quality Research Journal*, 31(1), 197-214.
- deBoer, G. J., & Satchivi, N. (2014). Comparison of Translocation Properties of Insecticides versus Herbicides That Leads To Efficacious Control of Pests As Specifically Illustrated by Isoclast™ Active, a New Insecticide, and Arylex™ Active, a New Herbicide. *American Chemical Society*, 1171, 75-93.
- Del Buono, D., Micheli, M., Scarponi, L., & Standardi, A. (2006). Activity of glutathione S-transferase toward some herbicides and its regulation by benoxacor in non-embryogenic callus and in vitro regenerated tissues of *Zea mays*. *Pesticide Biochemistry and Physiology*, 85(2), 61-67.
- Del Buono, D., Scarponi, L., & Espen, L. (2007). Glutathione S-transferases in *Festuca arundinacea*: Identification, characterization and inducibility by safener benoxacor. *Phytochemistry*, 68(21), 2614-2624.
- Delye, C., Zhang, X. Q., Michel, S., Matejcek, A., et al. (2005). Molecular bases for sensitivity to acetyl-coenzyme A carboxylase inhibitors in black-grass. *Plant Physiology*, 137(3), 794-806.
- DeRidder, B. P., & Goldsbrough, P. B. (2006). Organ-specific expression of glutathione S-transferases and the efficacy of herbicide safeners in *Arabidopsis*. *Plant Physiology*, 140(1), 167-175.
- Devine, M., Duke, S. O., & Fedtke, C. (1992). *physiology of herbicide action*. PTR Prentice Hall.
- Dixon, D., Cole, D. J., & Edwards, R. (1997). Characterisation of multiple glutathione transferases containing the GST I subunit with activities toward herbicide substrates in maize (*Zea mays*). *Pesticide Science*, 50(1), 72-82.
- Dixon, D. P. (1998). *Glutathione transferases in maize (zea mays)*. Durham University thesis.
- Dixon, D. P., Cole, D. J., & Edwards, R. (1998a). Purification, regulation and cloning of a glutathione transferase (GST) from maize resembling the auxin-inducible type-III GSTs. *plant molecular biology*, 36(1), 75-87.

- Dixon, D. P., Cole, D. J., & Edwards, R. (1999). Dimerisation of maize glutathione transferases in recombinant bacteria. *plant molecular biology*, 40(6), 997-1008.
- Dixon, D. P., Cummins, L., Cole, D. J., & Edwards, R. (1998b). Glutathione-mediated detoxification systems in plants. *Current Opinion in Plant Biology*, 1(3), 258-266.
- Dixon, D. P., Davis, B. G., & Edwards, R. (2002a). Functional divergence in the glutathione transferase superfamily in plants. Identification of two classes with putative functions in redox homeostasis in *Arabidopsis thaliana*. *The Journal of Biological Chemistry*, 277(34), 30859-30869.
- Dixon, D. P., & Edwards, R. (2010a). Roles for stress-inducible lambda glutathione transferases in flavonoid metabolism in plants as identified by ligand fishing. *The Journal of Biological Chemistry*, 285(47), 36322-36329.
- Dixon, D. P., Hawkins, T., Hussey, P. J., & Edwards, R. (2009). Enzyme activities and subcellular localization of members of the *Arabidopsis* glutathione transferase superfamily. *Journal of Experimental Botany*, 60(4), 1207-1218.
- Dixon, D. P., Laphorn, A., & Edwards, R. (2002b). Plant glutathione transferases. *Genome Biology*, 3(3), 3004-3001.
- Dixon, D. P., Laphorn, A. J., & Edwards, R. (2005). Synthesis and analysis of chimeric maize glutathione transferases. *Plant Science*, 168(4), 873-881.
- Dixon, D. P., Skipsey, M., & Edwards, R. (2010b). Roles for glutathione transferases in plant secondary metabolism. *Phytochemistry*, 71(4), 338-350.
- Duke, S. O. (2012). Why have no new herbicide modes of action appeared in recent years? *Pest Management Science*, 68(4), 505-512.
- Dutka, F., & Komives, T. (1987). MG-191 A new selective herbicide antidote. *Pesticide Science and Biotechnology*.
- Edwards, R., Dixon, D. P., Cummins, L., Brazier-Hicks, M., et al. (2011). New Perspectives on the Metabolism and Detoxification of Synthetic Compounds in Plants. *Organic xenobiotics and plants*, 8, 125-148.
- Edwards, R., Dixon, D. P., & Walbot, V. (2000). Plant glutathione S-transferases: enzymes with multiple functions in sickness and in health. *TRENDS in Plant Science*, 5(5), 193-198.
- Emanuelsson, O., Nielsen, H., Brunak, S., & von Heijne, G. (2000). Predicting subcellular localization of proteins based on their N-terminal amino acid sequence. *Journal of Molecular Biology*, 300(4), 1005-1016.
- ENV pesticide compliance. (accessed 2020).
- European_food_safety_authority. (2016). Peer review of the pesticide risk assessment of the active substance mesotrione. *EFSA Journal*, 14(3).
- FAO. (2012). World Agriculture Towards 2030/2050: The 2012 revision. http://www.fao.org/fileadmin/user_upload/esag/docs/AT2050_revision_summary.pdf, accessed 2020
- FAOSTAT. (Accessed 2020). <http://www.fao.org/faostat/en>.
- Ferro, M., Brugiére, S., Salvi, D., Seigneurin-Berny, D., et al. (2010). AT_CHLORO, a comprehensive chloroplast proteome database with subplastidial localization and curated information on envelope proteins. *Molecular & Cellular Proteomics*, 9(6), 1063-1084.
- Flury, T., Wagner, E., & Kreuz, K. (1996). An inducible glutathione S-transferase in soybean hypocotyl is localized in the apoplast. *Plant Physiology*, 112(3), 1185-1190.
- Foyer, C. H., Theodoulou, F. L., & Delrot, S. (2001). The functions of inter- and intracellular glutathione transport systems in plants. *TRENDS in Plant Science*, 6(10), 486-492.

- Frova, C. (2003). The plant glutathione transferase gene family: genomic structure, functions, expression and evolution. *Physiologia Plantarum*, 119(4), 469-479.
- Fuerst, E. P. (1987). Understanding the Mode of Action of the Chloroacetamide and Thiocarbamate Herbicides. *Weed Technology*, 1(4), 270-277.
- Fuerst, E. P., Irzyk, G. P., & Miller, K. D. (1993). Partial Characterization of Glutathione S-Transferase Isozymes Induced by the Herbicide Safener Benoxacor in Maize. *Plant Physiology*, 102(3), 795-802.
- Gachon, C. M., Langlois-Meurinne, M., & Saindrenan, P. (2005). Plant secondary metabolism glycosyltransferases: the emerging functional analysis. *TRENDS in Plant Science*, 10(11), 542-549.
- Gaillard, C., Dufaud, A., Tommasini, R., Kreuz, K., et al. (1994). A Herbicide Antidote (Safener) Induces the Activity of Both the Herbicide Detoxifying Enzyme and of a Vacuolar Transporter for the Detoxified Herbicide. *FEBS Letters*, 352(2), 219-221.
- Gasteiger, E., Gattiker, A., Hoogland, C., Ivanyi, I., et al. (2003). ExPASy: The proteomics server for in-depth protein knowledge and analysis. *Nucleic Acids Research*, 31(13), 3784-3788.
- Gonneau, M., Mornet, R., & Laloue, M. (1998). A Nicotiana plumbaginifolia protein labeled with an azido cytokinin agonist is a glutathione S-transferase. *Physiologia Plantarum*, 103(1), 114-124.
- Gouy, M., Guindon, S., & Gascuel, O. (2010). SeaView Version 4: A Multiplatform Graphical User Interface for Sequence Alignment and Phylogenetic Tree Building. *Molecular Biology and Evolution*, 27(2), 221-224.
- Gramss, G., Voigt, K. D., & Kirsche, B. (1999). Oxidoreductase enzymes liberated by plant roots and their effects on soil humic material. *Chemosphere*, 38(7), 1481-1494.
- Green, J. M. (2014). Current state of herbicides in herbicide-resistant crops. *Pest Management Science*, 70(9), 1351-1357.
- Greenbaum, D., Jansen, R., & Gerstein, M. (2002). Analysis of mRNA expression and protein abundance data: an approach for the comparison of the enrichment of features in the cellular population of proteins and transcripts. *Bioinformatics*, 18(4), 585-596.
- Grefen, C., Donald, N., Hashimoto, K., Kudla, J., et al. (2010). A ubiquitin-10 promoter-based vector set for fluorescent protein tagging facilitates temporal stability and native protein distribution in transient and stable expression studies. *The Plant Journal*, 64(2), 355-365.
- Gronwald, J. W., & Plaisance, K. L. (1998). Isolation and characterization of glutathione S-transferase isozymes from sorghum. *Plant Physiology*, 117(3), 877-892.
- Grossmann, K. (2010). Auxin herbicides: current status of mechanism and mode of action. *Pest Management Science*, 66(2), 113-120.
- Guengerich, F. P. (2001). Common and uncommon cytochrome P450 reactions related to metabolism and chemical toxicity. *Chemical Research in Toxicology*, 14(6), 611-650.
- Gupta, C. L., Akhtar, S., & Bajpai, P. (2014). in silico protein modelling: possibilities and limitations. *EXCLI Journal*(13), 513-515.
- Hatton, P. J., Dixon, D., Cole, D. J., & Edwards, R. (1996). Glutathione transferase activities and herbicide selectivity in maize and associated weed species. *Pesticide Science*, 46(3), 267-275.
- Hatzios, K. K. (1991). An Overview of the Mechanisms of Action of Herbicide Safeners. *Zeitschrift Fur Naturforschung C-a Journal of Biosciences*, 46(9-10), 819-827.
- Hatzios, K. K., & Burgos, N. (2004). Metabolism-based herbicide resistance: regulation by safeners. *Weed Science*, 52(3), 454-467.

- Hatzios, K. K., & Penner, D. (1982). *Metabolism of herbicides in higher plants*: Burgess Publishing Company.
- Hawkes, T. H., D.C. & Andrews, C.J. & Thomas, P.G. & Langford, Mike & Hollingworth, S. & Mitchell, G.. . (2001). Mesotrione: Mechanism of herbicidal activity and selectivity in corn. *The BCPC Proceedings-Weeds*, 2, 563-568.
- He, G., Guan, C. N., Chen, Q. X., Gou, X. J., et al. (2016). Genome-Wide Analysis of the Glutathione S-Transferase Gene Family in *Capsella rubella*: Identification, Expression, and Biochemical Functions. *Frontiers in Plant Science*, 7, 1325.
- Herrmann, K. M., & Weaver, L. M. (1999). The Shikimate Pathway. *Annual Review of Plant Physiology and Plant Molecular Biology*, 50, 473-503.
- Hershey, H. P., & Stoner, T. D. (1991). Isolation and characterization of cDNA clones for RNA species induced by substituted benzenesulfonamides in corn. *plant molecular biology*, 17(4), 679-690.
- Hoffman, O. L. (1969). Chemical antidotes for EPTC on corn. *Weed Science Society of America*, 12.
- Hoffmann, O. L. (1953). Inhibition of Auxin Effects by 2,4,6-Trichlorophenoxyacetic acid. *Plant Physiology*, 28(4), 622-628.
- Hoffmann, O. L. (1977). *Herbicide antidotes: from concept to practice*. Paper presented at the National Meeting of the American Chemical Society, New Orleans, Louis. (USA).
- Holt, D. C., Lay, V. J., Clarke, E. D., Dinsmore, A., et al. (1995). Characterization of the safener-induced glutathione S-transferase isoform II from maize. *Planta*, 196(2), 295-302.
- Horton, P., Park, K. J., Obayashi, T., Fujita, N., et al. (2007). WoLF PSORT: protein localization predictor. *Nucleic Acids Research*, 35(Web Server issue), W585-587.
- Hruz, T., Laule, O., Szabo, G., Wessendorp, F., et al. (2008). Genevestigator v3: a reference expression database for the meta-analysis of transcriptomes. *Advances in bioinformatics*.
- Hsu, F. C., Marxmiller, R. L., & Yang, A. Y. S. (1990). Study of Root Uptake and Xylem Translocation of Cinmethylin and Related-Compounds in Detopped Soybean Roots Using a Pressure Chamber Technique. *Plant Physiology*, 93(4), 1573-1578.
- Irzyk, G. P., & Fuerst, E. P. (1993). Purification and characterization of a glutathione S-transferase from benoxacor-treated maize (*Zea mays*). *Plant Physiology*, 102(3), 803-810.
- Islam, M. S., Choudhury, M., Majlish, A. K., Islam, T., et al. (2018). Comprehensive genome-wide analysis of Glutathione S-transferase gene family in potato (*Solanum tuberosum* L.) and their expression profiling in various anatomical tissues and perturbation conditions. *Gene*, 639, 149-162.
- Ito, J., Batth, T. S., Petzold, C. J., Redding-Johanson, A. M., et al. (2011). Analysis of the Arabidopsis cytosolic proteome highlights subcellular partitioning of central plant metabolism. *Journal of Proteome Research*, 10(4), 1571-1582.
- Jablonkai, I. (2013). Herbicide Safeners: Effective Tools to Improve Herbicide Selectivity. *Herbicides-Current Research and Case Studies in Use. IntechOpen*.
- Jablonkai, I., & Dutka, F. (1995). Uptake, Translocation, and Metabolism of MG-191 Safener in Corn (*Zea Mays* L.). *Weed Science*, 43(2), 169-174.
- Jablonkai, I., Hulesch, A., Cummins, I., Dixon, D. P., et al. (2001). The herbicide safener MG-191 enhances the expression of specific glutathione S-transferases in maize. *Proceedings of BCPC - Weeds*, 2527-532.
- Jepson, I., Lay, V. J., Holt, D. C., Bright, S. W., et al. (1994). Cloning and characterization of maize herbicide safener-induced cDNAs encoding subunits of glutathione S-transferase isoforms I, II and IV. *plant molecular biology*, 26(6), 1855-1866.

- Jiao, Y., Peluso, P., Shi, J., Liang, T., et al. (2017). Improved maize reference genome with single-molecule technologies. *Nature*, 546(7659), 524-527.
- Johnson, M., Zaretskaya, I., Raytselis, Y., Merezuk, Y., et al. (2008). NCBI BLAST: a better web interface. *Nucleic Acids Research*, 36(Web Server issue), W5-9.
- Joy, M., Abit, M., & Al-Khatib, K. (2009). Absorption, Translocation, and Metabolism of Mesotrione in Grain Sorghum. *Weed Science*, 57(6), 563-566.
- Jugulam, M. (2017). *Biology, Physiology and Molecular Biology of Weeds*. Boca Ratan CRC Press
- Klein, M., Burla, B., & Martinoia, E. (2006). The multidrug resistance-associated protein (MRP/ABCC) subfamily of ATP-binding cassette transporters in plants. *FEBS Letters*, 580(4), 1112-1122.
- Klein, M., Martinoia, E., Hoffmann-Thoma, G., & Weissenböck, G. (2000). A membrane-potential dependent ABC-like transporter mediates the vacuolar uptake of rye flavone glucuronides: regulation of glucuronide uptake by glutathione and its conjugates. *The Plant Journal*, 21(3), 289-304.
- Klodmann, J., Senkler, M., Rode, C., & Braun, H. P. (2011). Defining the protein complex proteome of plant mitochondria. *Plant Physiology*, 157(2), 587-598.
- Kocsy, G., von Ballmoos, P., Rueggsegger, A., Szalai, G., et al. (2001). Increasing the Glutathione Content in a Chilling-Sensitive Maize Genotype Using Safeners Increased Protection against Chilling-Induced Injury. *Plant Physiology*, 127(3), 1147-1156.
- Komives, T. (1992). Herbicide safeners: chemistry, mode of action, applications. *Weed Abstracts*, 41(12).
- Komives, T., & Hatzios, K. K. (1991). Chemistry and Structure-Activity-Relationships of Herbicide Safeners. *Zeitschrift Fur Naturforschung C-a Journal of Biosciences*, 46(9-10), 798-804.
- Konishi, T., & Sasaki, Y. (1994). Compartmentalization of two forms of acetyl-CoA carboxylase in plants and the origin of their tolerance toward herbicides. *Proceedings of the National Academy of Sciences of the U.S.A*, 91(9), 3598-3601.
- Kraehmer, H. (2012). Innovation: Changing Trends in Herbicide Discovery. *Outlooks on Pest Management*, 23(3), 115-118.
- Kraehmer, H., Laber, B., Rosinger, C., & Schulz, A. (2014). Herbicides as weed control agents: state of the art: I. Weed control research and safener technology: the path to modern agriculture. *Plant Physiology*, 166(3), 1119-1131.
- Kramer, W., & Schirmer, U. (2007). Modern Crop Protection Compounds. *Wiley-VCH*, 3.
- Kreuz, K., Tommasini, R., & Enrico Martinoia, E. (1996). Old Enzymes for a New Job: Herbicide Detoxification in Plants. *Plant Physiology*(111), 349-353.
- Lallement, P. A., Brouwer, B., Keech, O., Hecker, A., et al. (2014). The still mysterious roles of cysteine-containing glutathione transferases in plants. *Frontiers in Pharmacology*, 5, 192.
- Lallement, P. A., Meux, E., Gualberto, J. M., Dumarcay, S., et al. (2015). Glutathionyl-hydroquinone reductases from poplar are plastidial proteins that deglutathionylate both reduced and oxidized glutathionylated quinones. *FEBS Letters*, 589(1), 37-44.
- Lamberth, C., Jeanmart, S., Luksch, T., & Plant, A. (2013). Current challenges and trends in the discovery of agrochemicals. *Science*, 341(6147), 742-746.
- Lamoureux, G. L., & Rusness, D. G. (1993). Glutathione in the metabolism and detoxification of xenobiotics in plants. *Sulfur Nutrition and Assimilation in Higher Plants., The Hague, The Netherlands: SPB Academic Publishing*, 221-237.
- Lamoureux, G. L., Rusness, D. G., & Tanaka, F. S. (1991). Chlorimuron ethyl metabolism in corn. *Pesticide Biochemistry and Physiology*(41), 66-81.

- Larkin, M. A., Blackshields, G., Brown, N. P., Chenna, R., et al. (2007). Clustal W and Clustal X version 2.0. *Bioinformatics*, 23(21), 2947-2948.
- Laskowski, R. A., MacArthur, M. W., Moss, D. S., & Thornton, J. M. (1993). PROCHECK: a program to check the stereochemical quality of protein structures. *Journal of Applied Crystallography*, 26(2), 283-291.
- Laskowski, R. A., MacArthur, M.W., Thornton, J.M. (2006). PROCHECK: validation of protein-structure. *International Tables for Crystallography*, F(25.2), 722-725.
- Leah, J. M., Caseley, J. C., Riches, C. R., & Valverde, B. (1994). Association between elevated activity of aryl acylamidase and propanil resistance in Jungle-rice, *Echinochloa colona*. *Pesticide Science*, 42(4), 281-289.
- Leier I, J. G., Buchholz U, Cole SP, Deeley RG, Keppler D. (1994). The MRP Gene Encodes an ATP-dependent Export Pump for Leukotriene C4 and Structurally Related Conjugates. *The Journal of Biological Chemistry*, 269, 27807-27810.
- Letunic, I., & Bork, P. (2016). Interactive tree of life (iTOL) v3: an online tool for the display and annotation of phylogenetic and other trees. *Nucleic Acids Research*, 44(Web Server issue), W242-W245.
- Lewis, K. A., Tzilivakis, J., Warner, D., & Green, A. (2016). An international database for pesticide risk assessments and management. *Human and Ecological Risk Assessment: An International Journal*, 22(4), 1050-1064.
- Li, D., Xu, L., Pang, S., Liu, Z., et al. (2017). Variable Levels of Glutathione S-Transferases Are Responsible for the Differential Tolerance to Metolachlor between Maize (*Zea mays*) Shoots and Roots. *Journal of Agricultural and Food Chemistry*, 65(1), 39-44.
- Limmer, M. A., & Burken, J. G. (2014). Plant Translocation of Organic Compounds: Molecular and Physicochemical Predictors. *Environmental Science & Technology Letters*, 1(2), 156-161.
- Lin, F., Jiang, L., Liu, Y., Lv, Y., et al. (2014). Genome-wide identification of housekeeping genes in maize. *plant molecular biology*, 86(4-5), 543-554.
- Liu, Y. J., Han, X. M., Ren, L. L., Yang, H. L., et al. (2013). Functional divergence of the glutathione S-transferase supergene family in *Physcomitrella patens* reveals complex patterns of large gene family evolution in land plants. *Plant Physiology*, 161(2), 773-786.
- Loiseleur, O. (2017). Natural Products in the Discovery of Agrochemicals. *Chimia (Aarau)*, 71(12), 810-822.
- Low, K., & Tasheva, M. (2014). Mesotrione. *Journal of Medicinal Plants Research*, 241–305.
- Ma, R., Kaundun, S. S., Tranel, P. J., Riggins, C. W., et al. (2013). Distinct detoxification mechanisms confer resistance to mesotrione and atrazine in a population of waterhemp. *Plant Physiology*, 163(1), 363-377.
- MAIZE GROWERS GUIDE. from SeedCo Group. Accessed (2018). Retrieved from <http://www.seedcogroup.com/>
- Manners, C. N., Payling, D. W., & Smith, D. A. (1988). Distribution coefficient, a convenient term for the relation of predictable physico-chemical properties to metabolic processes. *Xenobiotica*, 18(3), 331-350.
- Marmagne, A., Ferro, M., Meinel, T., Bruley, C., et al. (2007). A high content in lipid-modified peripheral proteins and integral receptor kinases features in the arabidopsis plasma membrane proteome. *Molecular & Cellular Proteomics*, 6(11), 1980-1996.
- Marrs, K. A. (1996). The Functions and Regulation of Glutathione S-Transferases in Plants. *Annual Review of Plant Physiology Plant Molecular Biology*, 47, 127-158.

- Matola, T., & Jablonkai, I. (2007). Safening efficacy of halogenated acetals, ketals and amides and relationship between the structure and effect on glutathione and glutathione S-transferases in maize. *Crop Protection*, 26(3), 278-284.
- Mazzone, H. M. (1998). *CRC Handbook of Viruses: Mass-Molecular Weight Values and Related Properties*: CRC Press.
- McGonigle, B., Keeler, S. J., Lau, S. M., Koeppe, M. K., et al. (2000). A genomics approach to the comprehensive analysis of the glutathione S-transferase gene family in soybean and maize. *Plant Physiology*, 124(3), 1105-1120.
- Miller, K. D., Irzyk, G. P., & Fuerst, E. P. (1994). Benoxacor Treatment Increases Glutathione-S-Transferase Activity in Suspension-Cultures of Zea-Mays. *Pesticide Biochemistry and Physiology*, 48(2), 123-134.
- Minic, Z. (2008). Physiological roles of plant glycoside hydrolases. *Planta*, 227(4), 723-740.
- Mitchell, G., Bartlett, D. W., Fraser, T. E. M., Hawkes, T. R., et al. (2001). Mesotrione: a new selective herbicide for use in maize. *Pest Management Science*, 57(2), 120-128.
- Mittova, V., Theodoulou, F. L., Kiddle, G., Gómez, L., et al. (2003). Coordinate induction of glutathione biosynthesis and glutathione-metabolizing enzymes is correlated with salt tolerance in tomato. *FEBS Letters*, 554(3), 417-421.
- Miyoshi, K., Ahn, B. O., Kawakatsu, T., Ito, Y., et al. (2004). PLASTOCHRON1, a timekeeper of leaf initiation in rice, encodes cytochrome P450. *Proceedings of the National Academy of Sciences of the U.S.A*, 101(3), 875-880.
- Mizutani, M., & Sato, F. (2011). Unusual P450 reactions in plant secondary metabolism. *Archives of Biochemistry and Biophysics*, 507(1), 194-203.
- Monticolo, F., Colantuono, C., & Chiusano, M. L. (2017). Shaping the evolutionary tree of green plants: evidence from the GST family. *Scientific Reports*, 7(1), 14363.
- Moreland, D. E. (1993). Research on Biochemistry of Herbicides - an Historical Overview. *Zeitschrift Fur Naturforschung C-a Journal of Biosciences*, 48(3-4), 121-131.
- Morris, A. L., MacArthur, M. W., Hutchinson, E. G., & Thornton, J. M. (1992). Stereochemical quality of protein structure coordinates. *Proteins*, 12(4), 345-364.
- Mozer, T. J., Tiemeier, D. C., & Jaworski, E. G. (1983). Purification and characterization of corn glutathione S-transferase. *Biochemistry*, 22(5), 1068-1072.
- Mueller, L. A., Goodman, C. D., Silady, R. A., & Walbot, V. (2000). AN9, a petunia glutathione S-transferase required for anthocyanin sequestration, is a flavonoid-binding protein. *Plant Physiology*, 123(4), 1561-1570.
- Munoz, A., Koskinen, W. C., Cox, L., & Sadowsky, M. J. (2011). Biodegradation and mineralization of metolachlor and alachlor by *Candida xestobii*. *Journal of Agricultural and Food Chemistry*, 59(2), 619-627.
- Naylor, R. E. L. (2008). *Weed Management Handbook*. John Wiley & sons.
- NCBI-Resource-Coordinators. (2016). Database resources of the National Center for Biotechnology Information. *Nucleic Acids Research*, 44(D1), D7-19.
- Negi, S., Pandey, S., Srinivasan, S. M., Mohammed, A., et al. (2015). LocSigDB: a database of protein localization signals. *Database (Oxford)*, 2015.
- O'Connell, K. M., Breaux, E. J., & Fraley, R. T. (1988). Different rates of metabolism of two chloroacetanilide herbicides in pioneer 3320 corn. *Plant Physiology*, 86(2), 359-363.
- O'Sullivan, J., Zandstra, J., & Sikkema, P. (2002). Sweet corn (*Zea mays*) cultivar sensitivity to mesotrione. *Weed Technology*, 16(2), 421-425.
- Obojska, A., Berlicki, L., Kafarski, P., Lejczak, B., et al. (2004). Herbicidal pyridyl derivatives of aminomethylene-bisphosphonic acid inhibit plant glutamine synthetase. *Journal of Agricultural and Food Chemistry*, 52(11), 3337-3344.

- Ohkawa, H., Tsujii, H., & Ohkawa, Y. (1999). The use of cytochrome P450 genes to introduce herbicide tolerance in crops: a review. *Pesticide Science*, 55(9), 867-874.
- Oliveira, M. C., Gaines, T. A., Jhala, A. J., & Knezevic, S. Z. (2018). Inheritance of Mesotrione Resistance in an *Amaranthus tuberculatus* (var. *rudis*) Population from Nebraska, USA. *Frontiers in Plant Science*, 9, 60.
- Ota, H. (2013). National Museum of Nature and Science, Japan *Center of the History of Japanese Industrial Technology*.
- Oztetik, E. (2008). A tale of plant Glutathione S-transferases: Since 1970. *Botanical Review*, 74(3), 419-437.
- Pallett, K. E. (2003). *Herbicides, asulam*. In Encyclopedia of Agrochemicals.
- Pallos, F. M., Brokke, M. E., & Arneklev, D. R. (1972). Belgian Patent. *Patent number; 7821120*
- Pang, S., Duan, L., Liu, Z., Song, X., et al. (2012). Co-induction of a glutathione-S-transferase, a glutathione transporter and an ABC transporter in maize by xenobiotics. *PLoS One*, 7(7), e40712.
- Parliament, E. (2011). Commission regulation (EU) *Official Journal of the European Union*.
- Pataky, J. K., Meyer, M. D., Bollman, J. D., Boerboorn, C. M., et al. (2008). Genetic basis for varied levels of injury to sweet corn hybrids from three cytochrome P450-metabolized herbicides. *Journal of the American Society for Horticultural Science*, 133(3), 438-447.
- Peltier, J. B., Cai, Y., Sun, Q., Zabrouskov, V., et al. (2006). The oligomeric stromal proteome of *Arabidopsis thaliana* chloroplasts. *Molecular & Cellular Proteomics*, 5(1), 114-133.
- Perperopoulou, F., Pouliou, F., & Labrou, N. E. (2018). Recent advances in protein engineering and biotechnological applications of glutathione transferases. *Critical Reviews in Biotechnology*, 38(4), 511-528.
- Persans, M. W., Wang, J., & Schuler, M. A. (2001). Characterization of maize cytochrome P450 monooxygenases induced in response to safeners and bacterial pathogens. *Plant Physiology*, 125(2), 1126-1138.
- Pettersen, E. F., Goddard, T. D., Huang, C. C., Couch, G. S., et al. (2004). UCSF Chimera—a visualization system for exploratory research and analysis. *Journal of computational chemistry*, 25(13), 1605-1612.
- Pflugmacher, S., & Sandermann, H. (1998). Taxonomic distribution of plant glucosyltransferases acting on xenobiotics. *Phytochemistry*, 49(2), 507-511.
- Pimentel, D. (1997). *Techniques for Reducing pesticides: Environmental and Economic Benefits.*: Chichester, United Kingdom: Wiley.
- Prade, L., Huber, R., & Bieseler, B. (1998). Structures of herbicides in complex with their detoxifying enzyme glutathione S-transferase – explanations for the selectivity of the enzyme in plants. *structure*, 6(11), 1445-1452.
- Qin, G., Gu, H., Ma, L., Peng, Y., et al. (2007). Disruption of phytoene desaturase gene results in albino and dwarf phenotypes in *Arabidopsis* by impairing chlorophyll, carotenoid, and gibberellin biosynthesis. *Cell Research*, 17(5), 471-482.
- Rajcan, I., & Swanton, C. J. (2001). Understanding maize–weed competition: resource competition, light quality and the whole plant. *Field Crops Research*, 71(2), 139-150.
- Ramachandran, G. N., Ramakrishnan, C., & Sasisekharan, V. (1963). Stereochemistry of polypeptide chain configurations. *Journal of Molecular Biology*, 7(1), 95-99.
- Rani, R., & Juwarkar, A. (2015). Effect of Presence of Pesticides in Growth Medium on the Exudation Behaviour of Plants: A Study with Phorate (An Organophosphate Insecticide) and *Pisum Sativum* (L.). *International Conference on Biological, Environment and Food Engineering*.

- Rani, R., & Juwarkar, A. (2016). Influence of insecticide phorate on chemical composition and enzyme profile of root exudates and root extracts of *Brassica juncea*. *Journal of Environmental Biology*, 37(3), 413-419.
- Ranum, P., Pena-Rosas, J. P., & Garcia-Casal, M. N. (2014). Global maize production, utilization, and consumption. *Annals of the New York Academy of Sciences*, 1312, 105-112.
- Rao, V. S. (2014). *Transgenic Herbicide Resistance in Plants*: CRC Press.
- Rea, P. A. (2007). Plant ATP-binding cassette transporters. *Annual Reviews of Plant Biology*, 58, 347-375.
- Reinemer, P., Prade, L., Hof, P., Neuefeind, T., et al. (1996). Three-dimensional structure of glutathione S-transferase from *Arabidopsis thaliana* at 2.2 Å resolution: structural characterization of herbicide-conjugating plant glutathione S-transferases and a novel active site architecture. *Journal of Molecular Biology*, 255(2), 289-309.
- Rensen, J. J. S. v., & Hobé, J. H. (1979). Mechanism of Action of the Herbicide 4,6-Dinitro-o-cresol in photosynthesis. *Zeitschrift für Naturforschung*, 1021-1023.
- Reumann, S., Quan, S., Aung, K., Yang, P., et al. (2009). In-depth proteome analysis of *Arabidopsis* leaf peroxisomes combined with in vivo subcellular targeting verification indicates novel metabolic and regulatory functions of peroxisomes. *Plant Physiology*, 150(1), 125-143.
- A Review of Amino Acids. (Accessed 2019). Retrieved from <http://wbiomed.curtin.edu.au/biochem/tutorials/AAs/AA.html>
- Rice, P. J. (1996). The persistence, degradation, and mobility of metolachlor in soil and the fate of metolachlor and atrazine in surface water, surface water/sediment, and surface water/aquatic plant systems. *Iowa State University*.
- Riechers, D. E., Kreuz, K., & Zhang, Q. (2010). Detoxification without intoxication: herbicide safeners activate plant defense gene expression. *Plant Physiology*, 153(1), 3-13.
- Riechers, D. E., Zhang, Q., Xu, F., & Vaughn, K. C. (2003). Tissue-specific expression and localization of safener-induced glutathione S-transferase proteins in *Triticum tauschii*. *Planta*, 217(5), 831-840.
- Romano, M. L., Stephenson, G. R., Tal, A., & Hall, J. C. (1993). The Effect of Monooxygenase and Glutathione S-Transferase Inhibitors on the Metabolism of Diclofop-methyl and Fenoxaprop-ethyl in Barley and Wheat. *Pesticide Biochemistry and Physiology*, 46(3), 181-189.
- Samaras, P., Schmidt, T., Frejno, M., Gessulat, S., et al. (2020). ProteomicsDB: a multi-omics and multi-organism resource for life science research. *Nucleic Acids Research*, 48(D1), D1153-D1163.
- Santabarbara, S. (2006). Limited sensitivity of pigment photo-oxidation in isolated thylakoids to singlet excited state quenching in photosystem II antenna. *Archives of Biochemistry and Biophysics*, 455(1), 77-88.
- Sasan, M., Maryam, E., Fateme, M., Maryam, S., et al. (2011). Plant glutathione S-transferase classification, structure and evolution. *African Journal of Biotechnology*, 10(42), 8160-8165.
- Scalla, R., & Roulet, A. (2002). Cloning and characterization of a glutathione S-transferase induced by a herbicide safener in barley (*Hordeum vulgare*). *Physiologia Plantarum*, 116(3), 336-344.
- Scarponi, L., Alla, M. N., & Martinetti, L. (1992). Metolachlor in Corn (*Zea-Mays*) and Soybean (*Glycine-Max*) - Persistence and Biochemical Signs of Stress during Its Detoxification. *Journal of Agricultural and Food Chemistry*, 40(5), 884-889.

- Scarponi, L., & Del Buono, D. (2005). Benoxacor induction of terbuthylazine detoxification in *Zea mays* and *Festuca arundinacea*. *Journal of Agricultural and Food Chemistry*, 53(7), 2483-2488.
- Scarponi, L., & Del Buono, D. (2009a). *Festuca arundinacea*, glutathione S-transferase and herbicide safeners: A preliminary case study to reduce herbicidal pollution. *Journal of Environmental Science and Health Part B-Pesticides Food Contaminants and Agricultural Wastes*, 44(8), 805-809.
- Scarponi, L., Del Buono, D., Quagliarini, E., & D'Amato, R. (2009b). *Festuca arundinacea* grass and herbicide safeners to prevent herbicide pollution. *Agronomy for Sustainable Development*, 29(2), 313-319.
- Scarponi, L., Quagliarini, E., & Del Buono, D. (2006). Induction of wheat and maize glutathione S-transferase by some herbicide safeners and their effect on enzyme activity against butachlor and terbuthylazine. *Pest Management Science*, 62(10), 927-932.
- Schnable, P. S., Ware, D., Fulton, R. S., Stein, J. C., et al. (2009). The B73 maize genome: complexity, diversity, and dynamics. *Science*, 326(5956), 1112-1115.
- Sekhon, R. S., Lin, H., Childs, K. L., Hansey, C. N., et al. (2011). Genome-wide atlas of transcription during maize development. *The Plant Journal*, 66(4), 553-563.
- Sherwani, S. I., Arif, I. A., & Khan, H. A. (2015). Modes of Action of Different Classes of Herbicides. *Herbicides, Physiology of Action, and Safety*.
- Shone, M. G. T., & Wood, A. V. (1974). A Comparison of the Uptake and Translocation of Some Organic Herbicides and a Systemic Fungicide by Barley. *Journal of Experimental Botany*, 25(2), 390-400.
- Siminszky, B. (2006). Plant cytochrome P450-mediated herbicide metabolism. *Phytochemistry Reviews*, 5(2-3), 445-458.
- Sivey, J. D., Lehmler, H., Salice, C. J., Ricko, A. N., et al. (2015). Environmental Fate and Effects of Dichloroacetamide Herbicide Safeners: "Inert" yet Biologically Active Agrochemical Ingredients. *Environmental Science & Technology Letters*, 2(10), 260-269.
- Skipsey, M., Knight, K. M., Brazier-Hicks, M., Dixon, D. P., et al. (2011). Xenobiotic responsiveness of *Arabidopsis thaliana* to a chemical series derived from a herbicide safener. *The Journal of Biological Chemistry*, 286(37), 32268-32276.
- Smith, A. P., Nourizadeh, S. D., Peer, W. A., Xu, J., et al. (2003). *Arabidopsis* AtGSTF2 is regulated by ethylene and auxin, and encodes a glutathione S-transferase that interacts with flavonoids. *The Plant Journal*, 36(4), 433-442.
- Soranzo, N., Sari Gorla, M., Mizzi, L., De Toma, G., et al. (2004). Organisation and structural evolution of the rice glutathione S-transferase gene family. *Molecular Genetics and Genomics*, 271(5), 511-521.
- Sottomayor, M., Duarte, P., Figueiredo, R., & Ros Barcelo, A. (2008). A vacuolar class III peroxidase and the metabolism of anticancer indole alkaloids in *Catharanthus roseus*: Can peroxidases, secondary metabolites and arabinogalactan proteins be partners in microcompartmentation of cellular reactions? *Plant Signaling & Behavior*, 3(10), 899-901.
- Springett, R. H. (1965). The bipyridylum herbicides: their properties and use. *Outlook on Agriculture*, 4(5), 226-233.
- Stange, C., Fuentes, P., Handford, M., & Pizarro, L. (2008). *Daucus carota* as a novel model to evaluate the effect of light on carotenogenic gene expression. *Biological Research*, 41(3), 289-301.
- Stelpflug, S. C., Sekhon, R. S., Vaillancourt, B., Hirsch, C. N., et al. (2016). An Expanded Maize Gene Expression Atlas based on RNA Sequencing and its Use to Explore Root Development. *Plant Genome*, 9(1).

- Stephenson, G. R., & Yaacoby, T. (1991). Milestones in the Development of Herbicide Safeners. *Zeitschrift Fur Naturforschung C-a Journal of Biosciences*, 46(9-10), 794-797.
- Stryer, L. (1995). Biochemistry. In W. H. Freeman (Ed.), (4th ed.). NY.
- Su, L., Caywood, L. M., Sivey, J. D., & Dai, N. (2019). Sunlight Photolysis of Safener Benoxacor and Herbicide Metolachlor as Mixtures on Simulated Soil Surfaces. *Environmental Science & Technology*, 53(12), 6784-6793.
- Svec, D., Tichopad, A., Novosadova, V., Pfaffl, M. W., et al. (2015). How good is a PCR efficiency estimate: Recommendations for precise and robust qPCR efficiency assessments. *Biomolecular Detection and Quantification*, 3, 9-16.
- Sylvestre-Gonon, E., Law, S. R., Schwartz, M., Robe, K., et al. (2019). Functional, Structural and Biochemical Features of Plant Serinyl-Glutathione Transferases. *Frontiers in Plant Science*, 10, 608.
- Takahashi, Y., Hasezawa, S., Kusaba, M., & Nagata, T. (1995). Expression of the auxin-regulated parA gene in transgenic tobacco and nuclear localization of its gene products. *Planta*, 196(1), 111-117.
- Tamang, B. G., & Fukao, T. (2015). Plant Adaptation to Multiple Stresses during Submergence and Following Desubmergence. *International Journal of Molecular Sciences*, 16(12), 30164-30180.
- Tandzi, L. N., & Mutengwa, C. S. (2019). Estimation of Maize (Zea mays L.) Yield Per Harvest Area: Appropriate Methods. *Agronomy*, 10(1).
- Taylor, S. C., Laperriere, G., & Germain, H. (2017). Droplet Digital PCR versus qPCR for gene expression analysis with low abundant targets: from variable nonsense to publication quality data. *Scientific Reports*, 7(1), 2409.
- Theodoulou, F. L. (2000). Plant ABC transporters. *Biochimica et Biophysica Acta*, 1465(1-2), 79-103.
- Theodoulou, F. L., Clark, I. M., He, X. L., Pallett, K. E., et al. (2003). Co-induction of glutathione-S-transferases and multidrug resistance associated protein by xenobiotics in wheat. *Pest Management Science*, 59(2), 202-214.
- Thom, R., Cummins, I., Dixon, D. P., Edwards, R., et al. (2002). Structure of a tau class glutathione S-transferase from wheat active in herbicide detoxification. *Biochemistry*, 41(22), 7008-7020.
- Trenkamp, S., Martin, W., & Tietjen, K. (2004). Specific and differential inhibition of very-long-chain fatty acid elongases from Arabidopsis thaliana by different herbicides. *Proceedings of the National Academy of Sciences of the U.S.A*, 101(32), 11903-11908.
- Untergasser, A., Cutcutache, I., Koressaar, T., Ye, J., et al. (2012). Primer3: new capabilities and interfaces. *Nucleic Acids Research*(40).
- Usui, K. (2001). Metabolism and selectivity of rice herbicides in plants. *Weed Biology and Management*, 1(3), 137-146.
- Van Eerd, L. L., Hoagland, R. E., Zablotowicz, R. M., & Hall, J. C. (2003). Pesticide metabolism in plants and microorganisms. *Weed Science*, 51(4), 472-495.
- Vaughn, K. C., & Lehnen, L. P. J. (1991). Mitotic Disrupter Herbicides. *Weed Science*, 39(3), 450-457.
- Waterhouse, A., Bertoni, M., Bienert, S., Studer, G., et al. (2018). Swiss-Model: homology modelling of protein structures and complexes. *Nucleic Acids Research*, 46(W1), W296-W303.
- Waterhouse, A. M., Procter, J. B., Martin, D. M. A., Clamp, M., et al. (2009). Jalview Version 2—a multiple sequence alignment editor and analysis workbench. *Bioinformatics*, 25(9), 1189-1191.

- Wei, F., Coe, E., Nelson, W., Bharti, A. K., et al. (2007). Physical and genetic structure of the maize genome reflects its complex evolutionary history. *PLoS Genetics*, 3(7), e123.
- Whitcomb, C. E. (2016). An introduction to ALS-inhibiting herbicides. *Toxicology and Industrial Health*, 15(1-2), 232-240.
- Wiegand, R. C., Shah, D. M., Mozer, T. J., Harding, E. I., et al. (1986). Messenger-Rna Encoding a Glutathione-S-Transferase Responsible for Herbicide Tolerance in Maize Is Induced in Response to Safener Treatment. *plant molecular biology*, 7(4), 235-243.
- Wittenbach, V. A., Koeppe, M. K., Lichtner, F. T., Zimmerman, W. T., et al. (1994). Basis of Selectivity of Triflurosulfuron Methyl in Sugar Beets (*Beta vulgaris*). *Pesticide Biochemistry and Physiology*, 49(1), 72-81.
- Wloga, D., & Gaertig, J. (2010). Post-translational modifications of microtubules. *Journal of Cell Science*, 123(Pt 20), 3447-3455.
- Wosnick, M. A., Barnett, R. W., & Carlson, J. E. (1989). Total chemical synthesis and expression in *Escherichia coli* of a maize glutathione-transferase (GST) gene. *Gene*, 153-160.
- Xiang, Z. (2006). Advances in homology protein structure modeling. *Current Protein & Peptide Science*, 7(3), 217-227.
- Xie, F., Liu, H. J., & Cai, W. D. (2010). Enantioselectivity of racemic metolachlor and S-metolachlor in maize seedlings. *Journal of Environmental Science and Health B*, 45(8), 774-782.
- Xu, Y. L., Lin, H. Y., Ruan, X., Yang, S. G., et al. (2015). Synthesis and bioevaluation of pyrazole-benzimidazolone hybrids as novel human 4-Hydroxyphenylpyruvate dioxygenase inhibitors. *European Journal of Medicinal Chemistry*, 92, 427-438.
- Yenne, S. P., Hatzios, K. K., & Meredith, S. A. (1990). Uptake, Translocation, and Metabolism of Oxabetrinil and Cga-133205 in Grain-Sorghum (*Sorghum-Bicolor*) and Their Influence on Metolachlor Metabolism. *Journal of Agricultural and Food Chemistry*, 38(10), 1957-1961.
- Yu, C. S., Chen, Y. C., Lu, C. H., & Hwang, J. K. (2006). Prediction of protein subcellular localization. *PROTEINS: Structure, Function, and Bioinformatics*, 64(3), 643-651.
- Zadoks, J. C., Chang, T. T., & Konzak, C. F. (1974). A decimal code for the growth stages of cereals. *Weed Research*, 14(6), 415-421.
- Zhu, J. H., Li, H. L., Guo, D., Wang, Y., et al. (2016). Transcriptome-wide identification and expression analysis of glutathione S-transferase genes involved in flavonoids accumulation in *Dracaena cambodiana*. *Plant Physiology and Biochemistry*, 104, 304-311.
- Zybailov, B., Rutschow, H., Friso, G., Rudella, A., et al. (2008). Sorting signals, N-terminal modifications and abundance of the chloroplast proteome. *PLoS One*, 3(4), e1994.